Project Title:	**BRIDGE CONDITION ASSESSMENT USING REMOTE SENSORS**
Sponsoring Organization:	United States Department of Transportation Research and Innovative Technology Administration
Cooperative Agreement Number:	**DT0S59-10-H-00001**
Research Agency:	Michigan Technological University in cooperation with Center for Automotive Research Michigan Department of Transportation

Principal Investigators:

Theresa M. Ahlborn, PhD, PE, FPCI
Civil & Environmental Engineering

Robert A. Shuchman, PhD
Michigan Tech Research Institute

Lawrence L. Sutter, PhD
Michigan Tech Transportation Institute

Devin K. Harris, PhD
Civil & Environmental Engineering

Colin N. Brooks, MEM
Michigan Tech Research Institute

Joseph W. Burns, PhD
Michigan Tech Research Institute

Date: February 6, 2013

Volume I of II – Main Body

Michigan Tech

Abstract

The challenges of a deteriorating and aged infrastructure continue to challenge transportation authorities as they align maintenance and replacement priorities with decreasing funds. The United States is home to nearly 600,000 highway bridges of which nearly 12% are structurally deficient. This document reports the applicability of low cost, commercially available remote sensing technologies for assessing the condition of bridges.

Numerous remote sensing technologies were evaluated for their ability to measure associated high priority challenges at specific superstructure zones. Using quantifiable health indicators (e.g., percent spall, percent delamination, crack width) each technology was ranked based on criteria for applicability to enhance bridge inspection. Ranking criteria included commercial availability, measurement capabilities, cost, ease of data collection, complexity of analysis, stand-off distance and traffic disruption. Remote sensing technologies that scored as most promising included photogrammetric methods (3-D Optics, Bridgeviewer, GigaPan), passive infrared thermography, Light Detection and Ranging (LiDAR), digital image correlation (DIC), ultra-wide band imaging of GPR, synthetic aperture radar (SAR) and multispectral satellite imagery.

Based on these ranking results, promising technologies were further developed (with some technologies maturing into systems), evaluated, and compared to ground truth (e.g., hammer sounding, chain drag) via laboratory and field testing on in-service Michigan bridges. Spall and delamination maps were generated from the optical and thermal IR images using commercial software and an automatic detection algorithm. Integration of the maps into ArcGIS, a professional geographic information system, allowed for a streamlined analysis that included integrating the results of the complimentary technologies, including visual inspection and ground truth results.

It was found that no technology is a "solve all" solution to assessing the condition of a bridge. A web-interfaced decision support system was developed to display information and allow seamless fusion of the data collected by the chosen technologies. The DSS also supported a user-weighted evaluation system to compute bridge health. The system not only demonstrated how remote sensing results could be collected, synthesized and used effectively for bridge decision-making scenarios, but also how the technologies could be integrated with current assessment methods and strategies.

An economic evaluation was conducted to determine the cost-effectiveness for broad deployment of remote sensing technologies for bridge health monitoring, enhancing the inspection process and potentially improving the method of resource allocation for high priority maintenance and rehabilitation projects. It was found that remote sensing technologies are especially beneficial when combined and used in conjunction with a decision support system.

With a shrinking workforce of experienced bridge inspectors and increasing costs of rehabilitation and replacement, the use of low cost, commercially available remote sensing technologies is an efficient solution to enhancing and monitoring the condition assessment of bridges while supporting improved decision making.

'kk

Acknowledgements

Technical Advisory Committee:

Cook, Steve	Kolar, Dennis	Sweatman, Peter
Couto, C. Douglass	Otter, Duane	Trahey, Amy
Ishee, Charles	Ramsey, Keith	Verma, Krishna
Johnson, Michael	Roberts-Wollman, Carin	
Johnston, Dan	Surdahl, Roger	

Michigan Department of Transportation:

Beck, Steve	Kahl, Steve	Mahdavi, Ali
Cook, Steve	Katherns, Rich	Stallard, Tim
DeRuyver, Jason	Kelly, Bob	Staton, John
Juntunen, Dave	Knauff, Melissa	All Field Personnel

Center for Automotive Research:

Birmingham, Mark	Erickson, Joan	Hong, Qiang
Cregger, Josh	Forester, Mike	Wallace, Richard
Dennis, Eric	Hill, Kim	

Michigan Tech Research Institute:

Banach, David

Banda, Elizabeth

Billmire, Michael

Burns, Margaret

Dean, David

Dobson, Richard

Ebling, James

Endsley, K. Arthur

Gamberg, Peter

Hamermesh, Naomi

Hart, Benjamin

Howard, Matthew

Jason, James

Jessee, Nathaniel

Keefauver, D. Eric *(in memoriam)*

Kemker, Ronald

Koziol, Benjamin

Laubach, Zachary

LeBlanc, Joel

Leonard, Andrew

Leonard, Gregory

McCarty, Jessica

Morang, Melinda

Nesteruk, Alex

Nolte, Christina

Pablo, Leon-Luna

Papineau, William

Phillips, Lisa

Powell, Richard

Qadir, Shazeb

Roush, Benjamin

Roussi, Christopher

Sayers, Michael

Scarbrough, Kirk

Shazeb, Qadir

Subotic, Nik

Valenzula, John

Verploegh, Shane

Whitehead, James

Wienert, Michelle

Wilson, Brian

Yu, Angela

Michigan Tech Transportation Institute, Department of Civil & Environmental Engineering, and other personnel at Michigan Technological University:

Bershing, Scott

Colling, Tim

de Melo e Silva, Hernrique

Evans, Darrin

Gilbertson, Chris

Hannon, Pamela

Hoensheid, Ryan

Hoy, Elizabeth

Kiefer, John

Kus, Tammy

Longmire, Benjamin

Miller, Nathan P.

Oats, Renee

Seppala, Devin

Stein, James

Vaghefi, Khatereh

Weinmann, Nicholas

Yokie, Mike

Disclaimer

The views, opinions and findings expressed in this paper are those of the author(s) and do not represent the official policy or position of the United States Department of Transportation Research and Innovative Technology Administration, any state, or other entity.

Acronyms

2D - Two Dimensional

3D - Three Dimensional

3DOBS - Three Dimensional Optical-evaluation Bridge System

AADT - Annual Average Daily Traffic

AASHTO - American Association of State Highway and Transportation Officials

ACI - American Concrete Institute

ADT - Average Daily Traffic

API - Application Programming Interface

ASCE - American Society of Civil Engineers

ASNT - American Society of Non-destructive Testing

ASPRS - American Society for Photogrammetry and Remote Sensing

ASTM – ASTM International

AVMU - AKELA Radio Frequency Vector Signal Generator and Measurement Unit

BHRRP - Highway Bridge Replacement and Rehabilitation Program

BIRM - Bridge Inspector's Reference Manual

BVRCS - Bridge Viewer Remote Camera System

cm - Centimeter

CMA - Cost-minimization Analysis

ConnDOT - Connecticut Department of Transportation

CSV - Comma Separated Value

dB - Decibel

dBm - Decibel-meter

DDIT - Differential Digital Image Tracking

DIC - Digital Image Correlation

D-InSAR - Interferometric Synthetic Aperture Radio Detection and Ranging Displacement Mapping

DOM - Document Object Model

DOT - Department of Transportation

DSLR - Digital Single Lens Reflect

DSS - Decision Support System

EO - Electro-optical

ERD - Engineering Research Division

ERD - Entity Relationship Diagram

FEA - Finite Element Analysis

FFT - Fast Fourier Transform

FHWA - Federal Highway Administration

FLIR - Forward Looking Infrared RaDAR

FOV - Field of View

fps - Frames per Second

FRA - Federal Railroad Administration

ft - Feet

FY - Fiscal Year

GB - Giga Bite

GHz - Gigahertz

GigaPan - GigaPan System

GIS - Geographic Information System

GNSS - Global Navigation Satellite System

GP - Giga Pixel

GPR - Ground Penetrating Radio Detection and Ranging

GPS - Global Positioning System

GSSI - Global Survey Systems

HBP - Highway Bridge Program

HD - High Definition

HERMES - High-speed Electromagnetic Roadway Mapping and Evaluation System

HTF - Highway Trust Fund

HTML - Hypertext Markup Language

HTTP - Hypertext Transfer Protocol

Hz - Hertz

xkkk

I - Dwight D. Eisenhower National System of Interstate and Defense Highways (e.g., I-75)

IDS - Ingegneria dei Sistemi

INS - Inertial Navigation System

InSAR - Interferometric Synthetic Aperture Radio Detection and Ranging

IR - Infrared

IRI - International Roughness Index

IT - Information Technology.

JSON - Javascript Object Notation

kHz - Kilohertz

KIT - Karlsruhe Institute of Technology

km - Kilometer

KML - Keyhole Markup Language

LAMP - Linux-Apache-MySQL-PHP/Perl/Python

LAPP - Linux-Apache-MySQL-PHP/Perl/Python

LASER - Light Amplification by Stimulated Emission of Radiation

lb - pound

LiBE - Light Detection and Ranging-based Bridge Evaluation

LiDAR - Light Detection and Ranging

LRFD - Load and Resistance Factor Design

LVDT - Linear Variable Differential Transformer

m - Meter

M - Michigan State Highway System (e.g., M-26)

MB - Mega Bite

MBIS - Michigan Bridge Inspection System

MBRS - Michigan Bridge Reporting System

MDOT - Michigan Department of Transportation

MHz - Megahertz

mi - Mile

Michigan Tech - Michigan Technological University

mm - Millimeter

mp - Mega Pixel

mph - Miles per Hour

MS - Microsoft

MSI - Multispectral Satellite Imaging

MTO - Ontario Ministry of Transportation

MTRI - Michigan Tech Research Institute

MTTI - Michigan Tech Transportation Institute

MTU - Michigan Technological University

MVC - Model-view-controller

NASA - National Aeronautics and Space Administration

NB - North Bound

NBI - National Bridge Inventory

NBIS - National Bridge Inspection Standards

NCHRP - National Cooperative Highway Research Program

NDE - Non-destructive Evaluation

NDT - Non-destructive Testing

NHBP - National Highway Bridge Program

NHI - National Highway Institute

NHS - National Highway System

nm - Nanometer

ODOT - Oklahoma Department of Transportation

OGC - Open Geospatial Consortium

OS - Operating System

PDF - Portable Document Format

PennDOT - Pennsylvania Department of Transportation

PHP - PHP: Hypertext Preprocessor

PM - Preventive Maintenance

$ppft^2$ - Points per Square Foot

ppm^2 - Points per Square Meter

pps - Points per Second

z

RaDAR - Radio Detection and Ranging

REST - Representative State Transfer

RGB - Red-Green-Blue

RITA - Research and Innovative Technology Administration

RMA - Range Migration Algorithm

SAR - Synthetic Aperture Radar

SB - South Bound

SFCW - Stepped Frequency Continuous Wave

SHM - Structural Health Monitoring

SIA - Structure Inventory and Appraisal

SLC - Single-look Complex

SSD - Sun-squared Difference

SSI - Surveying Solutions Incorporated

TAC - Technical Advisory Committee

TARUT - Transportation Applications of Restricted Use Technology

Thermal IR - Thermal Infrared Imagery

ThIR - Thermal Infrared

TIF - Tagged Image File

TM - Technical Memorandum

TMS - Transportation Management System

TOF - Time of Flight

TTC - Transportation Technology Center

UNC Charlotte - University of North Carolina at Charlotte

US - United States

USDOT - United States Department of Transportation

UWB - Ultra Wide Band

WisDOT - Wisconsin Department of Transportation

WMS - Web Mapping Service

WSDOT - Washington State Department of Transportation

XML - Extensible Markup Language

YAML - Yet Another Markup Language

μm - Micrometer

zkk

Table of Contents /'Xqnwo g'Kqh'KK'O clp'Dqf {

Volume II of II: Appendices

List of Figures

List of Tables

1.   Introduction

The Michigan Tech Transportation Institute (MTTI) and Michigan Tech Research Institute (MTRI), in cooperation with the Center for Automotive Research (CAR) and the Michigan Department of Transportation (MDOT), completed a research study exploring the use of remote sensing technologies to assess and monitor the condition of bridge infrastructure and improve the efficiency of inspection, repair, and rehabilitation efforts. This project was sponsored by the United States Department of Transportation (USDOT) Research and Innovative Technology Administration (RITA) Commercial Remote Sensors and Spatial Information Program. Remote sensing technologies were correlated with in-place sensors to obtain bridge condition assessment data and evaluate them as part of an integrated decision support environment to move them towards practical use in structural health monitoring.

There is an imperative need to address the state of the aging and degrading infrastructure in the United States (US). The condition of the nation's infrastructure has gained increased attention in recent years, primarily as a result of catastrophic events such as the I-35W collapse in Minneapolis in 2007. However, deteriorating transportation infrastructure has burdened transportation agencies for many years. Bridges continue to age, and funds for the repair and replacement of this infrastructure are currently insufficient. As of December 2011, the US was home to 605,086 highway bridges, with 11.1% of these listed as structurally deficient in the National Bridge Inventory (NBI) (FHWA 2011). Structural deficiency, which describes the condition of significant load-carrying elements and adequacy of waterway openings, typically relates directly to the age of a bridge (AASHTO 2008).

This knowledge highlights the urgent need for replacing and/or upgrading existing bridge infrastructure and underscores the importance of quality inspection and assessment mechanisms to prioritize these efforts. In recent years, structural health monitoring (SHM) for bridges has adopted the "Level IV" approach with a primary focus of accurately monitoring in-situ behavior to assess in-service performance, detect damage, and determine condition of a structure (ISIS 2001). Recent advances in SHM have included novel sensing technologies and assessment methods such as: wireless sensors, strain sensing films and local damage identification, but a complete solution to the challenges facing our aging infrastructure. SHM is further complicated by the wide degree of variability in bridge types, materials, operating environments, and structural configurations Figure 1-1.
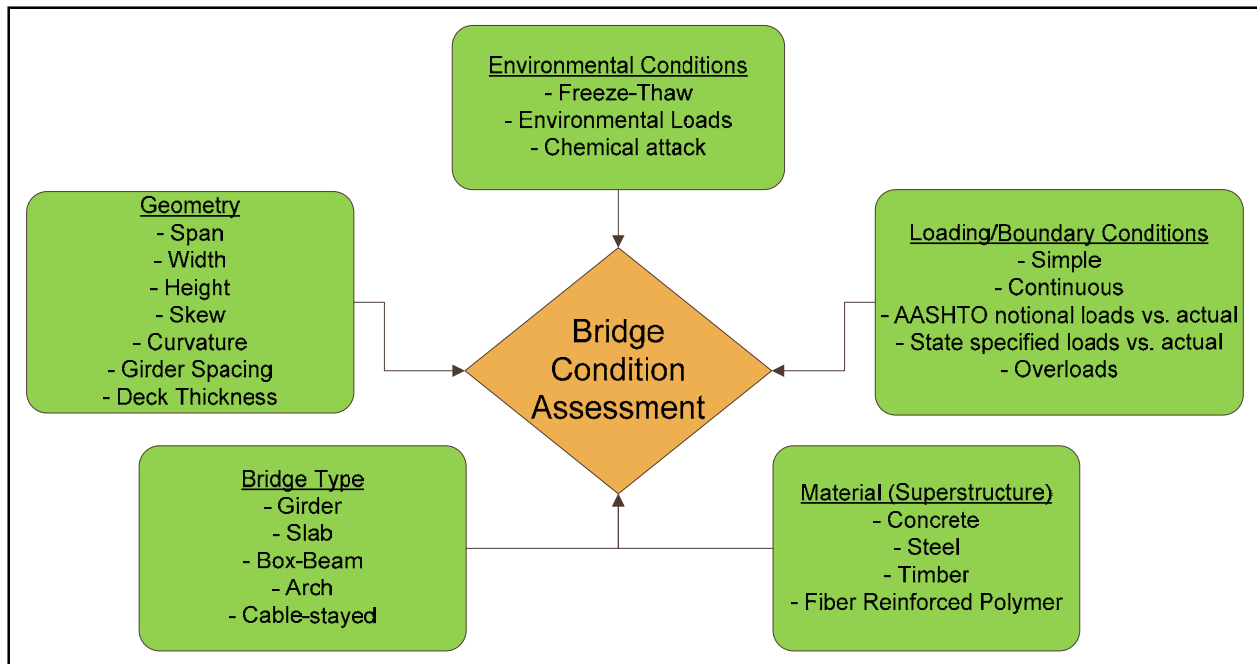
Figure 1-1: Variables influencing bridge behavior.

With a shrinking workforce of experienced bridge inspectors, the use of remote sensing technologies is an efficient solution to enhancing the condition assessment of bridges supporting improved decision making. The concept of remote sensing is often associated with satellite imagery and aerial photography for applications in the environmental and earth sciences; however, various remote sensing techniques have been used in infrastructure applications without being specifically labeled as such. Remote sensing is traditionally defined as the collection and measurement of spatial information at a distance from the data source, without direct contact. To the bridge engineer, remote sensing can mean the ability to assess the condition of the bridge at a distance, enhancement of the inspection process, all without traffic disruption. Current practices for condition assessment include visual evaluation, measurement of bridge response to known loading, and the use of specialized monitoring technologies for evaluating specific challenges.

No single SHM method exists that is capable of completely determining the condition of a bridge. Current assessment methods provide critical information about the condition of a bridge, but the data obtained must often be interpreted by a skilled professional and are typically limited to metrics, such as stress, strain, temperature, deflection, moisture, cracking and delamination. Remote sensing technologies offer the ability to combine several methods to obtain a more complete assessment. Currently, these methods exhibit a divide between metrics for structural response at the global level and material distress at the local level (Figure 1-2). The combination of these metrics provides a better picture of overall bridge condition.
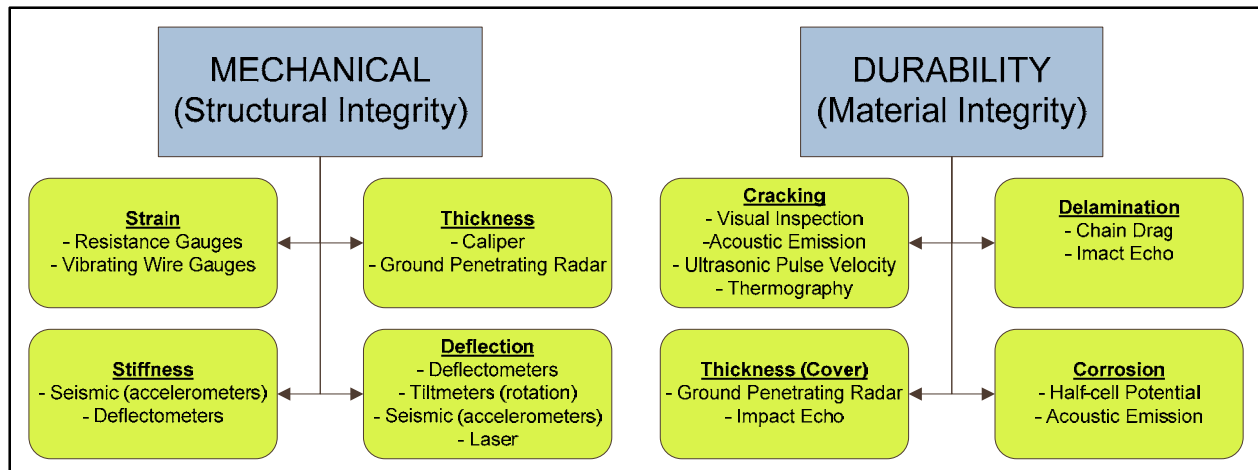
Figure 1-2: Overview of typical assessment measurements and techniques.

The Michigan Technological University (MTU) team (MTRI and MTTI) aimed to develop remotely sensed bridge condition signatures that will enhance the effectiveness of bridge inspection teams and improve asset management programs for transportation agencies. This approach integrates in-situ sensors, "local" remote sensing data (such as ground penetrating radio detection and ranging), and stand-off remote sensing data (such as satellite imagery) to create a unique bridge signature that provides an overall assessment of bridge structural health. The investigated technologies and developed systems consisted of:

- Three Dimensional Optical Bridge-evaluation System (3DOBS)
- Bridge Viewer Remote Camera System (BVCRS)
- GigaPan System (GigaPan)
- Terrestrial Light Detecting and Ranging (LiDAR)
- Thermal Infrared Imagery (Thermal IR)
- Digital Image Correlation (DIC)
- Ultra Wide Band Imaging Radio Detection and Raging System (UWBIRS)
- Synthetic Aperture Radio Detection and Ranging (SAR)
- Interferometric Synthetic Aperture Radio Detection and Ranging (InSAR)
- Multispectral Satellite Imagery (MSI)

The remote sensing technologies combined with a decision support system, which fuses data from multiple sources, offers several advantages compared to current bridge inspection and monitoring methods. It provides a meaningful bridge signature that can be used to rank and sort bridges by priority of needed repairs (as opposed to simply looking at each bridge's lowest PONTIS score), complementing and improving on bridge asset management systems.

This combined approach provides departments of transportation (DOTs) with a potentially cost-effective method for increasing the frequency with which bridges are examined (i.e., more than

once every two years), and it provides the field inspectors with an advanced decision support tool that is applicable regardless of whether or not remote sensing is used as a data source or not (Figure 1-3). The system adds value by providing bridge asset managers with a tool for obtaining an assessment of bridge condition without having to instrument the bridge. Also, by providing inspection teams with relevant preliminary condition assessment data, bridge inspection teams can focus their efforts on trouble spots identified by the sensors as evaluated through the bridge condition Decision Support System (DSS).

A computer-based DSS is a user-friendly web interface software tool, which integrates diverse sensor data and historical information. Monitoring how these signatures change over time will provide state and local engineers with additional information used to prioritize critical maintenance and repair of our nation's bridges. The ability to acquire this information remotely from many bridges without the expense of a dense sensor network provides more accurate and near real-time assessments of bridge condition. Improved assessments allow for limited resources to be better allocated in repair and maintenance efforts, thereby extending the service life and safety of bridge assets, and minimizing costs of service-life extension. With this approach, it is intended to save tax-payers' dollars by prioritizing allocated funds and maintaining structural integrity.
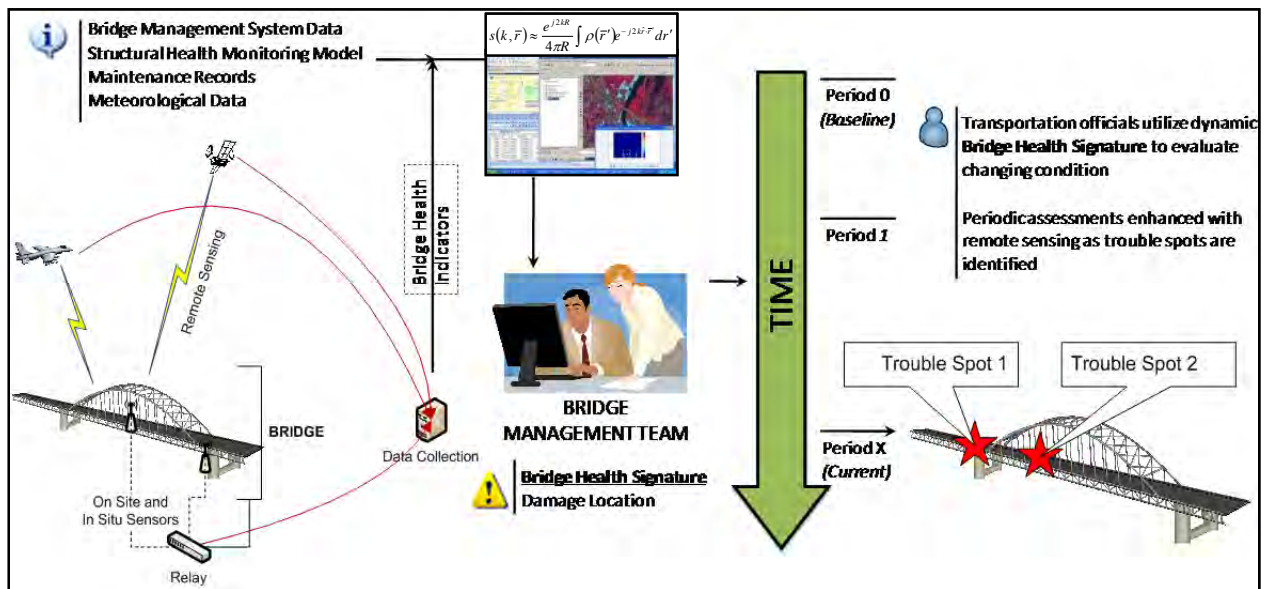
Figure 1-3: Remote sensing operation concept.

A primary outcome of this research effort was the creation of remotely sensed bridge health indicators that can be used in combination with physical inspections for condition assessment. Efforts were completed to combine these measures into a single, integrated bridge signature that can be used as an overall appraisal of bridge condition. The task of obtaining this integrated

bridge signature data and measurements was advised through a Technical Advisory Committee (TAC). The TAC served as a broad spectrum of stakeholders charged with evaluating the project approach, recommending methods and equipment, and reviewing the results from the study. The TAC helped to determine specific high priority bridge condition characteristics that would benefit most from the investigated remote sensors.

The economic evaluation examined the costs of the developed sensing techniques and also evaluated these costs in relationship to the added value that the techniques supply in terms of improved bridge health monitoring. The obtained bridge signatures from these technologies are expected to provide inspectors and transportation officials with both a baseline measure of condition and a measure of changes in bridge behavior over time. This approach will support bridge asset management by providing a method for easily obtaining an assessment of many bridges in one data collection. Figure 1-3 summarizes the concept of operation for the approach.

In this research effort, many tasks were completed including bridge condition characterization, commercial sensor evaluation, field demonstration, decision support system development and assessment (including technical and economic). The aspects of these tasks are discussed in the various chapters in this report.

A detailed literature review of the remote sensing technologies for bridge application and the state of practice for those technologies are presented. Characteristics of bridge condition challenges and their respective sensitivity (e.g., surface cracks at 1/32-1/16 in) were defined and evaluated for numerous remote sensing technologies. Details can be found in Chapter 2.

Chapter 3 involves a discussion on laboratory study of the selected technologies and incorporates the site selection details of the field demonstration work. Highlights of the submitted Technical Memorandums (TM) can also be found in this chapter discussion. More details of this evaluation can be found in Chapter 3.

Chapters 4-12 detail performance evaluations for each of the investigated technologies including highlights of the laboratory investigations, and field performance and analysis. Each technology is also evaluated for field readiness. More details can be found in Chapters 4-12.

The DSS serves as a GIS (geographic information system) web interface program that allows end users to easily map bridge information, access bridge inventory data and plot the remote sensing measurements for a comprehensive look at the overall condition. More details on this evaluation can be found in Chapter 13.

In addition to the technical evaluation of several remote sensing technologies, an economic assessment in which the financial applicability of these technologies for field implementations was evaluated. This analysis considers the costs of technology, labor and data, at a minimum, as well as considers the potential for decreasing marginal costs with broad deployment. More details on this evaluation can be found in Chapter 14.

Chapter 15 provides a final evaluation of the investigated technologies and their field readiness status for implementation. The concept of an overall bridge signature is developed and the path forward for wide spread use and acceptance is discussed.

Additionally, the report includes all supporting documentation including accompanying appendices (A-H), references, and an executive summary characterizing the project scope as well as other administrative support documentation.   In closing, MTU aimed to: establish remotely sensed bridge health indicators; develop a baseline bridge performance metric, the "signature," for benchmarking overall bridge condition; provide a system that enhances the ability of state and local bridge engineers to prioritize critical repair and maintenance needs for the nation's bridges. The contents within this report support the goals and accomplishments in meeting the project's initiative.

2. Background

The transportation infrastructure of the United States is in need of rehabilitation and repair. According the American Society of Civil Engineers (ASCE), more than 27% of the nation's bridges are either structural deficient or functionally obsolete. One succinct and startling statistic is that the average American bridge is now 43 years old. ASCE estimates that the total investment needed to bring the nation's bridge infrastructure up to code over five years is $930 billion, but in that time only $549.5 billion is projected to be spent (ASCE 2009). With a finite amount of funding, the allocation of such funds may make up the difference in the long run. Rehabilitation, for instance, is far cheaper than replacement when damage is minor. Better management of funds used to inspect and maintain existing bridge infrastructure could reduce costs.

Monitoring how damage or deterioration changes over time provides state and local engineers with additional information used to prioritize critical maintenance and repair of our nation's bridges. The ability to acquire this information remotely from many bridges without the expense of a dense sensor network provides more accurate and temporal assessments of bridge condition. Improved assessments allow for limited resources to be better allocated in repair and maintenance efforts, thereby extending the service life and safety of bridge assets, and minimizing costs of service-life extension. Current bridge inspection techniques consist largely of labor-intensive subjective measures for quantifying deterioration of various bridge elements. Some advanced non-destructive testing techniques are being implemented, however little attention has been given to remote sensing technologies.

For this project, the challenges of understanding deterioration common to bridges throughout our nation have been grouped into five broad areas:

- Deck surface
- Deck subsurface
- Girder surface
- Girder subsurface
- Global response

2.1. Current Evaluation Process

The standard evaluations used by the Federal Highway Administration (FHWA) have been limited to auditory tests and visual inspection since NBI was first developed (Chong et al. 2003) almost 40 years ago.

The performance evaluation starts with the inspection of the bridge to determine the present condition. This is completed in a variety of ways depending on the particular personnel and

department conducting the inspection of the bridge, but all inspections are completed in accordance with the National Bridge Inspection Standards (NBIS). The Bridge Inspector's Reference Manual (BIRM) aids the bridge inspector with programs, procedures, and techniques for inspecting and evaluating a variety of in-service highway bridges (FHWA 2006). The program emphasizes visual inspection techniques with manuals that provide photographs of the various types and degrees of deterioration in bridge elements.

Before an inspector is qualified, they are required to attend an inspection course that satisfies the requirement of the NBIS for a comprehensive training program. This is typically a one to two week course depending on the background of the inspector and types of inspections to be completed. To determine the overall condition of a bridge inspectors follow the guidelines provided for them, but also include personal or experience based judgments when assigning a rating for a particular bridge. This is where concern can come into play with structural health monitoring because of the limited consistency from one inspector's rating to the next inspector's rating; bridge inspectors are trained in identifying all the types of deterioration but there is a subjective component when dealing with the rating of the bridges.

According to NBIS, bridges must be inspected at least every two years. Some bridges with problem areas at the discretion of the owner may need to be inspected more frequently than two year minimum required. Any structure that has a span length of greater than 20 ft as defined by the NBIS regulations is required to be rated for NBI. There are currently 603,248 bridges rated within the NBI system as of December 2009. The number of bridges listed as structurally deficient as of 2009 was 71,179 (11.8%) and 78,462 (13.0%) were classified as functionally obsolete, demonstrating the need for a uniform rating system to ensure the correct bridges receive the appropriate attention and funding (FHWA 2010).

A general rating system is used to classify the condition on a 9 to 0 scale with 9 being a new bridge and 0 being out of service. A structurally deficient bridge would be rated at a "4" (poor) or less for superstructure, deck and/or substructure. A structurally deficient bridge could also have waterway adequacy that is rated at a "2" or less. Structural deficient bridges cannot support the intended traffic loads which results in postings to reduce weight and/or speed on the structure. In contrast functionally obsolete bridges do not typically represent a safety threat, but typically no longer have an adequate approach alignment, geometry, or clearance for the given traffic needs and are below current design standards (Amey 2010).

2.1.1. Visual Inspection

BIRM states the typical routine inspection performed for a bridge would be a review of the previous inspection and a visual inspection of all the different members from on top of the bridge and underneath the bridge. The second type of visual inspection would be the in-depth inspection of one or more elements at less than an arm's length from the inspector. With a visual inspection of the bridge, the inspector would be looking for various distress or signs of those

defects in the different members of the structure. If a defect is seen or suspected the inspector will often perform other inspection techniques to determine the extent of the defect on the structure. The location of fracture critical members is important when performing an inspection because these are often non-redundant members in the structure. The inspector pays particularly close attention to ensure that any defect that could potentially affect the capacity of a member or the bridge overall is closely inspected.

2.1.2.   Defects

Bridges are designed with a variety of materials with the three main materials being concrete, steel and timber. Each of these materials has special characteristic that determine which types of defects that the inspector must monitor to confirm the material still has adequate structural capacity for the member being inspected. The NBI is composed of 64.3% of concrete bridges and 30.9% of steel bridges. The use of timber is limited with about 4.2% of bridges being classified as a timber bridges along with only 0.3% of bridges being masonry (FHWA 2010). Table 2-1 shows the defects according to BIRM for the different materials that compose the different structural elements of the bridge. These defects are often associated with one or more structural groupings including deck, superstructure or substructure.

Table 2-1: Specific bridge materials and possible defects (BIRM).

Material	Defects
Concrete	cracking, scaling, delamination, spalling, chloride contamination, efflorescence, ettringite formation, honeycombs, pop-outs, wear, collision damage, abrasion, overload damage, reinforcing steel corrosion, prestressed concrete deterioration.
Steel	corrosion, fatigue cracking, overloads, collision damage, heat damage, paint failures
Timber	natural defects, decay, insects, chemical contamination, delaminations, loose connections, fire damage, weathering, warping, protective coating failure
Masonry	weathering, spalling, splitting, fire damage

When inspecting the deck of the bridge the inspector will look for key defects over the entire bridge. Of primary importance are the defects that affect ride quality of the bridge deck because the public often only feels irregularities from the riding surface. BIRM states that the inspector is typically looking for unevenness, settlement and roughness when determining the condition of the deck. Spalling is one of the defects that inspectors take into account with the safety of cars being of concern with falling concrete. Cracking is also of concern with rebar being exposed to elements possibly causing corrosion. Also the condition of the expansion joint is considered with the inspection of the deck. If there is a problem with the expansion joint it could lead to

superstructure degradation or alert the inspector to possible other damage in the bridge deck. The evaluation of bridge deck deterioration prompts deck repair, rehabilitation and replacement decisions. Sometimes asphalt is used to overlay the deck and the bridge inspector would then have to look for other signs of distress in the deck below the overlay.

The superstructure is of particular importance from a safety perspective, to ensure that the members are adequate for the loads supported by these members. The inspection of the superstructure includes searching for any of the defects in structural members. Some of the main defects that an inspector is looking for are exposed reinforcement, steel section loss and frozen bearing. The inspector should also confirm that the given members match those from plans. Additionally the bearing supports should also be checked thoroughly to ensure critical members are appropriately transferring the load from the superstructure to the substructure.

The substructure also has to be inspected for several different issues to be assured that it is not approaching failure. Some of the main defects the inspector would be looking for in the substructure members would be degradation, exposed rebar, cracking and corrosion. BIRM states that the inspector should determine the dimensions of the substructure to compare to those of the plan. Additionally, settlement of the substructure should be checked. According to BIRM this can be completed by looking along the superstructure to see if any of the vertical faces are tilting. Inspection of the substructure is typically finished with checking for scour or undermining of the structure.

2.1.3. Traditional Inspection Tools

BIRM suggests several tools that the inspector could use while performing the inspection to insure an accurate assessment of the structure's condition. The inspector should carry tools to clear debris (e.g., broom, wire brush, scraper, screwdriver, shovel), and an inspection hammer for sounding concrete, checking for sheared or loose connections and loosening dirt and debris. The inspection hammer can be used by the trained inspector to determine the condition of a member by the sound produced by tapping the hammer to the material. A chain drag apparatus is often used to determine the location of any delaminations that are located in the concrete bridge deck. The chains produce a clear ringing sound in areas where there are no delaminations and produce a dull or hollow sound where there is a delamination in the concrete; however this technique is ineffective where asphalt overlays are applied.

2.1.4. Advanced Inspection Techniques

When evaluation beyond the aforementioned basic techniques is required, more advanced inspections are typically performed. These advanced techniques often require specialized equipment and may require specialized personnel. The different types of inspection techniques available are numerous and are constantly evolving, but can generally be categorized into two types, destructive and nondestructive. A summary of these different techniques listed in BIRM

can be seen in Table 2-2. The purpose of a nondestructive test is to determine characteristics such as: strength and location of abnormalities, without compromising the integrity of the structure. This is important when inspecting a bridge because the less destructive tests required the better the structure will maintain its integrity. Destructive tests can affect the integrity of the structure, so the amount of testing is typically limited. Also the time required for destructive tests is extensive, often requiring the material samples to be delivered to a lab for testing. As a result, destructive tests are often used to confirm the findings of a nondestructive test. A typical example of confirmation destructive testing would be coring of concrete to confirm location and degree of delamination observed from an IR survey. Each individual test provides different information, so the inspector should use discretion for what test to use for the given situation.

Table 2-2: Materials, test type, and bridge testing methods (BIRM).

Material	Test Type	Tests
Steel	Nondestructive	acoustic emissions testing, corrosion sensors, smart paint, dye penetrant, magnetic particle, radiographic testing, computer tomography, ultrasonic testing, eddy current
Steel	Destructive	Brinell hardness test, Charpy impact test, tensile strength test
Concrete	Nondestructive	acoustic wave sonic, delamination detection machinery, ground-penetrating radio detection and ranging, electromagnetic methods, pulse velocity, flat jack testing, impact-echo testing, infrared thermography, laser ultrasonic testing, magnetic field disturbance, nuclear methods, pachometer, rebound and penetration methods ultrasonic testing
Concrete	Destructive	core sampling, carbonation, concrete permeability, concrete strength, endoscopes, videoscopes, moisture content, reinforcing steel strength, petrographic examination
Timber	Nondestructive	Pol-Tek, spectral analysis, ultrasonic testing, vibration
Timber	Destructive	boring, drilling, moisture content, probing, shigometer

2.1.5.　　Condition Rating

The rating of the condition of the three main components is done on a scale of nine (9; excellent condition) to zero (0; failed condition out of service) (see Table 2-3) according to the Recording and Coding Guide for the Structure Inventory and Appraisal of the Nation's Bridges (FHWA 1995). This guide was created to help promote uniformity in bridge structure rating. The bridge section of this guide is located between Items 58-62 and presents a detailed explanation of what

each rating of a structure stands for. The rating of the deck members that are integral with the superstructure are to be rated as a deck only not on how it influences the superstructure. Rating the deck, superstructure and substructure separately allows for an overall view of where the structural deficiencies are occurring. These ratings are then placed into the Pontis database system which forms the annual basis of the NBI. This inventory/rating database allows the federal government to get an accurate account of the condition of the United States bridge system. The rating system is key in providing a high-level summary of how and where work is need on the system of bridges and prioritizing funding on a national level.

Table 2-3: Condition ratings (FHWA).

Rating	Definition	Description
9	Excellent Condition	
8	Very Good Condition	No problems noted
7	Good Condition	Some minor problems
6	Satisfactory Condition	Structural elements show some minor deterioration
5	Fair Condition	All primary structural elements are sound but may have some minor section loss, cracking, spalling or scour
4	Poor Condition	Advanced section loss, deterioration, spalling or scour
3	Serious Condition	Loss of section, deterioration, spalling or scour have seriously affected primary structural components. Local failures are possible. Fatigue cracks in steel or shear cracks in concrete may be present.
2	Critical Condition	Advanced deterioration of primary structural elements. Fatigue cracks in steel or shear cracks in concrete may be present or scour may have removed substructure support. Unless closely monitored it may be necessary to close the bridge unless corrective action is taken.
1	"Imminent" Failure Condition	Major deterioration or section loss present in critical structural components or obvious vertical or horizontal movement affecting structural stability. Bridge closed to traffic but corrective action may put it in light service.
0	Failed Condition	Out of service – beyond corrective action

Another important rating criterion is load rating which defines the load limit on the structure to prevent catastrophic failure. The inventory level represents the live load that a bridge can safely

sustain for an indefinite period of time, whereas the operating level defines the level of permit load allowed across the bridge (Castro et al. 2010). According to the Manual for Bridge Evaluation (AASHTO 2008) there are three distinct procedures for the load and resistance factor rating of bridges: design load rating, legal road rating and permit load rating;

- The design load is a measure of how the bridge in its current condition performs under LRFD (Load and Resistance Factor Design) bridge design standards. If the bridge can support all the LRFD limit states the bridge would be satisfactory for legal loads.
- The legal load rating considers the effect of legal loaded truck traffic on the bridge. This can be the basis for posting load limits on the bridge or a bridge strengthening project.
- Permit load rating checks the effects of an overweight vehicle would have on the bridge taking into consideration the different factors on an individual permit basis.

2.2.   Condition Monitoring

Currently, SHM in the United States and most other developed nations is characterized by traditional visual inspection along with referencing of old inspection reports to maintain an accurate account of bridge condition.

As of 2005, about 40 long-span bridges (100 m or longer) worldwide have been equipped with sophisticated health monitoring instrumentation systems. These systems are lauded as "array[s] of inexpensive, spatially distributed, wirelessly powered, wirelessly networked, embedded sensing devices supporting frequent and on-demand acquisition of real-time information about the loading and environmental effects, structural characteristics, and responses" (Ko and Ni 2005). Despite these advantages, permanent, in-situ sensor networks are costly and can be difficult to install on some bridges or bridge elements, particularly when they were not considered during the construction phase.

Permanent networks of sensors are deployed on bridges with two distinct goals in mind: the generation of alerts for bridge managers and the viewing/analysis of continuous real-time structural data. These goals are achieved by networks that emphasize two discriminating factors: the time-scale of the change and the severity of the change. Traditionally, these networks have consisted of in-situ sensors coupled with structural elements and wired to both a data-acquisition system and a power source. Consequently, these networks are costly, cumbersome, and in some cases interrupt the normal operation of the structure (Kim et al. 2007).

In-situ sensor networks paved the way for modern bridge monitoring practices, including electronic data collection and distribution. Bridge inspection officials have indicated that the best way to improve the performance of bridge inspections is to allow for electronic data to be uploaded directly to a Bridge Management System (BMS); many have also cited the

establishment of such a system as a major accomplishment for their team (USDOT 2001). This is a popular idea in most conceptions of modern bridge monitoring by large, disseminated networks of permanent, in-situ sensors. Ideally, SHM should incorporate remote sensing techniques that provide the same capability for the remote collection of high-resolution (both spatial and temporal), real-time structural data without the need for costly hardware and its installation, calibration, and maintenance. Currently SHM consists of modern in-situ techniques (where sensors are in direct-contact with bridge elements), on-site surveys (where instrumentation is brought to the bridge to make measurements), as well as some standoff remote sensing techniques (where remote sensors are used far from the bridge).

In 1998, the FHWA surveyed the use of NDE techniques for SHM among state and Iowa county DOTs as well as independent contractors. From the 14 (out of 42) state DOT respondents, they learned that the most common NDE techniques being employed in the field, by American Society for Non-destructive Testing (ASNT) Level III personnel, were liquid penetrant testing, ultrasonic testing, and magnetic particle testing with a smaller number reporting expertise in radiographic and electromagnetic techniques. All of these techniques increased in reported use from 1993-98 according to three different surveys. Citing a similar survey from 1994, the FHWA concluded, from an increase of 19-33% response, that use of ASNT Level III certification has increased (USDOT 2001). Visual inspection dominated among NDE techniques then being used on existing bridges of all types, followed by the aforementioned techniques for steel bridges of all types, followed by the aforementioned techniques for steel bridges.

On concrete bridges, mechanical sounding was second to visual inspection, followed by some innovation such as electrical potential and RaDAR (Radio Detection and Ranging) measurements. While many state DOTs reported a variety of advanced NDE techniques such as these being used, almost no county or local agencies reported using anything other than visual techniques and mechanical sounding. It is important to note that of the state transportation agencies that use advanced NDE techniques, some indicated that they had ceased using techniques such as ultrasonic testing of pin/hanger connections, various pile testing, RaDAR, and acoustic emissions due to unreliable performance or other reasons.

2.3.   Remote Sensing

Remote sensing technologies can be used to assess and monitor the condition of bridge infrastructure and improve the efficiency of inspection, repair, and rehabilitation efforts. Most important, monitoring the condition of a bridge using remote sensors can eliminate the need for traffic disruption or total lane closure as remote sensors do not come in direct contact with the structure.

For the typical bridge engineer the concept of remote sensing is often associated with satellite imagery and aerial photography for applications in the earth sciences; however, additional remote sensing techniques have been used in infrastructure applications without being

specifically labeled as such. A general definition of remote sensing is the collection and measurement of spatial information about an object, area, or phenomenon at a distance from the data source, without direct contact (Falkner 1995; Aronoff 2005). Classic examples that may be familiar to the bridge engineer or inspector include satellite imagery, aerial photography, LiDAR, and GPR (ground penetrating RaDAR).

Remote sensing can also be understood as a form of "stand-off" SHM, and a form of NDE and NDT, where the device gathering data is not touching the object or feature being measured. Remote sensing does not include emplaced sensors such as strain gauges or temperature sensors, which are in direct contact with the feature whose characteristic is being measured, even if these data are being transmitted from the bridge to another location for remote monitoring. Being able to apply remote sensing techniques to the field of bridge inspection and monitoring has large potential value, especially considering the sheer number of bridges in the United States transportation infrastructure system and appropriate challenging funding environment for inspection, maintenance and rehabilitation (Ahlborn et al. 2010 a). The formal integration of remote sensing techniques into the bridge monitoring and condition assessment scheme has the potential to enhance inspection practices and also provide temporal assessments between inspection cycles, without traffic disruptions.

Each area has specific indicators that identify condition or deterioration (e.g., map cracking, delamination, and excessive vibration). A number of remote sensing technologies have been reviewed to evaluate potential applicability for monitoring bridge condition and structural health.

At the beginning of the project a pool of potential remote sensing technologies were evaluated in an unweighted, cumulative score of points system awarding a particular technology's capability in detecting a specific indicator of bridge structural health. The criteria for each technology-indicator appraisal was developed based on the experience, and each is intended to be an objective evaluation of remote sensing technology as it would be used in bridge condition assessment. The rating system is similar to the work of Gucunski, et al. (2010), where NDE/NDT techniques were assigned grades to assess their performance for various NDE/NDT applications. However, some of the same difficulties were encountered, particularly the lack of information in the literature regarding specific performance measures. The performance criteria that Gucunski, et al. (2010) used were: i) accuracy, ii) repeatability, iii) ease of data collection, analysis, and interpretation, iv) speed of data collection and analysis, and v) cost of data collection and analysis. For this project, each technique was rated for:

- Accuracy
- Commercial availability
- Cost of measurement
- Pre-collection preparation
- Complexity of analysis and interpretation
- Ease of data collection

- Stand-off distance
- Traffic disruption

A major component in the rating of technologies for bridge condition evaluation was a growing library of references that we initially generated for the State of the Practice Synthesis Report (Ahlborn et al. 2010 b). The highest level of detail and scope applicable to bridge-related remote sensing were used wherever possible for this commercial remote sensors rating methodology. Ideal inputs for the commercial sensor evaluation were papers that demonstrated a remote sensing technology in the field, attempted to characterize a potential defect or other relevant aspect of bridge condition, reported on the resolution or sensitivity they achieved, and estimated the error. In addition, the domain expertise of the project team, particularly in the areas of RaDAR, interferometry, digital image correlation, electro-optical imagery from both airborne and satellite instruments, as well as high-resolution "Street View-style" digital panoramas were critical to the evaluation.

All performance criteria receive a score from 0 to 2 (low to high). This narrow range was chosen so as to avoid artificially inflating scores. For all performance criteria, a higher score is more satisfactory; a score of zero indicates the technology does not satisfy that criterion. An emphasis on commercial availability and well-established practices was used in the literature search wherever possible to keep a focus on the potential for implementation. The commercial availability of these technologies has been represented, as detailed in the Commercial Sensor Evaluation report found in Appendix A. The State of the Practice report can be found in Appendix B.

Table 2-4 summarizes the rating results of each technology at the beginning of the project. The same rating was conducted again at the conclusion of the project and is discussed in Chapter 15 – Findings. Additionally, detailed information on these techniques is available in the State of the Practice report (Ahlborn et al. 2010 b) which can be found in Appendix B.

Table 2-4: Performance rating of commercial remote sensing technologies.

Location	Challenges	Indicator	Desired Measurement Sensitivity	GPR	Spectra	3D Photogrammetry	EO Airborne/satellite imagery	Optical Interferometry	LiDAR	ThermalIR	Acoustics	DIC	Radar (Backscatter/Speckle)	InSAR	Reflective Byte Photography
Deck Surface	Expansion Joint	Torn/Missing Seal		0	8	14	12	11	13	11	0	0	9	0	13
		Armored Plated Damage		0	0	14	12	11	15	11	0	0	0	0	13
		Cracks within 2 Feet	0.8 mm to 4.8 mm (1/32" to 3/16") width	0	8	14	0	12	12	11	0	0	9	0	13
		Spalls within 2 Feet	6.0 mm to 25.0 mm (1/4" to 1") depth	0	8	14	12	12	12	11	0	0	9	0	13
		Chemical Leaching on Bottom		0	11	0	0	0	0	0	0	0	0	0	0
	Map Cracking	Surface Cracks	0.8 mm to 4.8 mm (1/32" to 3/16") width	0	8	14	12	12	12	11	8	0	9	0	13
	Scaling	Depression in Surface	6.0 mm to 25.0 mm (1/4" to 1") depth	0	8	14	12	12	12	11	0	0	9	0	13
	Spalling	Depression with Parallel Fracture	6.0 mm to 25.0 mm (1/4" to 1") depth	0	8	14	12	13	12	11	0	0	9	0	13
	Delamination	Surface Cracks	0.8 mm to 4.8 mm (1/32" to 3/16") width	0	8	14	0	12	12	11	8	0	0	0	13
Deck Subsurface	Expansion Joint	Material in Joint		0	0	0	0	11	0	0	0	0	0	0	0
	Delamination	Moisture in Cracks	Change in moisture content	11	0	0	0	0	0	11	0	0	0	0	0
		Internal Horizontal Crack	Approximately 0.1 mm (0.004") level	0	0	0	0	0	0	11	8	0	0	0	0
		Hollow Sound		0	0	0	0	0	0	0	8	0	0	0	0
		Fracture Planes / Open Spaces	Change in signal from integrated volume	12	0	0	0	0	0	0	8	0	12	0	0
	Scaling	Depression in Surface	6.0 mm to 25.0 mm (1/4" to 1") depth	12	0	0	0	0	0	11	0	0	0	0	0
	Spalling	Depression with Parallel Fracture	6.0 mm to 25.0 mm (1/4" to 1") depth	12	0	0	0	0	0	11	0	0	0	0	0
	Corrosion	Corrosion Rate (Resistivity)	5 to 20 kΩ-cm	0	0	0	0	0	0	0	0	0	0	0	0
		Change in Cross-Sectional Area	Amplitude of signal from rebar	13	0	0	0	0	0	0	8	0	13	0	0
	Chloride Ingress	Chloride Content through the Depth	0.4 to 1.0 % chloride by mass of cement	12	0	0	0	0	0	0	0	0	12	0	0
Girder Surface	Steel Structural Cracking	Surface Cracks	< 0.1 mm (.004") hairline	0	8	11	0	12	0	11	0	0	0	0	0
	Concr. Structural Cracking	Surface Cracks	1 mm (.004")	0	8	11	0	12	0	11	8	0	0	0	0
	Steel Section Loss	Change in Cross-Sectional Area	Percent thickness of web or flange	0	0	11	12	0	13	11	0	0	11	0	0
	Paint	Paint Condition	Amount of missing paint (X%)	0	9	0	0	0	0	11	0	0	0	0	0
	Concrete Section Loss	Change in Cross-Sectional Area	Percent volume per foot	0	0	11	12	0	13	11	7	0	11	0	0
Girder Subsurface	Concr. Structural Cracking	Internal Cracks (e.g. Box Beam)	Approx 0.8 mm (1/32")	0	0	0	0	0	0	11	8	0	0	0	0
	Concrete Section Loss	Change in Cross-Sectional Area	Percent volume per foot	0	0	0	0	0	0	0	7	0	11	0	0
	Prestress Strand Breakage	Change in Cross-Sectional Area	Wire 2 mm or strand 9.5 mm diameter	9	0	0	0	0	0	0	8	0	9	0	0
	Corrosion	Corrosion Rate (Resistivity)	5 to 20 kΩ-cm	0	0	0	0	0	0	0	0	0	0	0	0
		Change in Cross-Sectional Area	Amplitude of signal from rebar	8	0	0	0	0	0	0	6	0	13	0	0
	Chloride Ingress	Chloride Content through the Depth	0.4 to 1.0 % Chloride by mass of cement	10	0	0	0	0	0	0	0	0	11	0	0
Global Metrics	Bridge Length	Change in Bridge Length	Accuracy to 30 mm (0.1ft) (smaller)	0	0	15	13	0	0	0	0	9	0	12	0
	Bridge Settlement	Vertical Movement of Bridge	Approximately 6 mm to 12 mm	0	0	12	0	0	12	0	0	9	0	12	0
	Bridge Movement	Transverse Directions	Approximately 6 mm to 12 mm	0	0	12	0	0	12	0	0	9	0	12	0
	Surface Roughness	Surface Roughness	Change over time	0	9	14	13	12	12	0	0	0	11	13	13
	Vibration	Vibration	5-20 Hz, amplitude?	0	0	0	0	12	0	0	0	10	12	12	0

Rating Based, in Part, on Theoretical Sensitivity for Measurement Technologies

3. Methodology

This section includes general discussion on the purpose of the laboratory study and field demonstration for each technology, in addition to the bridge selection methodology and field deployment plans. The detailed preliminary results of the laboratory tests are included in TM n° 11 and n° 15 (see Appendix C for all TMs) and Chapters 4-12 of this report.

3.1. Laboratory Study

The purpose of laboratory study in this research was to prove the methodology and potential of current commercially available remote sensors based on findings in literature. These commercially available remote sensors were selected based on the Commercial Sensor Evaluation report (Appendix A) and rating system that is included in Chapter 2 of this report. A discussion on the laboratory and preliminary studies for each one of these technologies is included in the following sections.

3.1.1. Three Dimensional Optical Bridge-evaluation System

3DOBS is mainly applicable for resolving surface challenges, such as spalling, scaling and cracking. The laboratory study for this technology included creating a 3D model of the surface and analyzing the results in commercially available software.

3.1.2. Bridge Viewer Remote Camera System

Unlike other technologies in this project, BVRCS is specifically designed to be used on a bridge site and when the camera is in motion and not in the laboratory environment. Therefore, the preliminary results of this study include collecting data on a bridge over US-23 south of Ann Arbor, MI.

3.1.3. Thermal Infrared Imagery

Thermal IR is commonly applicable for resolving the subsurface flaws such as delaminations and debondings on the concrete bridge element. The laboratory study for this technology included testing on several concrete specimens with simulated delaminations and monitoring the temperature change on the concrete surface above the flaw compared to the temperature change on the sound concrete area. Also, the effects of time of data collection and maximum depth of delamination were studied.

3.1.4. Digital Image Correlation

DIC is being used in this study to measure the deflection of the test specimens in the laboratory. These specimens include a section of a bridge pylon and a timber beam specimen.

3.1.5. Ground Penetrating Radio Detection and Ranging

Testing with UWBIRS was conducted inside the laboratory environment and using pavers and gaps to simulate the delaminations. Also, some testing was conducted on the remnants of a degraded prestressed box beam taken from a demolished bridge.

3.2. Field Demonstration

The aim of the field demonstration of this research was to evaluate the performance of selected remote sensing technologies in service. Pertaining to the two major structural components of concern in this research project, the deck (top and bottom surface) and superstructure, the following technologies/systems were evaluated during the field demonstration phase:

- 3DOBS
- BVRCS
- GigaPan
- LiDAR
- Thermal IR
- DIC
- UWBIRS

Four bridges were selected for this field demonstration. A summary of selection process and description of works is provided in the following sections.

3.2.1. Bridge Selection

The aim of the field demonstration selection process was to identify bridges that had varying degrees of degradation with the potential to be identified and quantified using multiple remote sensing technologies. To accommodate the multiple remote sensing technologies, selection parameters were established requiring numerous forms of degradation to be present in the selected bridges. The end goal of the site selection was to identify three bridges within the state of Michigan that could be inspected (visual and detailed), tested, and evaluated using both traditional structural health monitoring techniques (strain gages, deflectometers, accelerometers, live load vehicles, hammer-sounding, chain-drag) for correlation as well as remote sensing technologies/systems.

To allow for a more comprehensive assessment of each technology, the preliminary selection parameter was defined accordingly by using the NBI rating scale along with current MDOT assessment practices. The three bridges were broken down into separate categories, "poor", "fair", and "satisfactory" each of which had correlating NBI deck ratings of four, five and six (or better), respectively (MDOT 2011). Due to the nature of the tested remote sensing technologies a homogenous deck, superstructure and substructure material was preferred. To accomplish this additional parameter, the candidate bridges for each category were separated by item "43: Main span(s) material type" of the MDOT structure inventory and appraisal form (such as pre-stressed concrete box beam versus steel continuous). Once the bridges were broken down into their main material types, it was determined that the pre-stressed concrete I-girder material type bridges were to be further investigated due to the abundance of candidates in the three categories. In addition to, according to the national bridge inventory database, as of 2010, 79% (8,610 out of 10,928) of bridge decks in Michigan are either cast in place or precast concrete, and 53.5% (5,505 out of 10,928) of bridges are either normal reinforced or prestressed concrete which further justified the selection procedure (FHWA 2010).

Preliminary site visits and appraisals were conducted allowing for visual observation and validation of documented deficiencies recorded in past inspection reports. Following the completion of the preliminary site visits, photographs were collected and organized. An image database was developed and then used to generate discussion about each remaining bridge and the suite of technologies' implementation capability. All the technologies were judged individually for each bridge with a focus on four criteria; presence of sensing deficiencies, accessibility, setup and sampling. To generate a complete evaluation of the four established criteria the deck top surface, bottom surface and bridge superstructure were individually assessed. Upon completion of the bridge selection discussion, three field demonstration locations along with a supplemental selection had been established, each fulfilling the selection parameters for the three separate categories. The bridges selected were as follows:

- "Poor" condition; Mannsiding Road over US-127 north bound (NB)
- "Fair" condition; Willow Road over US-23
- "Satisfactory" condition; Freer Road over I-94
- "Supplemental" selection; Mannsiding Road over US-127 south bound (SB)

The field demonstration locations for the remote sensing technologies can be seen in Figure 3-1. The "Poor" and "Supplemental", "Fair", and "Satisfactory" locations are displayed in the provided figures as pin A, B, C, respectively. Due to the close proximity of the "Poor" and "Supplemental" bridge selections only one pin is displayed. Additional information for each selected field demonstration location is provided in the pertaining subsection and Appendices D.1-D.4.
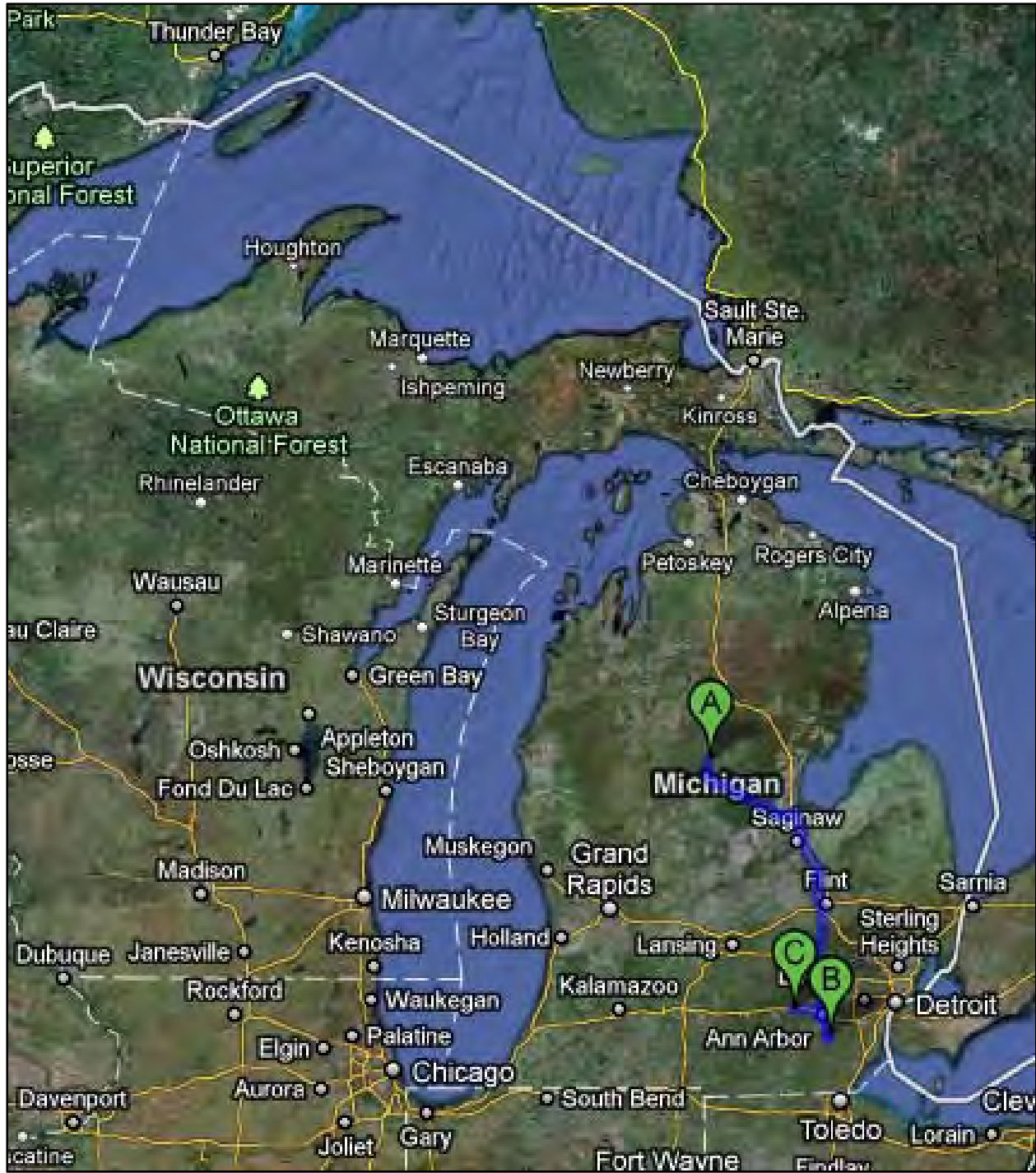
Figure 3-1: Locations of the selected field demonstration bridges.

3.2.1.1. "Poor" Condition Bridge

The selected "Poor" condition bridge, MDOT structure $n^{\underline{o}}$ 1713 – Mannsiding Road over US-127 north bound, is located in Clare County approximately 10 mi north of Clare, Michigan (Figure 3-2) and was determined to be the best candidate for field demonstration purposes.

The field demonstration candidate structure serves Mannsiding Road; a "Major Collector" road. The bridge was constructed in 1966 and is a 3-span prestressed concrete multiple I-beam composite structure. The structure is 130.92 ft in length and 31.17 ft in width, which translates into 26 ft of riding surface. During 1996, the average daily traffic (ADT) over the structure was found to be 1,000 with 3% being commercial (MDOT 2011).

Figure 3-2: "Poor" bridge selection – Mannsiding Road NB.

Currently the bridge has no posted speed limit restriction. The crossing spans north bound US-127; a National Highway System (NHS) route that is not within any federal-aid urban boundary. The bridge does not meet the desired minimum vertical clearance for NHS routes. The field demonstration location was located 2.3 mi south of M-61 (approximately 5.5 mi south of Harrison on US-127). The structure is part of an interchange serving the greater Harrison area,

which is considered to be a rural environment. Figure 3-3 (a) and (b) show photos of the bridge, one taken in 2008 during a MDOT scoping/inspection that provided detailed condition information, and the other by the research team during a site visit in June 2011.

The condition of the concrete deck surfaces, both top and bottom, were an area of major concern. A 2008 MDOT scoping inspection classified the deck with a NBI rating of "4". The scoping revealed that on the top surface of the concrete deck 176 ft^2 or 4.4% of the deck was delaminated. Additional testing on the bottom surface revealed that 623 ft^2 or 15% of the deck was in distress (MDOT 2011). The deck also possessed light scaling throughout and numerous transverse, longitudinal and diagonal cracks were present. Additionally, several high-load hits have resulted in scrapes and spalls of the superstructure underside, but currently there is no sign of exposed reinforcing steel or pre-stressing strands. The bridge is scheduled for complete replacement in 2012/13. Additionally, during the on-site inspection of the selected "Poor" bridge, it was found to have a complementing twin bridge, Mannsiding Road south bound overpass. The Mannsiding Road south bound overpass bridge is described in further detail in the "Supplemental" bridge selection section.

Figure 3-3: Mannsiding Road bridge NB deck condition in 2008 (a) and Mannsiding Road bridge NB deck condition in 2011 (b).

3.2.1.2. "Fair" Condition Bridge Selection

MDOT structure n$^{\underline{o}}$ 10892 – Willow Road over US-23 was selected for the "Fair" condition field demonstration bridge. The bridge is located in Washtenaw County approximately 3 mi north of Milan, Michigan. An aerial photograph of the selected site is shown in Figure 3-4.

The "Fair" field demonstration structure serves Willow Road; a "Major Collector" road. The bridge was constructed in 1962 and is a 4-span prestressed concrete multiple I-beam composite structure. The structure is 209 ft in length and 30.83 ft in width, which translates into 26 ft of

drivable surface with no availability for shoulder room. During 1997, the ADT over the structure was found to be 2,220 with 3% being commercial (MDOT 2011). Currently the bridge has no posted load limit restrictions. The crossing spans both north and south bound US-23; a NHS route that is not within any federal-aid urban boundary. The bridge does not meet the desired minimum vertical clearance for NHS routes. The structure is located in York Township within Washtenaw County.

Figure 3-4: "Fair" bridge selection – Willow Road.

The current condition of the deck surface is rated as a "5" on the NBI scale. In 2010, the inspection report indicated that open transverse cracks, diagonal cracks and areas of delamination were present throughout the deck. Concrete patching had been completed to help minimize deterioration and prolong the service life of the bridge. Additionally, areas on the bridge superstructure displayed desired sensing deficiencies over both the north and south bound lanes. This is attributed to several high-load hits, which had resulted in scrapes and spalls, but there was no sign of exposed reinforcing steel or prestressing strands. Figure 3-5 shows a photograph of the current condition of the concrete bridge deck.

Figure 3-5: Willow Road bridge deck condition.

3.2.1.3. "Satisfactory" Condition Bridge Selection

Lastly, the "Satisfactory" bridge was chosen to be the MDOT structure nº 10940 – Freer Road over I-94, located in Washtenaw County, approximately 1 mi east of M-52 in Chelsea, Michigan. An aerial photograph of the selected site is shown in Figure 3-6.

The field demonstration candidate structure serves Freer Road; a "Major Collector" road. The bridge was constructed in 1960 and is a 4-span prestressed concrete multiple I-beam composite structure. The structure is 209 ft in length and 30.83 ft in width, which translates into 26 ft of open roadway riding surface with no shoulder. During 1997, the ADT over the structure was found to be 150 with 3% being commercial (MDOT 2011).

Figure 3-6: "Satisfactory" bridge selection – Freer Road.

Due to the site's low ADT, this structure was the first to be tested, which allowed for the entire research team to work in an even safer environment while causing minimal disruption to local traffic going over the bridge. This site was the ideal location for the initial data collect to occur, allowing for the researchers to resolve any unforeseen issues on site prior to the inspection of the remaining two bridges, which possessed higher ADT volumes.

Currently, the bridge has no posted speed limit restrictions. The crossing spans both east and west bound I-94; a NHS route that is not within any federal-aid urban boundary. The bridge does meet the desired minimum vertical clearance for NHS routes with a measured clearance of 16 ft.

The NBI rating assigned to the concrete deck surface is a "6". In 2010, the inspection report indicated that there were several areas of concrete patching accompanied by few tight transverse and diagonal cracks present on the deck (MDOT 2011). Concrete patches were applied to help minimize deterioration and prolong the service life of the bridge. The report indicated that there were also areas of interest on the superstructure where the concrete material had spalled and cracked. These areas of interest were located at the beam-end locations on the bottom flange.

None of the spalled sections on the girders were deep enough to reveal any reinforcing steel or prestressing strands however some spalled areas on the underside of the deck were deep enough to allow for corrosion to occur as shown in Figure 3-7.

Figure 3-7: Freer Road bridge top and bottom surface conditions.

3.2.1.4. "Supplemental" Bridge Selection

The "Supplemental" bridge selection, MDOT structure n$^{\circ}$1712 – Mannsiding Road over US-127 south bound is located in Clare County approximately 10 mi north of Clare, Michigan and was not originally in the scope of work for the field demonstration. However, the close proximity of the bridge to the "Poor" selection location allowed for data acquisition with no additional traffic disruption and permitting. An aerial photograph of the selected site is shown in Figure 3-8.

The field demonstration candidate structure serves Mannsiding Road; a "Major Collector" road. The bridge was constructed in 1966 and is a 3-span prestressed concrete multiple I-beam composite structure. The structure is 130.92 ft in length and 31.17 ft in width, which translates into 26 ft of riding surface. During 1996, the ADT over the structure was found to be 1,000 with 3% being commercial (MDOT 2011).

Figure 3-8: "Supplemental" bridge selection – Mannsiding Road SB.

Currently the bridge has no posted speed limit restrictions. The crossing spans south bound US-127; a NHS route that is not within any federal-aid urban boundary. The bridge does not meet the desired minimum vertical clearance for NHS routes. The field demonstration location was located 2.3 mi south of M-61 (approximately 5.5 mi south of Harrison on US-127). The structure is part of an interchange serving the greater Harrison area, which is considered to be a rural environment. Figure 3-9 shows the general surface condition of the bridge deck.

When comparing the condition of the concrete deck surface, top and bottom, of the "Supplemental" and "Poor" bridge selections drastic differences in the state of deterioration were noted. The two bridges had been constructed at the same time, but large variations in the deteriorated state on the concrete deck are documented. An inspection conducted on this bridge in 2010, classified the deck with a NBI rating of "7" (MDOT 2011). The inspection notes stated that minor cracking and shallow scaling on the deck surface was present, however was not substantial enough to cause structural issues. When comparing the "Supplemental" bridge deck rating of "7" to the "Poor" bridge selection's deck rating of "4" on the NBI scale, questions of construction procedure, inspection consistency and environmental effects were raised.

Figure 3-9: Mannsiding Road bridge SB.

3.2.2.   Field Demonstration Design

The proposed field demonstration time was narrowed down to the first two weeks of August 2011. The first structure tested was the "satisfactory" condition bridge (MDOT $n^{\underline{o}}$ 10940), followed the "fair" condition bridge (MDOT $n^{\underline{o}}$ 10892), and the "poor" condition bridge (MDOT $n^{\underline{o}}$ 1713) respectively. The estimated allocated duration for data collection on each bridge was approximately between one to three days depending on weather condition. A scheduled time of data collection was assigned for each technology to allow for more efficient data collection and prevent the conflict on the data collection time between technologies.

For establishing ground-truth information, an MDOT certified bridge inspector was present during the field testing on each bridge and inspected the entire structure for correlation purposes (e.g., delamination maps, spall maps, crack maps, roughness) with all the remote sensing technologies being deployed on the three selected bridges. The detail plan and methodology for field demonstration of each technology is provided in Chapters 4-12. Further information regarding the technologies and bridge site selection are provided in TM $n^{\underline{o}}$ 20 and $n^{\underline{o}}$ 21 (Appendix C).

4. Designing and Deploying the Three Dimensional Optical Bridge-evaluation System

Photogrammetry is "the science or art of deducing the physical dimensions of objects from measurements on photographs of the objects" (Henriksen 1994). It includes the generation of three dimensional (3D) models from stereo pairs of imagery in order to obtain depth and height information, and is part of the larger field of 3D optics, and can be referred to as 3D photogrammetry. Stereo images have to be collected with an approximate 60% overlap in order to generate these models (McGlone et al. 2004). The project team's use of 3D optics/photogrammetry was a technology demonstration to apply a potentially low-cost remote sensing method not typically yet seen in transportation applications. At the distance used in this project, the deployment can be described as an implementation of close range photogrammetry (Luhmann et al. 2007). Several bridge condition indicators have been evaluated to see if they could be assessed with 3D optics, including spalling, scaling, cracking, and surface roughness. Along with assessing the accuracy of the technique, two different commercially-available 3D modeling programs were compared to see how they affected the outcomes of the measurements.

4.1. Methodology

Agisoft PhotoScan is a close range 3D photogrammetric commercial software program that can generate 3D models with minimal digital photographic inputs. This software was chosen over others due to the fact that it is relatively inexpensive and very easy to use, including by non-remote sensing experts in transportation agencies. Once photos are uploaded, the software processes them without having to calibrate cameras, user input of camera parameters or manually aligning the photos to generate a model. It is only when the user wants to output a digital elevation model (DEM) from the model that any user has to define markers with XYZ inputs.

Various experiments were performed to test the cameras and software limitations using a piece of foam board, which was used for its ease to shape and attach extra pieces. A wedge shape was carved into the board that allowed for the determination the horizontal resolution of the program, which relates to the width of cracks on bridges. Pieces of cardboard were arranged in a stair-step fashion that shows the programs limit to resolve height or depth measurements. Finally, different colored spheres were added to show if there would be problems with generating accurate models due to poor contrast and the different sizes show what the resolution is with respect to generating rounded features. Figure 4-1 is an example of one of the photos taken of the foam board used and Figure 4-2 is an example of the 3D model created with PhotoScan from the stereo overlapping digital photographs.
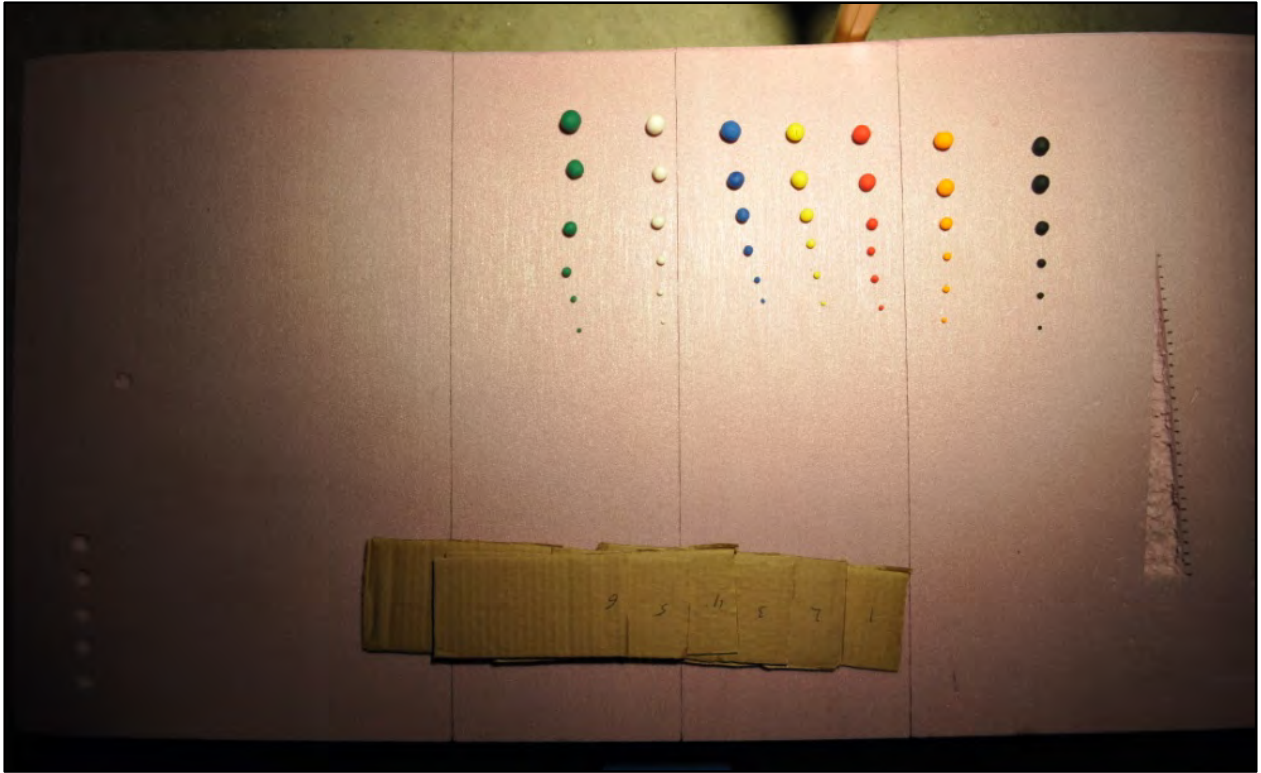
Figure 4-1: Photo taken of the foam board used to determine the restrictions of PhotoScan. The light source is directly overhead simulating conditions around noon where the presence of shadows is reduced.

Figure 4-2: The resulting PhotoScan model. A total of five photos were used to generate this model.

The camera was mounted above the board at a translation stage that allowed photos to be taken at precise intervals across the length of the board. Tests were also conducted with a single light source that illuminated the board from directly above, 45º from nadir and 80º from nadir to determine how the lighting and resulting shadows affected the model. All of the tests produced similar results and demonstrated that photos can be taken throughout daylight hours without concern over reducing resolution or accuracy.

Test runs were also performed to consider how the quantity of photos affected the resulting model. Models were generated using three, 20, and then 48 photos. This experiment showed that increasing the number of photos and coverage, noise was reduced and produced a clearer more accurate model without a change in resolution. Also differences in contrast did not appear to play a significant role in generating a model as all spheres greater than 10 mm in diameter were discernible in the 3D model for all colors as shown by the model produced in Figure 4-2.

The first in-field test was conducted by taking the camera and capturing spalls on the underside of the 6 Mile bridge over US-23 north of Ann Arbor, MI. 3D models of spalls were generated by taking four to six photos in a line, with the spalls being located approximately 2.5 m above where the photo was taken (Figure 4-3). Spalls at a distance were of importance to demonstrate how a 3D setup could be deployed to measure the length, width, and depth of spalls that would otherwise require equipment to reach.
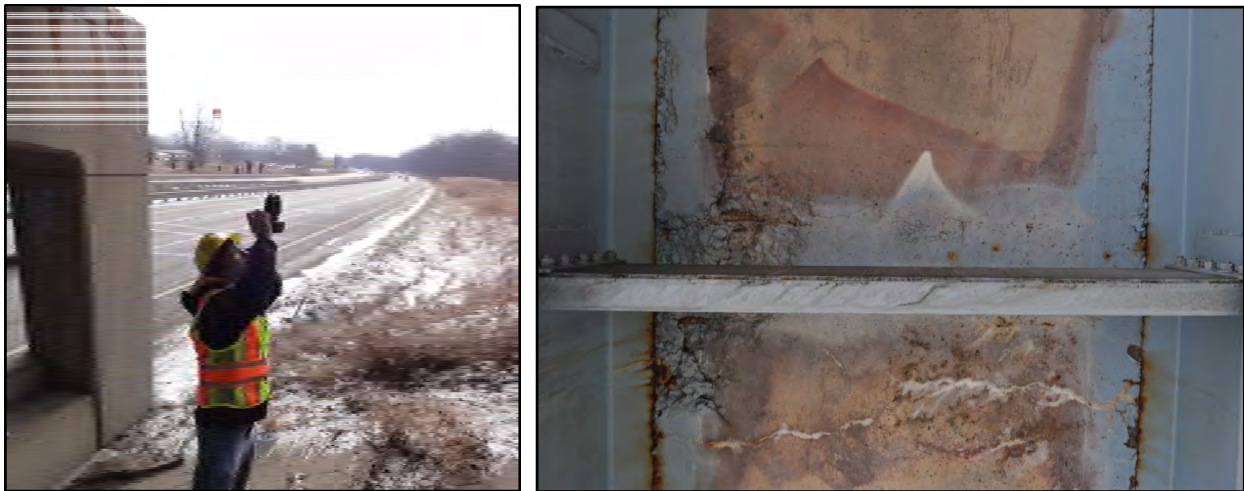
Figure 4-3: Taking photos of the underside of 6 Mile Road bridge over US-23. Image on the right is one of the photos used to generate a 3D model.

Additional testing was conducted on an asphalt parking lot. In this case the camera was hand held and walked over a spalled section (Figure 4-4). This would simulate a vehicle mounted camera driving across a bridge deck. For these tests the camera was about 1 m above the ground with at least a 60% overlap. These initial photos were used to develop techniques for analyzing the DEMs generated from PhotoScan. This analysis included calculating the deviations from a

plane. This helped in determining where there was a difference in elevation and helped to calculate the area and volume of the spall. For the initial testing, a Nikon D40 was used with a resolution of 6.1 MP and it was held about 3 ft off the ground.
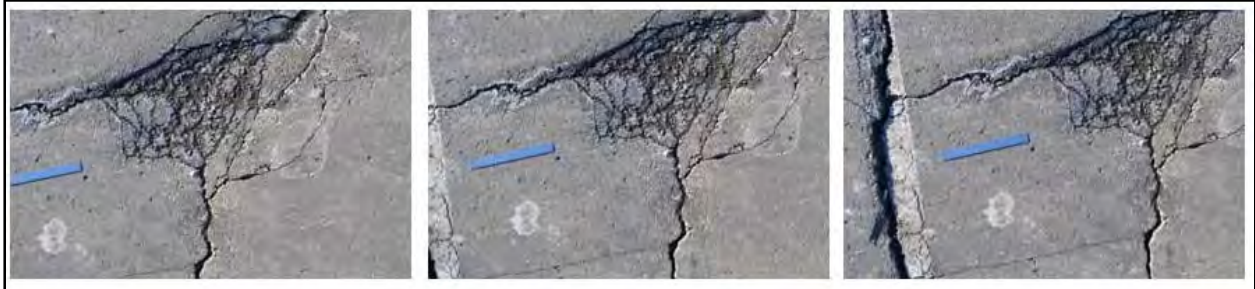
Figure 4-4: A series of photos that were taken from the parking lot test covering a spall that was used for initial testing with generating area calculations with the DEM outputs. Notice the 60% overlap.

From this initial hand held concept, a vehicle mount was constructed for use on a bridge deck (Figure 4-5). Calculations were made to determine the height necessary for the system to cover one lane per pass. For the Nikon D5000 DSLR (digital single-lens reflex) camera with a resolution of 12.3 MP and a 27 mm focal length lens, to cover a 12 ft wide lane, the camera needed to be mounted 9 ft above the bridge deck. In order to achieve this height a wooden vehicle mount was constructed to fit into the bed of a standard pickup truck. During field collections a programmed control board automated the camera to take pictures at a rate of one per second. At this rate, the truck was driven across the bridge deck at a speed of about 1 mph. This ensured that we captured a 60% overlap between the photos. However, faster speeds can be reached using higher-end, faster cameras. A full bridge deck was collected by driving each lane of the bridge.

In order to generate a DEM from the version of PhotoScan used in initial efforts, it was necessary to create reference points on the bridge decks as shown in Figure 4-6. These reference points were marked duct tape that was placed on the bridge deck in a grid pattern. The tape was place at 4 ft intervals in the transverse direction and at 10 ft intervals in the longitudinal direction. Carrier phase GPS points were collected with a Trimble GPS (with an accuracy of <50 cm) at each of the four corners and at various other points on the deck to be able to correctly spatially reference the data and to accurately reference the data with other data types. This reference pattern allowed for accurate georeferencing of the DEM and made it easier to line up and compare results between the different technologies.

Figure 4-5: 3DOBS vehicle mount in the bed of a pickup truck. The image on the left was taken on Willow Road bridge and the one on the right on Freer Road bridge.
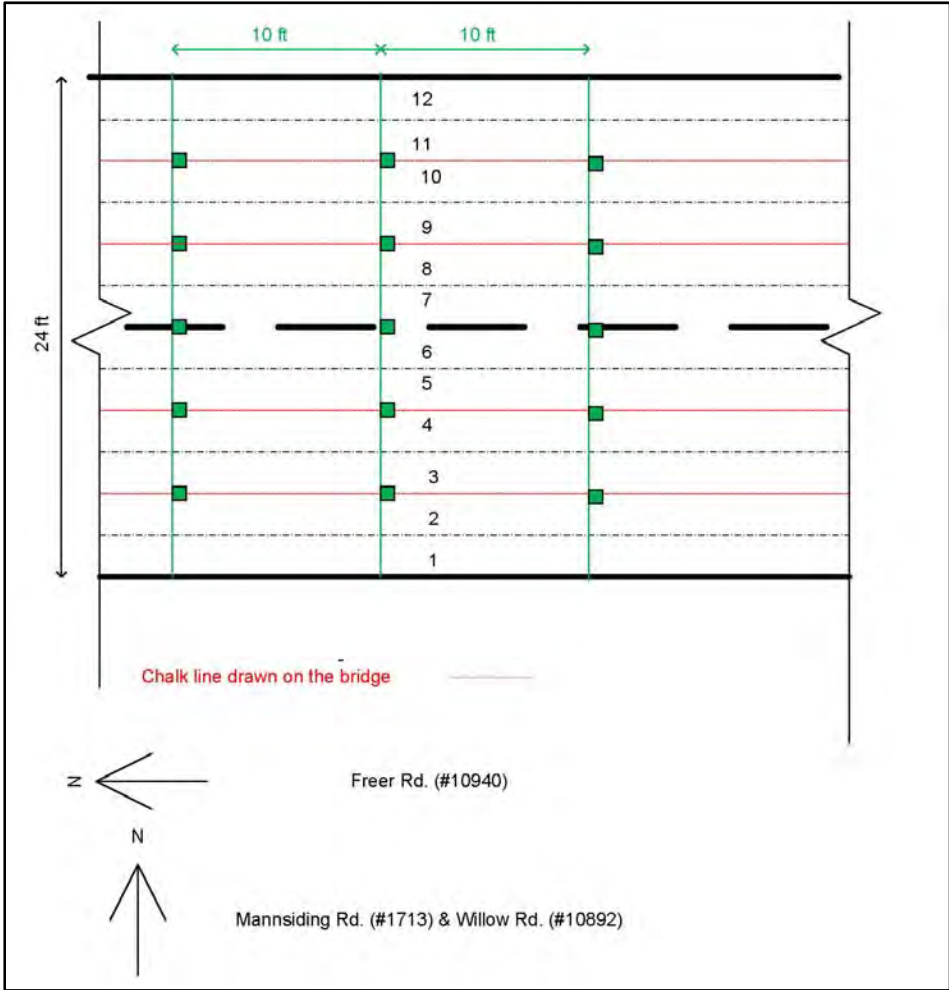
Figure 4-6: Diagram illustrating the grid pattern used for reference on all field demonstration bridges. The chalk line on the bridge deck was used for the Thermal IR data collects.

After 3DOBS was deployed to each of the three field demonstration sites (four bridges), the photos were processed in PhotoScan to generate DEMs of the three bridges. These DEMs were then used for two different methods in order to determine the condition of the bridge deck. First a spall detection algorithm was developed by the project research team using Python within ArcGIS so that spalls could be detected on an automated basis, and the tool could be extended to transportation agencies who had access to the leading commercial GIS software, ArcGIS. This algorithm generated a standard GIS shapefile that contained the extents of all the detected spalls as well as a CSV (Comma Separated Value) attribute file that contained area and volume calculations for each of the detected spalls.

The spall detection algorithm uses ArcPy to interface with ArcGIS and utilize some of Esri's available geospatial tools. The tool used to detect spalls is called Focal Statistics. This tool analyzes each cell in the raster and calculates statistics based on a specified neighborhood of cells around it. Figure 4-7 shows the difference in focal statistics output that is generated from using neighborhoods. For detecting spalls in the 3DOBS DEMs, a seven cell radius neighborhood was used and the standard deviation of the difference calculated. Additional functionality was added so that the user can remove bridge joints by creating a shapefile of the bridge joints. Spalls can also be detected based upon their area. This feature allows for the detected spalls to correspond to minimum size definitions and allow for the removal of small artifacts in the DEM (Figure 4-8). It is fully automated, and only requires the user to set the working directory, file names for the DEM and bridge joint shapefile, focal statistics sensitivity and the minimum spall size (Figure 4-9).
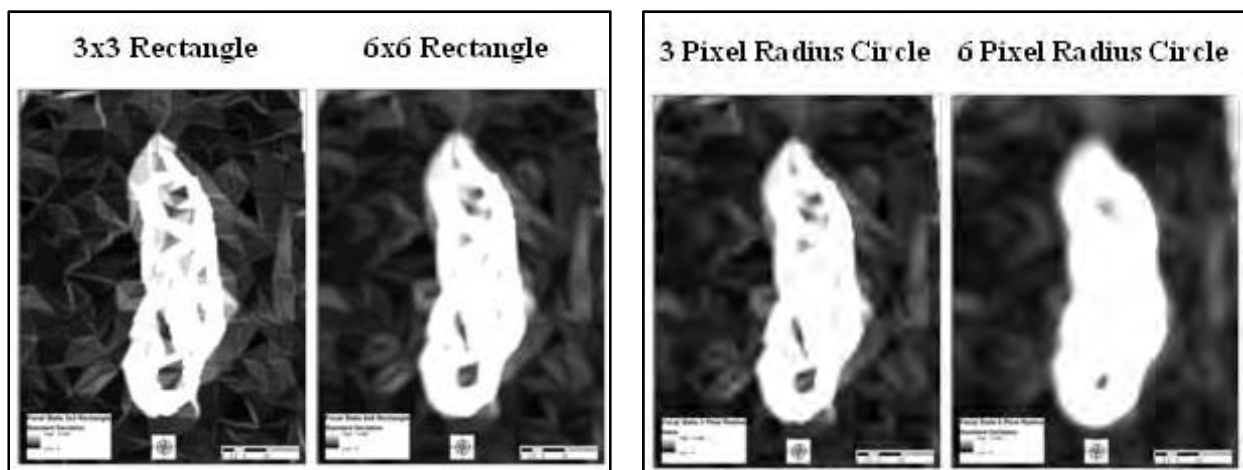
Figure 4-7: Different type of neighborhoods that could be used as applied to the DEM of Freer Road bridge. The image also shows how well a spall stands out against the bridge deck.
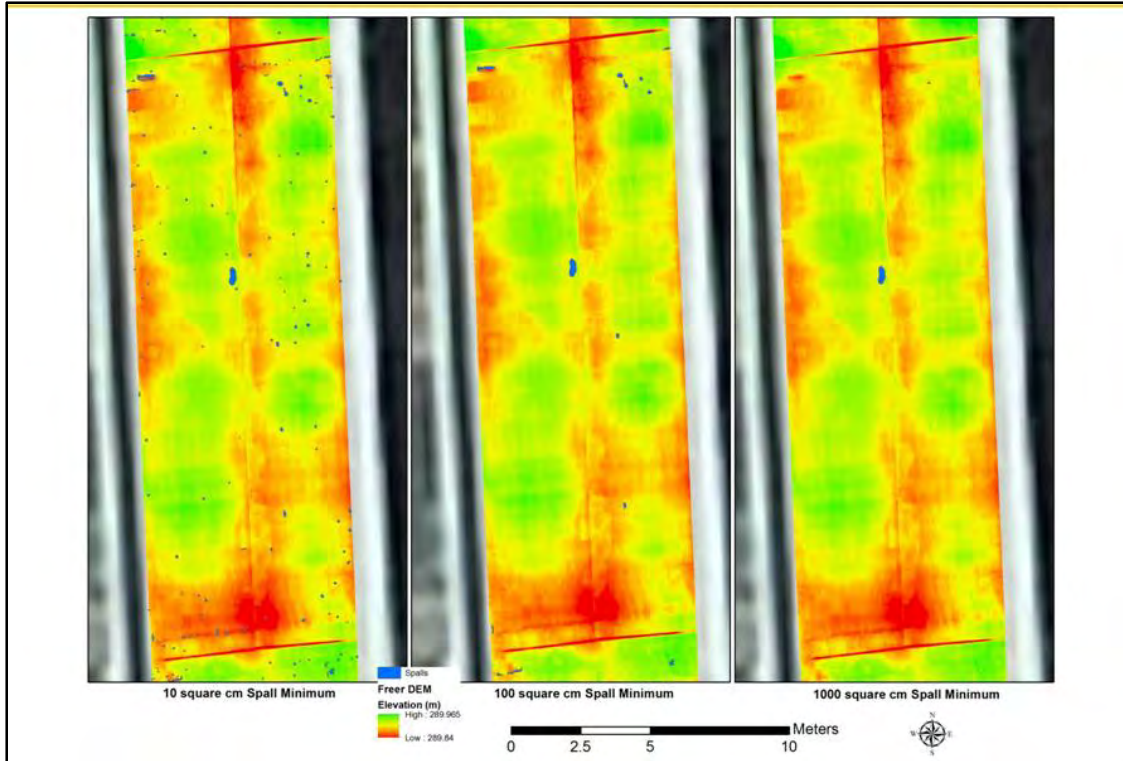
Figure 4-8: Differences in minimum spall sizes as from the spall detection algorithm. Starting on left, the images depict spalls larger than 10 cm^2, 100 cm^2, 1,000 cm^2 respectively. Data from Freer Road bridge.

Figure 4-9: Python shell running the 3DOBS algorithm. The "Max bridge" and "Min spall" pixel values correspond to the focal statistics values that were generated from the DEM. They allow the algorithm to distinguish which values represents the bridge deck and which are spalls. The "Min spall size" is used to define the minimum that would be considered a spall.

The spall results from the 3DOBS automated algorithm were compared to spalls manually digitized from the bridge overview high-resolution photo composite. This was done so that the 3DOBS algorithm could be compared to results representative of what a trained technician would interpret from visually assessing a high-resolution digital image of the bridge deck. The main benefit of having an automated method is to reduce the amount of time needed to process data. In order for the algorithm to be beneficial, it would need to produce similar results in less time.

The second method was to generate an IRI (International Roughness Index) numerical calculation for the bridge deck. This was done because the elevation data needed to calculate IRI was already available through having created the 3D bridge surface for spall detection. IRI is a profiling index that has ratings ranging from 0 m/km (or mm/m) to 20 m/km; indicating a perfectly smoothed surface and an extremely rough unpaved surface, respectively (see Figure 4-10) (Al-Omari and Darter 1994).
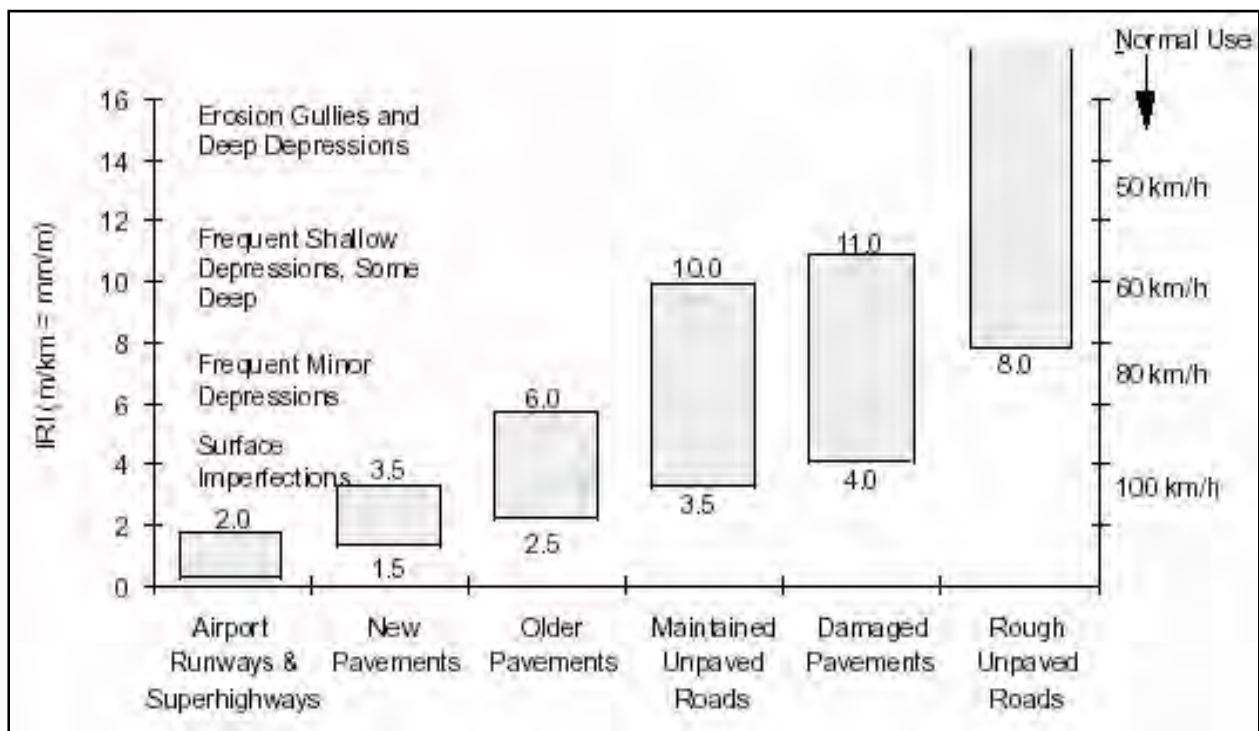
Figure 4-10: The IRI condition rating graph.

The ratings are based on a longitudinal profile of the pavement, which is then processed through the quarter-car and 250 mm wavelength models to simulate how a single wheel of a car would react to the condition of a pavement. Normally the longitudinal profile is created from a series of measurements made by an altimeter connected to a car, which is driven across the pavement. However, for the purposes of this project, the elevation measurements were collected using a

remote sensing methodology to determine where the three bridges would be positioned on the IRI graph and to validate if the results were similar to their real-world conditions. The profiling data was then formatted into an ERD (Entity Relationship Diagram) file that was imported into a computer profile graphing program. ProVAL then graphed the longitudinal profile, which was processed through the two models. The end result is an IRI value that is indicative of a single wheel path across the bridge.

3DOBS was also adapted to take a photo inventory and generate a 3D model of the underside of bridges. A separate attachment was made that attaches to the base of the vehicle mount. A Nikon D5000 along with the control board was still used to take regularly spaced photos as a vehicle was driven under the bridges. Two 500 watt work lights were attached to the mount to provide additional lighting so that features, particularly between the beams, could adequately illuminated. The truck was also driven at a speed of 2 mph to achieve overlap of the photos.

4.2. Results and Discussion

The initial lab testing proved that PhotoScan Pro was more than capable of generating 3D models of a surface. All of the models produced had a resolution of about 4 mm in the horizontal and vertical directions. More importantly, these test demonstrated that by using PhotoScan, 3DOBS would be capable of using photos from a variety of lighting conditions.

The initial parking lot testing helped to define the methodology for a successful 3DOBS collect. With the D40 we were able to produce a DEM with a resolution of 1 mm horizontal and 4 mm vertical (Figure 4-11). With this high resolution DEM, the project team started to look into the useful product that could be derived. The first step in characterizing the spall was to create an artificial plane which represents what should be the base elevation (Figure 4-12), above or below which represented deviations from the plane. Everything below this height was represented as spall. The DEM showed one large DEM that was 3,168 cm^2 in size.

During parking lot testing it was discovered that shadows do not affect the results of the 3D reconstruction. These shadows could be from trees or the vehicle-mount itself. Figure 4-13 shows example of the vehicle mount casting its shadow over the collect area as the truck was driving. Despite the shadow being captured in every photo, it does not affect the final DEM that was generated. This ability offers greater flexibility in deployment as collects are not restricted as to the time of day or specific direction of travel due to time of day.

During the field demonstrations at each of the selected bridges it was determined that it took about 30 minutes to collect one bridge. This time included 10 minutes for setup, 10 minutes for collecting the imagery and 10 minutes for break down. The vehicle mount was constructed so that it could easily be broken down and transported to different sites in the bed of a truck (Figure 4-14).
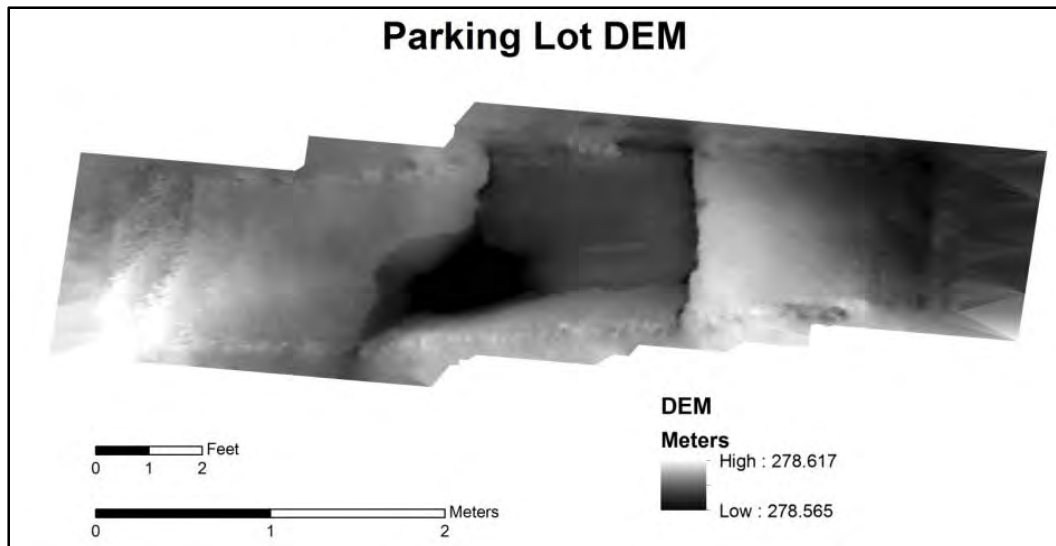
Figure 4-11: DEM of the walking test of 3DOBS in a parking lot. The DEM values are in meters above sea level. Note that over this 5 m area, elevation values change only by 0.05 m (5 cm), showing close range photogrammetric methods can detect small elevation changes.
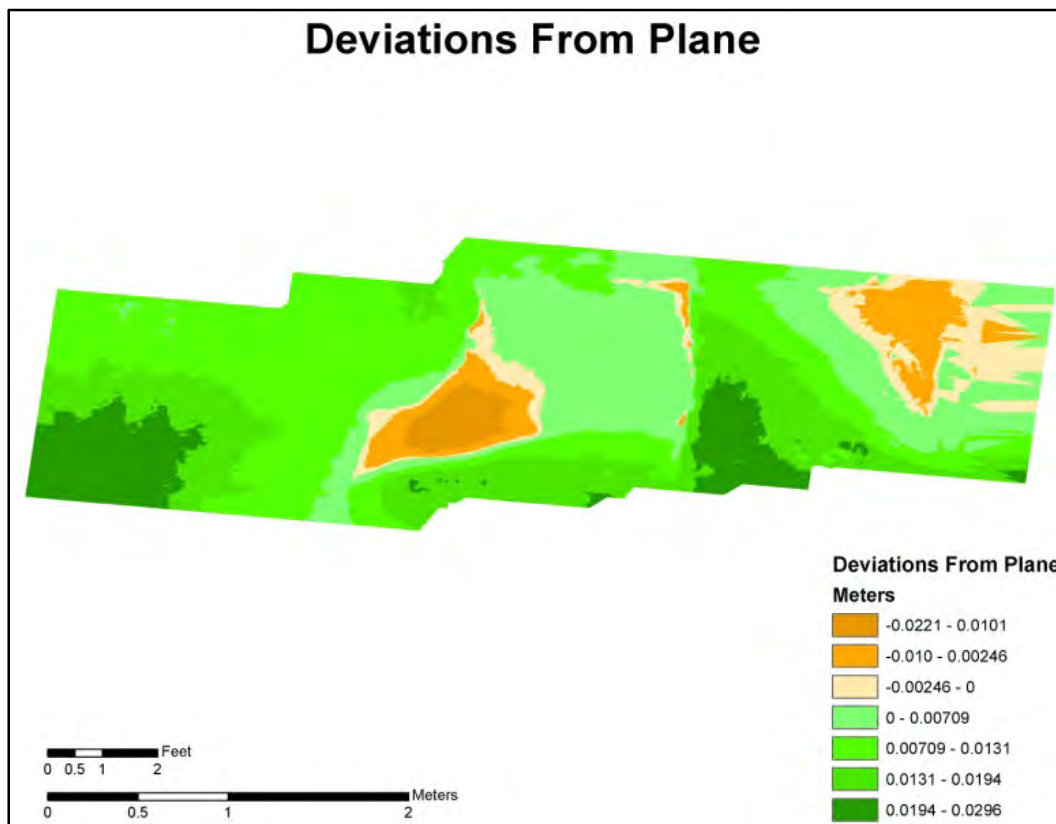
Figure 4-12: The deviations from a plane represent the elevation of a perfectly smooth surface. The values are in meters above and below the plane. The spall that was analyzed is clearly displayed.

4-10
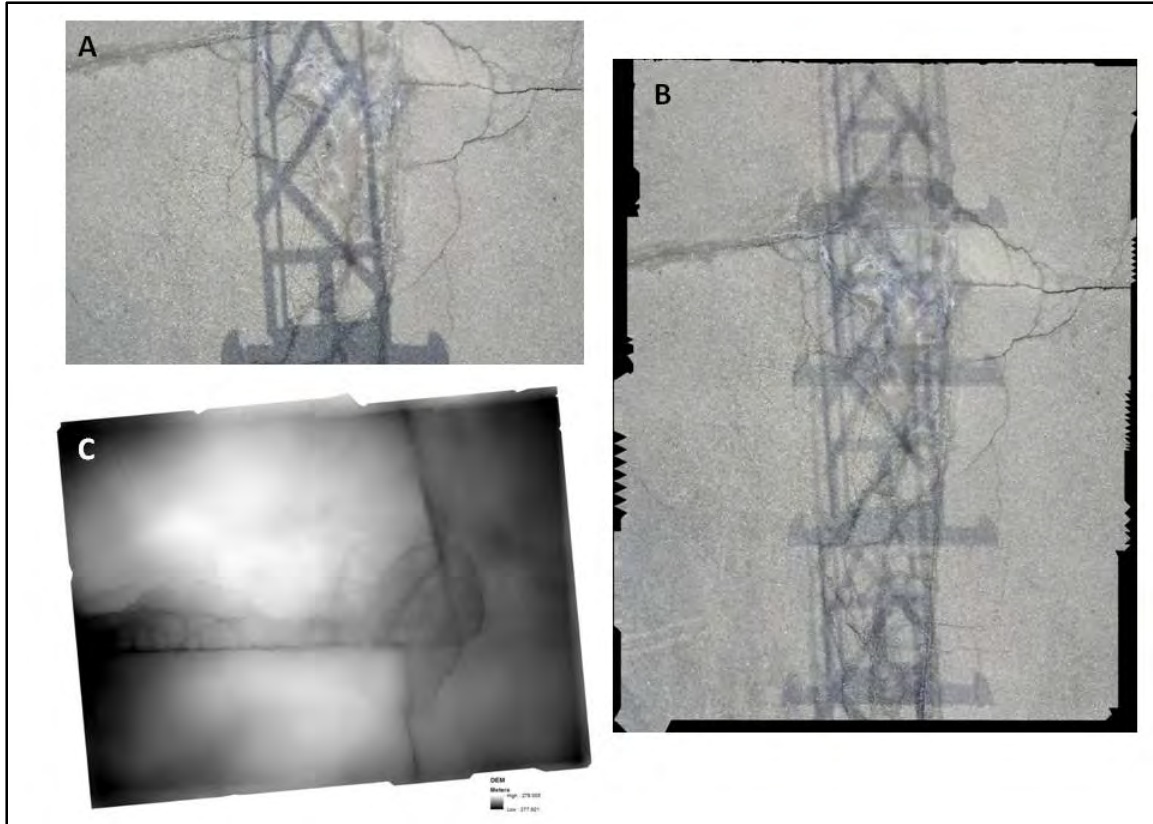
Figure 4-13: Photos captured by 3DOBS contained the shadow from the vehicle mount as shown in A. Despite the shadow PhotoScan was able to align the photos (B) and generate an accurate DEM (C) of the parking lot surface.

Figure 4-14: 3DOBS being transported in the bed of the collection vehicle.

One of the first results generated from 3DOBS imagery was a high resolution image of the entire bridge deck. This image had a resolution of 2 mm and it was made as a composite of all of the photos taken of each of the bridge decks. For Freer and Willow Road bridges (Figure 4-15) there were about 240 photos each and for the Mannsiding Road bridges (Figure 4-16) there were about 190 photos each. This bridge overview was useful as a base layer for all other data and it provided a reference for manually digitizing spall extents and delimitations for comparison with the optical and thermal technologies.
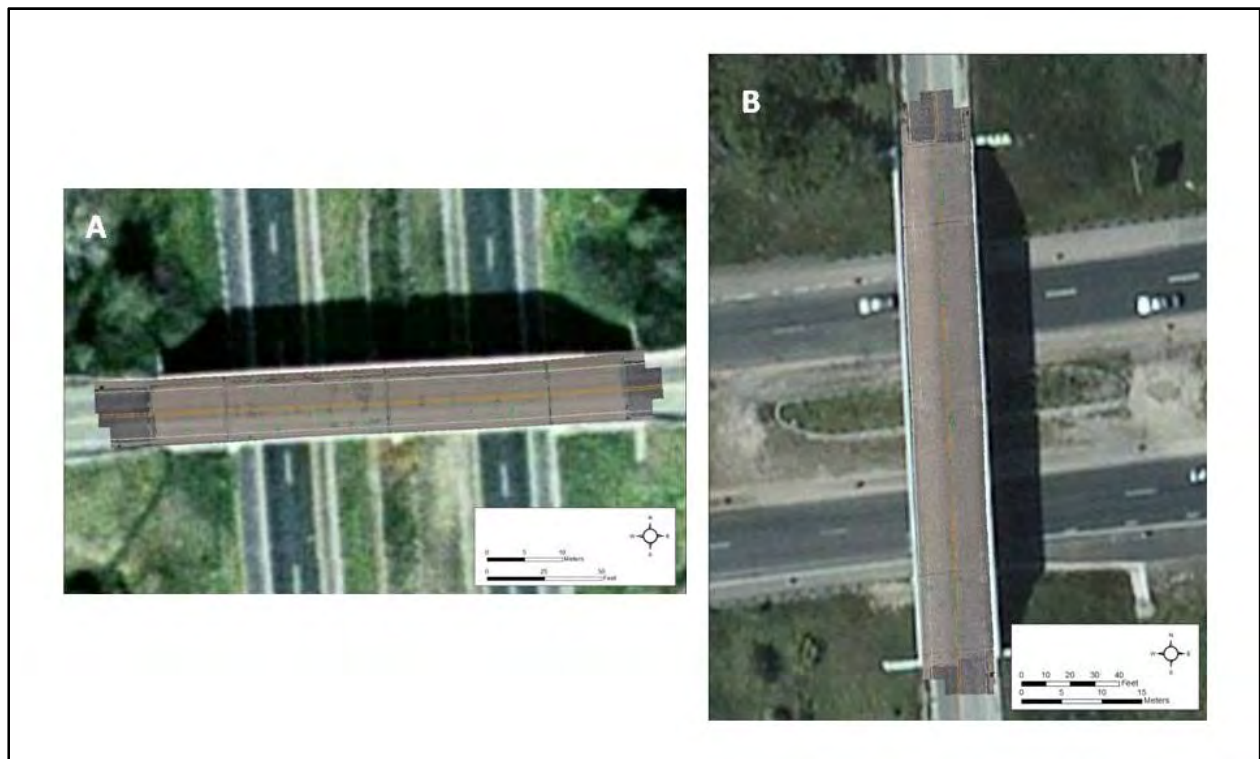
Figure 4-15: Overviews of Willow Road (A) and Freer Road (B) demonstration bridges.

The DEMs produced from PhotoScan (Figure 4-17 and Figure 4-18) had a resolution of 5 mm horizontal and 2 mm vertical. During the study, PhotoScan made several updates to PhotoScan which helped to get better than expected vertical resolution. The DEM was, however, restricted to 5 mm even though it could be produced at the same resolution as the overview image. This was done to reduce the size of the TIF (Tagged Image File) data file generated. Initial results were exported at a horizontal resolution of 1 mm but the file size for one lane was about 1.8 GB in size. The resolution was reduced to 5 mm, which still provided a high resolution product, but the file size for one lane was reduced to 73 MB.
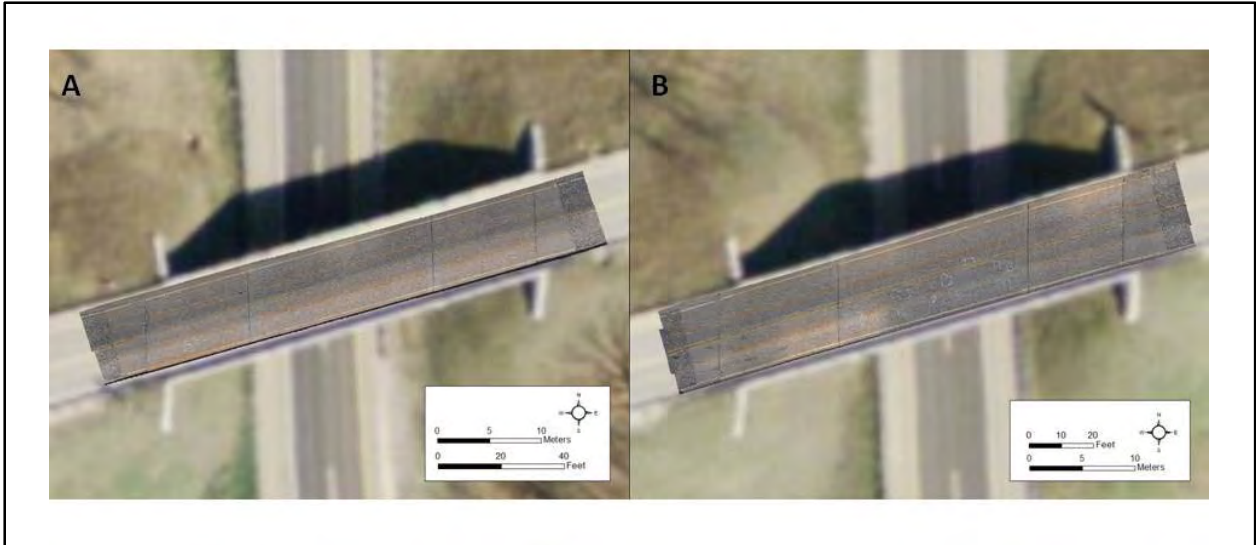
Figure 4-16: Overviews of Mannsiding Road brigde generated from 3DOBS. Image A is the Mannsiding Road bridge SB and B is Mannsiding Road bridge NB.

Figure 4-17: DEMs generated by 3DOBS of Willow Road (A) and Freer Road (B) bridges.

Early analysis of the DEMs proved that area and volume calculations were possible for the spalls from the field demonstration. Figure 4-19 is an example of a spall that was found on Willow Road. Once the spall was located on the DEM, it was manually digitized and the area and

volume calculations were done on the DEM that represented deviations from a plane. The spall detection algorithm would do this procedure with very little user input. This figure shows a spall that was 350 cm^2 in size and 299 cm^3 in volume.
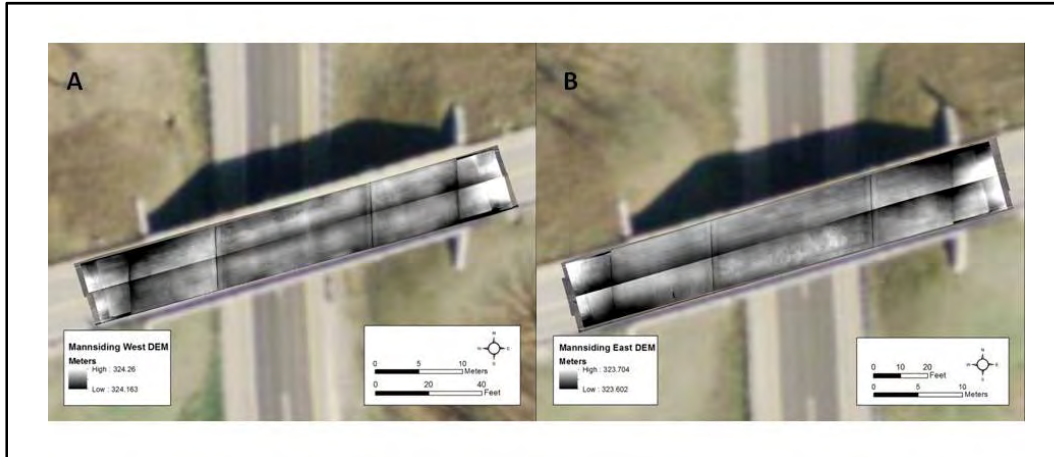
Figure 4-18: 3DOBS generated DEMs of Mannsiding Road West (A) and Mannsiding Road East (B) bridges.
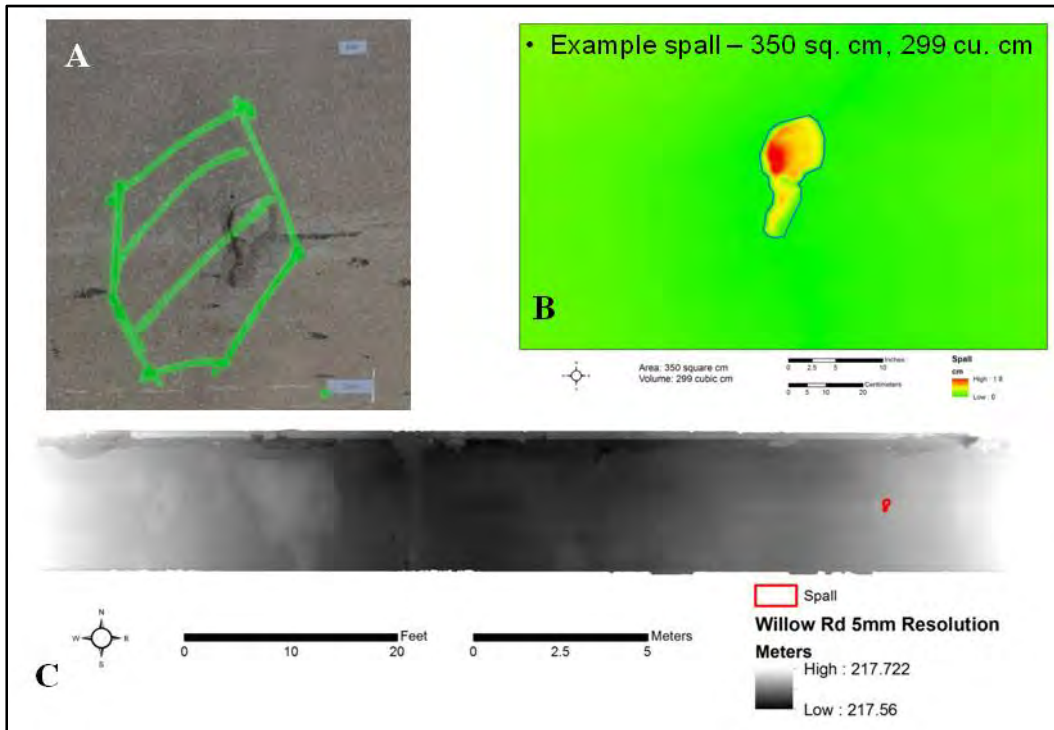
Figure 4-19: An example of manually deriving a spall from 3DOBS data. One of the original photos from 3DOBS is shown in image A and the digitized spall is shown in image B. An overview of the DEM of the lane the spall was found in is displayed in image C.

The results of the 3DOBS algorithm spall analysis are displayed in Table 4-1 along with the hand digitized results derived from the high-resolution images shown in Figure 4-15 and Figure 4-16. Both produced different results, where the 3DOBS algorithm consistently estimated a larger area. This is most likely due to how the 3DOBS algorithm locates spalls. Focal statistics produces standard deviation values for the amount of change in pixel value of a cell and its specified neighborhood. In the case of 3DOBS, a circular neighborhood of a radius of eight cells was used. Raster cells that are not part of a spall but are near one will have the spall cells as part of their neighborhood and therefore have lower standard deviation values. These lower values are similar to shallow or smaller spalls which are closer to the values of the bridge deck itself. This effect is minimized by adjusting the value used for "max bridge pixel value" in the algorithm. Another contributing factor is that the current algorithm simply detects a change in elevation. This becomes an issue when there are non-spall features that cause this change. An example would be areas where the bridge has been patched. These effects could be seen in a comparison of the two methods in Figure 4-20. This could be accounted for by adding in a localized detection of whether the deviation from the plane was down (a spall) or up (a raised area).

Table 4-1: Derived values form the hand digitized and 3DOBS algorithm spalls.

Bridge	Bridge Area (Sq. m)	Digitized Spall Area (Sq. m)	Digitized Percent Spalled	3DOBS Spall Area (Sq. m)	3DOBS Percent Spalled
Freer	565	0.80	0.14	3.80	0.67
Willow	529	18.05	3.41	27.29	5.15
Mannsiding East	368	0.78	0.21	1.73	0.47
Mannsiding West	327	0.32	0.10	1.74	0.53

IRI data was collected from 3DOBS DEMs to get further condition information from this technology. This was done by collecting the pavement's elevation changes on the Freer Road bridge involved using a DEM created using the 3DOBS. This process contained the necessary data to create a zero plane, in which all elevation deviations were based on. The profiling data was then formatted into an ERD file format that was imported into a computer program, The Transtec Group ProVAL, used to view and analyze pavement profiles. ProVAL then graphed the longitudinal profile, which was processed through the two models. The end result is an IRI value that is indicative of a single wheel path across the bridge.

Figure 4-21 and Figure 4-22 demonstrate the longitudinal profiles of two tire tracks for each side of the Freer Road bridge. The bridge deck-joints elevation data were removed from the profiles because they would misrepresent depressions on the bridge. After being processed through the two models, the northbound left tire track data produced an IRI value of 3.59 m/km, while the northbound right tire track data had an IRI value of 4.26 m/km. In addition, the southbound left

tire track produced an IRI value of 4.14 m/km, and the southbound right tire track had an IRI value of 3.71 m/km (see Table 4-2). All of these roughness values were classified as "older pavements" according to the IRI graph. To validate the results, they were compared against what was known about the bridge from site visits and the most recent MDOT inspection reports. Similar to the IRI graph, the Freer Road bridge has an older pavement, has frequent minor depressions, and is a paved surface; the June, 2010 Bridge Safety Inspection report shows a NBI Surface (element 58-A) rating of 6 ("Fair").
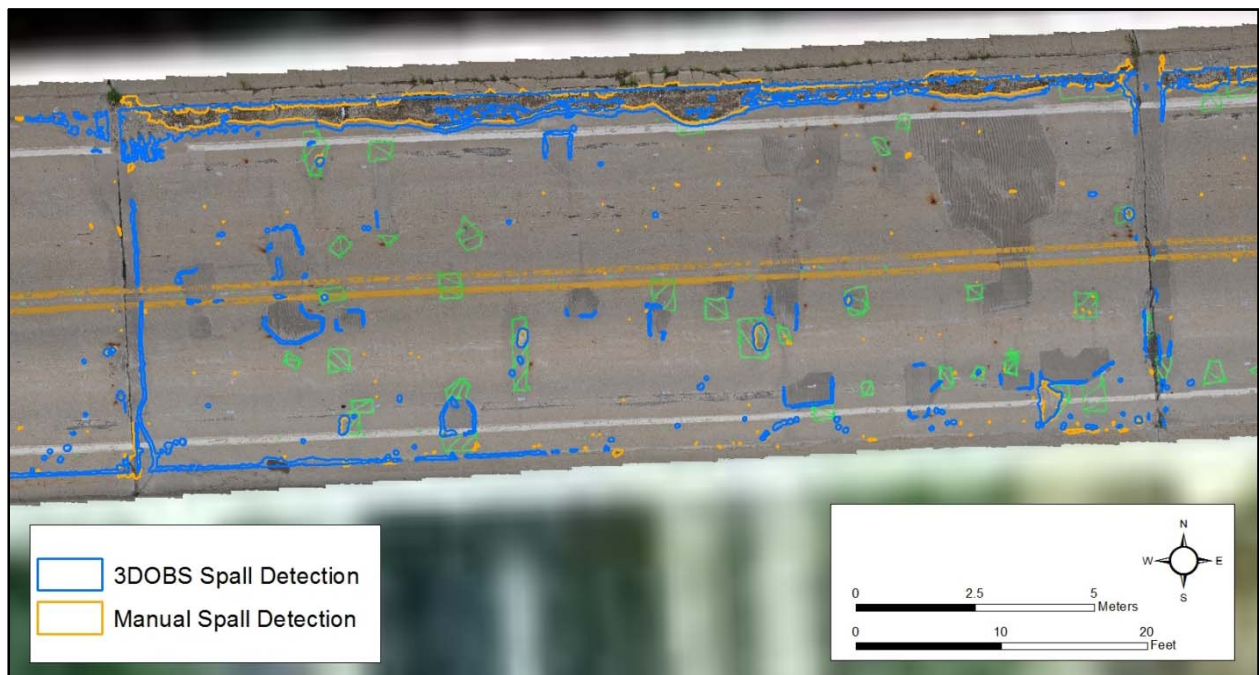
Figure 4-20: A Willow Road bridge comparison of 3DOBS detected spalls (blue polygons) and manual digitizing of spall locations (orange polygons). The green polygons were painted on to the bridge deck by MDOT personnel and represent delaminated areas as detected by the hammer sounding.
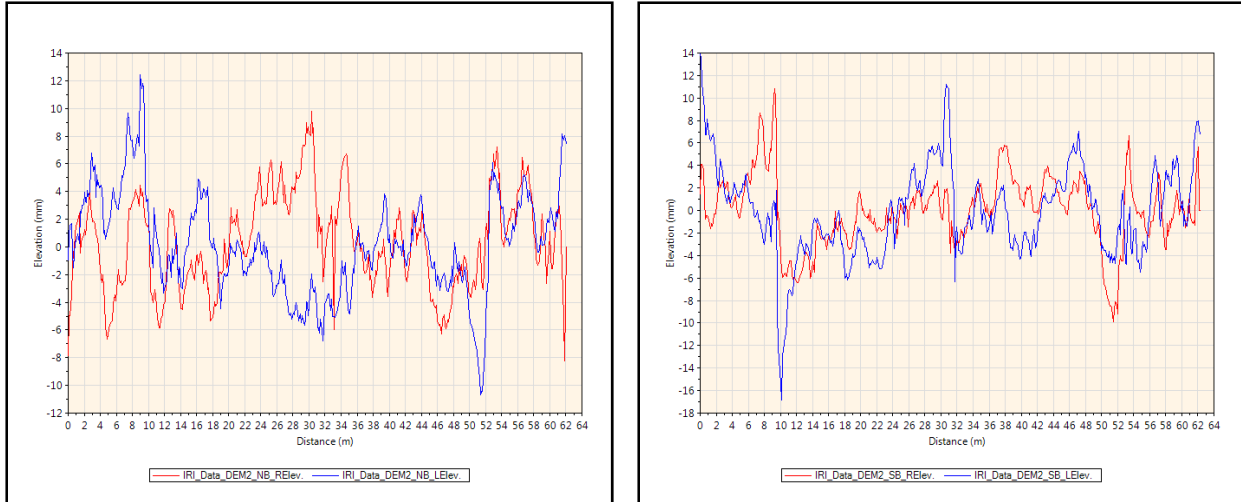
Figure 4-21: The longitudinal profiles of the NB (left) and SB (right) lanes of the Freer Road bridge.

Figure 4-22: A series of photos taken during a bridge underside collect with the 3DOBS system.

Table 4-2: IRI values for each tire track on Freer Road bridge.

IRI File	Profile	IRI (m/km)
IRI_Data_DEM2_NB	LElev.	3.59
IRI_Data_DEM2_NB	Relev	4.26
IRI_Data_DEM2_SB	LElev.	4.14
IRI_Data_DEM2_SB	Relev	3.71

Generating a photo inventory of the underside of a bridge was successful as the photos taken had some overlap and covered the entire lane from underneath. One issue that remains is that there still needs to be more powerful lights. If the conditions are mostly sunny the system is able to collect photos of the bridge underside but this is not the case for cloudy conditions. Figure 4-22 show a series of photos that was collected at Freer Road. These photos could not be used to generate a DEM since they do not contain any markings for PhotoScan to create a coordinate system.

PhotoScan also has issues generating models of the underside of the bridge deck since the beams create a situation where there is significant relief in a short distance. Since the camera was facing straight up it was unable to image the sides of the beams leading to missing or misplaced portions of the bridge underside in the model. To model the underside of bridges and locate spalls effectively, further development would be needed.

4.3.   Implementation and Next Steps

3DOBS, as developed for and deployed during this remote sensing project, was demonstrated to be a low cost, easily deployed and effective at deriving useful metrics of bridge deck condition, such as percent of a bridge decked that is spalled plus volume and area of spalls. The total system cost ($4,320) as currently developed is: $3,500 for PhotoScan Professional, $700 for the D5000 (including default kit lens), $20 for the camera triggering device, and $100 for the vehicle mount. The system cost is also one time purchase cost as the system can be deployed to several bridges after the initial purchase is made. The PhotoScan software can be purchased once and used to analyze multiple sets of 3DOBS bridge imagery.

The primary limitation on the current system is the speed at which data can be collected. This system limitation was due to the frame rate speed of the camera used. The current system used a relatively inexpensive D5000 that had a maximum sustained frame rate of 1 fps (frames per second). At that rate the maximum speed that the vehicle could travel would be about 2 mph. More advanced cameras would be needed to achieve near highway speeds of 40 mph with a rate of 19 fps or highway speeds of 70 mph with a rate of 33 fps.

HD (high definition) video has a frame rate of 24 fps or more depending on the model. This could get 3DOBS to near highway speeds, however, there is a resolution drawback. Full HD (1,920 x 1,080 pixels) is still only equivalent to 2 MP, versus a 12.3 MP photo from the D5000 or a 18 MP photo from the EOS 7D, meaning a significant sacrifice would be made in image quality and resulting resolution of the DEM products.

Another camera that is capable of up to 30 fps is the Red Scarlet <www.red.com/store/scarlet>. This camera, or one similar, would enable 3DOBS to operate a near highway speeds while still providing full frame resolution to generate high resolution DEMs. It is able to do 12 fps at a resolution of 15.4 MP and 30 fps at 8.3 MP. At these frame rates the system would have a max

speed of approximately 40 mph. The only drawback to the system would be that it is more expensive than the D5000. The cost for the Scarlett would be $30,000, which includes the camera body, lens and solid state hard drives. However, at near-highway speeds, this system could be deployed to collect 3D spall data at multiple bridges, helping defray the per-use cost.

5. Deployment of the Bridge Viewer Remote Camera System

The BVRCS is a dual camera system that can be mounted to any vehicle to take a photo inventory of a bridge deck and other bridge elements. This system was developed as a low-cost technology to capture location-tagged photos that can be used as a reference for assessing the current condition and comparing changes over time. Currently bridges are inspected by field crews visiting bridges and taking photos of only major problems that are found during inspections. The purpose of the BVRCS is to capture a location-tagged set of photographs of a bridge so that inspectors can easily and inexpensively review a bridge at a later point and over time as more photo inventories are taken, while working from the office. This is intended to optimize field time and enable review of high-resolution photos of a bridge, especially its deck. This system would allow inspectors to simply drive across each lane of the bridge deck with minimal disruption to traffic while keeping the inspector safe and collecting the photo inventory.

There are companies with dedicated equipment that will deploy their vehicles to take a photo inventory. Their systems take either HD video or use cameras somewhat similar to BVRCS. The main difference however is that the cost per deployment can be expensive. BVRCS costs less than $1,000 to put together from inexpensive components and can be mounted to any vehicle for deployment to multiple bridges without additional cost.

5.1. Methodology

BVRCS, as deployed for this project, consists of two Canon PowerShot SX110 IS cameras, a Garmin GPSMAP 76CSx, and a laptop with Breeze Systems PSRemote commercial camera control software installed and GPS-Photo Link software. PSRemote was loaded onto the laptop to control the cameras while they were mounted to the hood of a car while GPS-Photo Link is used to geo-tag the photos after a collect.

The cameras were mounted to the front of the vehicle and oriented so that the overall field of view would capture an entire lane width (Figure 5-1). The vehicle was driven at a speed of less than 5 mph while the cameras took pictures once every 4 seconds in order to capture the entire bridge using the inexpensive Canon cameras (Figure 5-1). This allowed the team to ensure that the digital photographs were not blurred and the detail of the bridge deck was preserved through in-focus photographs. Lighting conditions at the bridge did not affect the quality of the photos captured; these conditions ranged from sunny to completely overcast skies. This system can be and was set up, deployed, and broken down within 30 minutes during field demonstration at the three bridges.

Figure 5-1: BVRCS being deployed on Freer Road to capture a bridge photo inventory.

Once the photographs were taken, they were processed into a location-tagged, GIS and Google Earth-compatible files, such as KML (Keyhole Markup Language) and shapefiles, using the GPS-Photo Link commercial software program available from GeoSpatial Experts <www.geospatialexperts.com>. GPS-Photo Link has been used for a variety of projects needing to location-tag photos, primarily for natural resources and environmental field work (see Hagen et al. 2007; Kutser et al. 2007; DeLay et al. 2008 for examples), but this is the first known application for creating rapid, low-cost geospatial photo inventories of bridge infrastructure. While Google Street View provides similar digital imagery, transportation agency users have no control over when Google's photos are taken and cannot get updates of critical infrastructure on their own schedule whenever they need to.

The photo locations were displayed within ArcGIS and Google Earth and included hyperlinks to the full-resolution original photos; other geospatial software that can read shapefiles and KML files would also be able to use these data. A "watermarked" version including the GPS coordinates, date, and time showing where and when the photo was taken can also be linked to, as shown in Figure 5-2. The photos can reside on a transportation agency desktop computer, a server for multiple-user access within an office, or made accessible to a web server so they can be accessed in the field or from remote offices.

5.2. Results and Discussion

BVRCS was successfully deployed to all four demonstration bridges. Figure 5-3 and Figure 5-4 show the locations for all of the geo-tagged photos that were taken. Each bridge took less than 10 minutes to collect and set up and break down of the system took less than 30 minutes. This demonstrates that BVRCS is easily deployable with minimal time needed to collect a bridge. The downside to the current system is that it requires a vehicle to operate a speed of about 5 mph; however, higher-end digital cameras can be used to collect at faster speeds.
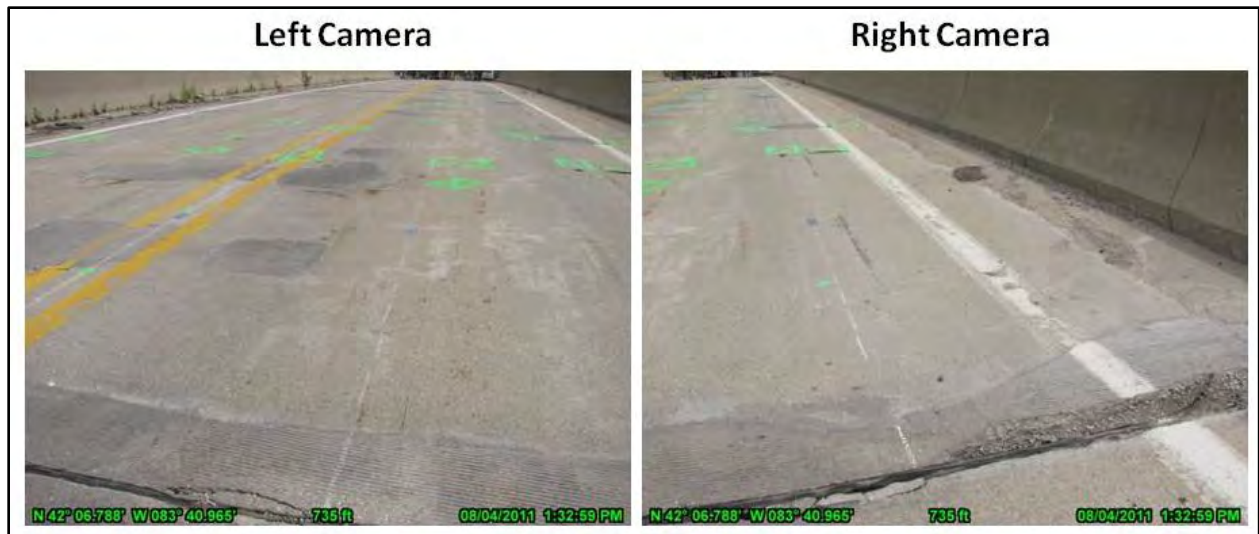
Figure 5-2: Example photos taken BVRCS on Freer Road bridge. These photos show that a full lane width was captured including overlap of the center of the lane. Note the coordinates and other image information recorded into each photographer through processing with GPS-Photo Link.
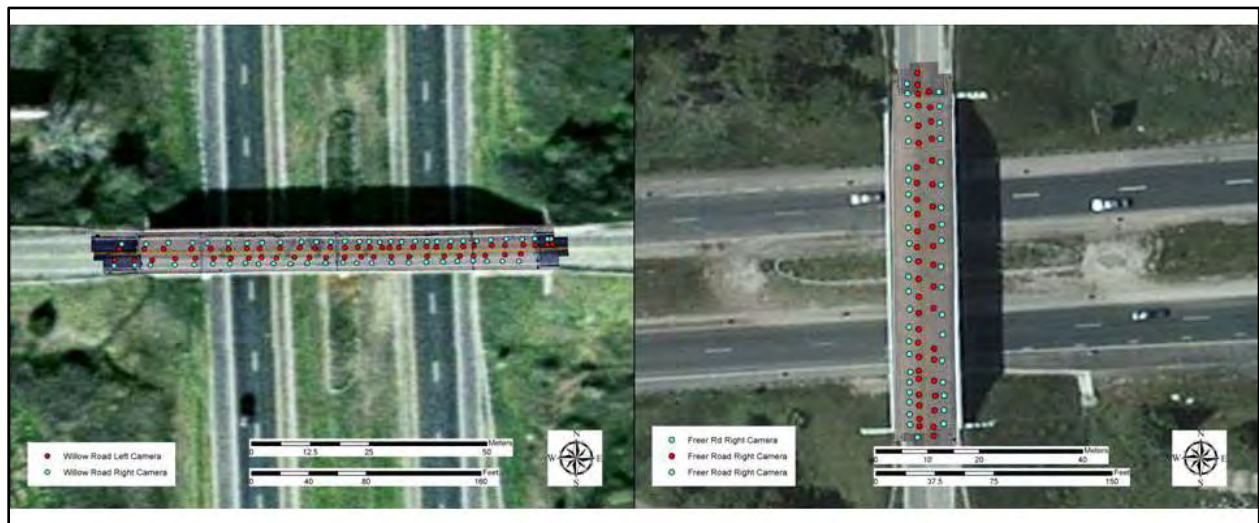
Figure 5-3: BVRCS deployment to Willow (left) and Freer (right) Road Bridges. The points are the locations of where each photo was taken and it is overlaying the bridge overview image created by 3DOBS.

Once the photos were collected they were processed using GPS-Photo Link add location information (geo-tagging) by linking the Garmin GPSMAP 76CSx tracklog to the photos based on the time the photos were taken. This process takes account of any time difference between the GPS time and the camera time by the user having taken a photo of the GPS screen showing the time to the second. This process only took a few minutes per bridge and generated water marked photos (Figure 5-2), a shapefile usable in Esri GIS and compatible software, and a KML file that can be loaded in Google Earth. The shapefile and KML outputs are very useful for displaying the locations of the photos on the bridge as well as helping users easily access at the

watermarked photos with user friendly geospatial environments such as Google Earth. Figure 5-5 shows the BVRCS photos being displayed in Google Earth. There were about 100 photos taken of each bridge and after processing the photos, each bridge used about 58 MB of space. These photos have also been integrated into the project's DSS. The DSS user can click on the photo point and bring a full-resolution picture taken at that location. As geo-tagged photo inventories are taken over time, such as during regular inspections every two years, these can be used to track and understand changes in the bridge deck condition.
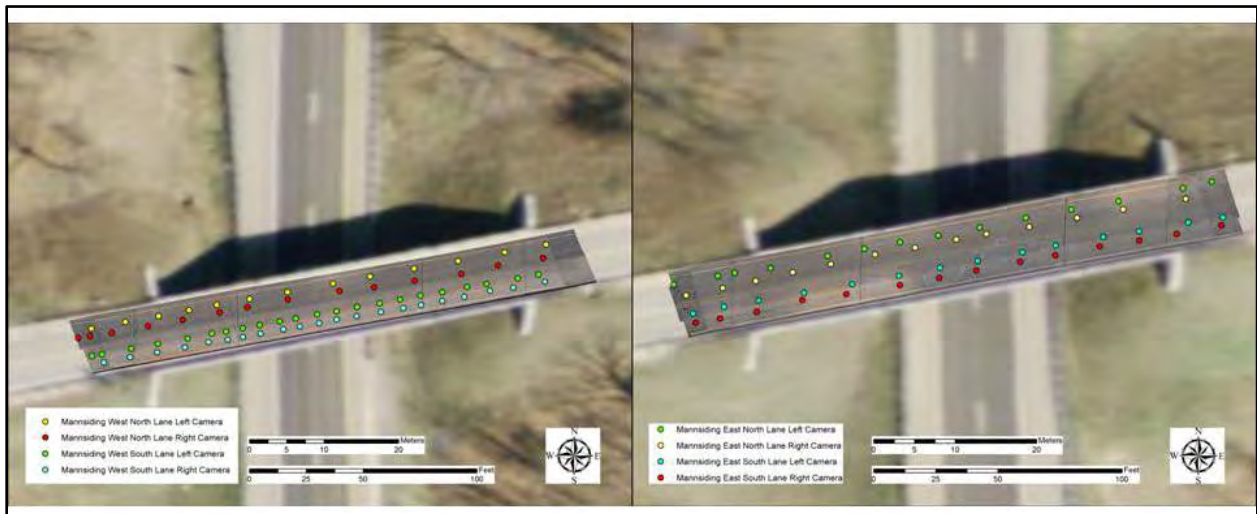
Figure 5-4: BVRCS deployment to Mannsiding Road bridges. Mannsiding East (NB) is on the right and Mannsiding West (SB) is on the left.

5.3. Implementation and Next Steps

The primary benefits of the current version of the BVRCS is that they can be deployed using inexpensive hardware, it can quickly be set up and taken down, taken in 10 minutes or less to collect data, it uses existing commercially-available software for photo processing, and the system creates an easily viewable photo inventory of the condition of a bridge that can be compared to future photos. The photos are location-tagged using GPS and can be accessed and queried using commonly available geospatial software such as ArcGIS and Google Earth. The photo inventory can also be easily loaded into the DSS. The total system cost as currently developed is $1,140, including $500 for two PowerShot SX100 IS cameras, $190 for PSRemote camera control software, and $350 for the GPS-Photo Link software (note that equivalent current cameras bring the total cost to below $1,000). The availability of a typical "Microsoft Windows" computer to process the photos is assumed.

The primary limitations of the system include the data collection speed, the need to assemble a working system from separate parts, and the use of non-high-end GPS. Similar to 3DOBS,

higher-end cameras would enable faster data collection. However, the PSRemote commercial software currently only works with certain cameras and cannot take photos faster than about once every four seconds (with the cost being $95 for the Canon version and $175 for the Nikon version, see <www.breezesys.com>). Ideally, the combined camera hardware, control, and photo processing system would be available from vendors that a transportation agency could contract with for services for field deployment. Taking BVRCS to the level of a commercially available but still inexpensive bundle is an option to make it more accessible to transportation agencies.

Figure 5-5: Example of the location of the digital photographs being displayed in Google Earth; each box contains a hyperlink to a full-resolution view of the photo taken at that location.

In order to take BVRCS to near highway speeds, the cameras would need to be upgraded so that they can acquire photos at a higher frame rate than 1 photo every 4 seconds (0.25 fps). Upgrading the system to use DSLRs instead of point and shoot cameras would be the preferred method. Some higher end cameras, such as the Nikon D700 at a cost (with lens) of about $2,800, are capable of capturing up to 8 fps continuously which would allow the BVRCS near highway speeds (around 40 mph).

6. Image Data Collection GigaPan System

The GigaPan Project <gigapan.com/cms/about-us> is a collaborative effort involving Carnegie Mellon University (CMU), NASA (National Aeronautics and Space Administration), with financial support from Google, with the goal of producing a low-cost hardware and software package to create panoramic images on the gigapixel (GP) scale (Frenkel 2010). As of 2012, GigaPan offers three different pieces of hardware: GigaPan EPIC, GigaPan EPIC 100, and GigaPan EPIC Pro <gigapan.com/cms/shop/store>. Each piece of hardware comes packaged with proprietary stitching software, GigaPan Stitch, which merges multiple digital photos into a single high-resolution image panorama. Other stitching software, such as Adobe Photoshop, can also be used.

Currently, GigaPan systems are being deployed by amateur and professional photographers around the world to capture composite high-resolution images of historical sites, geological formations, cityscapes <gigapan.com/gigapans/48492>, concerts < www.u2.com/gigapixelfancam/110626>, and the flight deck of the space shuttle Discovery <gigapan.com/galleries/8436/gigapans>. One of the first sites for which a GigaPan image was available in Google Earth was the Houghton-Hancock Portage Lake lift-bridge near MTU (Figure 6-1).

The fact that any part of the bridge could be seen at the same high resolution in a single web-accessible image inspired the application of GigaPan for this project (Endsley et al. 2012). Additionally, the MTRI part of the research team had the original GigaPan hardware already available through a previous imaging project. Deploying it as an additional technology to test and demonstrate its usefulness for creating high-resolution bridge images was a relatively simple and inexpensive project extension. The goal was to see if it could be deployed for creating an archival image set of bridge elements (such as fascia) that could be time and location stamped so that transportation agencies could use them to compare change over time for particular bridges.

6.1. Methodology

Prior to deploying the EPIC and the PowerShot SC110 IS, the hardware and software was tested around MTRI office to establish data collection speeds, optimal image processing, and testing for bridge deployment. Test example areas at the MTRI the office including the GIS lab, Intern work area, and an intern's vehicle were photographed. These data collections served two purposes. First the number of images a single set of batteries would take in both the EPIC robot (now $299), and in the PowerShot SX110 IS (which had cost $250). Secondly example data sets were needed to optimize use of the Stitch software. These data collects provided the team with the information that was needed to move forward with the implementation of the hardware and software.
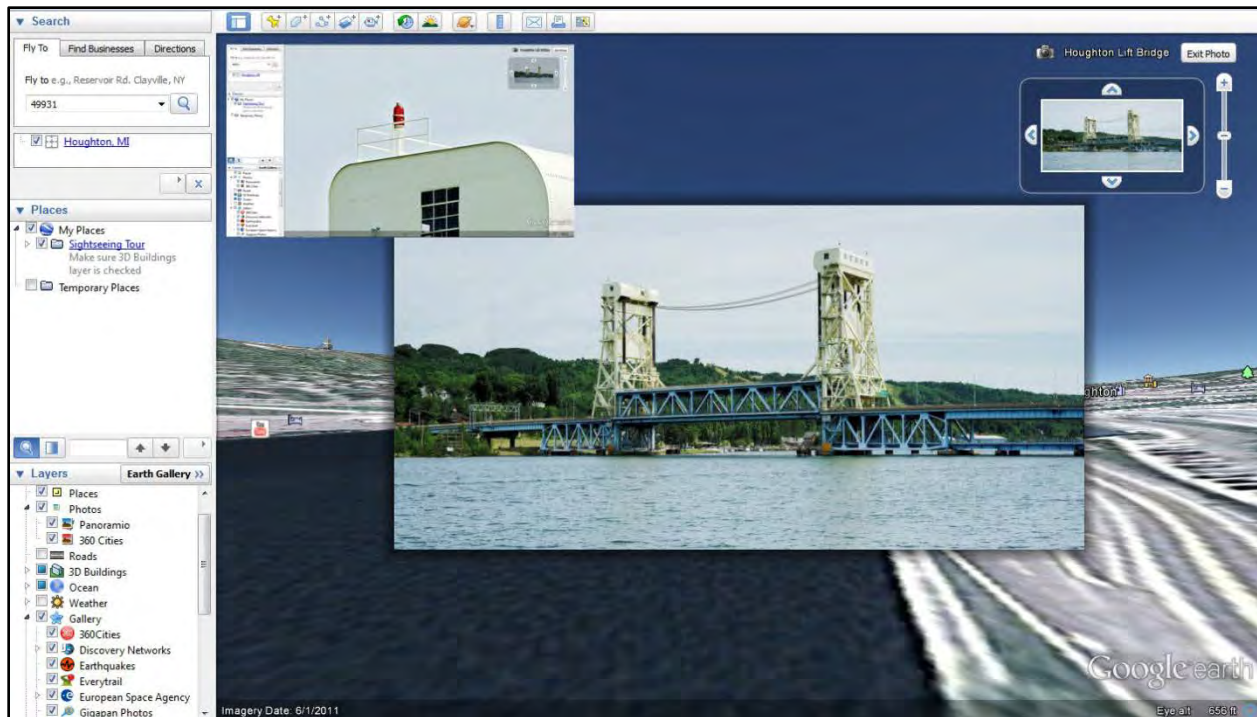
Figure 6-1: Example of GigaPan image for the Portable Lake lift-bridge; the same high resolution is available through the web and Google Earth at all parts of the bridge.

Throughout a series of visits to two of the selected bridge sites optimized collection methods were developed for the field demonstrations. Once data collections had started at actual bridge sites, further benefits of the GigaPan system were realized for assessing the condition of the bridges' superstructure. Small spalls on the bridge fascia could be magnified; spalls on the underside of bridge decks can be recorded in detail (Figure 6-2). Areas of leaching were readily visible in the images, as were fine cracks. This was the needed proof of concept. Over time, the GigaPan technology can be easily be used to take a yearly inventory of the condition of bridges to monitor changes over time, including some episodic events such as high-load hits.

The Stitch software is used to merge the multiple digital photographs together into a single GP, 1,000 megapixel (MP) or more, image and is straightforward to use. The commercial software is included when purchasing the GigaPan hardware. The images from a single collect are stored in one file on a network or local drive, and the user imports all of the images for one GigaPan collect. The user chooses whether the data was collected in rows or columns, and then adjust the number of rows/columns until the image is visible on the screen. The user clicks on the "Stitch" control and the Stitch software then automatically merges the images together into the single gigapixel image.

The biggest issue to day-to-day usage of the GigaPan hardware is collection times, and the fact that it cannot yet be done from a mobile platform. The user must set up the robot and camera on a tripod, configure the system, and wait for it to finish. If a point-and-shoot camera is used, this

can take between 30 minutes and three hours. A DSLR camera combined with the EPIC Pro ($895) greatly reduces the time for collects, so large panoramas could be collected in a more timely manner (about half the time, typically).
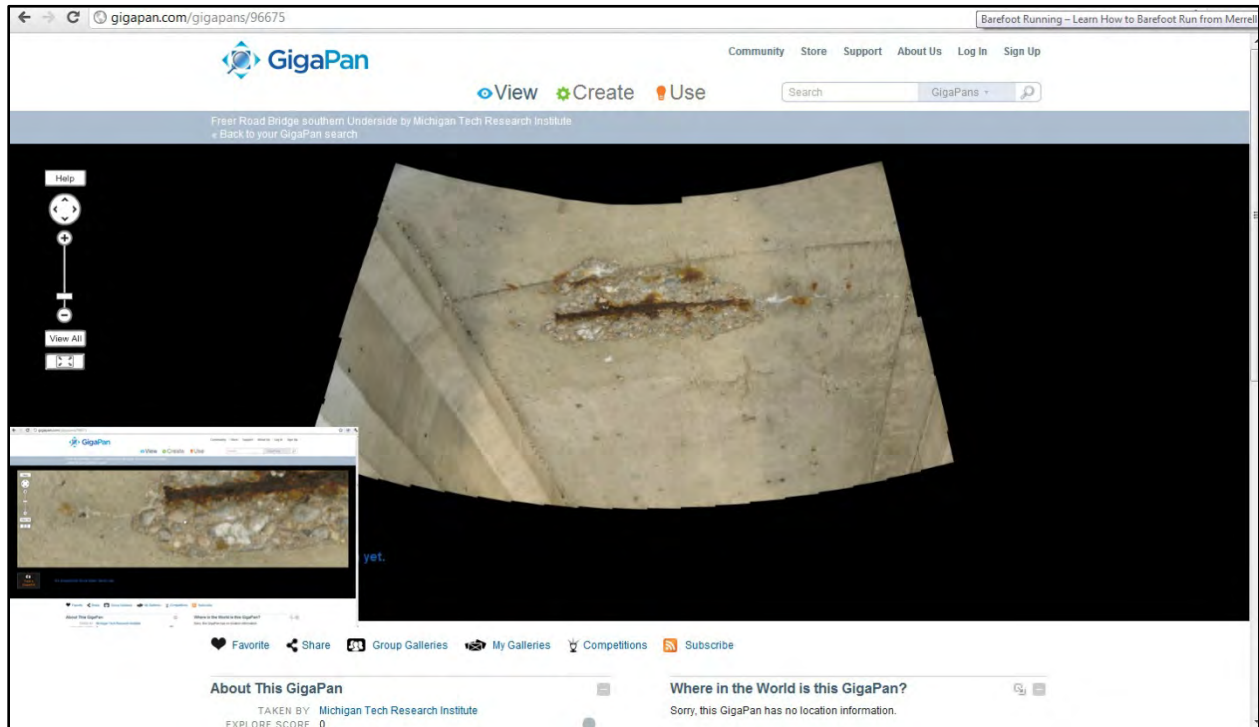
Figure 6-2: Example GigaPan image collected to test imaging of areas of deterioration on the underside of a Michigan bridge.

6.2.   Results and Discussion

The project team collected a series of GP images of the fascia, underside, and details of the four demonstration bridges using the GigaPan hardware (examples are shown in Figure 6-3 and Figure 6-4). These GigaPan images were very useful when the project team needed ground-truth details to compare the output from the LiDAR and 3DOBS systems and also provided examples of how the results could be useful to transportation agencies for creating high-resolution inventories of bridge infrastructure. The GigaPan images proved useful when something did not make sense with the data, and allowed for interpretation of a feature without having to send people back into the field to collect more ground-truth photography.
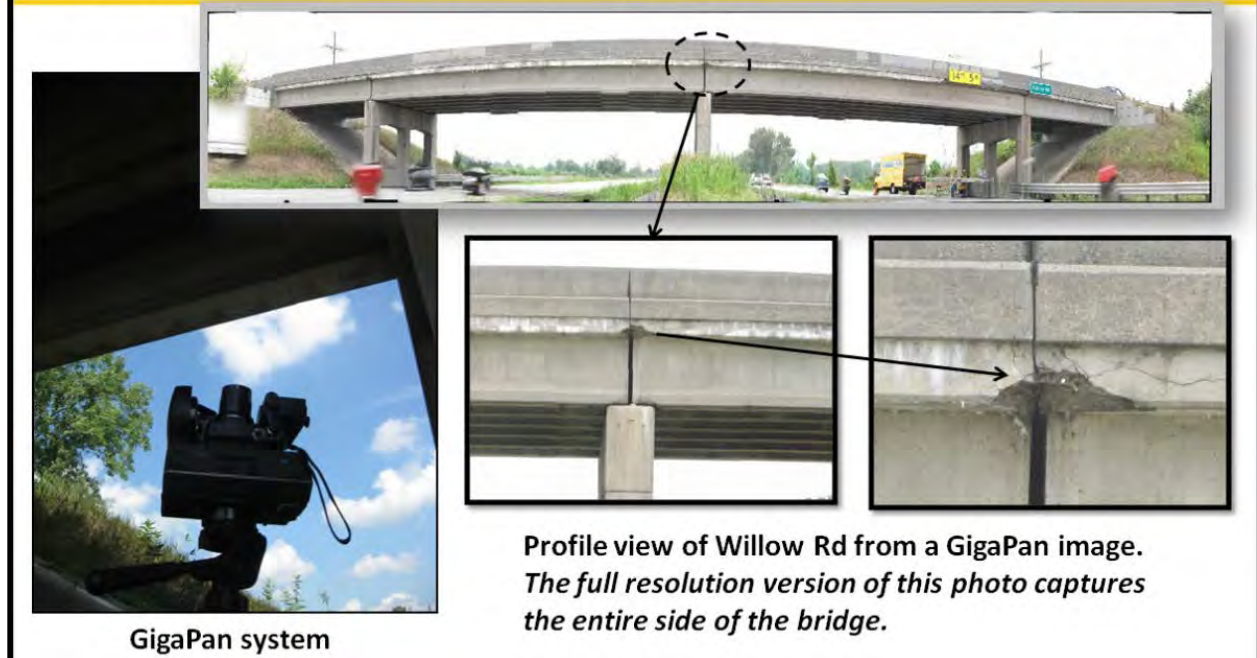
Figure 6-3: An example of the GigaPan image of a bridge fascia at the Willow Road bridge. The image is available online at <gigapan.com/gigapans/96672> where areas can be zoomed in on easily by end users. The EPIC robotic photo-taking hardware can be seen on the lower left.
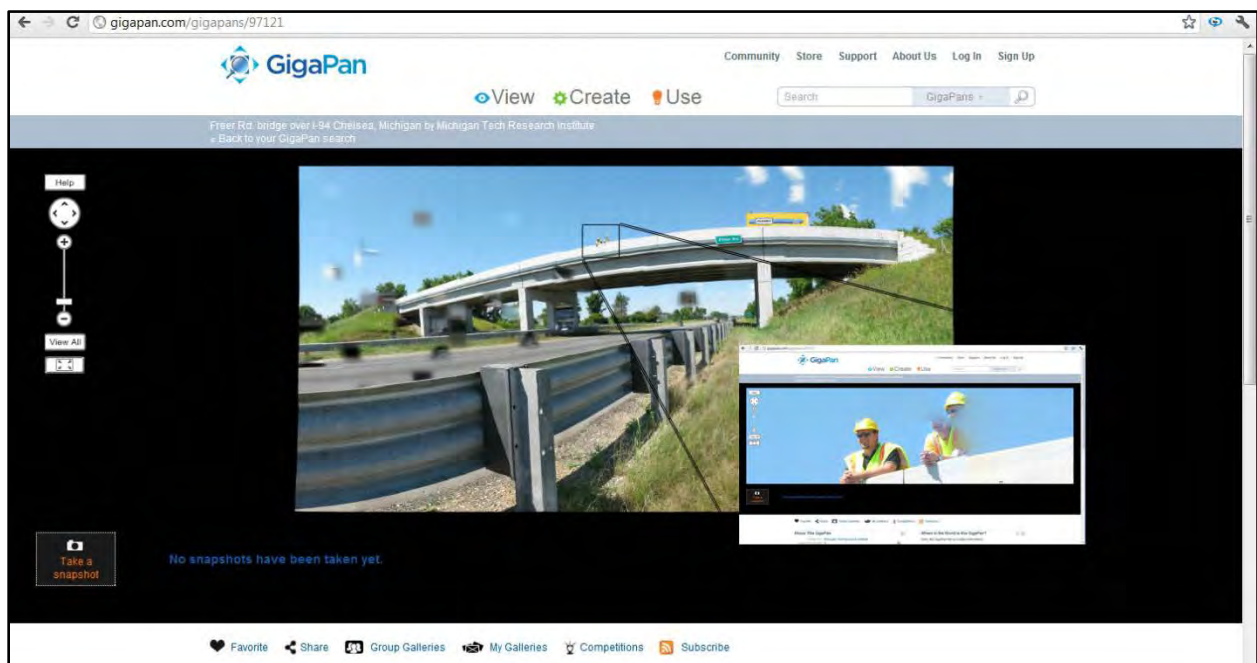
Figure 6-4: An example GigaPan image of a fascia from the Freer Road bridge. The bridge data collectors are shown as an example of the level of detail available when zooming in. The image is available at <gigapan.com/gigapans/97121>.

The testing revealed some limitations with the system as deployed. These were related to the camera being used, the version of Stitch that was available, and some of the locations of our data collects. An inexpensive point and shoot camera that worked with the older EPIC hardware was used that only collected one image every three seconds. While this is reasonable for photographing relatively small areas, it can be ineffective for large areas such as an entire bridge fascia, where there were collects that contained over 3,000 images. As mentioned, the $895 EPIC Pro with a DSLR camera <gigapan.com/cms/shop/epic-pro> is faster when paired with a DSLR camera (such as the $1,300 Canon EOS Rebel T3i).

Because of the speed of collection, changing light and traffic conditions washed out or obscured some of the features of the bridge. Another issue encountered was that the Stitch software version that was out when the image panoramas were being assembled did not include any vignette correction, and the early version of the hardware that was used did not have a very accurate stepper motor which caused shifts in columns of images that could not be corrected in post-processing. The vignette correction issue made taking GigaPan panoramas of the underside of bridge more challenging than it should have been. Newer software and newer GigaPan hardware do not experience these issues.

The project team demonstrated the integration of the GigaPan images with the DSS. The image panoramas have been made available through the DSS as point features tied to the locations where the photographs were taken from; the DSS then links directly to the images at <gigapan.com> (Figure 6-5). One advantage of the GigaPan system is that the end user (such as a transportation agency) does not have to host the composite panorama images – the GigaPan website hosts it instead at no cost. This means that transportation agencies do not have to manage the images as they are accessed by users, such as bridge managers or the general public.

The main benefits of using the GigaPan system for creating high-resolution panorama bridge inventory photos can be summarized as:

- Ultra-high resolution composite panorama images can easily be created.
- Periodic collections would allow for tracking of bridge condition changes and comparisons to other data.
- Individual setups are relatively inexpensive, and an array of cameras and GigaPan robotic hardware would allow for simultaneous, complete collects.
- The images can be very useful when compared to other remote sensing data such as LiDAR and 3DOBS.

Areas for improvement are:

- Slow collection times with most-inexpensive model (EPIC), up to 3 hours for a bridge fascia, for example. Collection times can be much faster with a DSLR and the EPIC Pro (estimated at 90 minutes or less for a bridge fascia).

- GigaPan data cannot be collected from a moving vehicle; the system has to be operated from a fixed location during the photograph collection.
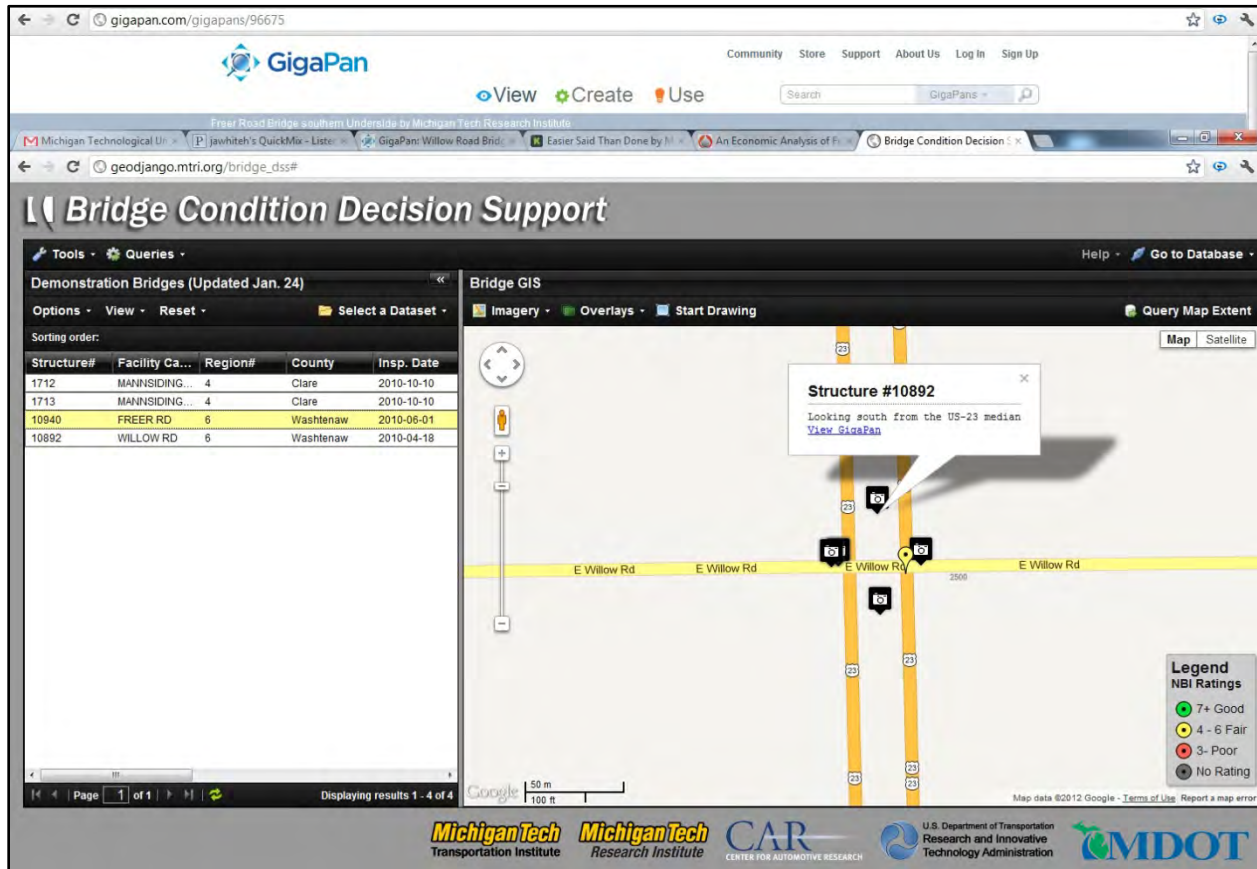
Figure 6-5: An example of the Willow Road bridge GigaPan images being made available through the DSS. The user clicks on the camera icon and is taken to the bridge panorama hosted at <gigapan.com>.

6.3.   Implementation and Next Steps

Implementation of this technology would require investing in one or more high-speed DSLRs (ranging from the $1,300 EOS Rebel T3i to higher-end and faster D700 with lens at $6,112), and a similar number EPIC Pro ($895 per robotic control system). Two systems, for example, would enable both fascias to be collected. The challenge with this technology is that it requires an operator to stop and set up at each bridge.

While the current version of the team's deployed GigaPan can be replicated for under $1,000 a rapidly deployable system that will allow for fast collects of the entire bridge will cost approximately $2,100-$7,000 per camera setup. The medium-range $2,100 system (EOS Rebel T3i plus EPIC Pro) has the potential to realistically be deployed by a transportation agency, with the results easily integrated into the DSS.

7.   Evaluation of Surface Defect Detection using Light Detection and Ranging

LiDAR is an optical remote sensing technology that determines distance to a target by measuring the time required for LASER (Light Amplification by Stimulated Emission of Radiation) pulses to travel to a target and return to the sensor (Vosselman and Maas 2010). A single LASER pulse transmitted and received can only determine the distance and angle from the sensor to the target. To define an object in three-dimensional space, the LiDAR scanner repeats the scanning process thousands of times per second. From the distance and the relative orientation of the LASER pulse, the XYZ coordinates (locations in a 3D environment) associated with each measured pulse can be determined in relative space (Chu 2011). The dataset containing the XYZ coordinates and associated intensity values for these millions of sensed data points is commonly referred to as a point cloud. From this point cloud, a user can access and visually display the collected data in virtual space. Software can be used to manipulate and extract features of interest present within the data. Compared to traditional surveying equipment, a LiDAR system can collect millions of data points in a single scan of a target, allowing a detailed 3D model of the scanned surface to be created.

LiDAR is generally collected using one of three techniques depending on project requirements: airborne, terrestrial and mobile. The fundamental data scanning principles are the same, measuring the distance between the sensor and a target using LASERs. The changes come in the hardware and software packages required to collect the data in a format appropriate for the desired use.

Airborne LiDAR uses a sensor mounted on or in an aircraft (helicopter or fixed wing) that is designed to measure the distance between the aircraft and surface with a high degree of precision. The dataset generated by airborne LiDAR is often used to generate digital terrain or digital surface models, which describe the terrain over which the sensor is flown (Figure 7-1). Generally the datasets collected by airborne sensors cover a relatively large area at moderate (0.5-5 m) post spacing (the average distance between LiDAR pulses on the surface). Large areas can be scanned relatively quickly, but the point of view of an airborne scanner is straight down – the sides of structures are generally not part of the dataset.

Terrestrial LiDAR uses a scanner unit, often mounted on a tripod, to scan a target area from a single vantage point at a time (Figure 7-2). When the scan is complete the unit is moved to the next pre-determined location until the project is complete. Scans are then registered to align the data using survey-grade GPS data (<10 cm accuracy) collected as part of the LiDAR effort, and then the scans are saved as a 3D point cloud which can be viewed using software capable of viewing LiDAR data. The multiple setups required to scan a structure or area take time but all sides of a structure such as a bridge or building can be represented in high definition.
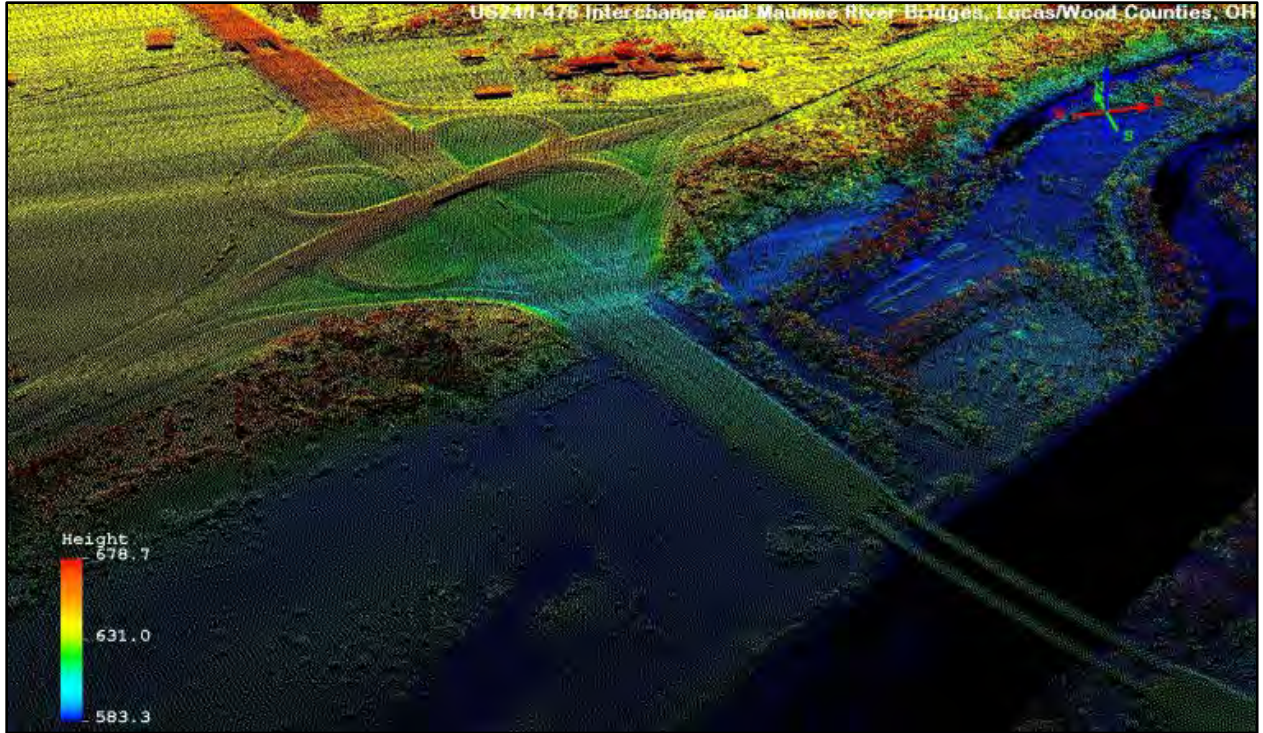
Figure 7-1: Airborne LiDAR point cloud of the US-24 and US-23/I-475 interchange and Maumee River bridges, Maumee, Ohio. Average post spacing during data collection was about 2 m.

Figure 7-2: An example terrestrial LiDAR scanner used to collect 3D data of the project's demonstration bridges. The unit was deployed by the project's Michigan DOT partners.

Mobile LiDAR is an adaptation of airborne LiDAR and terrestrial LiDAR hardware and software that allows LiDAR scanners to be mounted on a van or boat and collect data while the sensor is

in motion over a road, railway or waterway (Figure 7-3). Some of the advantages of using mobile LiDAR for data collection are faster data collection, data can be collected at off-hours, improved safety for survey crews and a reduced necessity for lane closures which minimizes the impact of data collection on traffic.

Figure 7-3: SSI Surveying Solutions Mobile LiDAR (MoLi) truck and LiDAR scan of the Mackinac Bridge and toll plaza.

Each acquisition method has strengths and weaknesses that should be considered when planning the data collection mission. Size of the area to be scanned, spatial resolution of the scanner, point cloud density required, wavelength of the LASER, and the number of setups required to scan the target are among the factors that must be considered when planning a data collect and selecting a scanner /acquisition platform (Park et al. 2007). When planning a data collect, it can extend the value of the data when users such as transportation agencies keep in mind other potential uses/users of the data that is collected, if budgets enable this. Small adjustments to the data collection methodology can make the data usable for multiple projects, increasing the value of the collected data to transportation agencies.

LiDAR is an active remote sensing technology, meaning that no other illumination source (such as the sun) is required. LiDAR data can be collected during off-hours – mid-day, evening or night based on traffic, weather or other project specific considerations. LiDAR works by illuminating a target with a LASER pulse and measuring the amount of time it takes for the pulse to return to the sensor to determine the distance to the target. This measurement technique is known as time-of-flight. LASER rangefinders use the same method of measurement, but rather than making a single distance measurement, terrestrial LiDAR scanners utilize spinning mirrors and a rotating base to collect millions of measurements over a scene (CFLHA 2011). LiDAR scanners generally use two techniques used to measure distance. Time-of-flight (TOF), discussed

briefly above is one, and phase shift, where a continuous sinusoidally modulated LASER beam is transmitted from the scanner is the other (Flood 2001). The distance to the target is calculated by comparing the phase of the returned pulse with the transmitted pulse <www.rp-photonics.com/phase_shift_method_for_distance_measurements.html> and <www.rp-photonics.com/time_of_flight_measurements.html>. The Leica ScanStation C10 and Riegl LMS-Z210ii LiDAR scanners deployed in this study are TOF sensors.

TOF LiDAR scanners measure the time it takes for a LASER pulse to travel to and from the target. A simple calculation is then automatically performed within the data acquisition and control system to determine the object's distance from the receiver. The calculation for determination of the travel distance of a pulse is shown in Equation 7-1.

$$Distance = \frac{(Speed\ of\ Light) \times (Time\ of\ Flight)}{2}$$

Equation 7-1

TOF scanners have multiple modulation frequencies that are utilized to increase the measurement accuracy. Additionally, TOF scanners can be used to measure different data sets bounded by the return time of the pulse. This feature is primarily used in forestry applications allowing for the generation of both a canopy profile with the "first return" and a ground surface profile with the "last return" (Reutebuch et al. 2005).

In phase-shift units, a continuous LASER beam with sinusoidally modulated optical power is projected from the transmitter and reflected off the suspect object. The reflected radiation wave is then sensed by the receiver and compared to the original emitted radiation to determine the present phase shift within the acquired data. Once the phase shift is determined, the TOF is then automatically calculated using Equation 7-2.

$$Time\ of\ Flight = \frac{(Phase\ Shift)}{2\pi \times (Modulation\ Frequency)}$$

Equation 7-2

The distance to the target is then calculated by substituting the determined TOF from Equation 7-2 into Equation 7-1.

TOF sensors are often used for longer range exterior survey and civil engineering applications such as roadway/bridge as-built surveys and mobile scanning applications. The working range of TOF sensors can extend to more than 250 m, depending on the requirements of the data collection. Phase based sensors have a working range of around 80 m and are frequently used for

as-built surveys of refineries/manufacturing plants and interior architectural spaces where distances to be measured are shorter.

Data collection using LiDAR requires an unobstructed path between the scanner and the target. When a LASER pulse reaches an opaque object (whether it is the desired target or not), some of the pulse is reflected back to the sensor. Nothing behind the object is 'visible' to the sensor. The line of sight nature of LiDAR highlights a potential issue - if the target has many faces, "shadows" or "blind spots" in the instrument's FOV (field-of-view) can occur. The line-of-sight issue can be resolved by repositioning the device to allow the shadowed surfaces of the complex object to be revealed. By combining the multiple point clouds collected from each scan a full three-dimensional rendering of the object after the multiple collection points are fused together can be created.

LiDAR returns usually include multiple attributes which can include RGB (red, green, and blue) and intensity (brightness) values in addition to XYZ location information. The MDOT LiDAR data processed here contain 8 bit or 256 levels of intensity (relative reflectivity) information which is useful when interpreting the elevation data. Information about the relative reflectivity of the bridge deck can provide an image similar to a black-and-white photograph of the study area.

7.1. Laboratory Testing, Proof of Concept, Software Description, and Field Deployment

LiDAR scans of the study areas were performed by an MDOT LiDAR crew during the field campaigns in August 2011 at the Freer Road, Willow Road, and the two Mannsiding Road bridges (Figure 7-4, left image). Twenty scanner setups were performed at the Freer Road site, eighteen setups were performed at Willow Road, and twelve setups each were performed for Mannsiding Road over NB (eastern lanes) and SB (western lanes) lanes of US-127. A ScanStation C10 terrestrial scanner owned by MDOT was used by the survey crew to collect LiDAR data for this study. Scanner setup locations were selected to provide the best possible coverage of the bridge structure with the fewest shadowed areas. Retroreflectors used by the survey crew to register the scans to each other were placed around the bridges. The location of each retroreflector and scan site was recorded using high resolution, survey-grade Leica GPS tied to the State of Michigan CORS (Continuously Operating Reference Station) network (for more information on CORS, see Snay and Soler 2008). Field sketches were made by the survey crew that documents the relative location of the retro-reflectors and scanner setups to each bridge (Figure 7-5). The sketches also contain information about the scanner settings at each scan setup. The LiDAR scans acquired from setups at each study site were merged together into a single registered and geo-referenced point cloud by the MDOT survey crew using Leica Cyclone software. MDOT provided the LiDAR data for each bridge to MTRI as a single registered, geo-

referenced point cloud in the industry-standard American Society for Photogrammetry and Remote Sensing (ASPRS) LAS (LASER) 1.2 format.

Figure 7-4: Typical terrestrial LiDAR units; MDOT's ScanStation C10 and MTU's Riegl LMS-Z210ii.

Some of the software packages considered for LiDAR data processing include Bentley MicroStation with the Certainty 3D TopoDOT add-on, Applied Imagery Quick Terrain Modeler, and the University of North Carolina at Charlotte (UNC Charlotte) Light Detection and Ranging-based Bridge Evaluation (LiBE) surface damage detection algorithm were a few of the promising post-processing software packages considered. Ultimately, LiDAR data processing was completed using ArcGIS, MicroStation with TopoDOT and Quick Terrain Modeler as the most time-efficient data processing method. The point cloud from each study site was cropped to the area of interest by MDOT, reducing the file size and eliminating data outside the study area (Figure 7-6 shows an example). Attributes in the LiDAR data include return intensity and elevation. The project team's staff further subset the data in order to analyze only the bridge deck surface (Figure 7-7 and Figure 7-8 show subsetted examples).
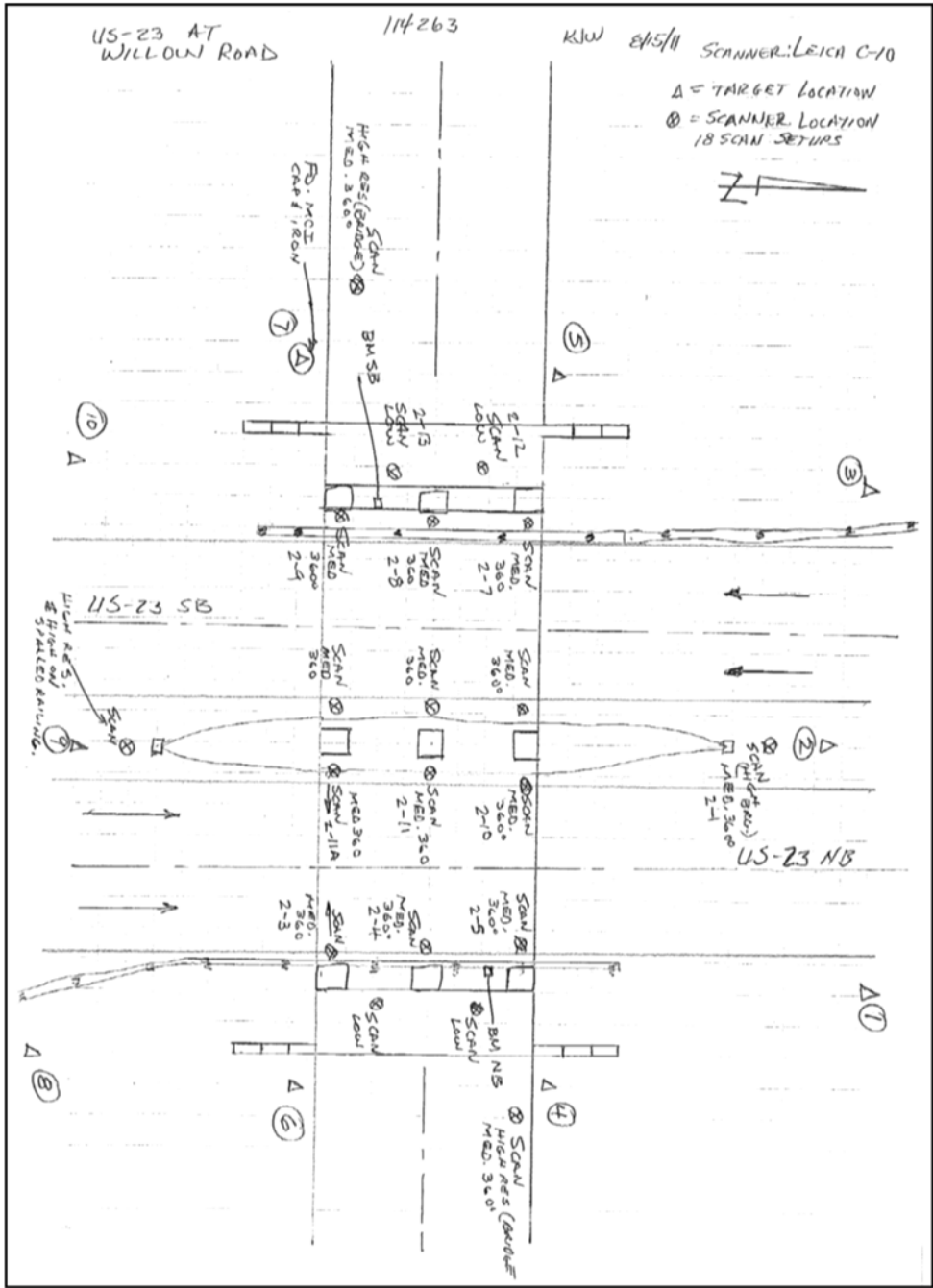
Figure 7-5: An example field sketch for the LiDAR data collection done by the MDOT survey crew at the Willow Road bridge. The sketch documents the site configuration, scan locations, location of retro-reflectors and bench marks and the resolution of the scans along with other information.
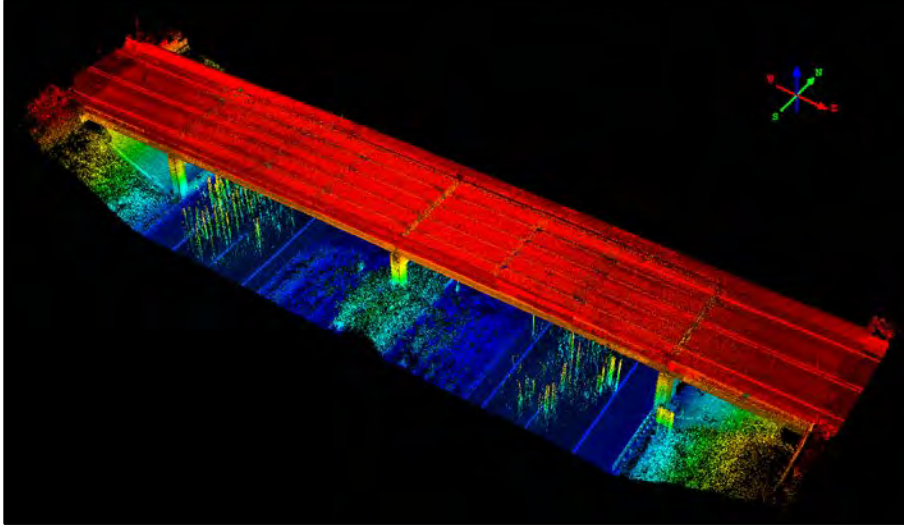
Figure 7-6: An example of geo-registered, geo-referenced LiDAR point cloud of the Willow Road as collected by MDOT. Point elevation (color) and intensity are displayed. This LiDAR point cloud contains more than 186 million points. Quick Terrain Modeler software was used to generate the point clouds and DEMs.
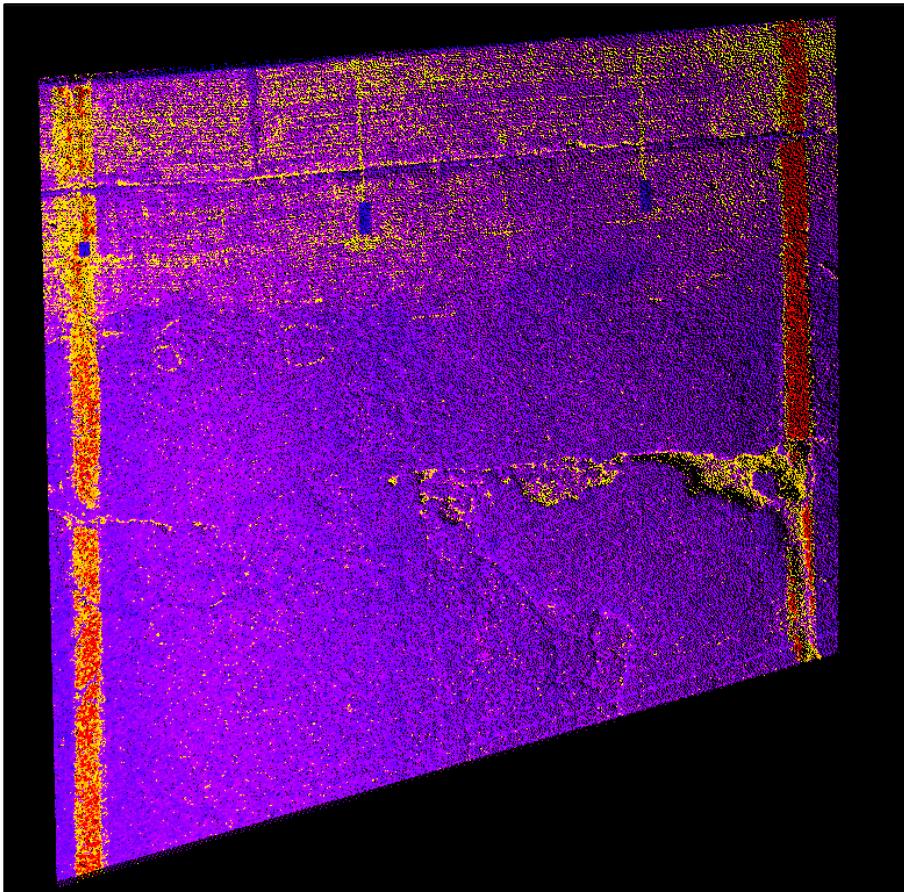
Figure 7-7: An example of LiDAR data displayed in TopoDOT of a Willow Road bridge subset deck extraction, color intensity display.
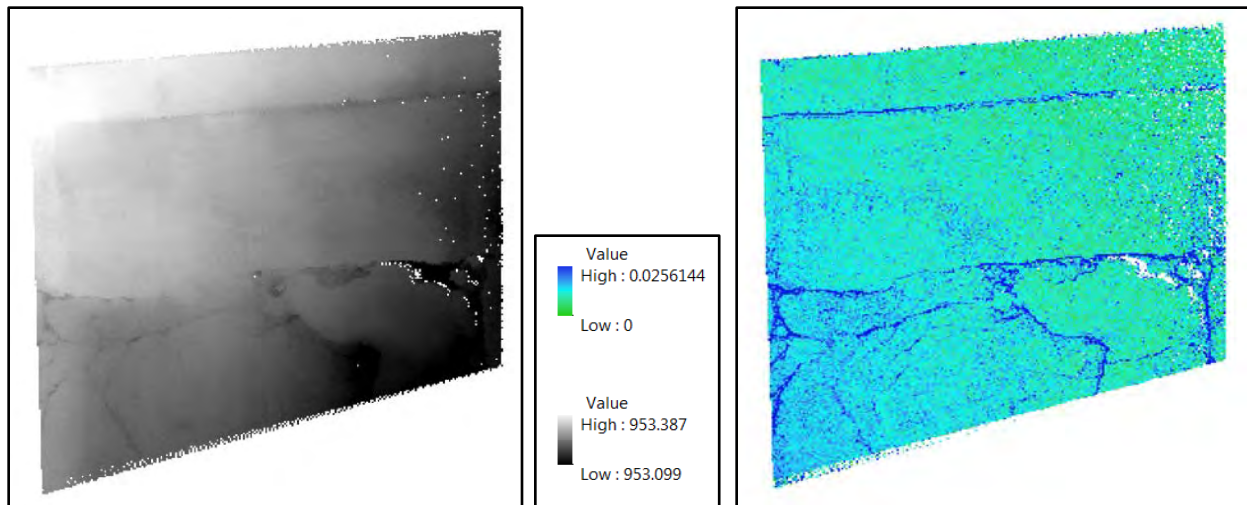
Figure 7-8: ArcGIS ArcMap Willow Road bridge subset deck DEM displaying point elevation (ft) for a LiDAR subsection displayed as a greyscale DEM (left) and a symbolized raster (right). Bridge deck features such as cracks can easily be seen the symbolized raster LiDAR image at right.

7.1.1.   Point Cloud Density Decay

The quantity and location of the scanner setups can significantly affect the point cloud density on the target surface and therefore the ability to detect features of interest such as spalls. A point cloud density image of the span of the Willow Road bridge over US-23 SB shows the dramatic drop in point cloud density with distance from the scanner setups, which were located on the east and west approaches of the bridge (Figure 7-9). The color ramp from red (high density) to blue (low density) represents a density range of from <12,000 points per square foot (ppft^2) near the scanner setup locations at each end of the bridge to <100 ppft^2 near the center of the bridge deck. The scan resolution, slope of the surface to be scanned toward or away from the scanner and size of and distance to the features to be resolved are all important attributes to be considered when designing how many times and where the scanner is set up at a site. Potential shadowing and the orientation of features to the scanner must also be considered when establishing scan locations. Even small features can be affected by shadowing and scanner setup position should take that into account. Figure 7-9 illustrates the fall-off in point cloud density as distance from the scanner increases. Features in the bridge deck that are closer to the scanner are characterized by more returns and can be more easily resolved than similar features further away from the scanner. Scanner setups and resolution information contained in the field sketches drawn by the survey crew (Figure 7-5) can provide a good idea about the point cloud density that can be expected in the point cloud at a particular scan location.
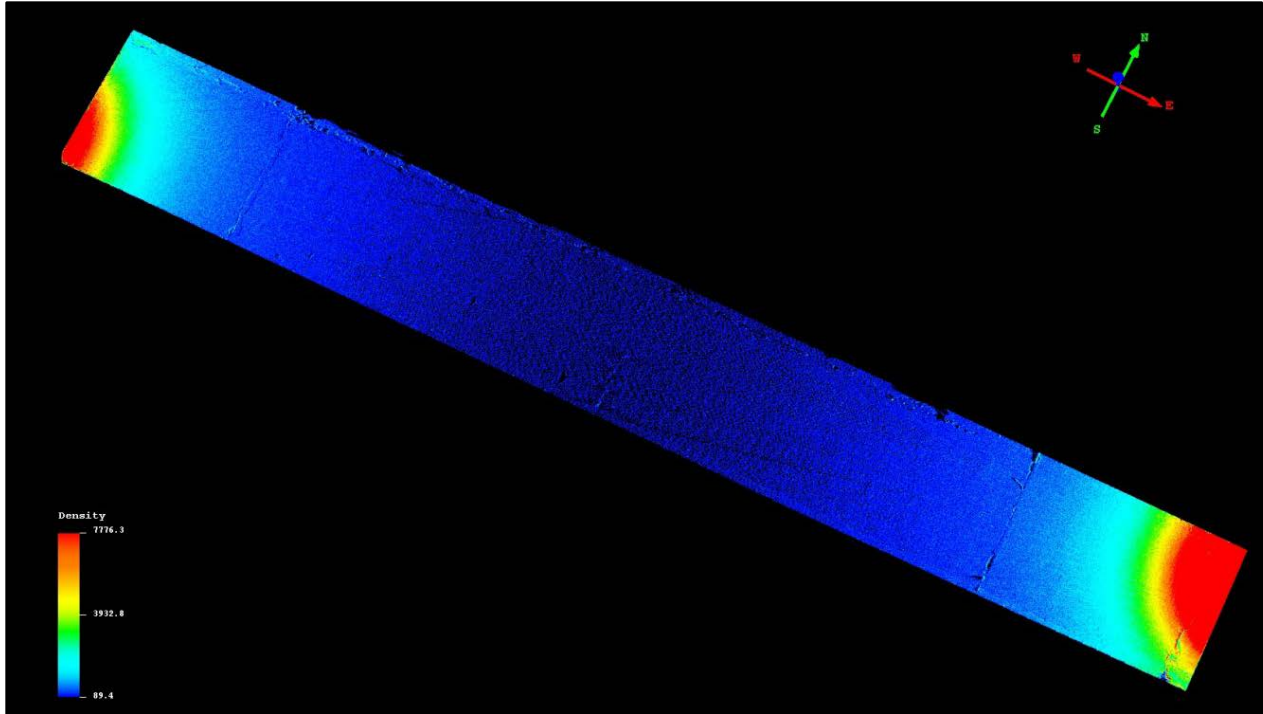
Figure 7-9: Point cloud density image of Willow Road bridge span over US-23. Note the dramatic fall-off in density of points from ends to center (red to blue, high to low). Features in the blue central areas are unlikely to be able to be resolved successfully.

During the field demonstration, two setups covering the bridge deck were performed at each study site. The setups were typically on the bridge approaches near the abutment at each end of the bridge. Most deck scans were performed at the highest resolution setting of available, with the exception of the eastern Mannsiding Road over US-127 NB overpass, which was collected at medium resolution due to time constraints. The scan settings at the Mannsiding Road NB overpass data collect was not documented on the field sketch. Regardless of the resolution a pattern in the data became evident during the post-processing of all four bridge decks. In each case, the point cloud showed a rapid decline in point cloud density with distance from the scanner.

Further analysis of the data shows that the point cloud density decays at an exponential rate rather than the originally anticipated linear decay rate (Weibring et al. 2003). Figure 7-10, Figure 7-11, Figure 7-12, Figure 7-13, Figure 7-14, Figure 7-15, Figure 7-16, and Figure 7-17 help to visually illustrate the point cloud decay. Areas represented in red are locations near scanner setups and the blue represents the lowest point cloud density captured on the bridge deck surface. The densest recorded reading for all four bridge decks was 7,736.3 ppft^2) (83,186 points per square meter (ppm^2)), while the least populated section was 18 ppft^2 (193.5 ppm^2). The graphs below each deck show a longitudinal profile of each bridge deck.

The curve in each graph consists of individual data points along a longitudinal profile near the centerline of each bridge (such as Figure 7-11, Figure 7-13, Figure 7-15, and Figure 7-17). In each case, what appears to be a solid line resolves into individual data points near the center of the bridge as the point cloud density decreases. This effect is more pronounced on longer bridges (Freer Road and Willow Road bridges) or where the scanner is set up further from the abutment (Mannsiding Road over US-127 NB). In each case, the graph mirrors the point cloud density decay phenomenon seen in the graphic above it.

To explain the originally unexpected severity of the exponential point cloud decay, data collection and processing methods were reviewed and the literature was further reviewed. By relying on two stationary collection locations at a fixed collection height, the angle of incidence greatly influences the obtainable surface information. Figure 7-18 and Figure 7-19 show that as the distance from the receiver increased, the angle of incidence initially increased rapidly and asymptotically approached 180 degrees. The established relationship for the angle of incidence resulted in an equal reduction in the coverage angle. Also, Weibring et al. (2003) review that LiDAR data has a falloff of $1/Range^2$; as scanned areas are further away, there is exponential falloff in the LiDAR signal. When sensing a planar surface for topographical defects, a coverage angle of nearly 180 degrees (the surface is normal to the scanner) would be ideal. However, with terrestrial LiDAR units, the coverage angle for a bridge deck is substantially less than the desired 180 degrees.
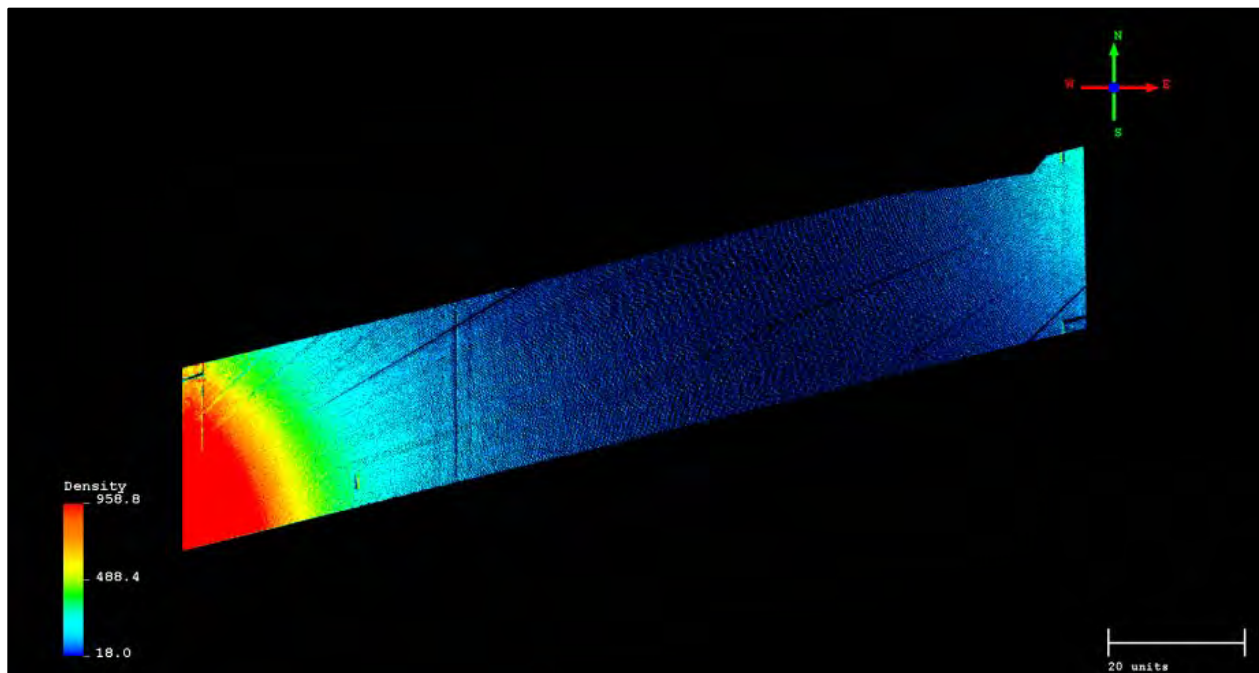
Figure 7-10: Mannsiding Road bridge over US-127 NB point cloud density texture for visual representation.
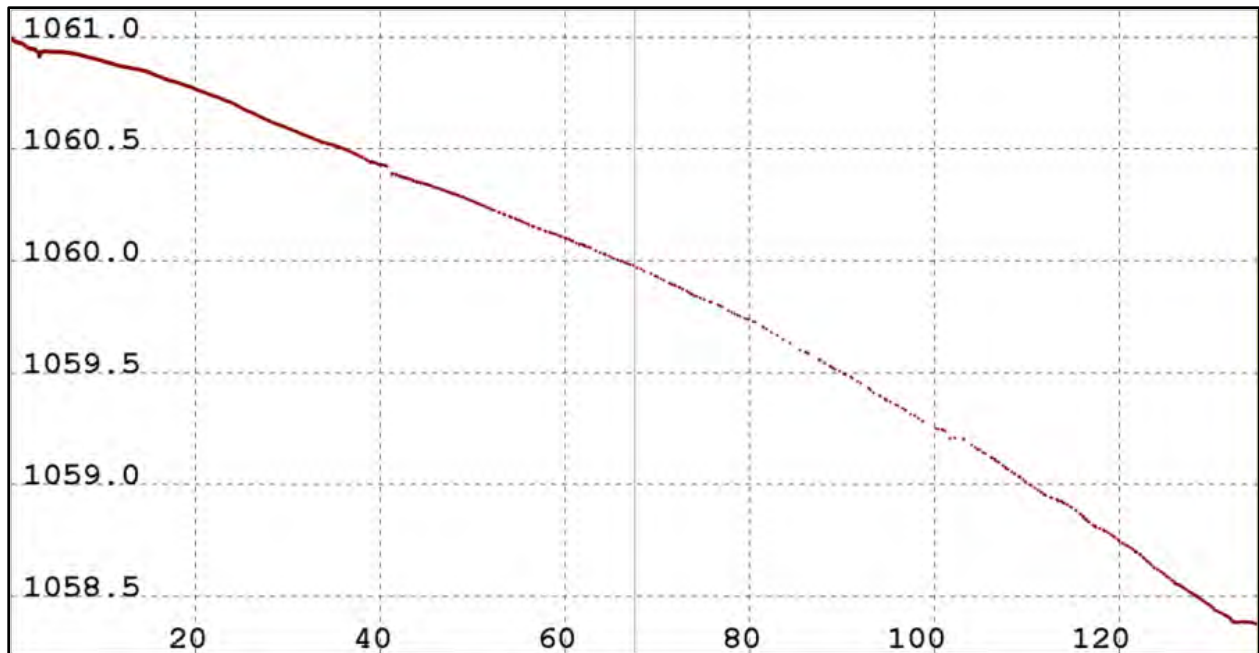
Figure 7-11: Mannsiding Road NB longitudinal elevation profile; elevation in feet (Y-axis) and distance along the centerline in feet (X-axis).
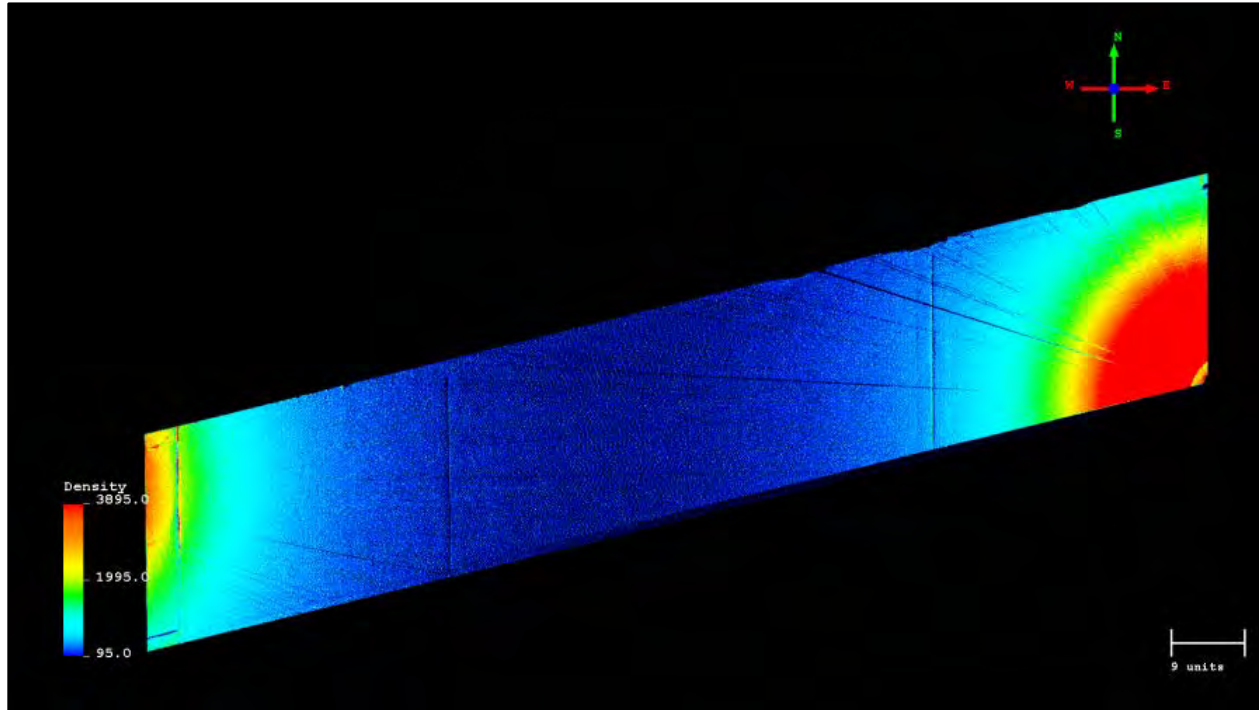
Figure 7-12: Mannsiding Road over US-127 SB point cloud density texture for visual representation.
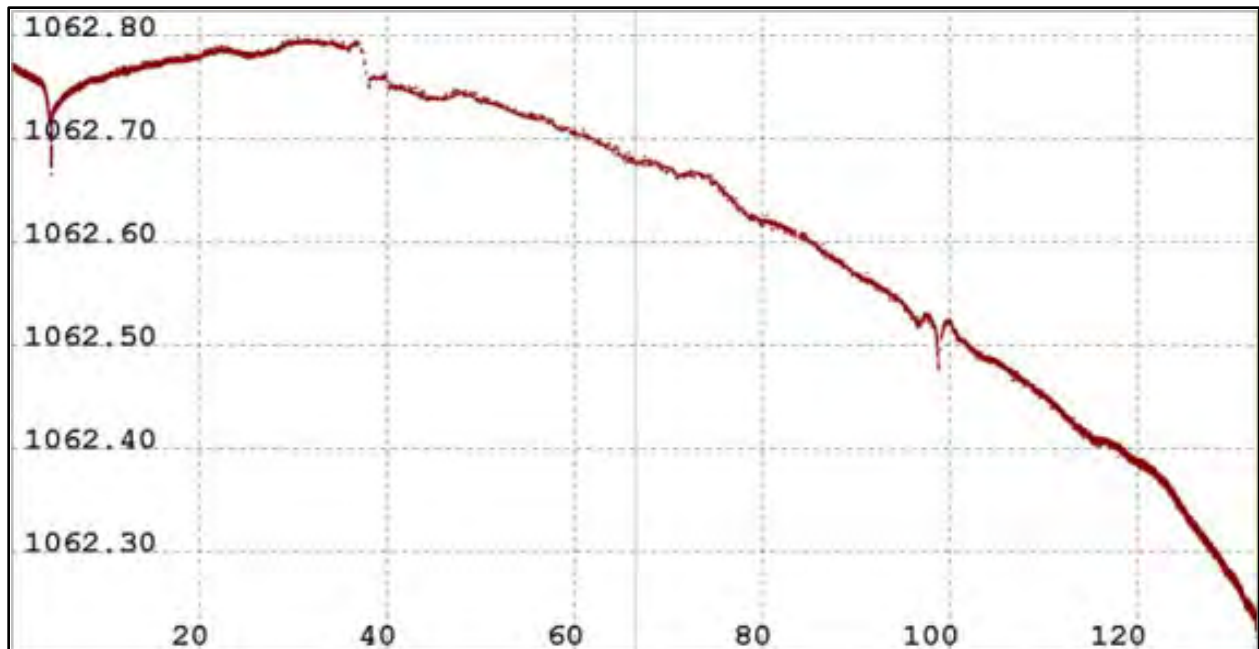
Figure 7-13: Mannsiding Road SB longitudinal elevation profile; elevation in feet (Y-axis) and distance along the centerline in feet (X-axis).
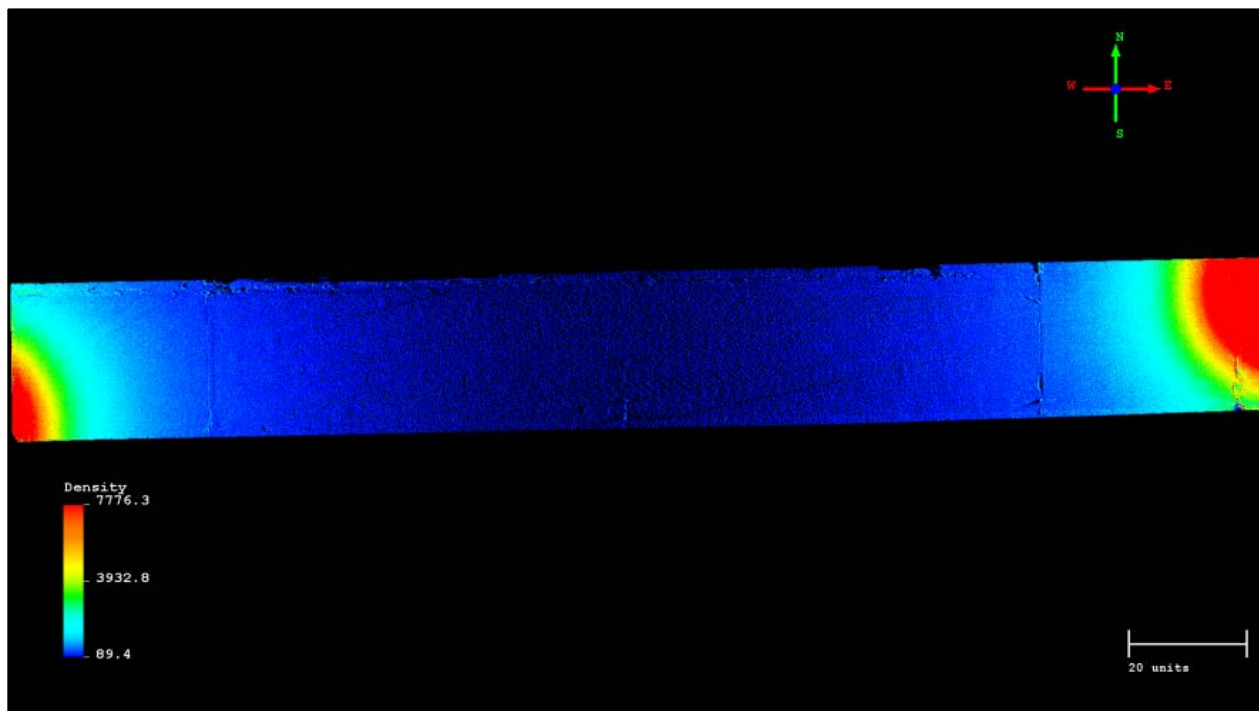
Figure 7-14: Willow Road point cloud density texture for visual representation.
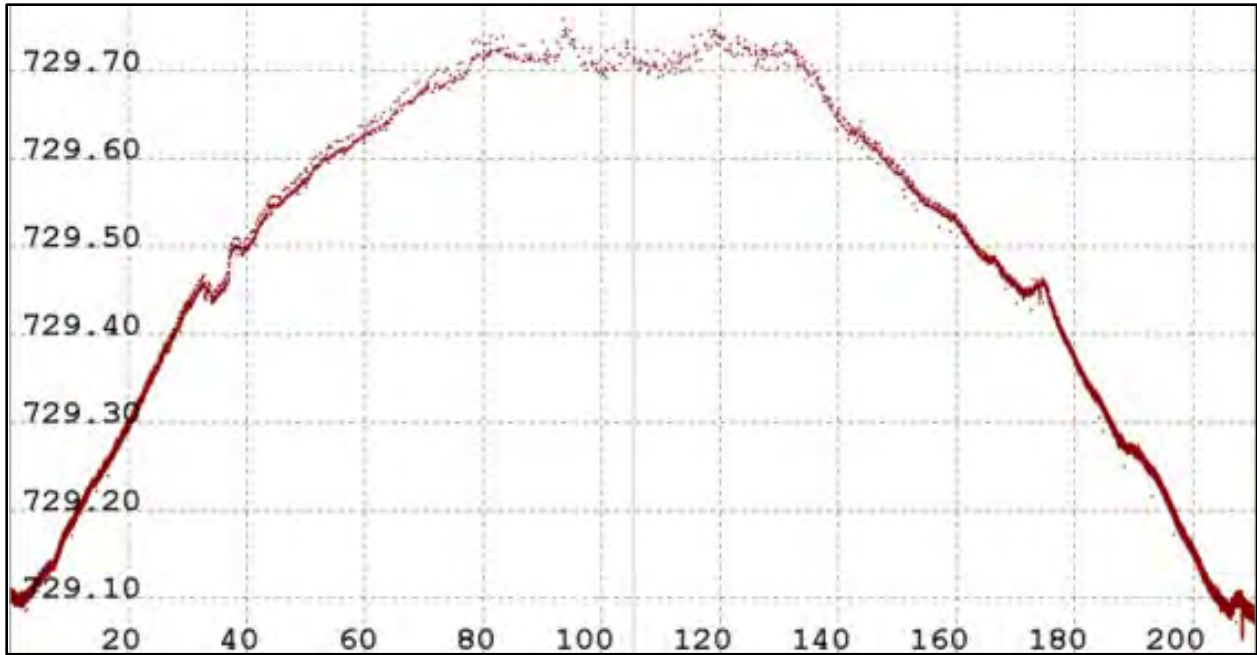
Figure 7-15: Willow Road longitudinal elevation profile; elevation in feet (Y-axis) and distance along the centerline in feet (X-axis).
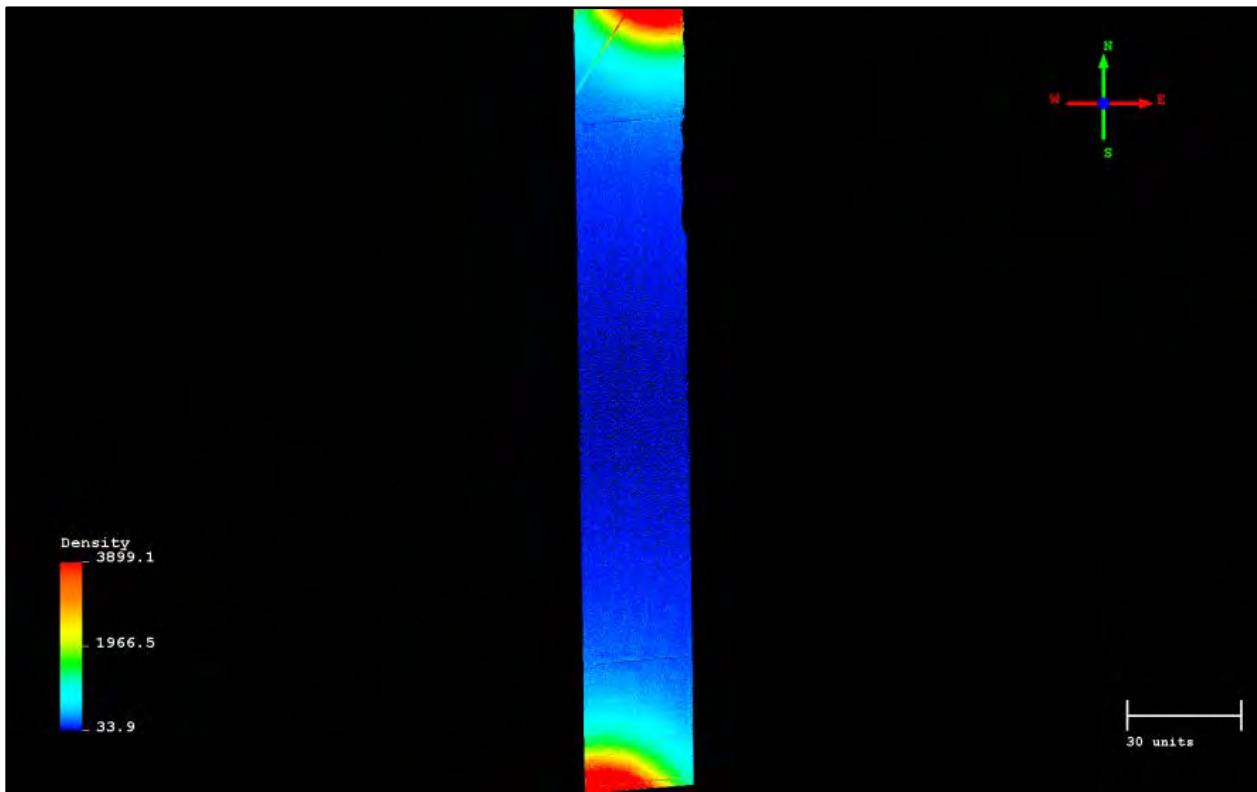
Figure 7-16: Freer Road bridge point cloud density texture for visual representation.
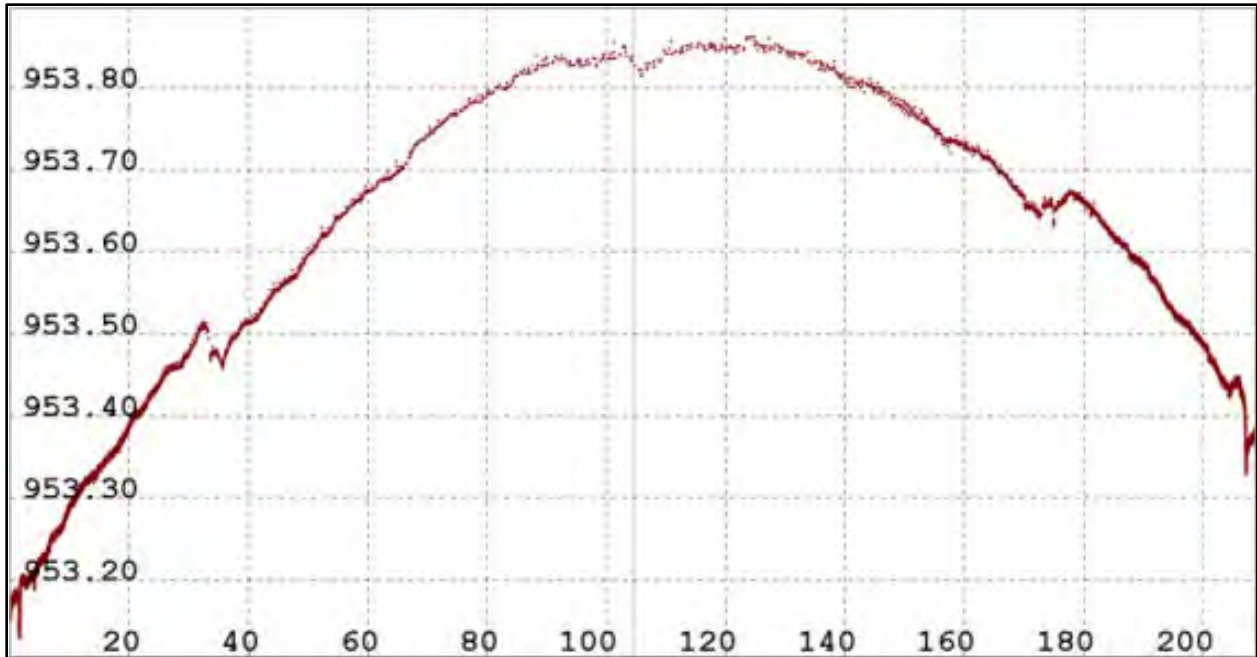
Figure 7-17: Freer Road bridge longitudinal elevation profile; elevation in feet (Y-axis) and distance along the centerline in feet (X-axis).
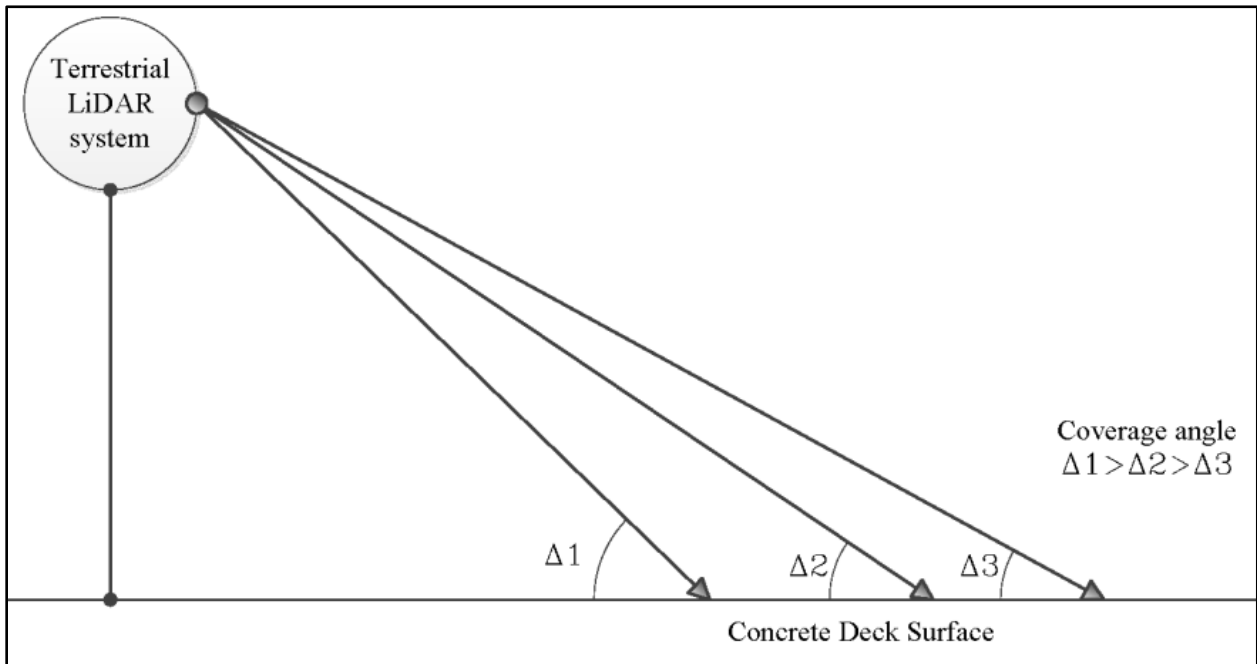
Figure 7-18: Visual representation of the reduction in coverage angle over distance.

The "arching" (camber) found in many bridge decks contributes to point cloud density decay. As the deck begins to slope away from the scanner beyond the center of the bridge, the coverage angle approaches zero. A bridge deck that slopes down away from the scanner can have a similar

effect. The coverage angle on bridge deck that rises with distance from the scanner will not have as significant drop in coverage angle. The Mannsiding Road bridge over US-127 NB (Figure 7-10 is an example of this effect, where the bridge elevation falls away from the scanner, which can be seen in the graph (Figure 7-11). As shown in the longitudinal elevation profile graphs, the camber of the bridges were captured during the data acquisition. The maximum arch present in the four test cases was estimated to be 0.65 ft of elevation change (on Freer Road from abutment to the middle span).
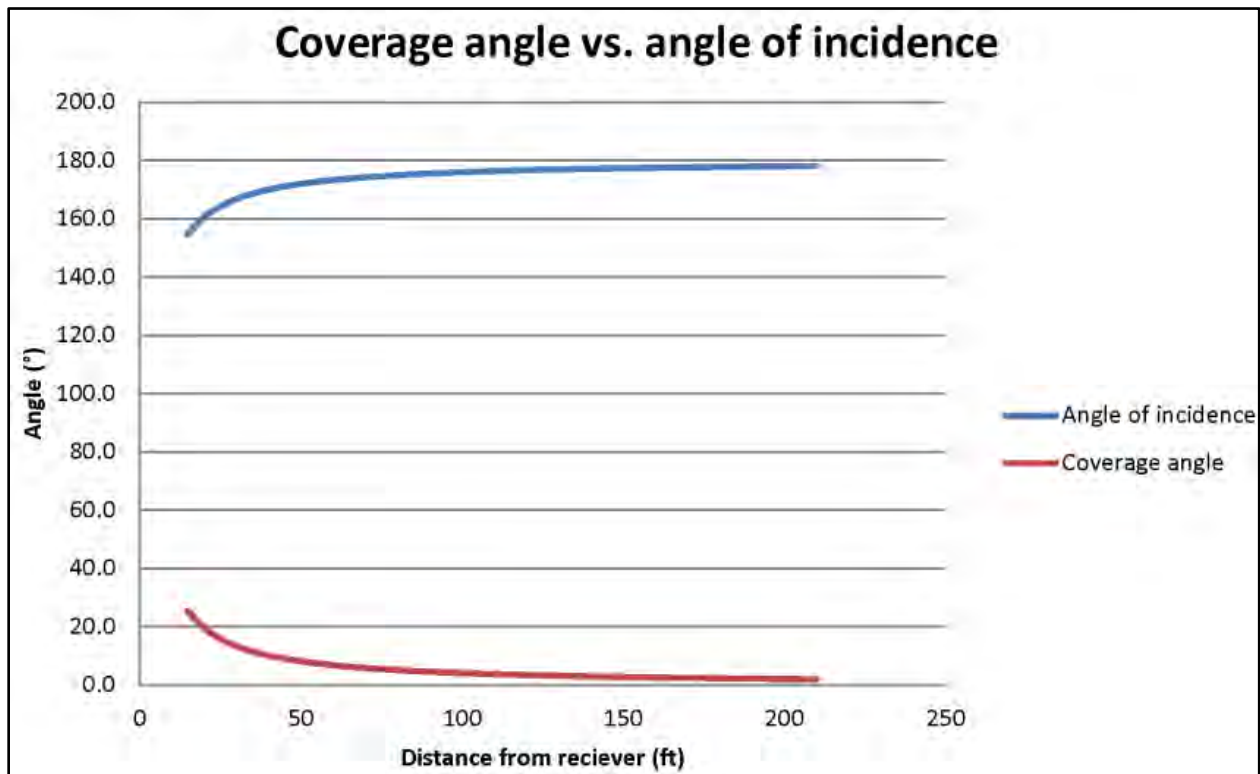
Figure 7-19: The coverage angle and angle of incidence as the distance from the scanner increases.

7.1.2. Maximum Radius of Capture

This project was able to create high-resolution bridge surface DEMs from both 3DOBS and LiDAR technologies, enabling both comparisons and sharing of algorithm-based analysis methods. When applying the 3DOBS spall detection algorithm results for LiDAR derived DEMs, the estimated spalled area increased as the distance from the terrestrial LiDAR unit increased. The cause of the increasing overestimation of spalled area is attributed to the exponential point cloud density decay seen in the graphs and illustrations. By comparing the optical master deck images of each case study bridge and the algorithm results, a maximum radius of data capture was generated for the ScanStation C10 when set at the highest resolution

setting. By measuring the distance from the edge of the approach slab to the point of error saturation, a maximum radius of capture trend was established. The individual bridge measurements for maximum radius of capture are listed in Table 7-1 at 50,000 points per second (pps). The average radius of capture, when considering all terrestrial LiDAR locations where a high resolution scan was collected, is 56.2 ft (17.1 m). The established radius of collection of 56.2 ft only pertains to the case study collection parameters. This study is focused on bridge deck condition and requires the ability to resolve small (~40 cm^2) features such as spalls on a bridge deck. It is important to keep in mind that this radius reflects only point cloud density on the bridge deck, not the range accuracy of the scanner, which is accurate out to a significantly greater distance. The number of scanner setups required to obtain an adequate point cloud density will vary based upon project requirements and the length of the bridges being assessed.

Table 7-1: Maximum radius of capture for ScanStation C10 at 50,000 pps.

Field Demonstration Location	Approach Slab	Radius of Capture (ft)
Mannsiding Road NB	Northeast	Not collected
	Southwest	50.78
Mannsiding Road SB	Northeast	66.48
	Southwest	66.48
Freer Road	North	51.59
	South	52.09
Willow Road	East	50.76
	West	55.37

LiDAR point clouds or LiDAR-derived DEMs superimposed over ortho-photographs of the bridge deck is a useful technique to verify visual and quantitative analysis of the data. In this example a high resolution geo-referenced mosaic of bridge deck images captured by the 3DOBS close range photogrammetry system is used to help confirm the analysis of the deck condition seen in the LiDAR data. In Figure 7-20 and Figure 7-21, patches made to the bridge deck that are not flush with the existing deck can be seen (arrows) as areas of slightly higher elevation. A spall can also be seen in Figure 7-20, Figure 7-21, and Figure 7-22 as an area somewhat lower in height than the surrounding bridge deck. The patches are 0.25-0.625 in (0.635-1.59 cm) higher

than the surrounding bridge deck and the spall is about 0.375 in (0.953 cm) deep at its deepest point.
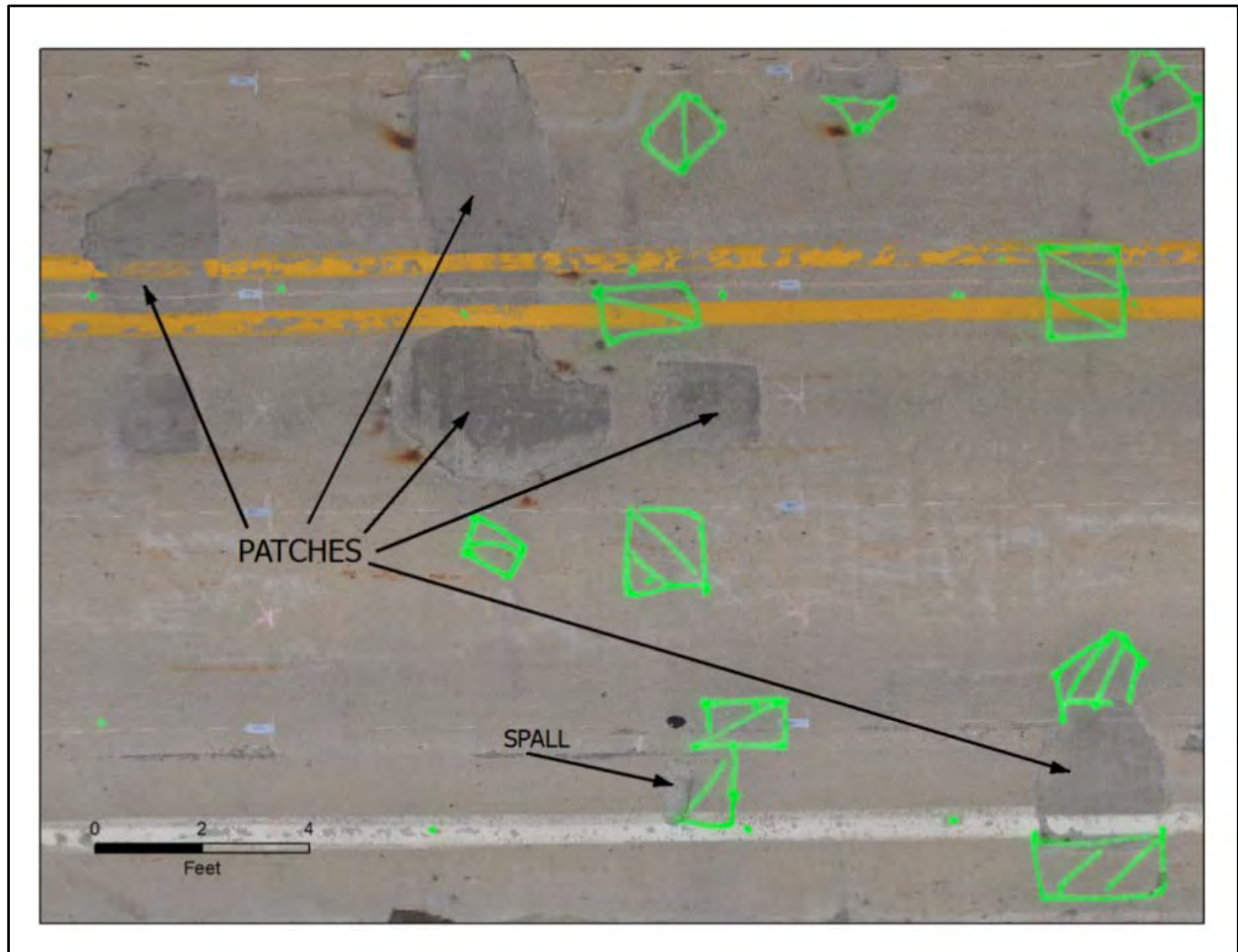
Figure 7-20: Section of the ortho-photo of the Willow Road bridge deck illustrating patches and a spall. The green pavement markings outline areas of subsurface delamination as determined by inspection performed by MDOT bridge inspectors using the hammer (metal rod) sounding technique.
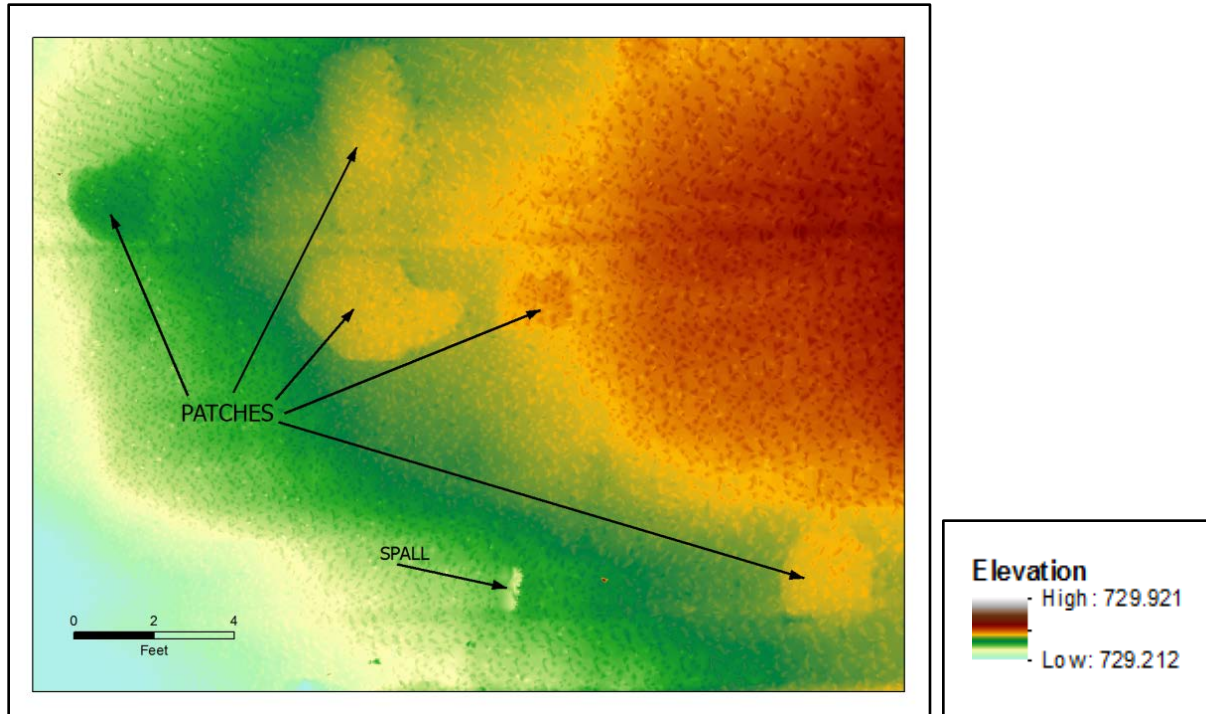
Figure 7-21: DEM with a color ramp applied of the same area of the Willow Road bridge deck. Note that the higher areas of the concrete patches and missing material from the spall correlate well between the ortho-photo and DEM. The patches (correctly) appear higher than the surrounding bridge deck and the spall appears lower than surrounding deck.
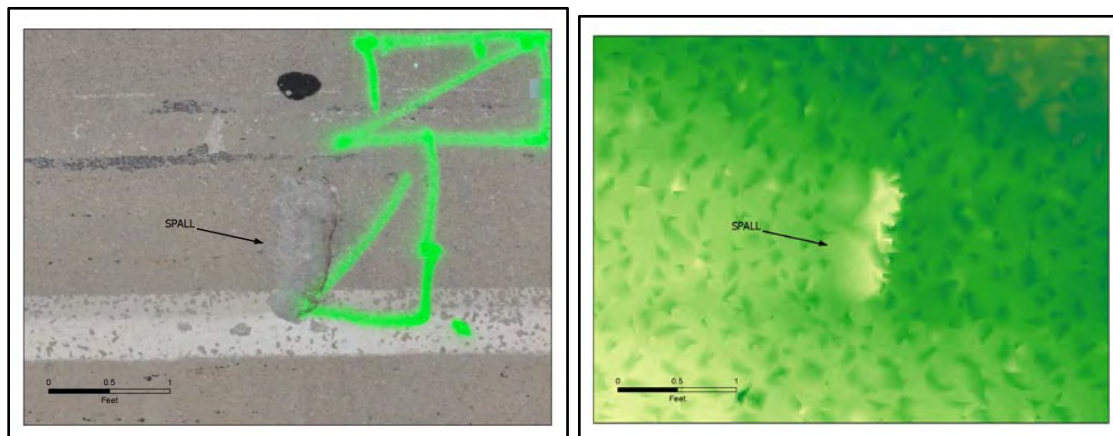
Figure 7-22: Close up of the spall on the Willow Road bridge deck. The spall is clearly visible in the ortho-photo as well as in the DEM (the light yellow color is lower than the green).

7.1.3. Mobile Light Detection and Ranging

As noted previously, LiDAR is a line-of-sight instrument and may require repositioning of the scanner to illuminate shadowed areas. This requirement can increase collection time and required labor during data collection and post processing. The dramatic falloff in point cloud density with distance from the LiDAR scanner discussed above means features further away from the scanner are characterized with fewer points than similar features near the scanner. Mobile LiDAR has the potential to reduce the collection time and increase the resolution versus terrestrial LiDAR by collecting at a consistent resolution across the entire bridge deck, reducing the problem of point cloud density decay, as discussed in TM nᵒ 21. Surveying Solutions (SSI) of Standish, MI completed a mobile LiDAR scan of the US-23 and I-96 interchange in Brighton, MI for MDOT during the summer of 2011. This data was shared by MDOT with MTRI and evaluated as an additional potentially useful technology for the assessment of bridge deck condition.

Mobile LiDAR is a vehicle-mounted LiDAR data collection system that creates a point cloud along a path followed by the scanning vehicle (Tao and Li 2007). A typical mobile LiDAR scanning unit consists of two LiDAR scanners, an Inertial Navigation System (INS), and a high accuracy GNSS (Global Navigation Satellite System, such as GPS, the US-run Global Positioning System) receiver mounted on a vehicle. The integrated scanning unit is most often mounted on the roof of a full size vehicle, although the systems can be mounted on boats or rail equipment, depending on the requirements of the project (Figure 7-23). The scanners are mounted at an angle that allows each scanner to "see" areas not visible to the other, which improves the coverage of the LiDAR point cloud. A data cable runs between a control unit mounted inside the vehicle and the roof mounted measuring head which contains the scanners, GNSS and INS (Figure 7-23, right).

Mobile LiDAR data can be collected at near highway speeds (35-50 mph) depending on point cloud density required. The mobile LiDAR point cloud is generally linear and as is the case with other LiDAR scanning technologies, the return density decreases sharply with distance from the centerline of the scanning unit.

Mobile LiDAR systems can collect data at very high spatial resolutions near the scanner. The same falloff in point cloud density with increasing distance that occurs with terrestrial scanners also occurs with mobile scanners, but only in the transverse direction. Like fixed terrestrial systems, multiple scan passes are registered together to create a point cloud of the project area. Figure 7-24 below is a composite of multiple scans of the I-96 and US-23 interchange near Brighton, MI. The image consists of four passes through the interchange by the data collection vehicle that were clipped to the approximate right of way of the highway. Each of the data sets can contain multiple passes over the highway. Note that like other forms of LiDAR, mobile LiDAR can capture features that are sometimes at a significant distance. Depending on scanner settings and the size and reflectivity of the target, returns from objects up to 800 m away from

the sensor can be detected. A typical working range is 75-100 m, but the density to detect most spalls is likely to be shorter. Point cloud density and sample rate can be adjusted based on project requirements; some scanner setups can collect up to ~500,000 pps (two scanners at 250,000 pps each, such as the Riegl VQ-450 and VMX-250).

Figure 7-23: The VMX-250 scanner mounted on an SUV. Image on the right shows a close-up of the scanner heads, GNSS receiver, and Processing/Inertial Navigation Unit.
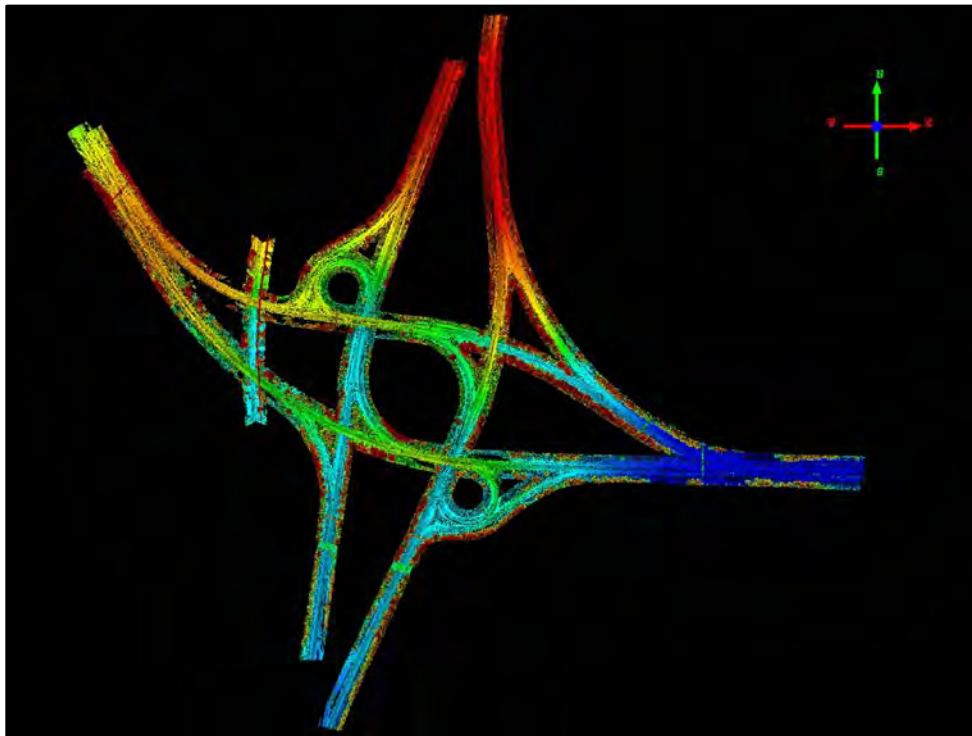
Figure 7-24: Synoptic view of the point cloud collected by mobile LiDAR at the US-23 and I-96 interchange near Brighton, MI. Data collected in August 2011.

As is the case with other LiDAR sensors, mobile LiDAR can be configured to collect attributes such as number of returns, classification, intensity and RGB values which enhance the analyses that can be performed with the data. Unlike other LiDAR sensor configurations, there are usually two sensors in a mobile LiDAR unit, angled in such a way as to minimize shadowing. This configuration results in a crosshatch pattern on the pavement below the sensors. The spacing of the lines in the crosshatch is directly related to vehicle speed and the rotational speed of the scanner mirror. As a result, the point cloud density and scan line spacing required to define features must be known in advance of a scan in order for the correct speed and sensor sampling rate to be established. Figure 7-25 illustrates the change in point cloud density that results from a change in vehicle speed. The project vehicle traveled 45 mph on the lanes of the main road and 35 mph on ramps. The change in distance between scan lines on the travel lanes (generally left to right in the image) and on the ramp coming up from the lower right is noticeable.
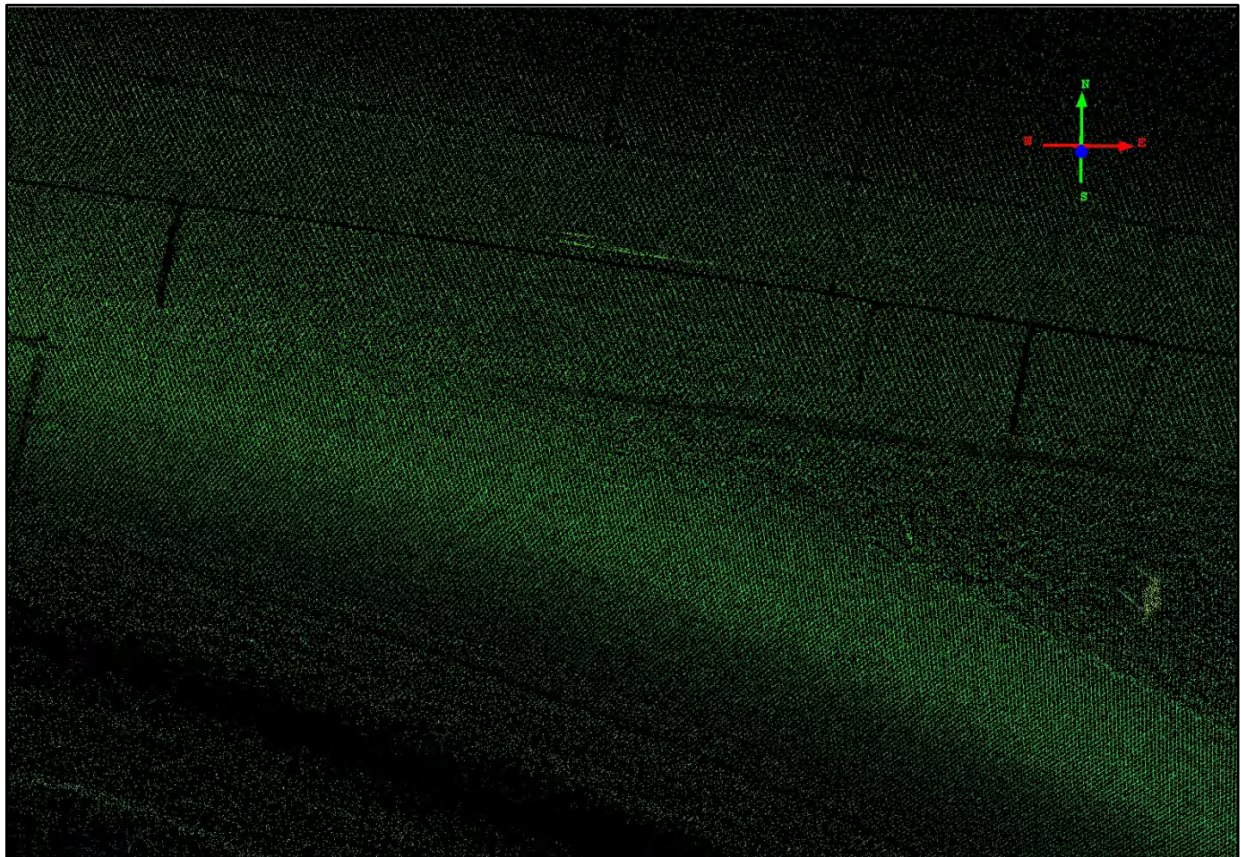
Figure 7-25: Close up of the LiDAR return pattern where a ramp where data was collected at 35 mph meets the main road where data was collected at 45 mph. The distance between scan lines increases with vehicle speed. The ramp diverges from the main road to the lower right in this image. Elevation and intensity values are displayed in this image.

Mobile LiDAR does not suffer the falloff in point cloud density along the path of the project vehicle, although it does fall off transverse to the direction of travel. Spacing between scan lines varies with vehicle speed so care must be taken to ensure the point cloud density on the target surface is adequate to allow extraction of the desired features.

Figure 7-26 is an example of passes over US-23 NB and the ramp from I-96 westbound to US-23 NB near Brighton, MI. During the pass on the ramp the survey vehicle was moving from the lower right of the image at approximately 35 mph as the data were collected. The pass on US-23 NB was collected at approximately 45 mph. The color ramp in Figure 7-26 is point cloud density per square meter. Note the relative difference in average points per square meter between the ramp (darker red, higher density) and US-23 NB (orange, lower density). The point cloud density on US-23 NB increases as the ramp gets closer and the point clouds from the ramp and main road begin to overlap. The highest point cloud density is within a few meters of the centerline of the scanning unit as it moves down the road. This should be kept in mind as project requirements are developed. If high point cloud density will be required on each lane, it may be necessary for the scanning vehicle to drive each lane of multi-lane divided highways. If pavement condition is a project requirement, care should be taken to accurately register the individual scans. Vertical registration is particularly important since poor vertical registration can appear as rough pavement when the data are processed.
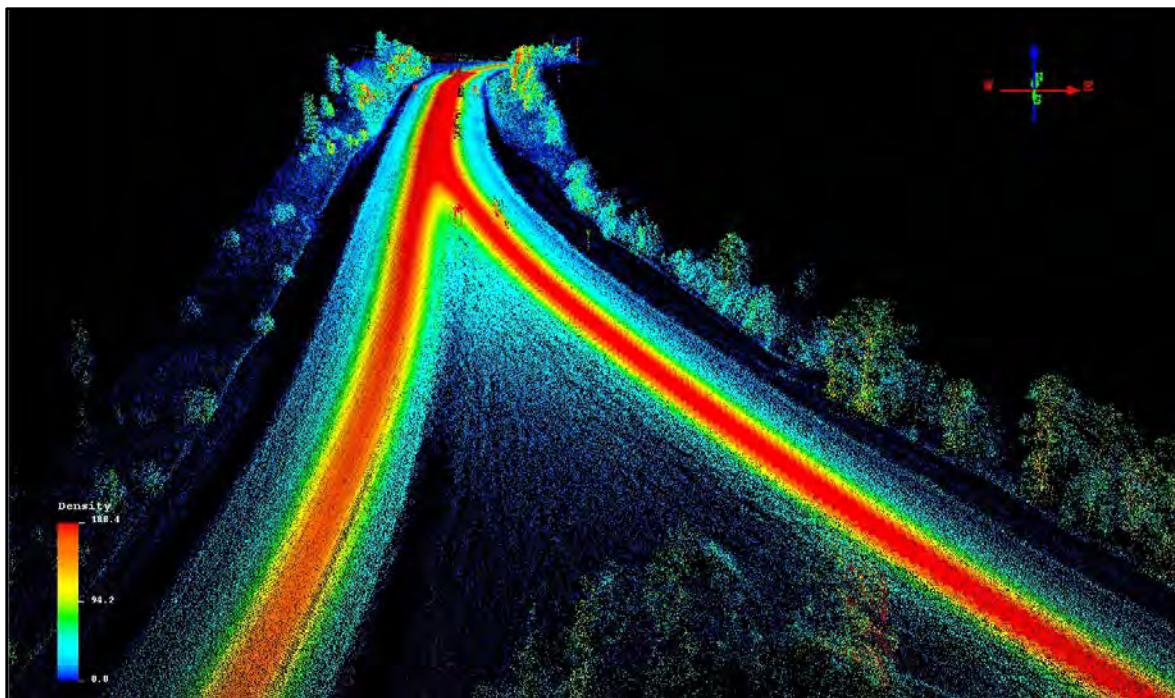
Figure 7-26: An example of the point cloud density decreasing from scanning-vehicle /scanner-centerline. Image shows US-23 NB (left) I-96 (right) merging. Vehicle speeds; ~45 mph (US-23) and ~35 mph (I-96).

7.2. Field Demonstration Results and Discussion and Integration into the Decision Support System

7.2.1. Three Dimensional Optical Bridge-evaluation System Spall Detection Algorithm

As part of the larger bridge condition assessment project, MTRI developed an algorithm for 3DOBS (Chapter 4), to automatically detect spalls and calculate associated areas and volumes of any spalls present using bridge deck DEMs and is briefly reviewed here. The algorithm was written in Python, and utilizes a software component called "ArcPy" to access geospatial analysis tools in ArcGIS to evaluate data. For identification and characterization of defect spalls, the algorithm uses a statistical method available in ArcGIS, called focal statistics. Focal statistics evaluates individual cells by establishing boundaries around each cell referred to as "neighborhoods" (Unwin and Unwin 1998). Then the change in cell value is evaluated and compared to surrounding "neighborhoods". User defined parameters within the algorithm allowed for establishment of critical values defining cell value change, which would constitute a spall.

The 3DOBS spall detection algorithm evaluates elevation data in a DEM, allowing for sudden elevation changes to be detected and compared with user defined spall characteristics. For proof of concept, MTRI performed analysis on a single spall, varying the user defined minimum spall size to be considered, allowing for the establishment of minimum size criteria. The user defined minimum spall sizes evaluated were 10 cm^2, 100 cm^2 and 1,000 cm^2 allowing for a trend to be forecasted. From the testing, MTRI concluded that a minimum detection size of about 40 cm^2 (6.2 in^2 or an area approximately 2.5 x 2.5 in) would be optimal for detecting spalls of interest to transportation agencies.

The spall detection algorithm was developed to accept any geospatial DEM. LiDAR derived geotiff DEMs exported from Quick Terrain Modeler were processed using the 3DOBS spall detection algorithm in the same way as DEMs created using close-range photogrammetry. Analysis was performed on areas of known spall volume and compared with a secondary surface defect detection technology to validate results. Figure 7-27 shows a particular area of more focused analysis, demonstrating the ability to predict surface defects when comparing to a high-resolution image of the bridge surface taken with 3DOBS.
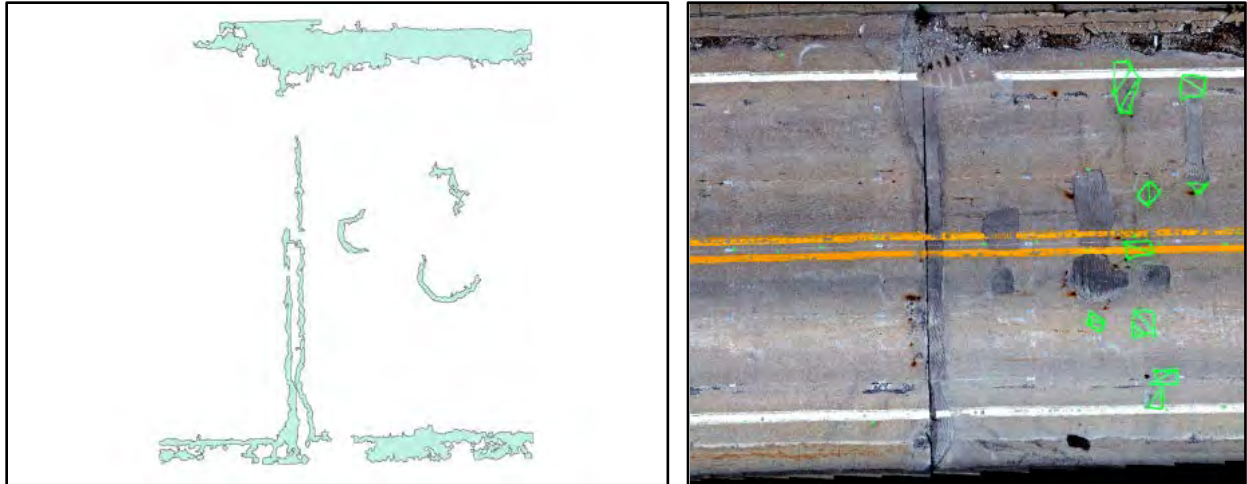
Figure 7-27: Comparison of the results of the spall detection algorithm (left) to a high-resolution composite image of the bridge deck taken with 3DOBS.

7.2.2. Light Detection and Ranging Data Derived Digital Elevation Models and Processing in the 3D Optical Bridge-evaluation System Spall Algorithm

LiDAR point spacing is important to getting spall detection results similar to 3DOBS close range photogrammetry. Falloff in point cloud density with distance from a terrestrial LiDAR scanner can be dramatic even at high data collection rate settings as discussed previously. DEMs created using terrestrial LiDAR must be processed from point clouds collected with the point density decay in mind.

Subsets of the LiDAR data from the study bridges that included only the bridge deck were created to isolate the bridge deck data. This allowed the examination of the deck of the bridge while excluding the balance of the bridge structure. A property of LiDAR discussed previously is the rapid falloff of the point cloud density (measured in points per unit area). The Figure 7-28 illustrates the falloff in point cloud density on the Freer Road bridge. This falloff with distance occurs with all LiDAR scanners and must be taken into account when planning the number, location and resolution of scanner setups.
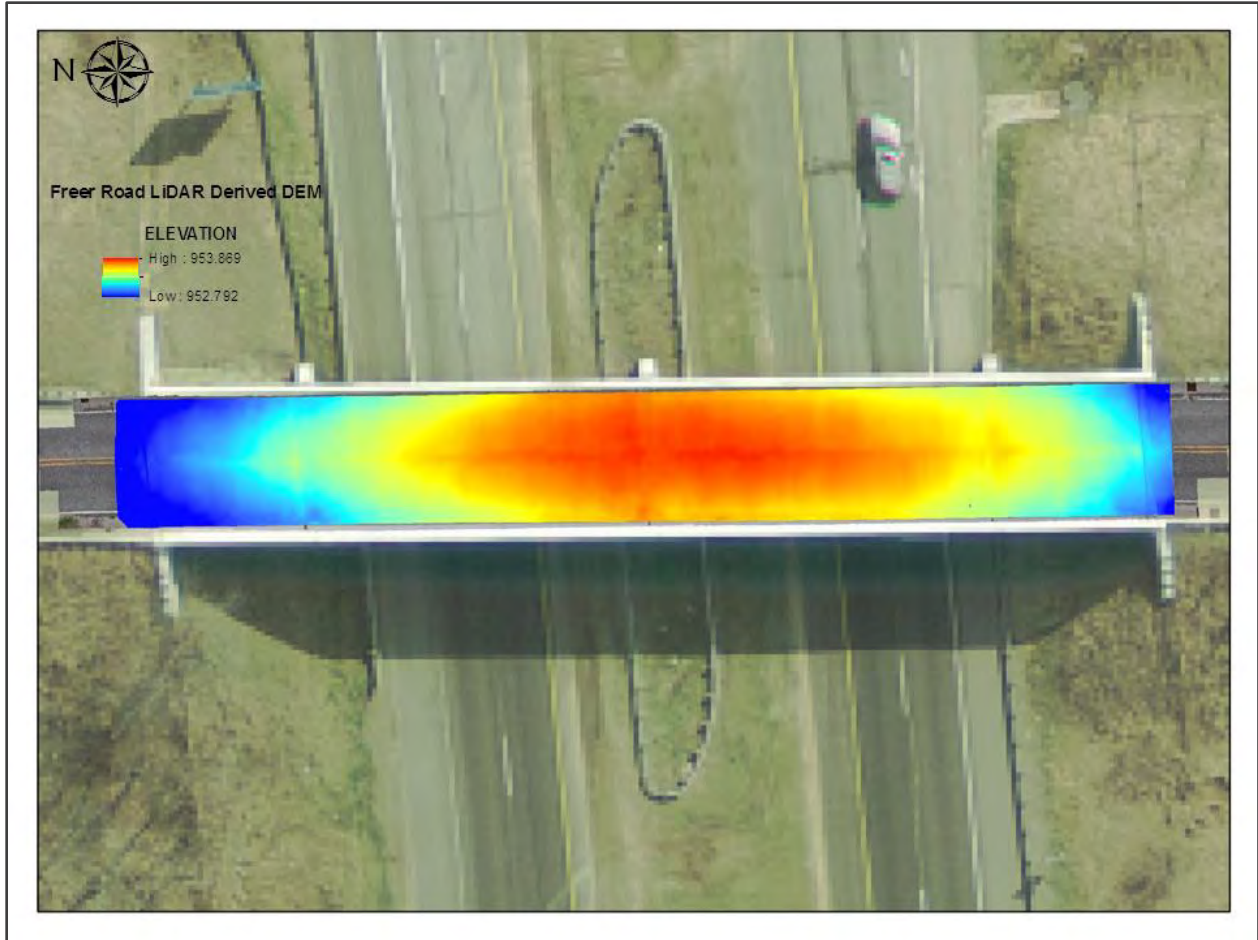
Figure 7-28: The Freer Road bridge deck DEM over one foot per pixel aerial imagery and the high resolution orthophoto of the Freer Road bridge deck. The DEM is approximately 220 ft long with a spatial resolution of 3 cm per pixel.

The point cloud density in this data set runs from 3,800 ppft^2 (red) near the scanner location to 33 ppft^2 (blue) at the center of the bridge (see Figure 7-29). At both ends of the bridge, the scanner setup was on the bridge approach rather than on the deck itself. Small features (spalls, for instance) near the scanner can be easily resolved in the LiDAR data while similar sized features further from the scanner may not be resolved as easily, if at all. An example in this graphic is the expansion joints visible as a line across the bridge deck near each end. There is a similar joint at the center of the span that is difficult to see or detect in the LiDAR data.
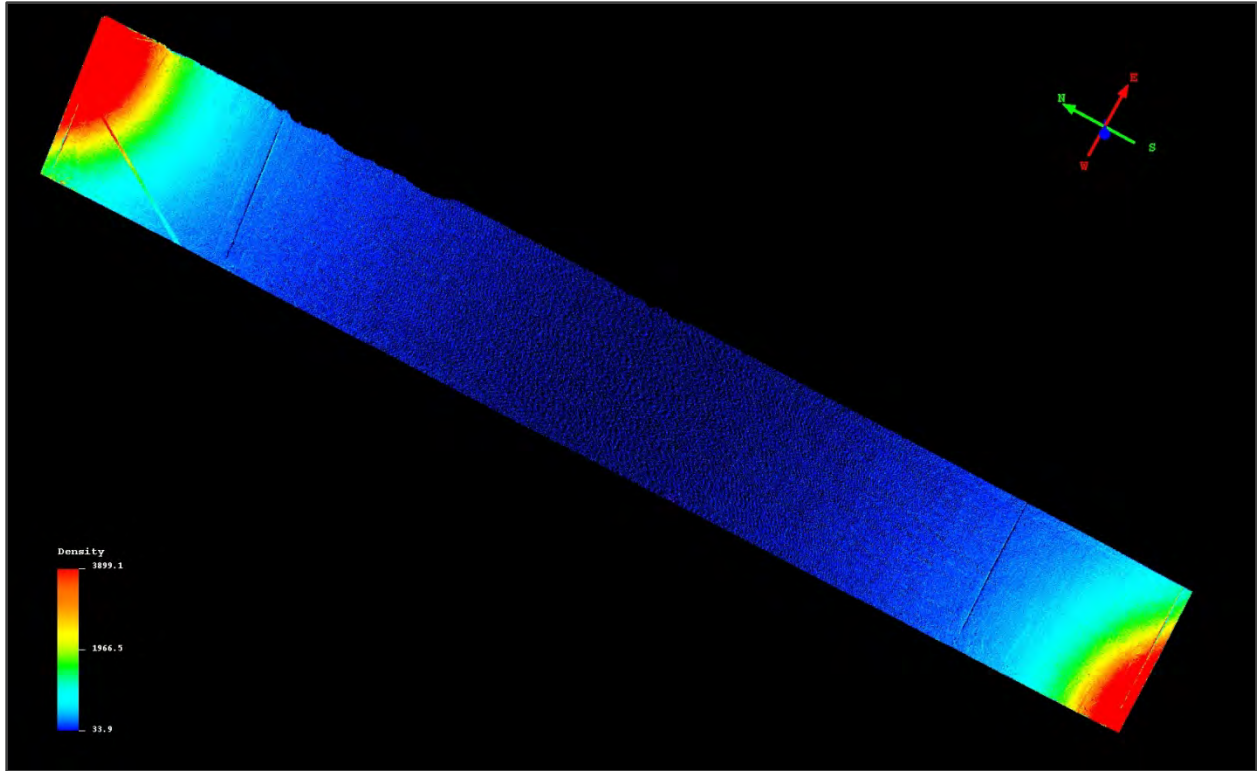
Figure 7-29: Freer Road bridge deck point cloud density map. The rapid falloff in point cloud density (red high density to blue low density) with distance from the LiDAR scanner is clearly visible.

The falloff in point cloud density can be a significant issue when creating a DEM from LiDAR data. When data are sampled to create a DEM, software may average the point density over the entire dataset, potentially under representing the resolution of the data set in some areas and over representing the resolution in others. The underrepresentation of the data does not improve the accuracy of the data and may in fact introduce errors.

Because of the two DEMs of the Willow Road bridge being collected with two different technologies (LiDAR and 3DOBS); the results when displayed in geospatial software appear different even though they both show an elevation model of the bridge surface (see Figure 7-30). The color ramp for the top DEM in Figure 7-30 was derived from a LiDAR data set, and the values represent elevation relative to sea level. The bottom DEM was extracted by close range photogrammetry from images of the bridge deck collected by the 3DOBS system. Both DEMs were effective at detecting the spalls and patches - 3DOBS across the entire bridge deck, and for LiDAR where these was sufficient point density before range falloff issues resulted in insufficient data (a distance of about 56 ft as described above). The same color ramp was applied to both datasets.
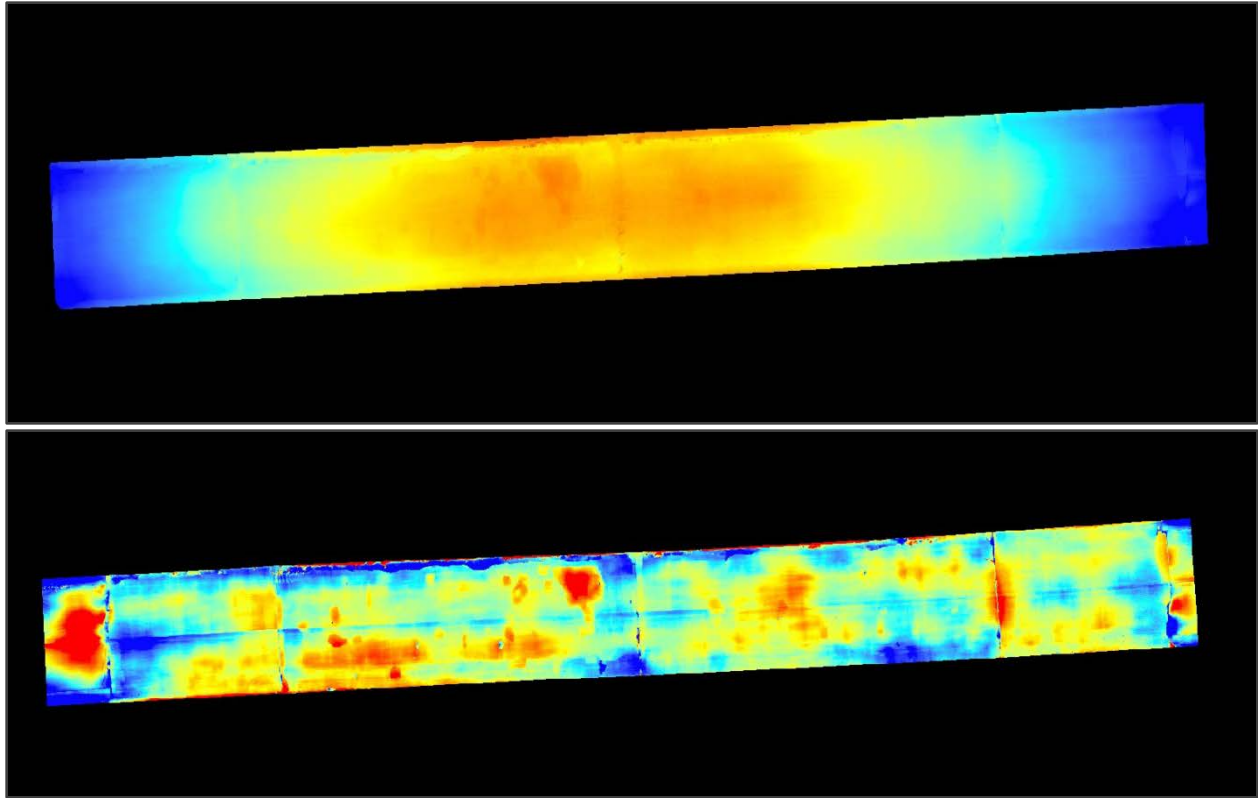
Figure 7-30: A comparison of DEMs derived from LiDAR data (top) and the 3DOBS close range photogrammetry system (bottom).

With the understanding of the exponential point cloud decay and the maximum capture radius, individual evaluation of the bridge decks was conducted. To reinforce the two general findings, full deck evaluations for surface defects were conducted; results are provided and compared with an established ground truth measure. For the algorithm to successfully process the eight subsets for each bridge, consistent spall algorithm parameters were established. The spall parameters used in the spall detection algorithm were as follows:

- Max bridge pixel value: 0.004
- Min spall pixel value: 0.0040001
- Min spall size: 1.0

Known surface defects located within the established 56.2 ft coverage radius were further evaluated allowing for a determination of the effectiveness of the technology, data collection and processing methods under ideal conditions. The extracted surface defects were processed at different input parameters then what the entire bridge decks were processed at. In addition, each comparative ground truth measure was processed at similar input parameters allowing for a fair comparison.

7.2.3.   Ground Truth Measure for Comparison

High resolution DEMs created through 3DOBS, were used to compare to the LiDAR DEMs. 3DOBS utilizes close range photogrammetry to generate 3D models from stereo pairs of electro-optical (EO) imagery. The developed models provide depth and height information that could not otherwise be determined from individual EO images. A DSLR, high-quality camera is the main component of the field system. The system implemented during the field demonstration consisted of a D5000 DSLR camera, vehicle mount and a camera triggering device as shown in Figure 7-31 (de Melo e Silva and Brooks 2011).

Figure 7-31: 3DOBS data collection system field demonstration

MTRI conducted laboratory testing on 3DOBS; the results showed that the technology is capable of detecting vertical changes 0.079 in (2 mm) in depth, and even smaller with certain configurations. With the current bridge inspection standard of 0.25 in (6.35 mm) for minimum consideration criteria of an elevation change to be a potential spall, the 3DOBS technology exceeds the established criteria (de Melo e Silva and Brooks 2011).

As discussed previously, a characteristic of LiDAR data is the falloff in point cloud density with distance from a terrestrial scanner. This becomes an important factor when DEMs are derived from the LiDAR data and run through the 3DOBS spall detection algorithm. The falloff is manifested in the DEM as greater variation in elevation between DEM cells as the point cloud density declines. The 3DOBS algorithm uses a technique called focal statistics to identify sudden changes in elevation in a DEM. Where the point cloud density is high enough, the 3DOBS algorithm correctly identifies patches and spalls. As the point cloud density declines, the space between LiDAR pulse returns becomes large enough for the algorithm to classify the area between pulses as a spall, artificially increasing the area classified as spalled. For a detailed explanation of how the spall detection algorithm works, see the 3DOBS final report section.

Two sets of bridge data are reviewed here, one where the LiDAR derived DEM was effective at characterizing spalls near the LiDAR scanner and another where the falloff in point cloud density made the data unusable for detecting spalls on the bridge deck.

7.2.3.1. Mannsiding Road Over US-127 North Bound

With the deteriorated state of the medium-resolution LiDAR point cloud and over saturation of the predicted defect metrics, the overall determination of the spalling amount for the reinforced concrete deck to any accuracy was impossible. As a result of the lowered resolution data capture on the northeast approach, the estimated percentage of defect surface area from the ScanStation C10 data was 57% of the total bridge deck surface area. The established ground truth measure, 3DOBS, predicted that the defect surface area to be 1.07% of the total bridge deck surface area. Details of the findings are shown in Table 7-2.

However, a spall of significant size was present within the established 56.2 ft capture radius of the southwest approach scan allowing for an evaluation of the capabilities of terrestrial LiDAR under ideal conditions. Figure 7-32 shows the location of the spall in reference to the entire deck, which is highlighted in red. The spall was evaluated with the algorithm under the established input spall parameters. Results from the analysis estimated that the surface area, volume and percent surface area were 2.065 ft^2 (0.285 m^2), 0.067 ft^3 (0.002 m^3) and 0.06% respectively. Figure 7-33 shows an optical image and the predicted spall area image from the algorithm for visual comparison. The green color in the predicted spall area image represents the area assumed to be a spall.

Table 7-2: Results from the Mannsiding Road NB full deck evaluation.

Items of Comparison	Total deck evaluation		Difference (%)
	LiDAR	3DOBS	
Bridge surface area	3,458.93 ft^2 (321.3 m^2)		-
Predicted defect area	1,965.1 ft^2 (182.8 m^2)	37.07 ft^2 (3.47 m^2)	5201
Predicted defect volume	777.3 ft^3 (21.8 m^3)	2.66 ft^3 (0.07 m^3)	291
Predicted defect area (%)	57	1.07	5227

(Table header: **Results for Mannsiding Road NB**)
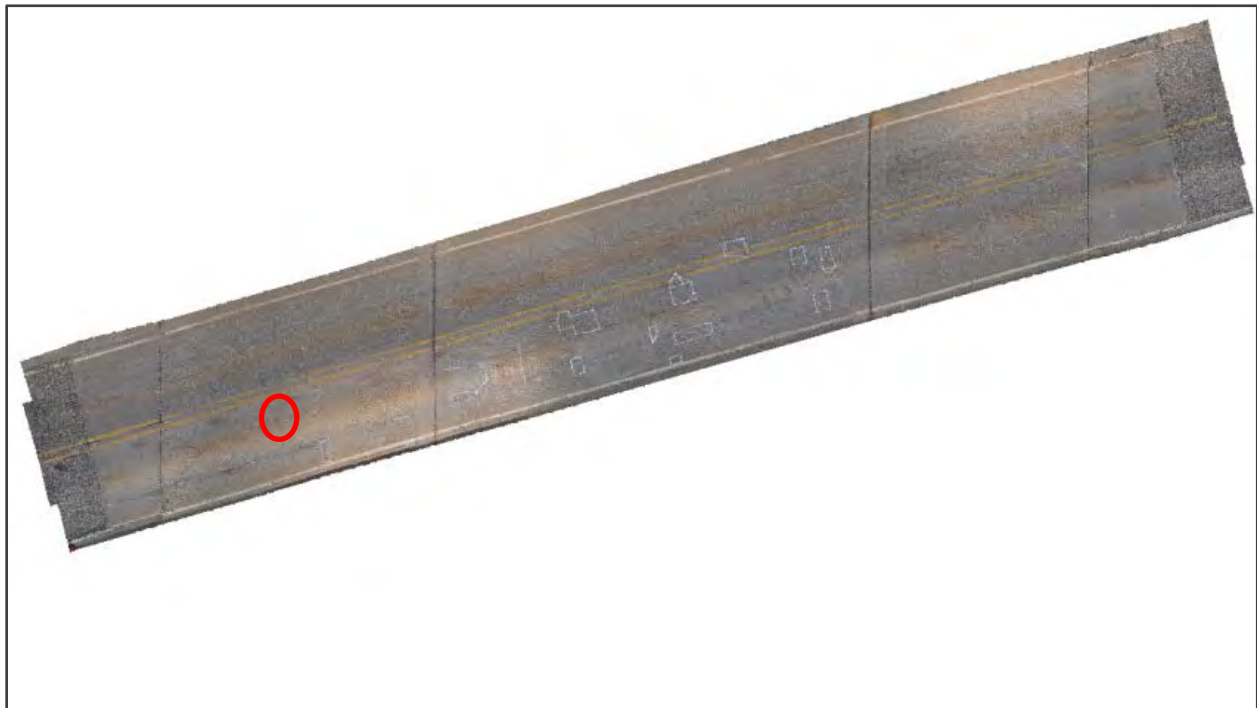
Figure 7-32: Optical image of Mannsiding Road NB showing evaluated spall location.
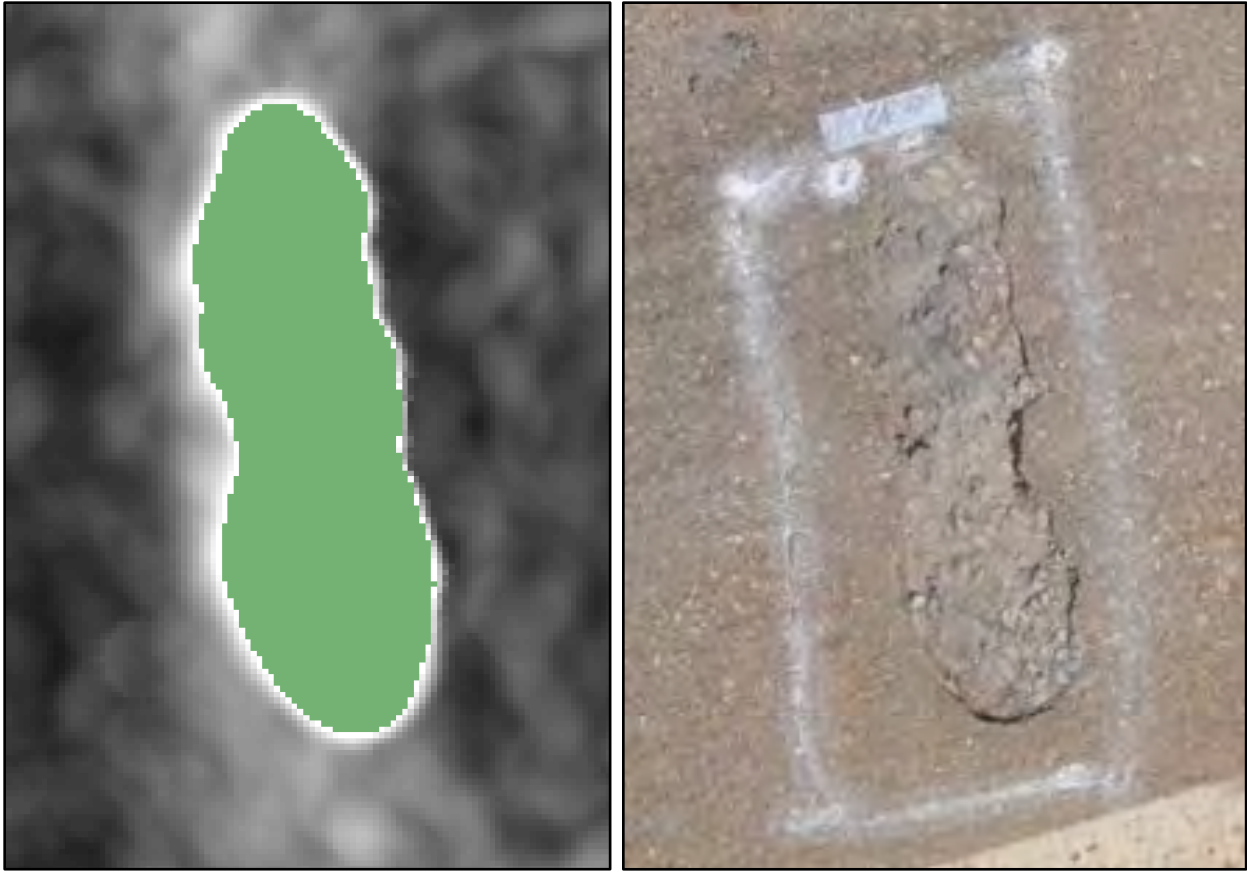
Figure 7-33: Optical image and the predicted spall area image for visual comparison.

3DOBS estimated that the selected spall surface area, volume and percent surface were 1.696 ft^2 (0.158 m^2), 0.064 ft^3 (0.002 m^3) and 0.049%, respectively. The differences in the three measures were 21.8%, 4.7% and 22.4% demonstrating that terrestrial LiDAR possesses the capabilities of detecting surface defects to an acceptable degree of accuracy when sufficient point density has been collected. Table 7-3 lists dimensions of the evaluated spall for LiDAR, 3DOBS and the difference. The Mannsiding Road NB demonstrated the sensitive nature of the data acquisition procedure and when a suspected defect is within the established maximum radius of capture, determination of the surface condition is possible.

Table 7-3: Isolated section within capture radius on Mannsiding Road NB.

Isolated section within capture radius			
Items of Comparison	LiDAR	3DOBS	**Difference (%)**
Predicted defect area	2.065 ft^2 (0.285 m^2)	1.696 ft^2 (0.158 m^2)	21.8
Predicted defect volume	0.067 ft^3 (0.002 m^3)	0.064 ft^3 (0.002 m^3)	4.7
Predicted defect area (%)	0.06	0.049	22.4

7.2.3.2. Willow Road Over US-23

For Willow Road, the two data collection methods pertaining to the evaluation of the bridge deck condition were high-resolution allowing for the densest point cloud generation possible. With the two deck scans being located on opposite abutments, the point cloud decay was evident along the bridge deck surface once the 56.2 ft maximum radius of capture was exceed from each approach slab. The predicted spall area from the algorithm with the established input parameters was saturated with error in the center portion of the deck point cloud. The estimated percentage of defect surface area from the ScanStation C10 data was 41.9% of the total bridge deck surface area. The established ground truth measure, 3DOBS, predicted that the defect surface area to be 7.34% of the total bridge deck surface area. Details of the findings are shown in Table 7-4.

With the deteriorated state of the point cloud and over saturation of the predicted defect metrics, the overall determination of the reinforced concrete deck to any accuracy was not possible. To further evaluate the capabilities of the technology in ideal conditions, a section of the north shoulder of the deck was selected, which was in a severely deteriorated state. The selected section of the north shoulder was within the 56.2 ft maximum radius of capture. Figure 7-34 shows the location of the selection section of the north shoulder in reference to the entire deck, which is highlighted in red. The shoulder was evaluated with the algorithm under the established input spall parameters. Results from the analysis estimated that the surface area, volume and percent surface area were 9.910 ft^2 (0.922 m^2), 0.647 ft^3 (0.018 m^3) and 0.18% respectively. Figure 7-35 shows an optical image and the predicted spall area image from the algorithm for visual comparison. The green color in the predicted spall area image represents the assumed spalled area.

Table 7-4: Results from the Willow Road full deck evaluation.

Items of Comparison	Total deck evaluation		Difference (%)
	LiDAR	3DOBS	
Bridge surface area	5,416.8 ft^2 (503.7 m^2)		-
Predicted defect area	2,272.3 ft^2 (211.3 m^2)	397.6 ft^2 (37.0 m^2)	472
Predicted defect volume	300.1 ft^3 (8.4 m^3)	70.7 ft^3 (2.0 m^3)	325
Predicted defect area (%)	41.9	7.3	474

Note: "Results for Willow Road" is the table's overall header spanning all columns.
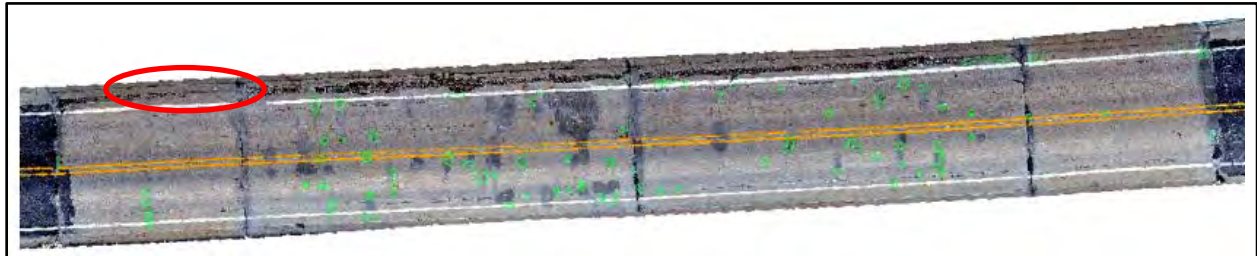
Figure 7-34: Optical image of Willow Road showing evaluated surface defect location

3DOBS estimated that the selected spall surface area, volume and percent surface were 8.310 ft^2 (0.772 m^2), 0.600 ft^3 (0.017 m^3) and 0.15%, respectively. The variations in the three measures were 19.3%, 7.8% and 20.0%, showing that when LiDAR is used within its limitations of maximum capture radius and resolution, accurate quantification of metrics can be made. Table 7-5 lists dimensions of the evaluated spall for LiDAR, 3DOBS and the difference.
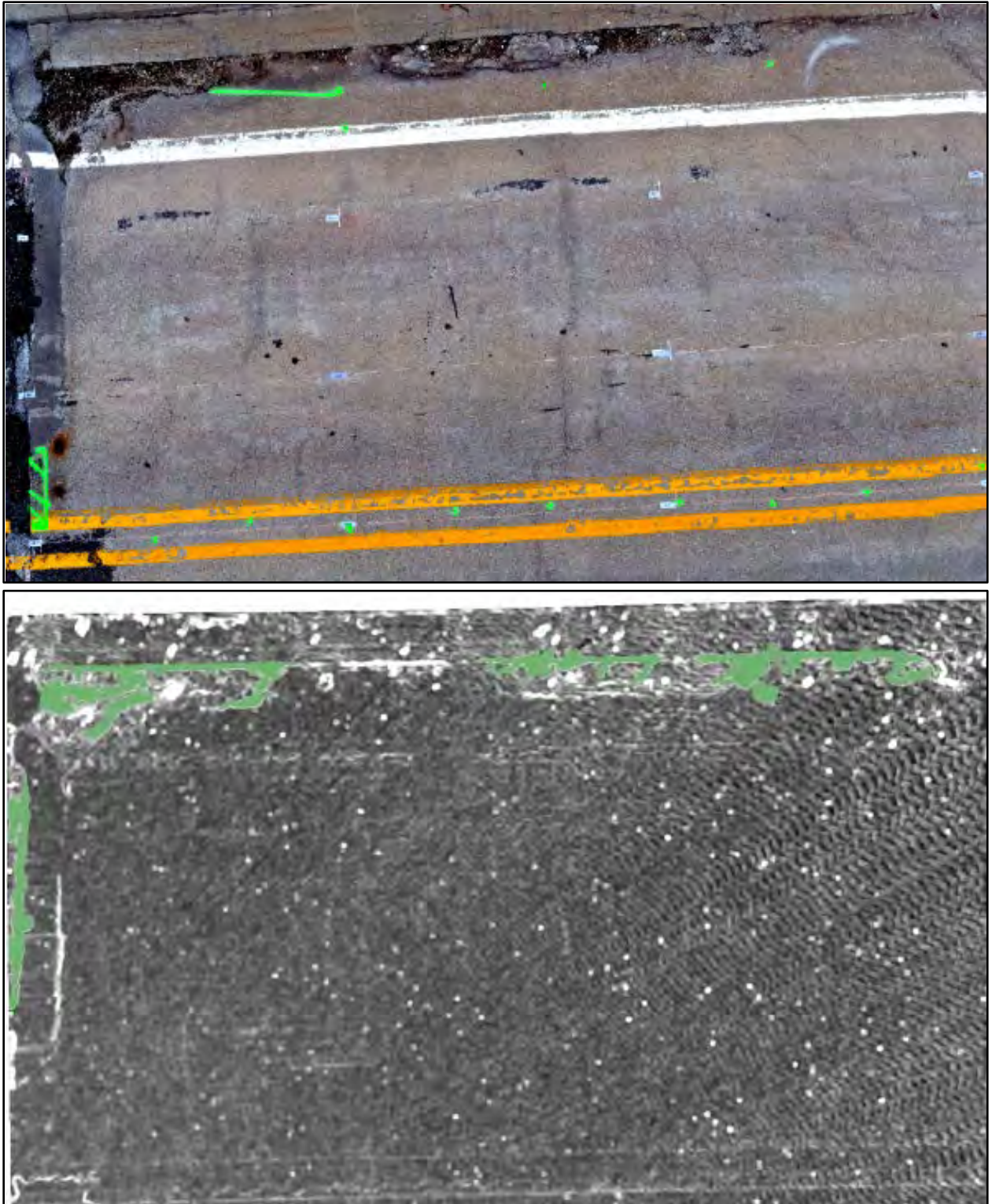
Figure 7-35: Optical image and the predicted spall area image for visual comparison.

Table 7-5: Isolated section within capture radius on Willow Road bridge.

Isolated section within capture radius			
Items of Comparison	**LiDAR**	**3DOBS**	**Difference (%)**
Predicted defect area	9.91 ft^2 (0.922 m^2)	8.310 ft^2 (0.772 m^2)	19.3
Predicted defect volume	0.647 ft^3 (0.018 m^3)	0.600 ft^3 (0.017 m^3)	7.8
Predicted defect area (%)	0.18	0.15	20.0

7.2.3.3. Freer Road over I-94

For Freer Road, the two data collection methods pertaining to the evaluation of the bridge deck condition were high-resolution allowing for the densest point cloud generation possible. With the two deck scans being located on opposite abutments, the point cloud decay was evident along the bridge deck surface once the 56.2 ft maximum radius of capture was exceed from each approach slab. The predicted spall area from the algorithm with the established input parameters was saturated with error in the center portion of the deck point cloud. The estimated percentage of defect surface area from the ScanStation C10 data was 15.5% of the total bridge deck surface area. The established ground truth measure, 3DOBS, predicted that the defect surface area to be 0.89% of the total bridge deck surface area. Details of the findings are shown in Table 7-6.

With the deteriorated state of the point cloud and over saturation of the predicted defect metrics, the overall determination of the reinforced concrete deck to any accuracy was not possible with the collected LiDAR data. Differing for Mannsiding Road NB and Willow Road field demonstrations, Freer Road contained few significant surface deterioration or shoulder distress. Evaluation under ideal conditions was unable to be completed on Freer Road due to the limited quantity of surface defects. The limited quantity of surface defects was expected; the selection parameters established during the field demonstration selection desired a case study bridge with a rating of "satisfactory" (aka "fair") under the NBI rating system (as of 2010, Freer Road bridge NBI deck surface rating was 6 according to the most recent MDOT inspection report). The result from this particular field demonstration shows the overestimation of the LiDAR system, when no surface defects are present to accentuate the spall area and volume estimations. The overestimation is caused by the rapid point cloud density decay.

Table 7-6: Results from the Freer Road full deck evaluation.

Items of Comparison	Total deck evaluation		Difference (%)
	LiDAR	3DOBS	
Bridge surface area	5805.7 ft^2 (539.9 m^2)		-
Predicted defect area	896.8 ft^2 (83.4 m^2)	51.8 ft^2 (4.8 m^2)	1631
Predicted defect volume	72.5 ft^3 (2.0 m^3)	2.9 ft^3 (0.08 m^3)	2400
Predicted defect area (%)	15.45	0.89	1636

Results for Freer Road

7.2.3.4. Mannsiding Road Over US-127 South Bound

For Mannsiding Road SB, the short span of the bridge and the collection of data from the two established locations at high-resolution produced the most dense point cloud over the entire bridge deck. Limited point cloud decay was visible in the spall algorithm output. The estimated percentage of defect surface area from the ScanStation C10 data was 3.1% of the total bridge deck surface area. The established ground truth measure, 3DOBS, predicted that the defect surface area to be 1.4% of the total bridge deck surface area. Details of the findings are shown in Table 7-7.

With the short span and high-resolution data collection techniques performed at the two established scan locations, the estimated defect metrics were similar. Also to be noted is that the profile graph provided in the previous section showed that the bridge had negligible camber and was sloped from the southwest to the northeast approach. The absence of the arch and the sloped surface allowed for an increase in the coverage angle, further allowing for increased line of slight from the receiver to the middle span of the bridge.

Table 7-7: Results from the Mannsiding Road SB full deck evaluation.

Results for Mannsiding Road SB			
Items of Comparison	**Total deck evaluation**		**Difference (%)**
	LiDAR	3DOBS	
Bridge surface area	3403.2 ft^2 (316.5 m^2)		-
Predicted defect area	106.4 ft^2 (9.9 m^2)	46.5 ft^2 (4.32 m^2)	129
Predicted defect volume	6.6 ft^3 (0.18 m^3)	2.94 ft^3 (0.08 m^3)	125
Predicted defect area (%)	3.1	1.4	121

The evaluation under ideal conditions was unable to be completed on Mannsiding Road SB due to the limited quantity of surface defects. The limited quantity of surface defects was unexpected because the "Supplemental" bridge was not initially investigated and surface defects were not documented. However, the results showed that the potential for the arch and angle of the bridge could greatly affect the clarity of collected data. Unfortunately, no additional testing was performed on this matter, but further research could evolve this hypothesis allowing for a better understanding on the technology's capabilities and limitations.

7.2.4. International Roughness Index Using Light Detection and Ranging Digital Elevation Models

LiDAR technology was also incorporated to measure the roughness of the bridge deck surface. The roughness was measured using the IRI, as was done with 3DOBS. Using the DEMs derived from the LiDAR data, the roughness would be measured remotely, therefore determining if IRI results from the LiDAR data could be comparable to the success of the 3DOBS system.

In order to determine the IRI for each bridge using LiDAR technology, the same methodology was used as when the 3DOBS evaluated bridge deck surface roughness. The ratings were dependent upon a longitudinal profile, the quarter-car and 250 mm wavelength models that simulate the response of a tire to the bridge's pavement. The longitudinal profile was created from the DEM, which was processed through the two models in ProVAL. The final result was the IRI number ranging from 0 m/km to 20 m/km; a perfectly smooth surface and an extremely rough unpaved surface, respectively (Figure 7-36).
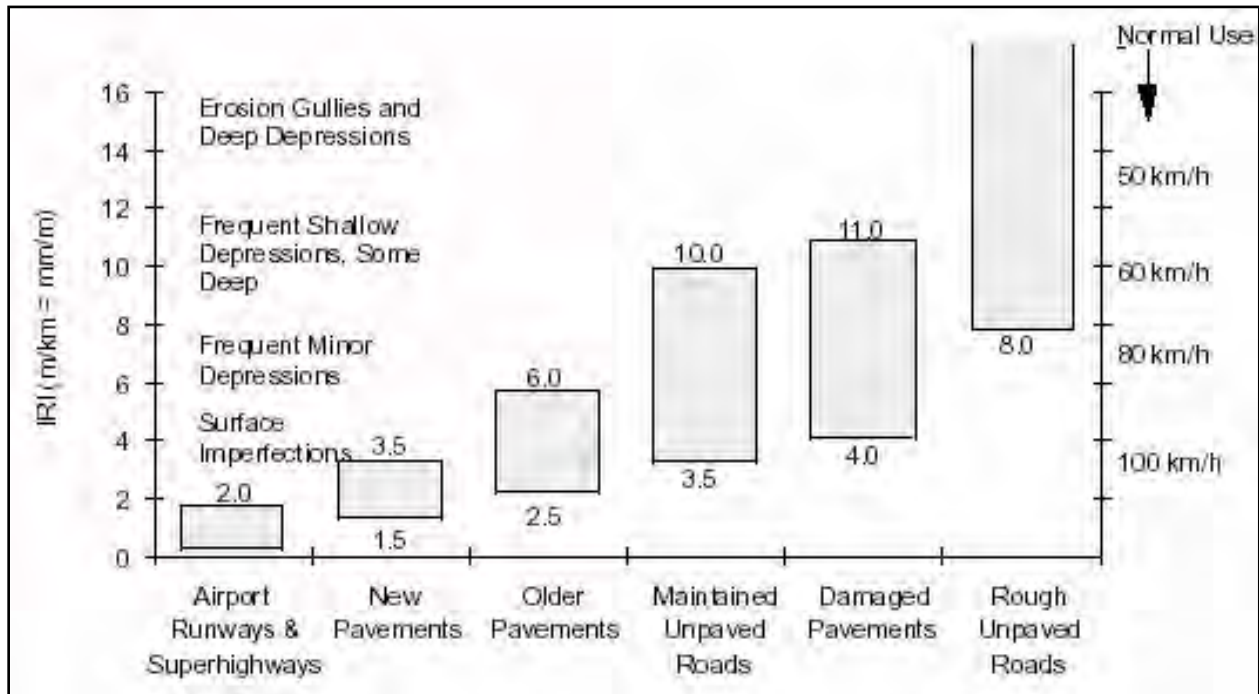
Figure 7-36: The IRI graph

While it was demonstrated that these methods would work using the 3DOBS and produced reasonable results, the LiDAR results proved to be not as reliable. During the first trials, the LiDAR profiles were not representative of the entire bridge deck surface, but still clearly indicated that they looked different from the profiles created using the 3DOBS (Figure 7-37). Instead of representing the bridge deck surface roughness, it appeared to represent the pavement's crowned profile. After running these two profiles through the quarter-car and 250 mm wavelength models, the IRI values were evaluated to be between 12.41 m/km and 15.01 m/km. According to the IRI graph, this would classify the bridge at Freer Road as rough and unpaved. However, the 3DOBS classified the bridge as a more realistic older pavement with IRI values between 3.59 m/km and 4.26 m/km (Figure 7-38). Given that Freer Road Bridge is known to be an older paved surface, the LiDAR IRI results and methodology were determined to be erroneous and the processing methodology was revised.
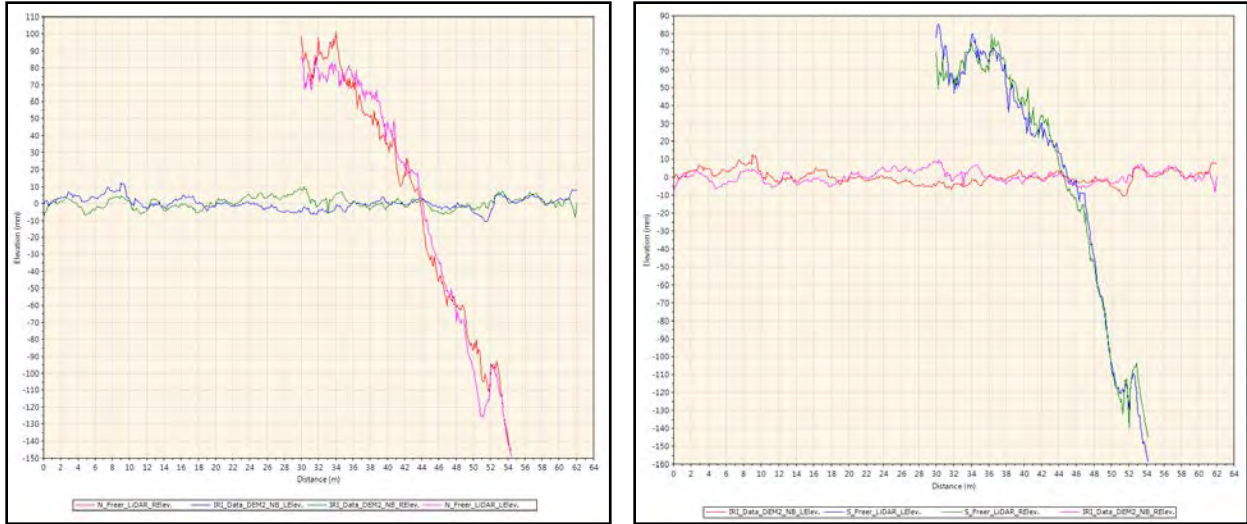
Figure 7-37: 3DOBS/LiDAR longitudinal profiles of north Freer Road (left) and south Freer Road (right).

	File	Profile	IRI (m/km)
>	N_Freer_LiDAR	LElev.	12.87
	N_Freer_LiDAR	RElev.	15.01
	S_Freer_LiDAR	LElev.	12.41
	S_Freer_LiDAR	RElev.	12.52

	File	Profile	IRI (m/km)
>	IRI_Data_DEM2_NB	LElev.	3.59
	IRI_Data_DEM2_NB	RElev.	4.26
	IRI_Data_DEM2_SB	LElev.	4.14
	IRI_Data_DEM2_SB	RElev.	3.71

Figure 7-38: IRI values for LiDAR (left) and 3DOBS (right) transects across Freer Road.

The first revision incorporated residuals calculated from the LiDAR longitudinal profiles. The residual plots were meant to represent the bridge deck surface roughness and therefore lower the IRI values. However, after completing the analysis the IRI values were reduced to 1.38 m/km and 1.17 m/km; values associated with airport runways and superhighways (Figure 7-39). A potential source of IRI error in the LiDAR measurements is the decrease in point cloud density with distance from the scanner as discussed previously. As the distance from the sensor increases, the point cloud density decreases. As a result, the problem may exist because as the profile line transects the data, it is not able to collect as much data towards the middle of the bridge. To resolve this, elevation data was collected closer to the sensor's location and in a smaller quantity. This was demonstrated by using a line segment of 3 m located near the highest point density. Once the shorter segment data was extracted from the DEM and processed through the two models, the IRI results improved to more likely values, similar to the 3DOBS results. The longitudinal profile still looked different from the 3DOBS profile, but produced IRI values of 4.56 m/km and 4.86 m/km (Figure 7-40). Both of these values would place the deck surface into the older pavement category.

Figure 7-39: The residual longitudinal profile and IRI values of Willow Road Bridge.
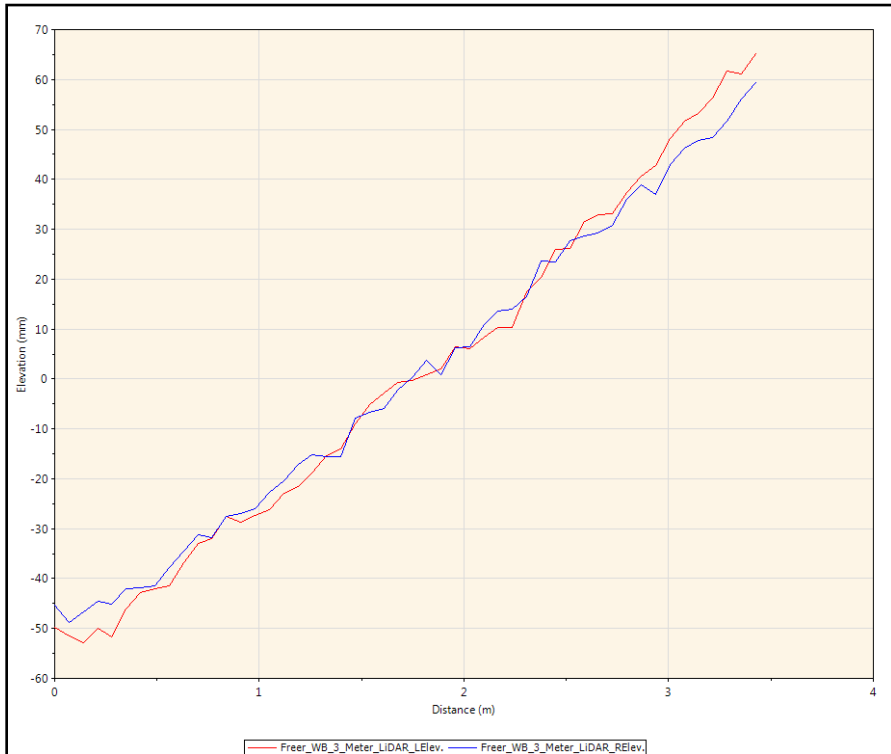
Figure 7-40: LiDAR longitudinal profile and IRI values, 3 m.

Although the LiDAR based IRI results eventually produced reasonable values, the methodology behind attaining them made the process less readily usable than the 3DOBS data. The biggest problem seemed to be due to the fact that the sensor is kept stationary while collecting the raw data. This caused the point cloudy density to change along the bridge and therefore the IRI data to only be useful in small increments near high point cloud areas. As evident by the multiple LiDAR IRI test that were completed, an entire bridge span worth of LiDAR IRI data is less practical due to set up and data collection time. Changes, such as the use of mobile LiDAR, would have to be incorporated to create an even point cloud density along the entire bridge span. This may change how the longitudinal profile looks and cause it to look more like a 3DOBS profile. With these modifications, a direct comparison between the two technologies and their ability to measure surface roughness would be possible.

7.3. Challenges for Implementation, Costing Comments, Data Fusion With Other Technologies, and Future Plans

Terrestrial LiDAR shows the potential to be a useful technology for characterizing concrete bridge deck condition when sufficient point density is collected. With the increasing acceptance of terrestrial LiDAR in the civil engineering industry as an as-built surveying tool and an inventory data generator, limited changes to the data collection process would be required to use a LiDAR dataset to assess bridge condition. The technology is applicable to any concrete or asphalt surface inspection, allowing for accurate generation of surface condition metrics if appropriate data collection protocols are followed.

The data collection process used during the full-scale field demonstration required bridge and lane closure to minimize the exposure of the survey crew to traffic hazards. To minimize the requirement for lane restrictions, mobile LiDAR is an option that should be further explored. Testing and evaluation of mobile LiDAR scanners should be considered to develop hardware and software (along with scan configuration procedures) capable of collecting and processing useful bridge surface data at near highway speeds.

The nature of terrestrial LiDAR and the findings from this research demonstrate that the remote sensing system utilizing terrestrial LiDAR to characterize bridge deck condition would not be practical without significant traffic disruption. However, terrestrial LiDAR has the potential to assess other parts of the bridge structure, such as areas on the underside and fascia, which would be difficult for mobile LiDAR or 3D photogrammetric systems to accurately characterize. Ultimately, terrestrial LiDAR has the capability to accurately characterize bridge deck condition. With further research into the capabilities of mobile LiDAR, a remote sensing, highway speed surface defect detection system could be feasible.

7.3.1.   Sensing Bridge Surface Condition

The research conducted concluded that the point cloud decay rate is not linear, but rather exponential. When the data was collected at a rate of 50,000 points/second, the exponential decay resulted in the establishment of a maximum coverage radius of 56.2 ft. Evaluation of the entire bridge deck data was performed to reinforce the conclusion of the exponential point cloud decay and the maximum coverage radius.

Full bridge deck results when compared to the established ground truth of 3DOBS demonstrated that the limited point cloud density in the middle of the field demonstration data developed an overestimation of the damage surface. The difference in the calculated percentage of damage surface area for the "Poor", "Fair" and "Satisfactory" between the LiDAR and 3DOBS data was 55.93%, 34.6%, and 14.56% respectively. No definitive trend can be established, because of the limited amount of unique field demonstration locations.

However, the two damaged features located within the maximum radius of coverage on Mannsiding Road NB and Willow Road showed the potential of the technology. The difference in the calculated percentage of the damaged features located on Mannsiding Road bridge NB and Willow Road bridge between the LiDAR and 3DOBS data were 0.011% and 0.03%, respectively.

The small variation between the two technologies definitively shows that terrestrial LiDAR has the capabilities of sensing surface defects to an acceptable accuracy.

7.4.   Conclusions

The goal of this thesis was to evaluate the surface defect detection capability of terrestrial LiDAR for reinforced concrete bridge decks. LiDAR, whether collected from a terrestrial scanner or by a mobile platform can only sense the surface of the bridge structure. It should be considered as part of a remote sensing package, along with other technologies (e.g., Thermal IR, SAR) capable of determining the subsurface condition of the bridge structure.

The evaluation of the terrestrial LiDAR system was accomplished through the collection and processing of data from four separate field demonstration locations. Processing allowed for characterization of the minimum resolvable surface defect, maximum conservable distance from LiDAR unit for detection, determination of point cloud density decay and algorithm limitations. While these characterizations allow for current federal, state and private agencies to repurpose current terrestrial LiDAR systems to enhance the reinforced concrete bridge deck inspection practice, there are still many improvements which can be made.

The evaluated data collected by the ScanStation C10 unit can sense surface defects to a high degree of accuracy, but is dependent on five parameters; angle of incidence, coverage angle,

collection rate, reflectivity, height of collection platform. The coverage angle was shown to rapidly decrease the further away from the terrestrial LiDAR unit. The angle of incidence increased at a similar magnitude to the coverage angle. The result was limited return of scattered light the further away from the receiver the object of interest became. The increase in coverage angle and angle of incidence resulted in a decrease in point cloud density with distance from the scanner location. Point cloud density does not decay in a linear fashion, but rather as an exponential function that approaches an asymptote between the centers of the two scan locations. The result of the exponential point cloud decay was the establishment of a maximum radius of capture of 56.2 ft for the ScanStation C10, collecting at the highest data collection settings of 50,000 pps.

Surface damage sensed within the maximum coverage radius was comparable to the established ground truth measure, 3DOBS, with reasonable accuracy. The difference in the calculated percentage of the sample damaged features located on Mannsiding Road NB and Willow Road between the LiDAR and 3DOBS data were 0.011% and 0.03%, respectively. The small variation between the two technologies shows that terrestrial LiDAR has the capabilities of sensing surface defects to an acceptable accuracy.

7.5.   Potential Future Work

Areas have been identified where future studies are warranted. These areas were outside the scope of the current research and would require additional study and/or testing to fully investigate. Suggestions for future work include the following:

Current literature regarding performance evaluation research for terrestrial LiDAR systems has mainly performed spherical target recognition precision testing. Spherical target always presents a constant detectable surface area, which allows for limited angle of incidence to be developed. By evaluating a planar surface at varying distances, a firm understanding of the target recognition precision would be established to better model bridge surface defects. With the issue of the dramatic point cloud density fall off as the object distance from the terrestrial LiDAR system increased, it was theorized that the reduction in the coverage angle associated with the bridge induced camber. A study to test the relative effect of volume estimation by introducing camber into a test specimen with a constant artificial defect present.

An investigation into alternative LiDAR platforms, such as aerial and mobile for highway infrastructure inspection purposes, should be conducted. By transitioning to a moving platform LiDAR system, uniform and sufficient point cloud density to analyze bridge surface defects such as spalls maybe obtainable. A literature review should be conducted pertaining to the state of the practice to gain a complete understanding of the moving LiDAR platforms. Laboratory and field testing could follow, if deemed feasible.

Research seems warranted into the capabilities of multi-platform LiDAR systems for evaluation and surface defect detection of aged asphalt. With aged asphalt, the light reflectance index is raised due to the loss of asphalt binder, which may allow for substantial contrast development. A study should consider the elevated light reflectance between aged and fresh asphalt. Detectable surface defects should be evaluated, if found feasible.

8.   Implementation of Thermal Infrared Imagery

Critical conditions of highway bridges within the nation highlight the need for an easily deployable non-destructive tool with the ability to provide meaningful condition information for bridge inspectors and management teams. Delaminations within the concrete bridge decks are one of the indicators of the bridge deteriorating condition, therefore accurate assessment of total area and location of these delaminations can provide invaluable information for prioritizing maintenance funding, during the decision making process. Current practices for detecting delaminations include sounding concrete with a hammer or chain drag. These methods require lane closure over the bridge deck and are not necessarily easy to conduct during a routine bridge inspection. In addition, past studies have demonstrated significant variations in the results from deck delamination surveys carried out by these sounding techniques (Moore, Phares et al. 2000).

Thermal infrared (IR) has been recognized as a non-destructive tool for detecting delaminations and subsurface defects that are not visible to the human-eye. This technology has been cited in the ACI 222 report as a potential tool for detecting delaminations (ACI 2001). ASTM D4788 describes the test method, equipment and environmental conditions for detecting delaminations in concrete bridge decks using this technology (ASTM 2007). This remote sensing technology can yield both qualitative and quantitative indicators of condition. A delamination map, created from the outputs of a Thermal IR bridge inspection, can help to document delaminations and can be used to determine the total area and percentage of delamination over the entire bridge deck. The purpose of this paper is to summarize the results of the laboratory study and deployment of this technology on three concrete bridge decks in Michigan as well as discuss the challenges that a bridge inspector may face during data collection and processing. Applying this technology can provide transportation agencies with useful measures for maintenance and repair decision making.

8.1.   Concepts of Application for Concrete Bridge Evaluation

Thermal IR is a technology based on collecting surface radiant temperature and converting that temperature measurement into a visual image. Thermal IR radiant energy is emitted from all objects that have a temperature greater than absolute zero. The radiant temperature (T_{rad}) of an object is defined by the amount of electromagnetic energy exiting the object in two electromagnetic spectrum windows: 3-5 and 8-14 μm. This value is slightly lower than the true kinetic temperature (T_{kin}) of any object due to the fact that objects are not perfect emitters (Jensen 2007).

Emissivity of the material is the factor that affects the radiant temperature measurement of the material surface and defines the correlation between the true kinetic temperature and the radiant temperature of an object. This correlation is defined with Equation 8-1. Emissivity depends on the amount of radiant flux (the amount of electromagnetic energy exiting an object) emitted from a material and has the value between 0 and 1. This value is typically greater than 0.9 for concrete. Characteristics such as surface roughness, color, moisture content, viewing angle and field of view are some of the factors that can influence the emissivity of objects (Jensen 2007).

$$\varepsilon = \left(\frac{T_{rad}}{T_{kin}}\right)^4$$

Equation 8-1

A thermal IR camera is a tool for collecting the surface radiant temperature data of an object and generating a thermal IR image. Radiation, conduction and convection are three methods of heat transfer that can affect the heat flow through concrete. Although radiated energy is the parameter that can be measured by the camera, the heat conductivity within the concrete and heat convection around the concrete can also influence this measurement. The appropriate emissivity value should be inserted as an input on the camera software while collecting data, in order to achieve temperature results close to the true kinetic temperature. In this project, the emissivity value of 0.95 has been input to the software during both laboratory study and field demonstration. Materials with reflective surfaces, such as duct tape, have lower emissivities compared to concrete therefore these materials will appear with lower temperatures on the image.

The concept behind the application of this technology in concrete bridge evaluation is that the anomalies and subsurface delaminations interrupt the heat transfer through the concrete and appear with different temperatures on the image compared to the area of surrounding sound concrete. During the day, as the ambient temperature increases, concrete absorbs heat and starts emitting radiant energy. Delaminations and air voids within the concrete will resist the heat transfer and warm up at a faster rate compared to the area of the surrounding sound concrete, thus delaminations will appear as hot areas on the thermal IR image. However, during the night, as the ambient temperature decreases, the area of the sound concrete around the delaminations loses heat at a lower rate compared to the delaminations, thus the delaminations appear as cold areas on the thermal IR images (Washer, Fenwick et al. 2009 a).

According to ASTM D4788, a thermal IR camera (0.1˚F thermal resolution), video recorder, video camera, distance measurement device, test vehicle and contact thermometer are the equipment required for this test. A vehicle mounted thermal IR camera and a video recorder are driven over the center of each lane on a bridge deck. The thermal IR camera needs to be mounted on the vehicle in a way that allows the minimum image width of 14 ft. The conventional video

image camera is used with the infrared image to separate patches and surface defects. Bridge deck dryness is a factor that has to be considered during data collection with this method; as moisture on the surface can affect emissivity and reduce the thermal contrast on the thermal IR image (ASTM 2007).

Time of data collection is the most critical factor in a thermal IR bridge inspection. Not all materials in the environment have the same response to ambient temperature change; this causes the variation of the objects' radiant temperature during a 24-hour period for different materials. The term thermal inertia refers to the thermal response of a material to temperature changes. Thermal conductivity, density and thermal capacity are factors that can influence the thermal inertia of the materials. Two thermal crossover times can be identified in the diurnal graphs of radiant temperature of materials. These two times are roughly the local sunrise and local sunset; when the radiant temperatures of the materials are the same and appear with the same temperature on the thermal IR image.

Concrete materials and delaminated areas on a bridge have similar behavior with respect to ambient temperature changes. In a study conducted by Washer et al. on developing thermal IR inspection technology for bridges, it was found that the effective time to perform a test depends on the depth of the delamination. The most contrast appears on the thermal IR image approximately 4 hours after sunrise for a 2 in deep delamination and 7 hours after sunrise for a 3 in deep delamination (Washer, Fenwick et al. 2009 a).

8.2. Limitations of Application and Environmental Effects

Previous studies on thermal IR applications for bridge inspection have reported several limitations that should be considered. Clark et al. highlighted the fact that emissivity of the concrete surface can vary based on the extra materials on the surface, thus the brightness of the materials on the surface does not necessarily correlate with the subsurface concrete defects (Clark, McCann et al. 2003). Factors such as soil, moisture, oil spills, and staining on the concrete surface can appear as hot spots and affect the results of thermal imagery; therefore, taking optical (visible) images of the concrete surface is necessary to enable the inspector to separate these areas from delaminations.

Wind speed, solar energy, ambient temperature and humidity are environmental factors which influence thermal IR images (Washer, Fenwick et al. 2009 b). More advanced thermal IR cameras models have the option to adjust the image based on the relevant humidity and ambient temperature occurring at the time of data collection. The minimum ambient temperature of 32˚F and the maximum wind velocity of 30 mph have been highlighted as upper limits on environmental criteria for performing Thermal IR of concrete bridge decks in ASTM D4788 (ASTM 2007). Washer et al. investigated the effects of variable environmental conditions on

concrete bridge inspections and suggested a maximum wind speed of 8 mph on a sunny day and 10 mph when the surface is not directly exposed to solar energy. Also, it has been noted that consistent solar loading on the concrete can provide a better contrast on a thermal IR image (Washer, Fenwick et al. 2009 b).

Thermal IR inspection is mostly applied for shallow delaminations. The maximum depth of 3 in has been noted in the literature as a limitation of this technology in detecting delaminations. What needs to be considered when interpreting a thermal IR image is the fact that deeper delaminations manifest as areas with less temperature values compared to shallower delaminations.

8.3.   Advantages for Bridge Inspections

The ability of Thermal IR to detect subsurface defects and delaminations, commercial availability, remote sensing, ease of data collection and image interpretation are the advantages which can be beneficial to the regular/biennial bridge inspection practices (Ahlborn, Shuchman et al. 2010). Lab studies for concrete slabs show that this technique is capable of detecting shallow (up to 3 in) delaminations, which can help bridge inspectors identify areas of unsound concrete before they turn into spalls (Ahlborn, Shuchman et al. 2011 b).

Evaluating the top surface of concrete bridge decks has been noted in literature as the main application of thermal IR for bridge inspection as this element is exposed to direct sunlight. This technology also has the potential to be applied at near highway speed over the bridge deck which can help to conduct bridge inspections more frequently and at a faster rate.

Several studies have demonstrated that this technology can also be applied for detecting delamination and damage underneath the deck and within the bridge soffits, which can be critical for passing traffic under the bridge (Washer 2010). Remote sensing characteristic of Thermal IR can reduce traffic disruption and lane closures on and underneath the bridge, as no direct contact is required. Results from can be imported and stored in ArcGIS, thus it allows a bridge management team to review the bridge information easier and facilitates the decision making procedure.

8.4.   Methodology

8.4.1.   Laboratory Experiment

Laboratory experiments have been conducted to prove the concept of for evaluating the concrete bridges. These experiments have been reported in previously submitted technical memorandums (Ahlborn, Shuchman et al. 2011 a; Ahlborn, Shuchman et al. 2011 b). This section summarized the results of laboratory studies that were conducted during this research project.

Laboratory experiments for this study included two phases; (I) Monitoring the variation in surface temperature of a concrete slab and determining the percentage of delamination in a controlled laboratory condition and (II) Investigating the effects of environmental conditions and time of data collection as well as determining the depth of delamination that can be measured.

The FLIR i7 and the FLIR ThermaCAM SC640 were the thermal IR cameras that were used in this research. The i7 camera is a handheld camera which costs about $2,000. Although this camera is easy to use and has the ability to produce similar results as the more expensive cameras, it is not as efficient. This camera has a lower field of view and lower resolution than the more expensive cameras. Not having the options of taking thermal IR images at time increments and taking optical images, as well as thermal IR images, are the main disadvantages of this camera. The ability of the thermal IR camera to take images at time increments is necessary to use this technology at near-highway speed. Taking optical images of the bridge, as well as thermal IR images, is one of the important components of data collection to help bridge inspectors to re-visit the collected data at a later time and separate the surface staining from the delaminated areas. The analysis software is not included in the price of this camera and is purchased separately.

The ThermaCAM SC640, used in this field demo, has the option to collect data at time increments of every one second or less (up to 30 Hz) which helps in collecting the data at near-highway speed and creates a sequence of images for each pass. Also, this camera has the option to collect optical images, as well as thermal IR images, of the surface which helps bridge inspector to collect images and store the data in one device. The proprietary software of this camera has the option to analyze the images and help in detecting and calculating the area of delaminations. The price of this research and development camera is around $40,000.

8.4.1.1. Phase I

The ThermaCAM SC640 and proprietary software were used to monitor the change in temperature and determine the subsurface anomalies within a concrete slab. Laboratory testing was conducted on 6 in deep concrete slab which was built with simulated delaminations. The layout and size of the inclusions are given in Figure 8-1.

The slab was placed outside during winter (around 10 to 20˚F) for over 24 hours and then brought into the lab, which was at a significantly higher temperature than outside (a temperature differential of 71˚F). Thermal IR images were taken inside as the specimen was warming up. Figure 8-2 shows the set-up of this test.

A: 3.5" x 2.75"x1.5" wood located at 2" from the top surface
B: 2 x # 3 rebars located at 4.5" from the top surface
C: 6" x 6"x ¼" Corroded plate located at 2.5" from the top surface
D1: 2.75" x 6" x 5/8" Styrofoam located at 4" from the top surface
D2: 2.5" x 6" x 1.5" Styrofoam located at 4" from the top surface
E: 2" x 12" x 1/8" metal bar located at 4" from the top surface
F1: 2.75" x 6" x 5/8" Styrofoam located at 2" from the top surface
F2: 2.5" x 6" x 1.5" Styrofoam located at 2" from the top surface
G: 4" x 3.5" x 1.5" and1" x 3" x ½" Galvanized scrap metal located at 4" from the top surface
H: 6"x 9"x 0.003" Plastic bag located at 2" from the top surface

Figure 8-1: Layout plan of 48 x 48 x 6 in slab with simulated defects.
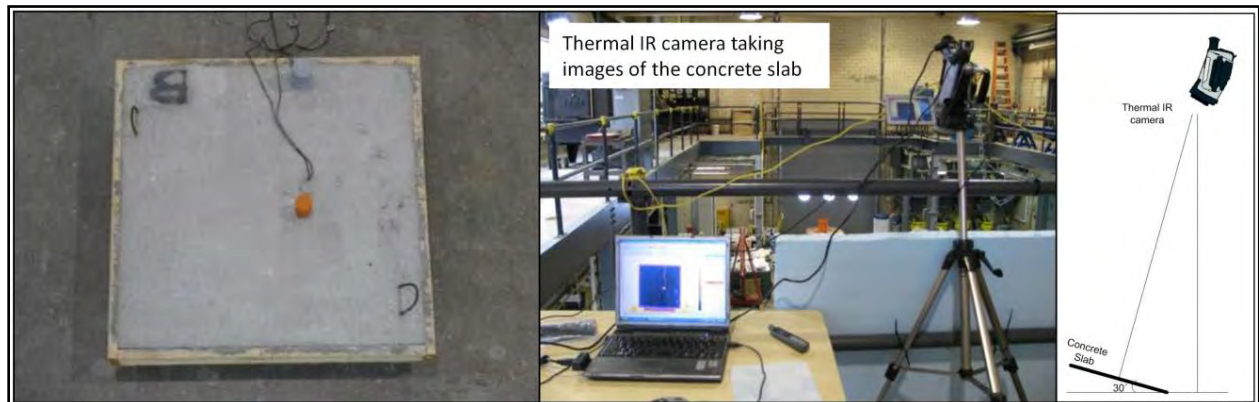
Figure 8-2: Laboratory experimental set-up for a thermal IR test.

The thermal IR camera was set up at a distance of 16.67 ft above the slab to take images every 10 minutes during a seven hour period (9:28 am to 4:30 pm). The indoor lab temperature was 72.3˚F and the relative humidity was 13%. The emissivity was assumed to be 0.95 for the concrete slab Figure 8-3 shows the thermal IR image of the test specimen and the graphs of the temperature change during the seven hour period. Areas 3 and 4 on the image correspond to the F1 and F2 delaminations.
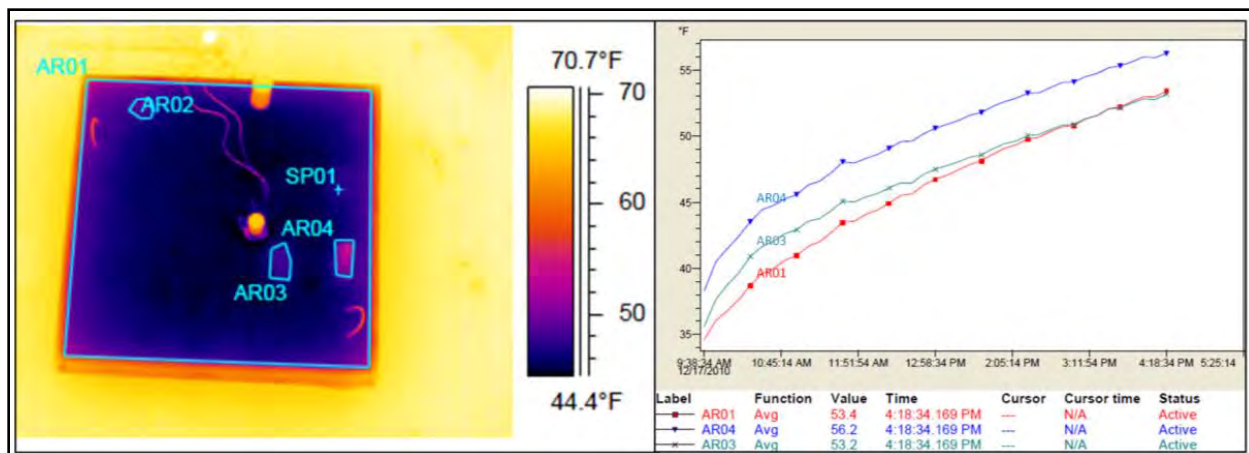
Figure 8-3: Thermal IR image and graphs showing the temperature change of each defect compared to the average temperature of the slab.

8.4.1.1.1.   Proposed Method for Calculating the Area of Delamination

Determining the percentage of delaminated area was one of the objectives of this phase of study to provide valuable information for determining the deficient areas on the concrete bridge deck, soffits and prestressed girders. Note that taking thermal IR images at a normal angle to the slab (camera perpendicular to the slab) provides more accurate results than any other angles.

Two methods were considered to calculate the percentage of delaminated areas. The first one used the thermal IR camera proprietary software to draw boxes around the warmer areas and count the number of pixels within the box. The percentage of delaminated area in this test was determined by using Equation 8-2.

$$Delaminated\ Area\ (\%) = \frac{Number\ of\ Pixels\ of\ Hot\ Area}{Number\ of Pixels\ of\ Slab} x\ 100 \qquad \textbf{Equation 8-2}$$

The second method involved saving the data in a CSV file format and using a spreadsheet to count the number of pixels. In this test, the spreadsheet was set up to highlight the number of pixels within the specific temperature range that best match the thermogram and counted the number of pixels in that range.

One of the errors that appeared in this test was the effect of the thermal gradient from the edge, which made it difficult to assign a pixel to delaminated areas close to the edges. The percentage of delaminated areas can be calculated by using the same equation as the first method. A sample thermal IR image and the associated highlighted Microsoft (MS) Excel spreadsheet are presented

in Figure 8-4. Because delaminations appear with higher temperature, pixels with higher temperatures than a threshold value can be highlighted in a way to match the bright area on the associated thermal IR image. This threshold value is different for each image due to the various temperature ranges between images taken at different time and environmental conditions. Matching the area between the spreadsheet and thermal IR image is subjective and based on the user interpretation of the thermal IR image. For comparison purposes, the actual percentage of delamination was 1.78%. The proprietary software computed 1.61% and the simplified post-processing using a spreadsheet computed 1.84% of the concrete slab area was delaminated.
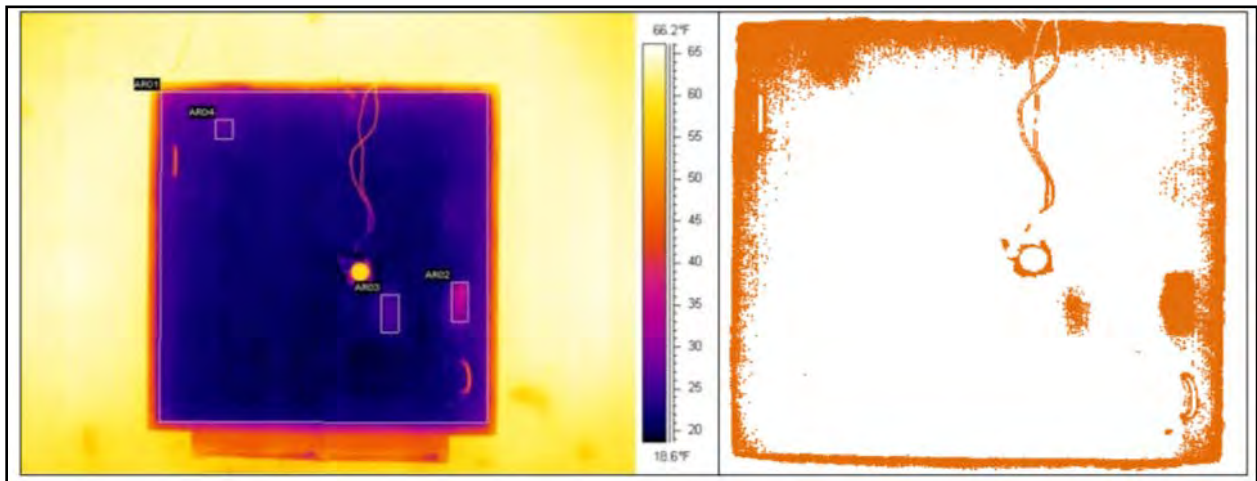
Figure 8-4: Thermal IR image and the associated Excel spreadsheet.

8.4.1.2. Phase II

To study the effect of time of day in data collection, the same concrete specimen that was used for the previous phase was put outside and thermal IR images were taken at two different times. Figure 8-5 shows these images which were taken at 8:18 am and close to 10:59 am to highlight the time of day factor affecting Thermal IR. A i7 handheld thermal IR camera was used for this phase of the experiment.

Determining the depth of delamination that can be identified was the next step of this phase. To achieve this objective, a concrete slab was built with simulated delaminations (6 x 6 x 1/8 in cardboard squares placed at different depths; 0.5, 1, 1.5, and 2 in) and a thermal IR image was taken around noon to have the maximum contrast on the image. Figure 8-6 demonstrates the plan layout of the concrete slab with the simulated delaminations and spot temperature readings on the thermal IR image. As it has been noted, the deeper delaminations manifest themselves with lower temperatures compared to shallower delaminations.
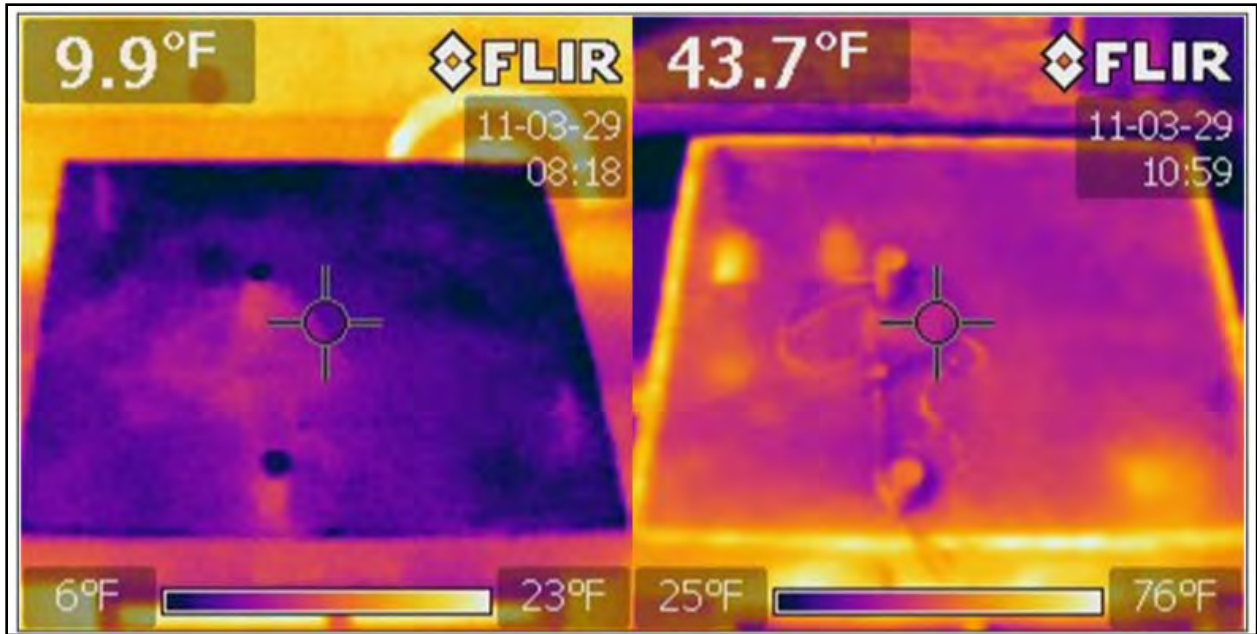
Figure 8-5: Comparison of images of the concrete slab with simulated delaminations, captured at 8:18 am and 10:59 am.
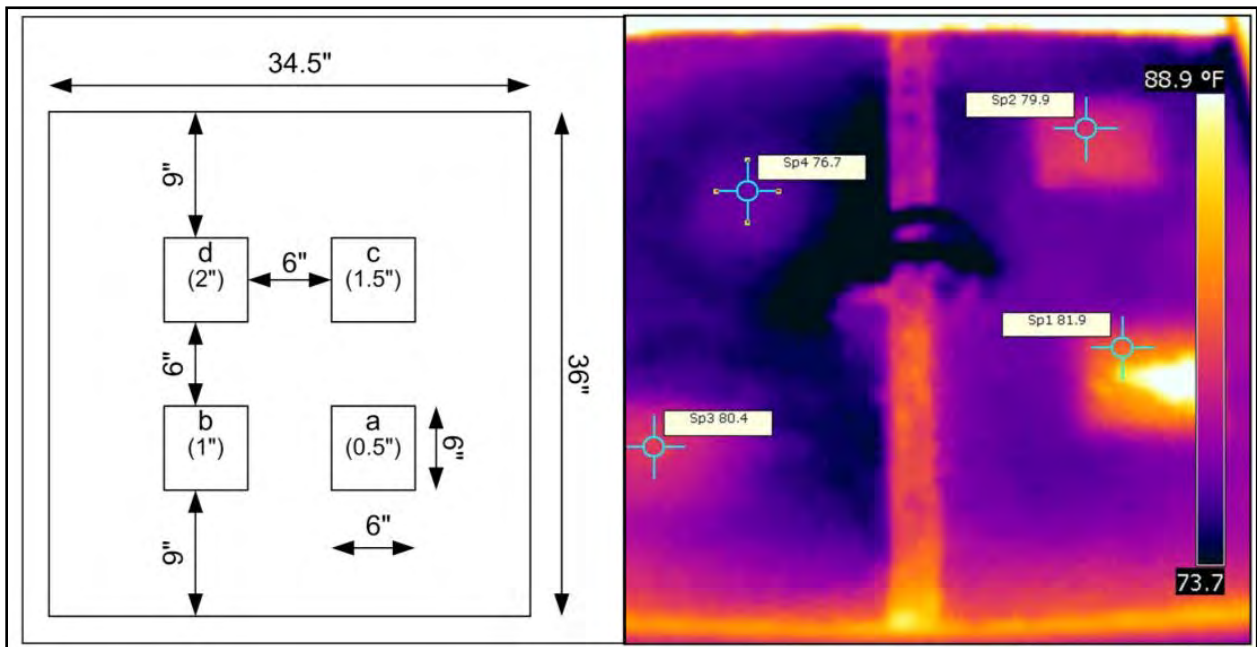
Figure 8-6: Plan layout of the concrete slab with simulated delaminations and the thermal IR image showing the temperature data placed at different depths; 0.5, 1, 1.5 and 2 in.

Figure 8-7 highlights the importance of distinguishing actual delaminations from soil, moisture, oil spills and staining. This figure shows how a surface concrete stain (a residual chemical

released from a cardboard square) on the concrete surface can affect the results by appearing as a higher temperature on the thermal IR image.
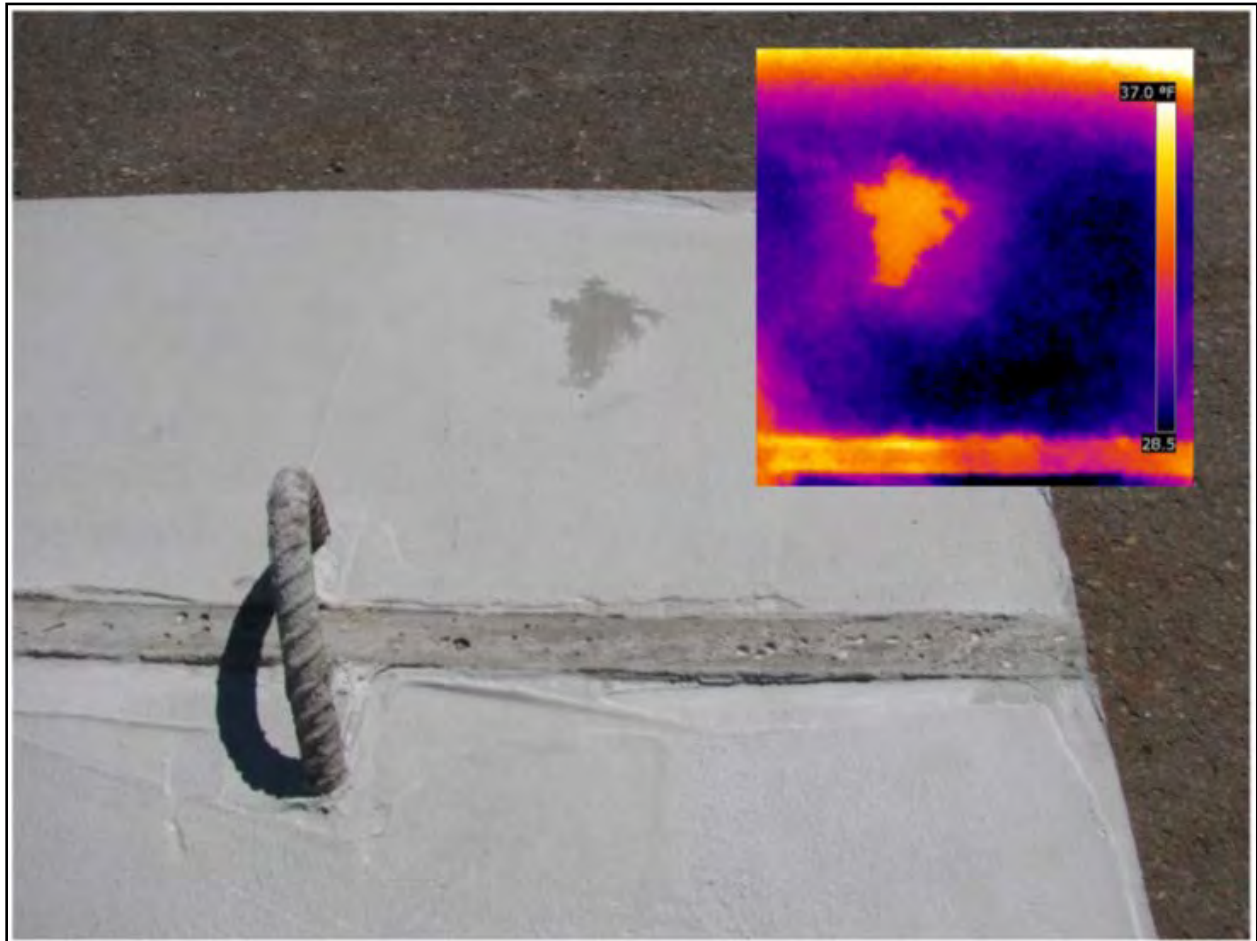
Figure 8-7: Thermal IR image of the chemical staining on the concrete specimen.

8.4.2. Field Deployment Methodology

Implementation of in the field and on a bridge deck is highly dependent on the type of camera and lens. The best possible option is to cover at least one lane (10-12 ft width) in each pass. Increasing the distance between the camera lens and the bridge deck will extend the field of view of the camera and helps in collecting the data in fewer passes over the bridge. The ThermaCAM SC640 that was used in this project had a 24 x 18 (in degrees) lens. This means that this camera should be located 24 ft above the concrete bridge deck to cover the whole lane width in one image, which is not a practical method in the field. Therefore, to collect images on the bridge with this type of camera, several passes were required to cover a single lane. In this field demonstration, the thermal IR camera was installed at 6.2 ft above the deck which could cover a

8-10

2.6 x 2 ft FOV. Images were collected by pulling a cart with the mounted camera over the bridge in ten to twelve passes (5-6 passes for each lane) at walking speed to cover the entire bridge deck.

A grid pattern was laid on the bridge deck before testing. Duct tape was used on the bridge deck every 10 ft in the longitudinal direction and every 4 ft in the transverse direction, to provide reference points on the bridge deck. Duct tape has a reflective surface and low emissivity compared to concrete; therefore, it appears on the thermal IR image with a lower temperature. The use of duct tape enabled the merging of individual images for creation of a full bridge deck thermogram. Figure 8-8 shows a sample grid pattern for field deployment and a working mobile configuration for the camera system on a cart. This proposed data collection method was specific to the camera model and lens that were being used in the study herein. A wider-angle lens could be used to achieve a more ideal data collection scenario.
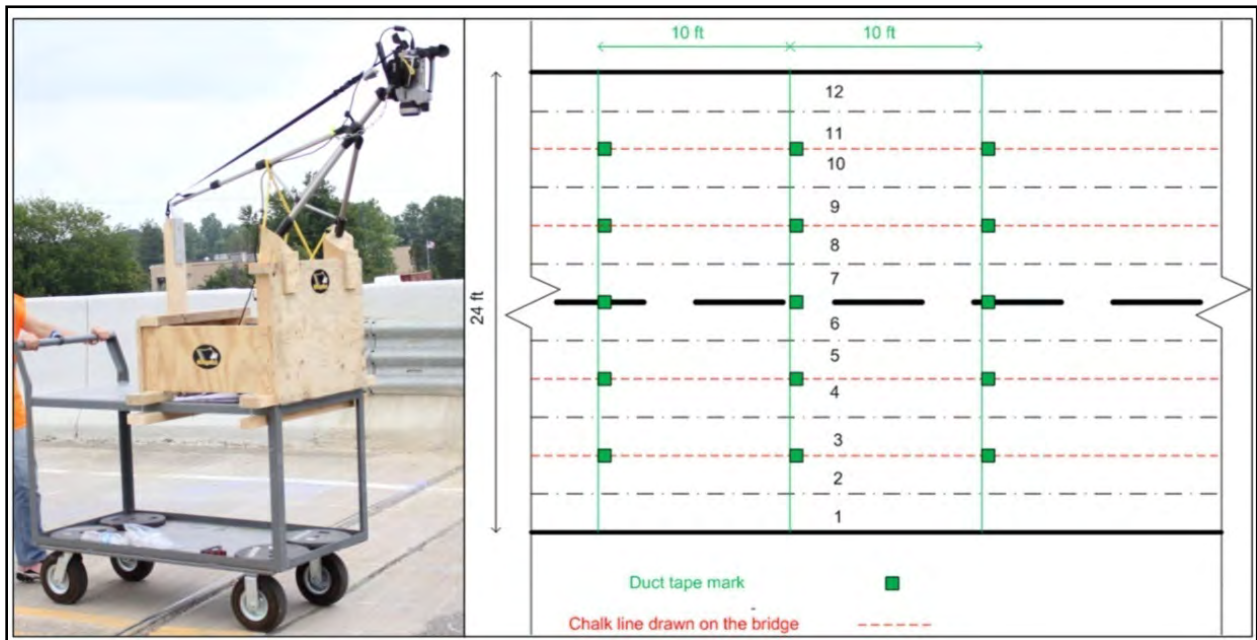
Figure 8-8: Thermal IR camera mobile system and sample grid pattern on the bridge deck.

8.4.2.1. Displaying Field Deployment Results in ArcGIS

The development of a GIS thermal IR map layer in ArcGIS involved the use and conversion of a remotely sensed, high-resolution thermal IR raster dataset into a usable geospatial format. This data was produced in multiple tiles, which were then joined manually in MS PowerPoint to form plan view of the bridge deck and potential delaminations. Conversion of the image to a compatible GIS file was necessary to be able to make measurements and inferences in ArcMap and integrate the data into the bridge condition DSS. First, the PowerPoint image was converted

into a PDF (Portable Document Format) file, and then into a tiff. Because the tiff file is compatible as a GIS layer, no further conversions were required.

Separation of the bridge deck and potential delamation images within the tiff file had to be completed before georeferencing could take place. Using masks created for both sections, each was extracted out of the former PowerPoint slide, and saved as their own tiff file. The bridge deck layer could then be georeferenced to the merged image, which was created by 3DOBS (Figure 8-9). However, the potential delamination layer still had to be edited to remove the borders of tiles that made up the overall image. Manual edits were made in Adobe Photoshop, and afterwards the potential delamination layer was loaded into ArcMap and georeferenced to the high-resolution thermal IR bridge deck. This was possible because during the day, delaminations have a higher temperature than the surrounding sound concrete deck, and appear brighter on the thermal IR image (Figure 8-10).
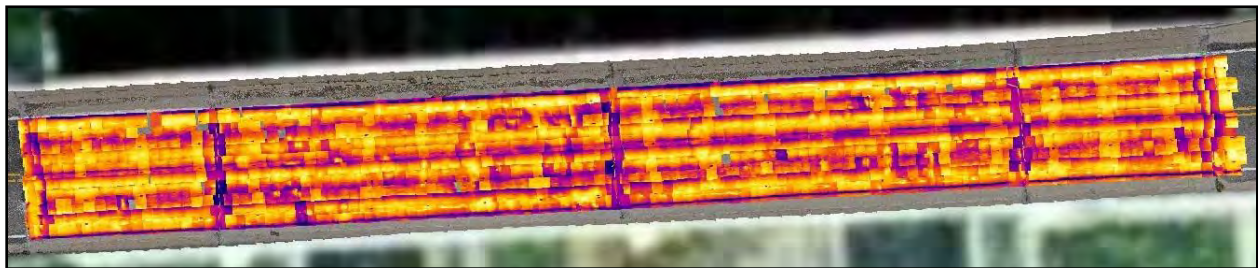
Figure 8-9: Geo-referenced thermal IR map of Willow Road bridge on ArcGIS.

Once the delaminations were positioned correctly, the data was processed through ArcGIS's raster calculator in order to eliminate any excess pixels that were incorrectly labeled as part of a delamination. This procedure reassigned all of the pixel values within this layer; pixels with a red value of "210" or less were given a new value of "1" while pixels with other values were set as "null." The raster calculator layer was then used as a mask to extract pixels from the original delamination layer. These extracted pixels best represented the thermal IR delamination in both size and area. Prior to eliminating these pixels, the total delamination area was very different than results from other methods of area calculation. The delaminations were then converted from a raster layer to a vector polygon layer. The vector layer consisted of delaminations that had interior polygons labeled separately, even though they existed within the same entity. Therefore, all polygons were dissolved, which eliminated the borders of polygons within the same delamination. All remaining polygons then had their areas calculated.
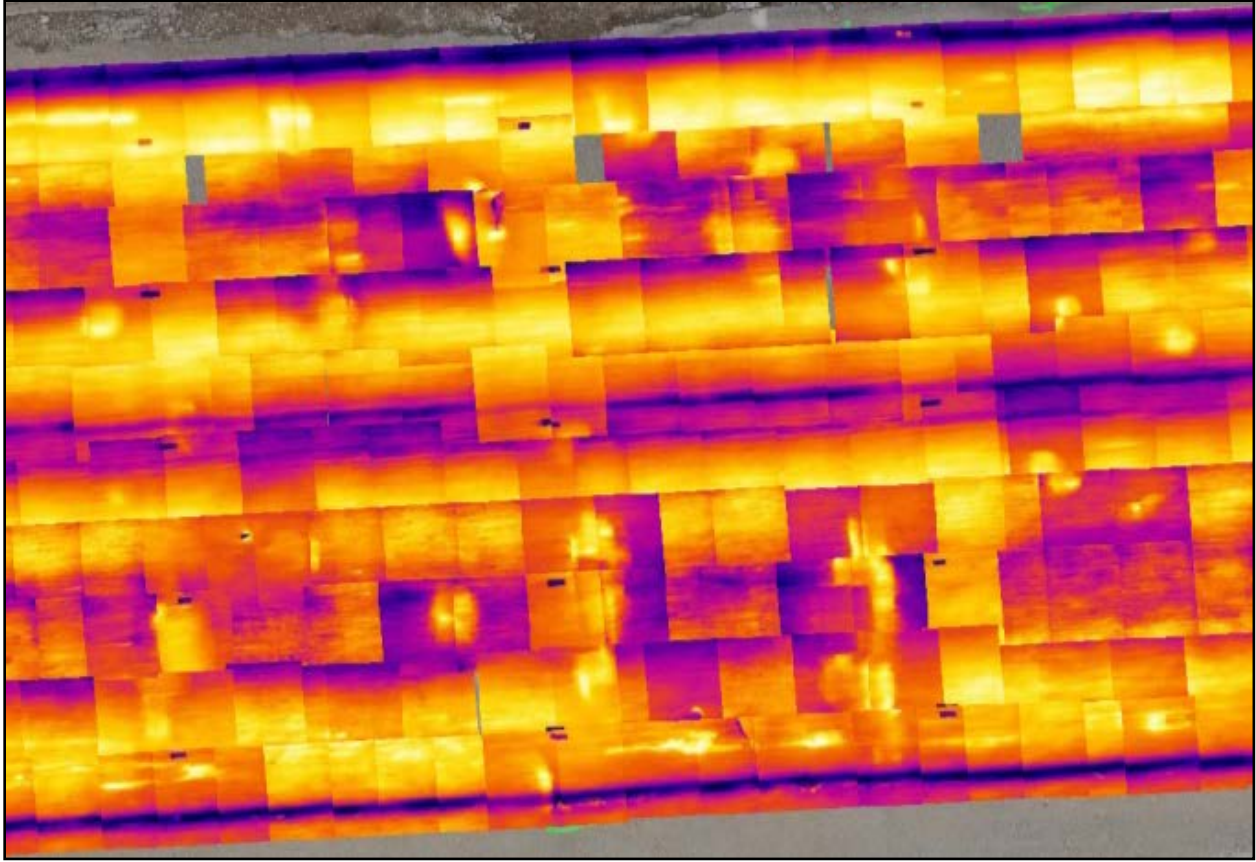
Figure 8-10: Georeferenced thermal IR image on ArcGIS.

8.5.   Results and Discussion

The Thermal IR survey was conducted on three prestressed I-beam bridges with concrete decks in Michigan during August 2011. These three bridges were selected based on their NBI rating to represent for a poor, fair and good condition bridge deck. Results and images of these three selected bridges are discussed in the following sections. Although, the main focus and challenge of this study was trying to collect information from the top of the bridge deck at speed, some images were also taken from the underside of the bridge deck and girders to capture an overall condition for these elements.

8.5.1.   Inspection Results for Top of the Bridge Deck

The Thermal IR survey over the bridge deck was conducted according to the aforementioned described data collection method. Environmental conditions at the time of data collection and the overall rating based on the last inspection are summarized in Table 8-1. Time of data collection specified in this table was the starting time of data collection for each bridge. The total time of data collection for each bridge took approximately one to one and a half hours. Ambient

temperature and humidity were added as inputs in the thermal IR data collection software. Sun direction was another factor that was considered while collecting the data to avoid having any shadow on the images.

Table 8-1: Environmental condition and overall rating (0-9) for each bridge.

Bridge	Last Inspection Date	Overall Condition	Deck NBI rating	Time of Data Collection	Weather Condition	Ambient Temperature (˚F)	Humidity (%)
Freer Road	06/02/2010	Good	6	12:00 pm	Partly Cloudy	96.6	45
Willow Road	04/19/2010	Fair	5	10:50 am	Mostly Cloudy	86.7	54.5
Mannsiding Road (NB)	10/11/2011	Poor	4	11:50 am	Mostly Cloudy	96.4	35.3

After completion of the data collection on the bridge, thermal IR images for each bridge were merged to create an overall map of the bridge deck. A delamination map was created and the percentage of delaminated area was calculated based on the abovementioned proposed spreadsheet method. The thermal IR map and delamination map for Freer Road bridge, Willow Road bridge and Mannsiding Road bridge are demonstrated in Figure 8-11, Figure 8-12 and Figure 8-13, respectively. Although having duct tape on some of the thermal IR images was helpful to create a thermal IR map of the bridge deck, delaminations on these images were not as apparent as the rest of the thermal IR images. Also, the rubber expansion joints on the bridge appeared with higher temperature on the image due to the higher emissivity factor of rubber and it induced some difficulties to detect delaminations within these areas.

8.5.1.1. Comparing Results with Chain Drag and Hammer Sound Inspection Techniques for Bridge Deck

Concurrent with the field deployment, MDOT conducted a delamination survey on these three bridges. The hammer sound technique was used on Freer Road and Willow Road bridges and the chain drag was used for Mannsiding Road bridge. Both of these methods are sounding techniques and based on the bridge inspector expertise in hearing the hollow sound in a delaminated area compared to the surrounding intact area. Delaminated areas for all these three bridges were marked on the bridge deck. Optical (digital) images of the marked areas were taken and merged together to produce a composite image of the entire bridge deck with the sounded delaminations highlighted.
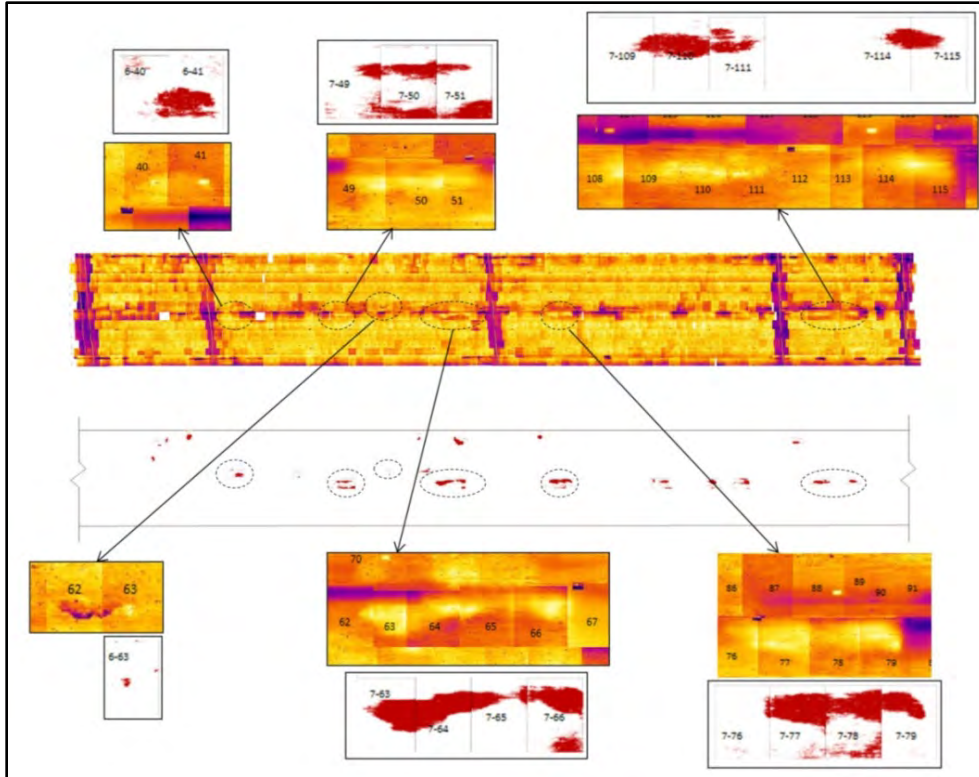
Figure 8-11: Deck delamination map of Freer Road bridge, using Thermal IR and post-processed output data results for a typical spreadsheet analysis.
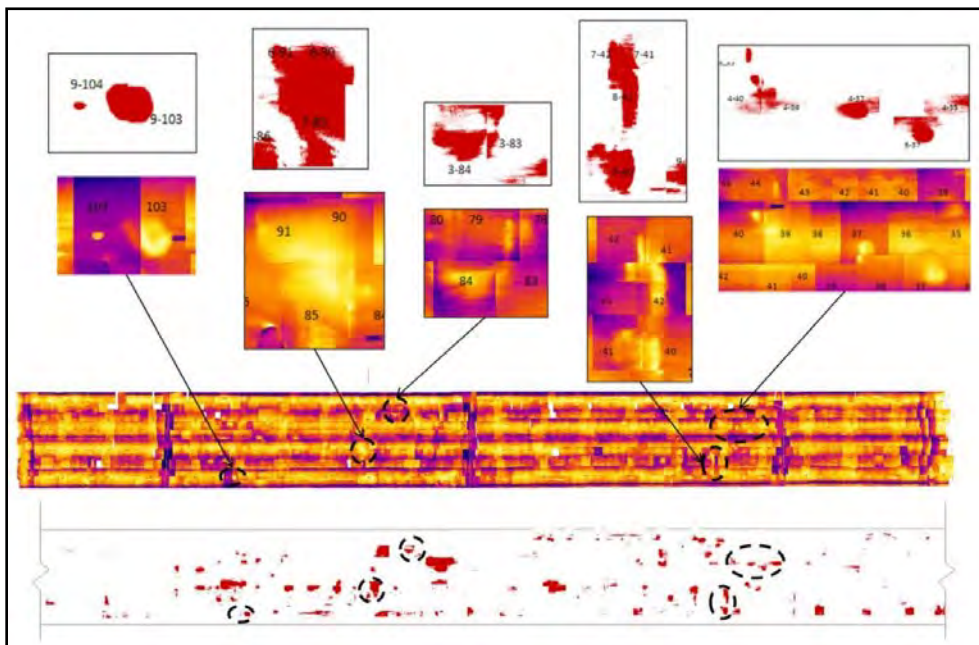
Figure 8-12: Deck delamination map of Willow Road bridge, using Thermal IR and post-processed output data results for a typical spreadsheet analysis.
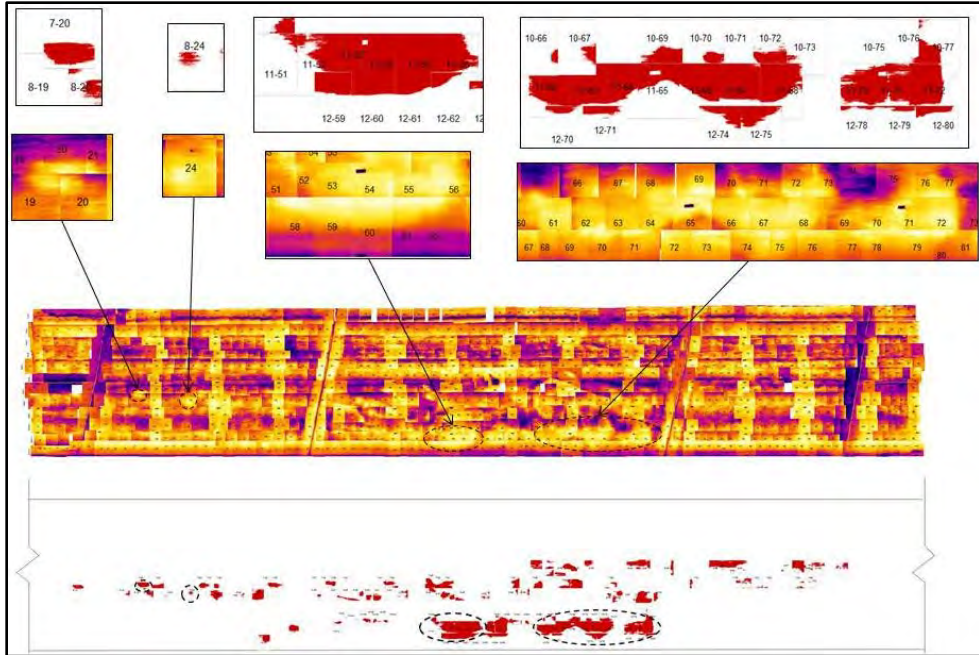
Figure 8-13: Deck delamination map of Mannsiding Road bridge, using Thermal IR and post-processed output data results for a typical spreadsheet analysis.

Delamination maps from both MDOT and Thermal IR surveys were imported into ArcGIS as two separate layers to compare the location and area of each delamination that was detected with each method. The total area of delamination calculated based on the MDOT and Thermal IR surveys for these three bridges as well as the overlapped area between these two surveys have been summarized in Table 8-2. Total area of delamination is the union of the delaminated area that can be detected by sounding or Thermal IR survey. Overlapped area is the intersection between the delaminated areas detected by each method and is the common delaminated area between the two methods.

Table 8-2: Total area of delamination using Thermal IR and MDOT sounding techniques.

Bridge	Delaminated Area (ft^2)						
	MDOT Method	MDOT	Thermal IR	Overlapped Areas	Only MDOT	Only Thermal IR	Thermal IR and MDOT
Freer	Hammer Sound	101.74	29.25	14.13	87.6	15.11	116.8
Willow	Hammer Sound	159.54	157.83	17.49	142.05	140.34	299.9
Mannsiding (NB)	Chain Drag	127.3	136.13	21.43	105.87	114.7	242

Table 8-3 demonstrates the percentage of delaminations, detected by each method, over the entire bridge deck, as well as the percentage of the total delaminations that could be detected by both methods or only by one of the two methods. The overlapped delaminated area between the two methods is also reported as a percentage of the total delaminated area, detected by each method. Delaminated areas presented in these two tables were obtained from the ArcGIS delamination layers. Percentages of the total overlapped area of the bridge was somewhat surprising; however, further analysis were performed on the displayed data on ArcGIS to compare these areas on the small sections over the bridge deck. These analyses are discussed in the following sections for each bridge.

Table 8-3: Percentage of delaminated areas calculated from the results of each delamination survey.

Bridge	Delamination (%)		Percentage of total delamination (%)			Correspondence with each method (%)	
	MDOT	Thermal IR	Common Areas	Only MDOT	Only Thermal IR	MDOT	Thermal IR
Freer	1.80	0.52	12.1	74.97	12.93	13.89	48.31
Willow	3.05	3.02	5.83	47.37	46.8	10.96	11.08
Mannsiding (NB)	3.63	3.88	8.85	43.75	47.4	16.83	15.74

8.5.1.1.1. Freer Road Bridge

Figure 8-14 shows the thermal IR and hammer sound delamination maps for Freer Road bridge displayed as two layers on ArcGIS. The main cause of variation between the results of the MDOT and Thermal IR surveys on the Freer Road bridge is that most of the delaminations on this bridge were around the construction joint and overlapped with the painted centerline on the bridge deck. Reflective paint on the bridge deck has lower emissivity than concrete; therefore, it will appear on the thermal IR image with lower temperature and cause some difficulties in detecting delaminations in those areas. Also, delaminations are most likely to occur around spalled or patched areas, which can help to detect exact location of delaminations based on the thermal IR and optical images.

In order to compare the variations between hammer sound and thermal IR inspections, a virtual grid pattern (4 x 10 ft) was created over the bridge deck in ArcGIS. Delaminated area within each cell that could be detected by either hammer sound or thermal IR camera or both was calculated in ArcGIS and presented in Appendix E. The total area of intersection between Thermal IR and sounding techniques are 12.1% of the total area of delamination that can be

detected by either one of the technologies. Higher correspondence was observed for some sub-section areas such as cell E-13 which shows 40.3% correspondence between Thermal IR and sounding within the total union delaminated areas. Correspondence of this overlapped area with the area detected with Thermal IR and sounding surveys are 72.7 and 47.5%, respectively. This shows that the sounding survey in this specific location detected more delaminations than what was obtained from Thermal IR survey. On the other hand, for cell H-10, total correspondence between Thermal IR and delamination surveys is 9.81%. The overlapped area has a correspondence of 14.4 and 23.5% with the area detected with thermal IR and sounding techniques, respectively. In this cell, contrary to cell E-13, more area of delamination was detected with Thermal IR survey as opposed to sounding.

Larger correspondence was observed for delaminated areas detected by the Thermal IR survey within most grid cells on this bridge. This can be due to overestimating the delaminated area by the sounding survey. However these results must be interpreted with caution due to the effect of the painted centerline influencing the thermal IR images obtained on site. In-depth inspection of data is required to make a decision on the potential areas of delamination that were detected by only one of the two methods and the variances in the results obtained from these two surveys.

8.5.1.1.1. Willow Road Bridge

Delamination and hammer sound maps for Willow Road bridge are demonstrated in Figure 8-15. To compare the variations between hammer sound and thermal IR inspections, the same virtual grid pattern (4 x 10 ft) as Freer Road bridge was created over the bridge deck on ArcGIS (Figure 8-16. Delaminated areas were calculated within each cell and results from both methods were compared. Appendix E provides a summary of this analysis. Total delaminated area for cell G-4 calculated from thermal IR and hammer sound methods are 4.43 and 5.72 ft^2, respectively. The overlapped delaminated area between these two methods in this cell is 3.24 ft^2. Intersection between the results of Thermal IR and sounding surveys for this specific cell is 56.7% of the total delaminated area detected by sounding survey and 73.12% of the total delaminated area detected by Thermal IR inspection. However, the correspondence of the overlapped area with the total delaminated areas that can be detected by either one of the techniques is 46.93%. Values for percentage of correspondence vary between the specified cells and this fairly high correspondence may not be achievable for other areas. Therefore, the total correspondence between the results of Thermal IR and hammer sound surveys for this bridge was calculated as 10.96 and 11.08% of the total delaminated area detected by MDOT and Thermal IR surveys, respectively. This variation was anticipated due to the variations in hammer sound results and not having the ideal environmental condition for Thermal IR during the inspection day.

Figure 8-14: Thermal IR and sounding delamination map and the virtual grid pattern over the Freer Road bridge displayed on ArcGIS.

8.5.1.1.2. Mannsiding Road Bridge North Bound

Figure 8-17 shows thermal IR and hammer sound delamination maps for Mannsiding Road NB on ArcGIS. Similar to the other two bridges, there are some variances between the results of these two techniques that are demonstrated in this figure. A virtual grid pattern, similar to the aforementioned bridges, was created on ArcGIS to compare the results of the two inspection methods considered in this study (Figure 8-18).
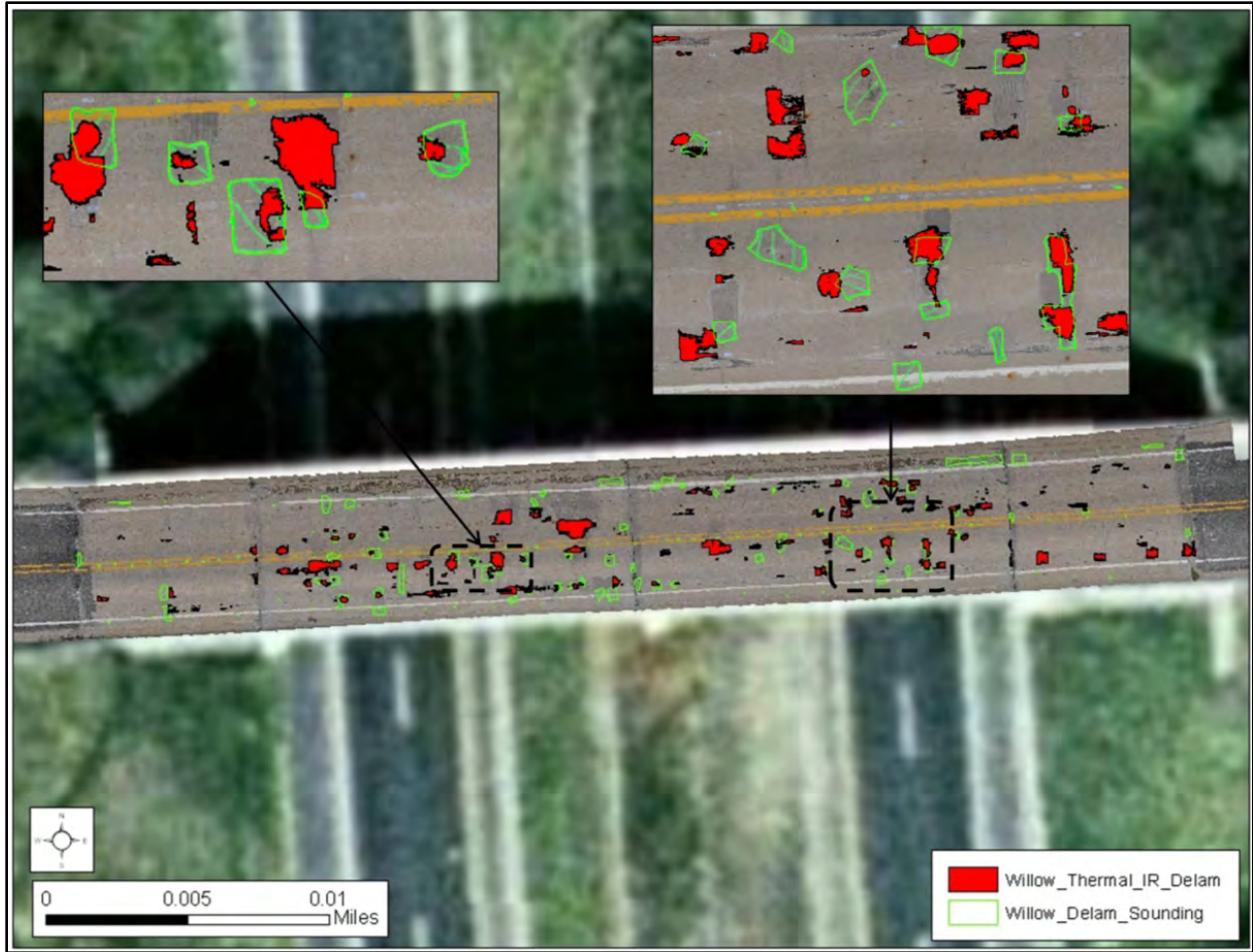
Figure 8-15: Thermal IR delamination map and sounding delamination map of Willow Road bridge displayed on ArcGIS.
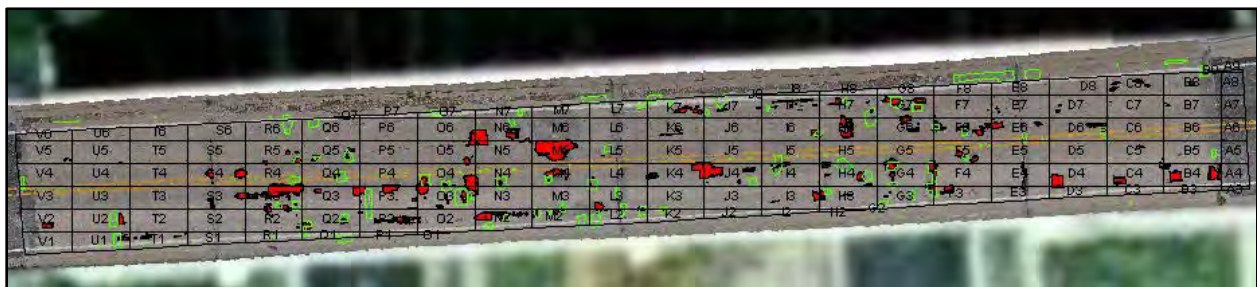
Figure 8-16: Virtual grid pattern over the Willow Road bridge deck.

Figure 8-17: Thermal IR delamination map and sounding delamination map of Mannsiding Road bridge displayed in ArcGIS.
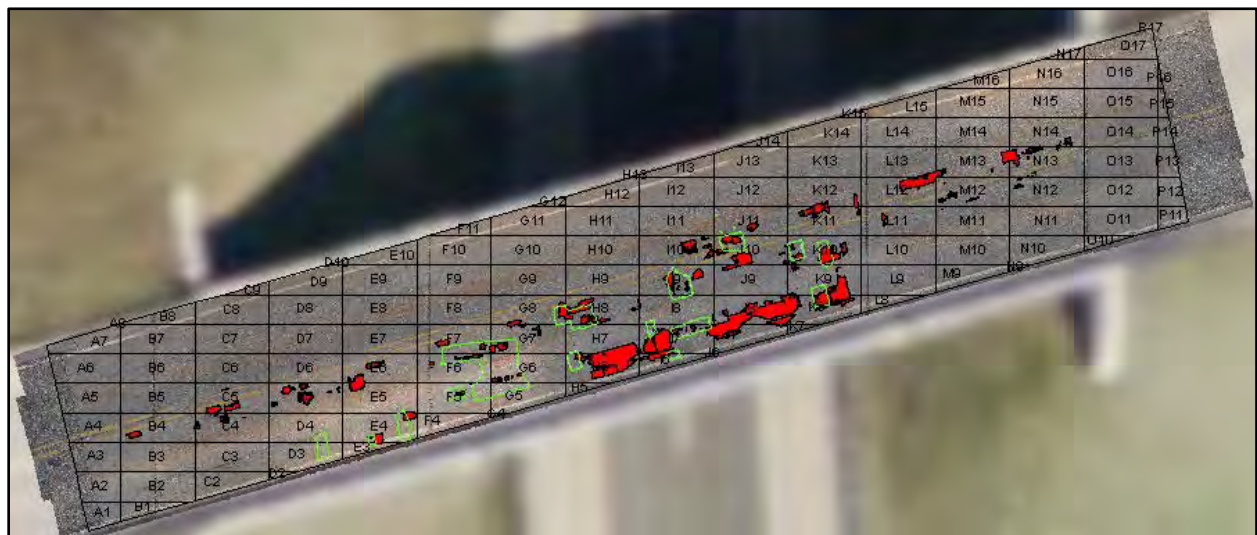
Figure 8-18: Virtual grid pattern over the Mannsiding Road bridge deck.

Maximum correspondence between the results of the Thermal IR and sounding surveys was scrutinized in cell K-10, which shows 33.45% correspondence between the results. For this bridge, deck percentage of correspondence between the overlapped area and the area detected with Thermal IR and sounding surveys are 63.76 and 41.29%, respectively. Similar to the other two bridges, the calculated delamination area and percentages within each cell is included in Appendix E.

Figure 8-19 shows the deck survey results from sounding conducted by MDOT in 2008. Most delaminations were observed on the south side of the bridge in span 2, and this somewhat reflects the sounding and Thermal IR surveys that was conducted in this study in 2011. However, the total delaminated area that was found in the survey performed in 2008 was 176.5 ft^2 (4.4%). The chain drag survey conducted in 2011 found 127.3 ft^2 (3.63%) of delaminated area and reflects the variation that was anticipated within the results of a sounding study.

Due to the variances in the results obtained by sounding and Thermal IR survey, in-depth scoping surveys with destructive methods such as coring are required to make the decision about the exact location of delaminations on this bridge deck.
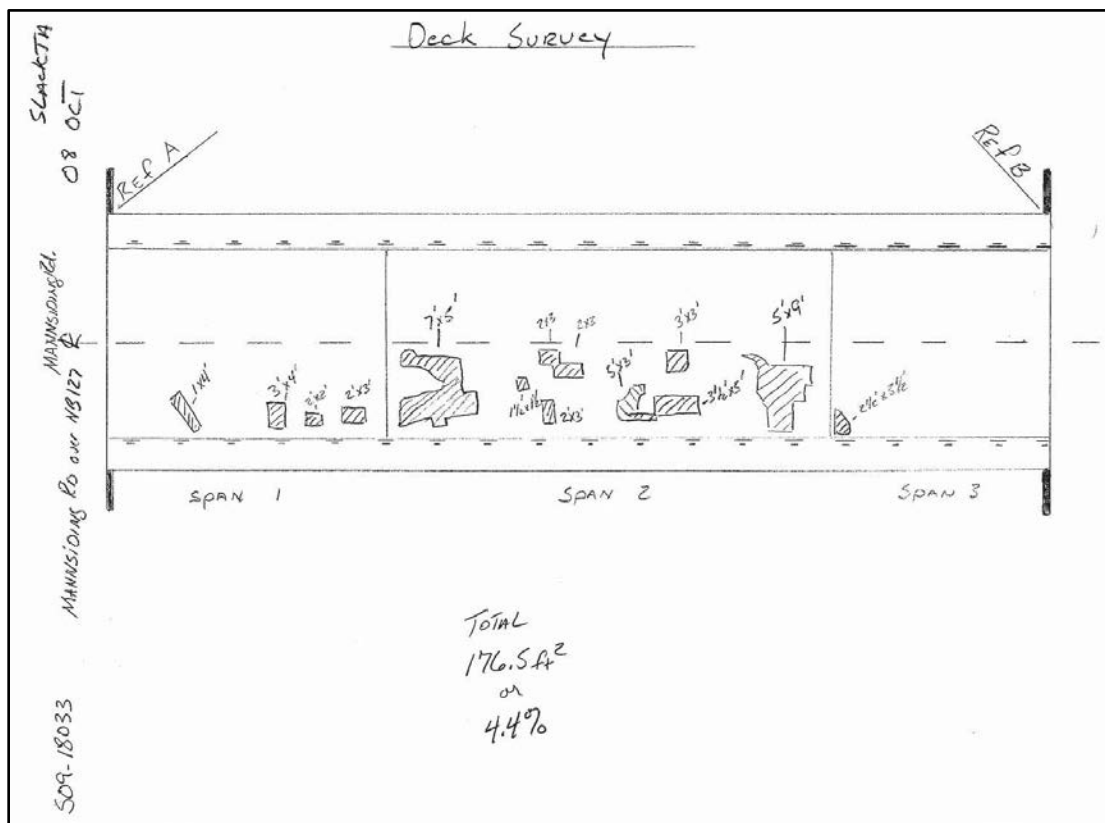
Figure 8-19: Deck survey map for Mannsiding Road Bridge NB developed by MDOT in 2008.

8.5.2. Ground Truth Results

To validate the results obtained from Thermal IR and chain drag surveys on the Mannsiding Road bridge, 10 cores (∅ 12 in) were extracted from the Mannsiding Road bridge deck .The coring was conducted before the partial deck replacement of the Mannsiding Road bridge NB by MDOT.   Figure 8-20 shows the proposed coring locations.

Cores were obtained on the bridge deck by drilling the concrete and pulling out the core with a pry bar. On those locations that no delaminations were present, MDOT inspectors were not be able to extract the cores out. Figure 8-21 shows the coring procedure and Figure 8-22 shows the cores extracted from the bridge deck.
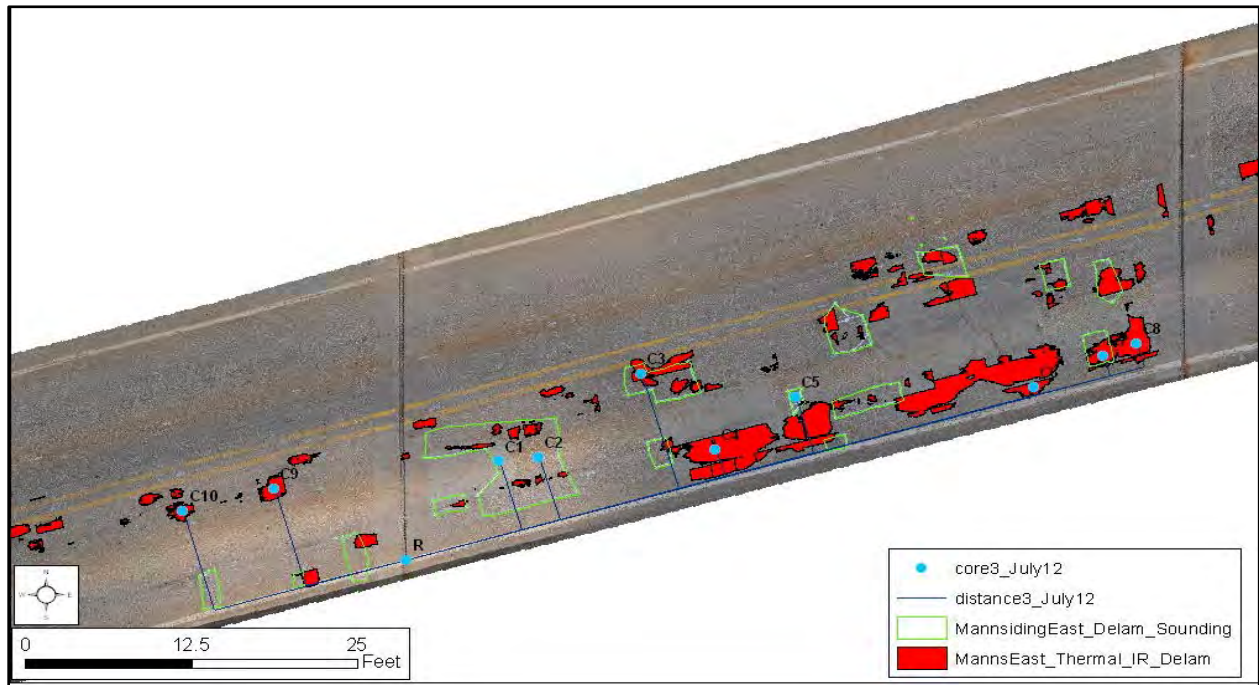
Figure 8-20: Coring plan (blue dots) for Mannsiding Road bridge.

The depth of delamination and repair condition for each core is summarized in Table 8-4. Seven out of the 10 cores showed visible damage. Four out of seven delaminated cores were evident in Thermal IR results. Cores C2 and C5 were 3 in or deeper (3.125 in), thus no delaminations were detected with Thermal IR. This result may be due to the effects of time of data collection and/or overcast conditions.

Figure 8-21: Drilling a core on the bridge deck (a), pulling out the drill (b), and pulling out the core with a pry bar (c).

Figure 8-22: Six of the 10 cores extracted from the Mannsiding Road bridge deck.

Cores C4, C9 and C10 were intact (therefore not included in Figure 8-22) and no delaminations were found within the 3.5 in of the top surface for these locations. The reasons for not properly distinguishing between the delaminated and solid (sound) areas in these locations (C4, C9, and

C10) can be due to delaminated areas possibly being smaller than the $\varnothing 12$ in core or patched areas with different concrete properties that influence the emissivity factor.

Location of delaminated areas on five cores was properly detected using chain drag. Delaminations on cores C6 and C8 were only detected by Thermal IR. These delaminations were closer to the surface. Overall, further investigation is required to determine the efficiency of Thermal IR for detecting delaminations within patched areas or deeper than 3 in.

Table 8-4: Summary of the cores condition and depth of delaminations.

Core	Repair Condition	Ground Truth Results	Chain Drag	Thermal IR
C1	Patched	Delamination at 2.75 in	Yes	No
C2	Not patched	Delamination at 3.125 in	Yes	No
C3	Not Patched	Delamination at 2 in	Yes	Yes
C4	Patched	No delamination	No	Yes
C5	Not patched	Delamination at 3 in	Yes	No
C6	Not Patched	Delamination at 2.75 in	No	Yes
C7	Not patched	Delamination at 3 in	Yes	Yes
C8	Patched	Delamination very close to surface	No	Yes
C9	Not Patched	No delamination	No	Yes
C10	Not Patched	No delamination	No	Yes

8.5.3.   Inspection Results for Bridge Deck Underside and Bridge Girders

Previous literature has suggested that Thermal IR can also be used for bridge soffits and girders (Washer 2010). The possibility of using Thermal IR has been investigated on the three case studies of the research herein. Because all these three bridges were prestressed I-beam bridges, the main challenge was end-beam cracking. No delaminations were found along the girders using either thermal IR or hammer sound inspection. The bridge soffit was another element that was investigated in the current study. Figure 8-23 and Figure 8-24 were taken from the Willow Road and Mannsiding Road bridges. Delaminated areas on these images appeared as cold areas. This may be due to the rainy weather conditions the day before testing and mostly cloudy conditions for both bridges during thermal IR inspection.
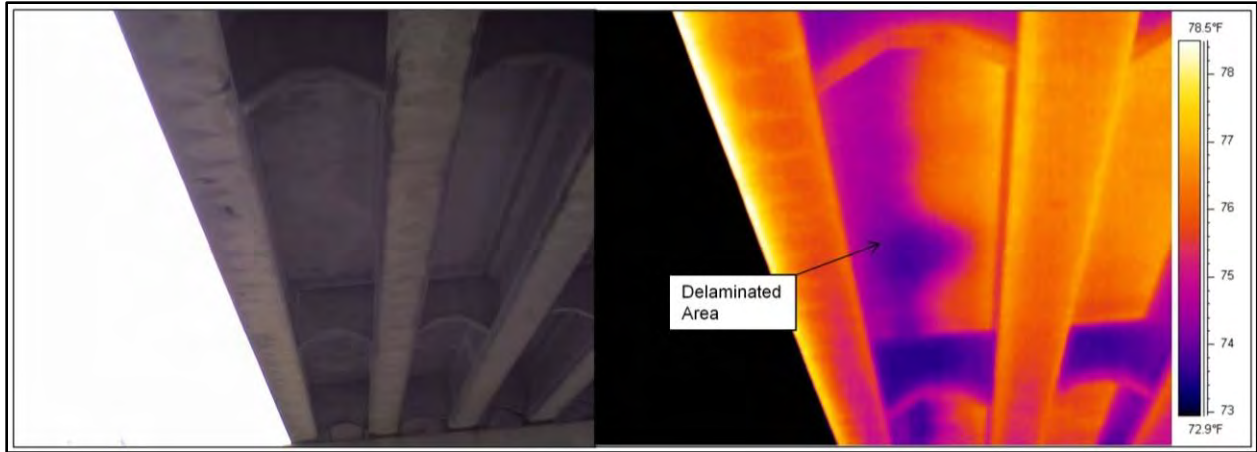
Figure 8-23: Digital and thermal IR image of Willow Road bridge soffit.
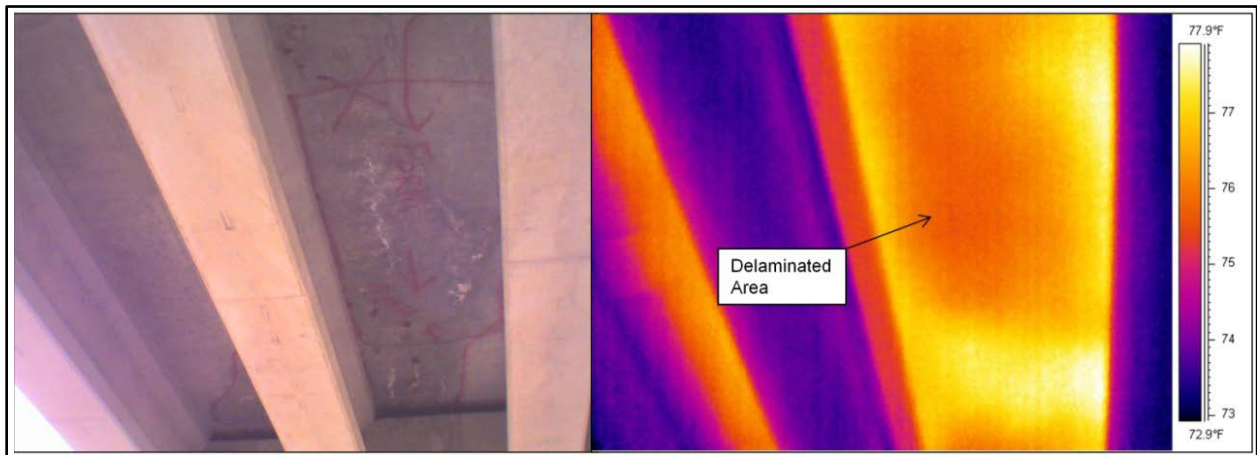
Figure 8-24: Digital and thermal IR image of Mannsiding Road bridge soffit.

Figure 8-25 and Figure 8-26 show digital and thermal IR images taken from the bridge piers under Willow Road and Mannsiding Road bridges. These areas were shown as bright areas (higher temperature) on the thermal IR image.

8.6.   Implementation and Next Steps

Identifying the location and area of delaminations on the bridge deck has always been an important challenge for bridge inspectors during routine bridge inspections. Thermal IR can be a useful tool for bridge inspectors to overcome this challenge by providing qualitative and quantitative information for delaminated areas on the bridge deck. The thermal IR data collection method is highly dependent on the camera system and field of view of the camera being used. However, the main challenge is creating a merged map with highlighted delaminations from thermal IR data that is useful to the bridge management team and bridge inspectors responsible

for ratings. Another important challenge is to remove the bright areas that are not delaminations and just appeared on the thermal IR image due to the differences in emissivity values.
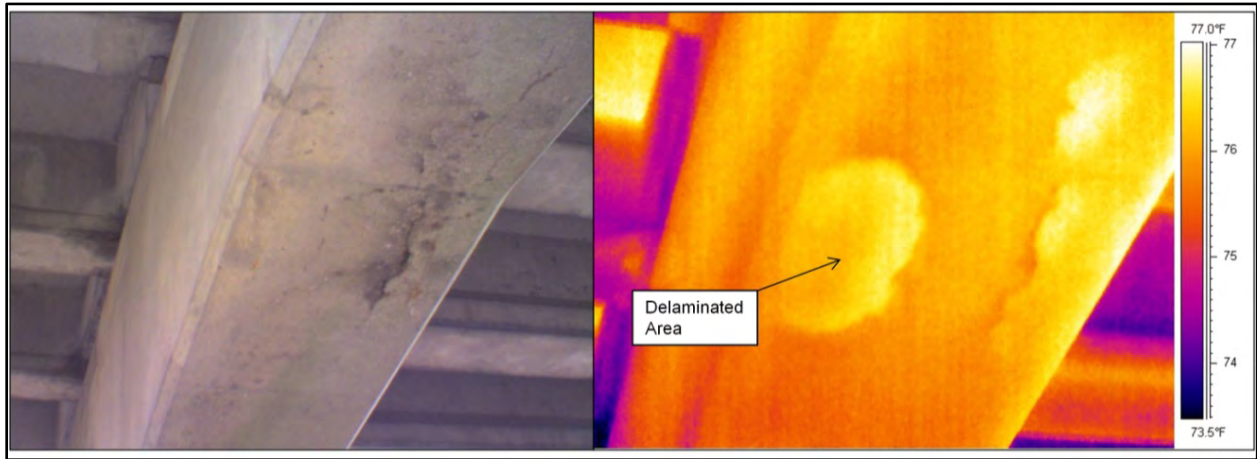
Figure 8-25: Digital and thermal IR image of bridge pier under Willow Road bridge.
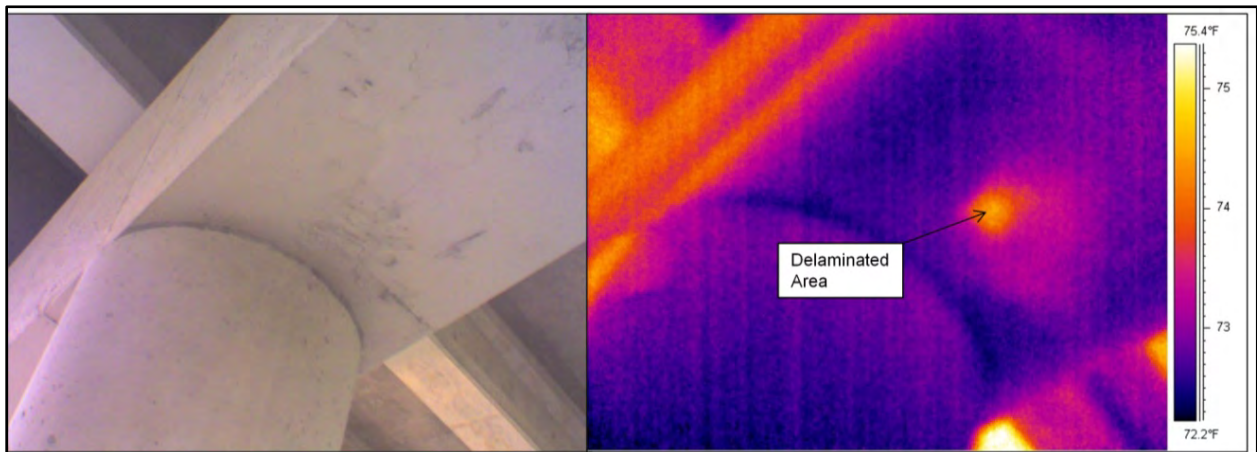
Figure 8-26: Digital and thermal IR image of bridge pier under Mannsiding Road bridge.

Having a grid pattern on the bridge deck is necessary to merge and assign the specific coordinate system, however this can affect the results and it will be more practical to use less duct tape on the bridge deck. Having a camera with larger field of view can solve this issue to some extent, and having less images on the overall bridge deck can make the data procedure faster and more practical. However, caution must be applied in using the wide-angle lens for the thermal IR camera as the edges of the thermal IR images may be distorted and not viable for calculating the number of pixels and area of delamination. Presenting the results of thermal IR bridge inspection in the ArcGIS environment allows for faster location and analysis of bridge deck delaminations.

Also, it will help the bridge management team to compare their results with other delamination survey practices, or combine the results with other inspection methods.

In general, a Thermal IR survey provides a good overview of delaminated and debonded areas within the bridge deck. However, results are highly dependent to the time of data collection. Several inspections during the day may be required to capture delaminations located at different depths, as the shallower delaminations appear on the thermal IR image earlier than the deeper delaminations. Results from this study were compared to the sounding techniques such as hammer sound and chain drag performed by MDOT inspectors. However, the results of these surveys may vary depending on the inspector teams. Therefore, ground truth information is required to validate the results of the Thermal IR survey.

The present study confirms previous findings and contributes additional evidence that suggests Thermal IR is a well-established non-destructive tool for concrete bridge deck inspection. However, further study needs to be conducted to develop an easily deployable system and a less subjective data processing method. Conducting a Thermal IR survey and obtaining quantifiable information will help transportation authorities in prioritizing the maintenance needs during the decision making process.

9.   Evaluation of Digital Image Correlation Method

The condition of transportation infrastructure, specifically bridges, has received a great deal of attention in recent years as a result of catastrophic failures, deteriorating conditions, and even political pressure. The condition of the nation's bridges highlights the necessity for deployable non-destructive techniques for condition assessment. In particular, there is a need to monitor global level behavior with traffic and loading conditions that bridges endure daily. Current bridge inspection techniques consist largely of labor-intensive subjective measures for quantifying deterioration of various bridge elements, but often these assessment methods focus on degradation and not much on the system behavior.

While there have been advances in non-destructive testing techniques such as fiber optics, wireless sensors strain gages, and accelerometers that are used for bridge evaluation, little attention has been given to the application of remote sensing technologies.

The concept of using remote sensing involves using sensor technology to monitor and detect information in a non-contact manner.   Remote sensing technologies can be used to assess and monitor the condition of bridge infrastructure and improve the efficiency of inspection, repair, and rehabilitation efforts while also enhancing safety during evaluation.

Common remote sensing technology can include satellite, RaDAR, and LiDAR; but the non-contact definition recognized allows for incorporation of non-traditional sensors as well when referring to condition assessment for bridges. Reducing the traffic disruption or lane closure is one of the advantageous features of using remote sensing technologies; the sensors do not come in direct contact with the structure.

Therefore, innovative technologies that can obtain structural condition measurements optically could be very efficient in bridge evaluation practices. DIC is one of these innovative techniques. DIC is an optical based remote sensing technology suited for challenges on the global metric level of the bridge system. Digital images before and after loading are used to track details about the structure's deformation. Automatic change detection algorithms are used to calculate changes between photographs and correlate these changes with measurements of deformation in the image plane. These deformations can be rigid or global displacements as well as local deformation.

The focus of this chapter is to provide an overview of this technique, elaborate on laboratory and field studies as well as to provide limitations and advantages of this technique in addition to future investigations.

9.1. Background

DIC was developed in the 1980s during the early ages of digital image processing and numerical computing. Continued investigations of the method lead to further applications in crack initiation, stress intensity factors for brittle materials and analyzing the effect with mixed mode loading simulations (Zafar 2008). DIC is a method that has been extensively investigated and significantly improved for achieving high accuracy deformation measurements and expanding application range.   This method was heavily based in mechanical behavior studies. By the 1990s, further investigations of this method lead to additional advancements including: three dimensional effects in crack analysis as well as determinations of plastic deformation patterns in ductile materials in which deformations were found in micron and nanometer scales (Zafar 2008). In the early 2000s, DIC was applied to examine larger deformations and tracking crack growth curves for functionally graded materials (Zafar 2008).

9.1.1. Theory

The measurements of DIC involve mapping of pixel gray level patterns between subsequent digital images of a deformation object. This measurement technique is based on spatio-temporal mapping considering change in velocity field between successive images (Besnard et al. 2011). This technique employs these algorithms to determine the motion vectors of small traced particles from image to image (Sutton et al. 2009). In routine implementation of the two-dimensional method, the calculation area in the reference image should be defined in virtual grids. The displacements are computed at the points on the virtual grid of the deformed image. This can be demonstrated in Figure 9-1. The displacement vectors will reveal the magnitude and direction of movement.
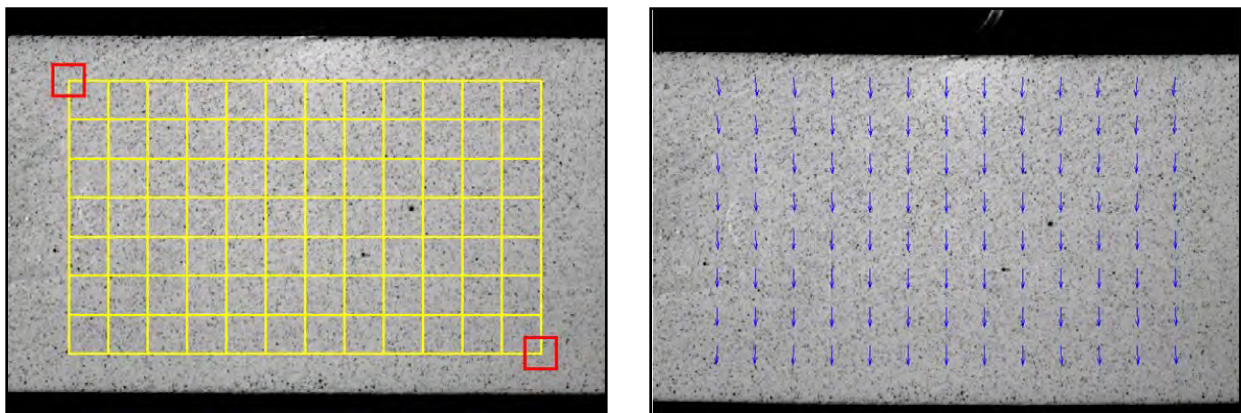
Figure 9-1: Sample grid for DIC Methods Displacement Calculations (Pan et al. 2009). Subset grid used for interpolation correlation on left and deformed vectors on the grid on right.

In order to compute the displacements of point P, a square reference subset of pixels centered at point $P(x_0, y_0)$ from the reference image location $P(x,y)$ are chosen to compare in the consecutive deformed image. A square subset is chosen for matching the wide variation of gray scales in the subset grid and therefore can be more uniquely identified in the deformed image. To evaluate the similar degree between the reference subset and the deformed subset, a cross-correlation criteria or sum-squared difference (SSD) correlation must be defined. To improve the accuracy of displacement measurements, certain sub-pixel registration algorithms are applied. Iterative spatial cross-correlation algorithms are used for correlating and matching of patterns (Pan et al. 2009).

The matching procedure is completed through searching the peak position of the distribution of correlation coefficient. So for example, a cross correlation function will be produced as a moving body moves between two images. The correlation function gives a peak value at the best matching ordinate through the function. This peak value will indicate the magnitude and direction of the displacement of the body. This is shown in Figure 9-2 below. Before implementation of the DIC process, a region of interest should be identified to help in the correlation procedures.
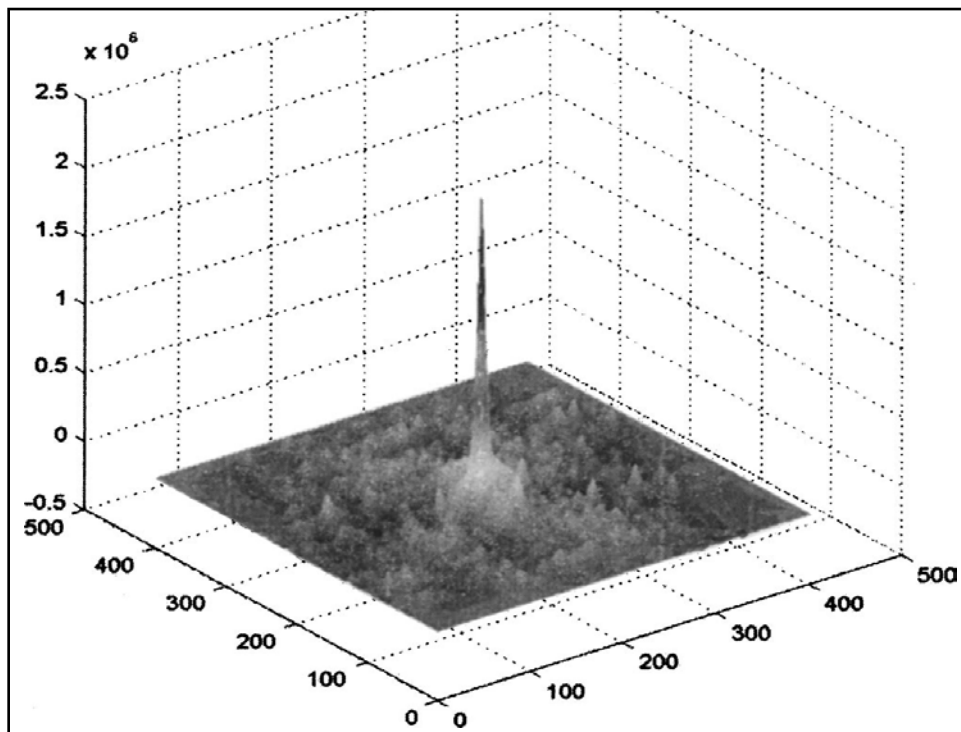
Figure 9-2: Cross correlation function identifying peak values (Sadek et al. 2003).

DIC is a path independent approach as typically the computed displacement and strains at the current point are used in the initial guess of the next point according to the continuous deformation assumption   3D DIC processes, stereovision principles are incorporated in the fundamental principles of two dimensional correlation concept (Lava et al. 2011). Synchronization acquisition of pairs of images simultaneously during loading is imperative of 3D measurements.   For swift calculations, the cross correlation function is applied to the images in the frequency order to the fast Fourier Transform (FFT) (Sadek et al. 2003).

9.1.2.   Concept

DIC is an optically based remote sensing technology proposed in this study for measuring challenges on the global metric level of the bridge system (Ahlborn et al. 2010). DIC technique consists of correlation, typically, on a pixel by pixel basis, of two or more electro-optical images separated in time or space. This measurement can be a surface plane measurement, 2D (two dimensional) as well as full-field measurement, out of plane measurement in more of a stereo-vision approach, 3D. The 2D concept is shown in the Figure 9-3.

The system generally uses charge coupled device (CCD) cameras for a combination of high resolution and speed (large number of frames), but DSLR cameras have also been used. Regardless of the camera essentials, it is significant for the cameras to be equipped with distortion free lenses to avoid lens induced errors (Shukla and Dally 2010). DIC tracks the change in position of the physical points shown in a referenced image relative to the specimen in the deformed image.   This change in position can detail displacement measurements and further extract displacement fields to determine strain in structures. Therefore, deflections in structures during loading processes can be determined. In addition, DIC has been useful on structures under dynamic loading for vibration measurements and frequency detection.   This can allow static and dynamic bridge behavior measurements to be determined. The planar surface of the specimen is typically sprayed with paint to provide a target pattern for image comparisons under white light illumination of the surface; this illumination is expected to contain mixed gray scale intensity measurements at each specified pixel location of the CCD camera array on the specimen's surface.

In the DIC technique, square subsets of pixels are identified on the speckle pattern of the selected area of interest and are traced on each corresponding photograph. In this selection, various parameters are considered such as speckle size, speckle density and subset size, and gray scale level intensity (Yang et al. 2010).   These parameters are typically the input factors and can alter the image detection processes. These are user selective and will depend on the individual analysis.   As discussed a great grey scale level contrast is suggested and the speckle pattern should be random and balanced in size (not too large or small) for efficient image tracking (Correlated Solutions 2010).
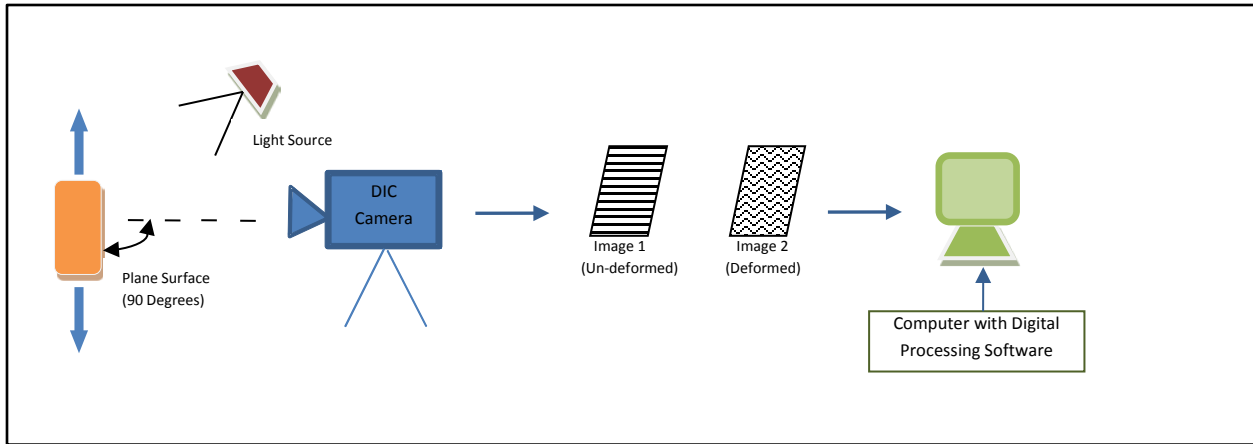
Figure 9-3: 2D DIC system setup.

Throughout this project study, DIC was determined to have great potential for bridge condition measurements. This method was regarded as most effective for global metric behavior on a bridge system (Ahlborn et al. 2010). Global metric behavior focuses more at the structure's physical response (as a unified or complete system) due to the daily vehicle traffic and environmental conditions observed by the bridge. These challenges may not be observable during routine inspections of the bridge or of individual elements. However, their influence on the system behavior has the potential to change the bridge member's condition.

As was demonstrated by the I-35W collapse (Wolchuk 2011), it is important to be able to monitor changes and variations in element and system behavior to help prevent catastrophic failures. Implementing an optical method to enhance inspection observations for those global metrics would be beneficial to the bridge inspectors from a far standoff (distance) location or even close to the bridge. In evaluating the global behavior of bridges, four challenges were identified on the global level for which DIC could be applicable including detecting a change in bridge length, measuring bridge settlement, measuring transverse bridge movement, and measuring the vibration or the live-load deflection of a bridge or a structural element (such as a girder) (Ahlborn et al. 2010). In this study, the focus was geared toward the vibration or live load challenge as the others were deemed more long-term monitoring and not an ideal use of the technology.

9.1.3.   Literature Review and State of Practice

9.1.3.1. Research

DIC has been used for many types of tests and research areas. DIC is a simple technique that leads to a huge range of potential applications including automotive, industrial and aerospace. DIC allows for materials testing that can incorporate a diverse range of specimens and even at varied temperature dynamics (McCormick and Lord 2010). Typically, the process involves

detection of the strain fields to determine the displacement of the specimen being analyzed. This method is able to provide full field displacement measurements. The process of procedures generally follows the live field strain measurement captured through the speckle strain pattern and then displacement is tracked through the deformation vector field. With the digital processing, the strain field can be determined as shown through Figure 9-4 (Zafar 2008).

In this figure the pattern field (on the area of interest) is shown for the reference *(t)* and deformed image *(t+dt)*, and the deformation field from that movement is tracked which is used to calculate the strain field. This type of procedure can be used for various components and is heavily used in mechanical testing of materials. These mechanical tests can also include tensile material tests. In Besnard's testing, there was tensile testing completed on a metal split Hopkinson pressure bar. The temporal spatial map details a 201 x 351 pixels in space and time and this represents a size equal 165 μm. In this case, the DIC method produced the corresponding velocity, displacement, and engineering strains found on the tensile bar using a frame rate of 30,000 fps (2011).
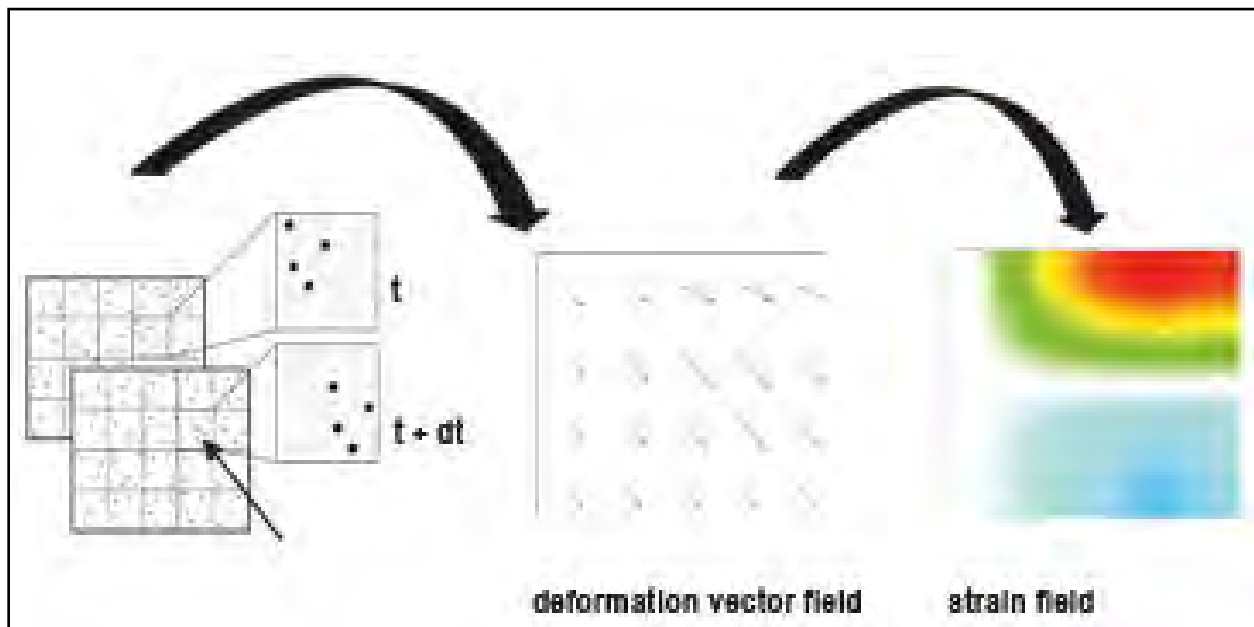
Figure 9-4: DIC Process for strain field (Zafar 2008) showing the pattern field, deformation live field, and the strain field.

It has been researched that DIC technique can detail high spatial resolution; with previous project experiments confirming that 1/10 in resolution (2.5 mm) can be achieved at close stand-off. There is, however, a compromise between spatial resolution and extent; in order to achieve higher spatial resolution, only a small coverage area can be imaged and thus, for larger targets, multiple images must be stitched together. The frequency response is dependent on the camera used, and may not be sufficiently high enough for measuring the

vibration of some bridges. This will greatly depend on the qualities of the camera used. To its advantage, the camera-target geometry ensures that data collection will not interfere with bridge traffic as it will be in a location not disrupting traffic, but the target surface preparation is a part of the measurement that demands contact with the bridge structure. If the bridge's girder surface or testing location is not full of contrast for DIC movement detection, an implemented pattern will be physically be placed on the surface. Hutt and Cawley (2009) describe their collection using a 2-camera system developed by Dantec Dynamics and processing using GOM ARAMIS, which consisted of simple-windowed block matching where correlations took from a few seconds up to several minutes. Kuntz et al. (2006) used Correli 3D and a fast FFT algorithm to measure displacements of 1.4 μm as well as cracks (Ahlborn et al. 2010).

DIC has been reviewed as a developing application for obtaining measurements for civil infrastructure such as bridges. On bridges, there are various loading classifications including two primary categories such as dynamic and static loading. It is crucial to monitor these loads for the in-service traffic loads and dead load on the bridge itself. There have been studies conducted on investigating DIC measurements on bridge structure. Yoneyama (2007) conducted vertical bridge deflection measurements on a small one lane (with walkway) steel girder bridge. The bridge was about 23 ft wide with a small elevation, near 1 m between underside ground level. Because the bridge was fairly low to the ground so displacement transducers were placed under the bridge. A magnet pattern was placed on the steel girder for the digital single-lens reflex camera lens setup on the underside ground level. In this study, the measured results from the transducers and DIC showed agreeable patterns.

In Gamache and Santini-Bell's (2009) study, a DIC system was implemented on a near 110 ft steel reinforced prestressed girders bridge (concrete deck). There was a test pattern created for testing at 100 ft from the bridge. A loading truck of 37.5 kip was driven on the bridge and vertical shift of the girder was detected. A 95% confidence after de-trending was shown within this test study when compared with the FEA (finite element analysis). In this study, it was stated that there was a noticeable drift in results due to wind gusts, air turbulence and even thermal effects (Gamache and Santini-Bell 2009).

This could also be prevalent in the confidence gap received from measurement results. It was also shown how this type of data collection can lead to detailing bridge performance information where this data can be further developed into estimation of load rating. Santini-Bell et. al (2011) also conducted field testing for composite bridge deflection measurements of a steel girder, but also revealed that bridge testing adds challenges to DIC that would not be customarily encountered as in the laboratory environment. One of the greatest challenges in DIC field measurements was identified as maintaining a static camera position (Santini-Bell et al. 2011).

9.1.3.2. Commercially Available Systems

A number of commercial vendors currently offer digital imaging correlation packages and systems. A few of the companies are described below. Dantec Dynamics is a company that provides laser optical measurement systems and sensors. Dantec Dynamics offers integrated measurement systems for various applications including full field image analysis methods in which contours and displacements of objects can be investigated (Dantec Dynamics 2012) Correlated Solutions is a company that investigates non-contacting measurements solutions and provides customized testing for various types of specimens. Correlated Solutions offers non-contact shape and deformation measurement solutions for materials and product testing to its consumers (Correlated Solutions 2010).   Correlated Solutions can provide individual merchandise or complete packages including camera, lenses, calibration equipment and analysis software. Commercial vendors such as these can provide 2D and 3D DIC measurement systems that can be useful for mechanical applications where an understanding of deformation is essential.

9.2.   Methodology

To fully explore DIC, a series of laboratory investigations were performed. In this compilation of laboratory tests multiple computer algorithms and software packages were used for validation of measurements. This testing scheme allowed for exploration of DIC parameters such as lighting concerns, speckle pattern design and flexibility in testing materials. The following section below details the extension of these testing and software algorithm used.

9.2.1.   Computer Software Algorithms

In the preliminary investigation of using DIC for bridge behavior evaluation, two systems were evaluated. These packages consisted of an open source The MathWorks MATLAB algorithms and Correlated Solutions Vic-2D software.

9.2.1.1. MATLAB Algorithm

The MathWorks open source DIC and DDIT (Differential Digital Image Tracking) MATLAB routine was developed by Dr. Christoph Eberl, head of the Microreliability Junior Research Group at the Karlsruhe Institute of Technology (KIT) in Germany. In this algorithm, an area of interest on the specimen is user defined. An analysis grid is formed and compared on each image in the set of tested images. A random spray pattern is applied to the specimen surfaces and serves as the high contrasting background when post-processed, as demonstrated in Figure 9-5. This image shows the surface plane of the illuminated specimen's surface, (left) and is examined in the software algorithm (right).
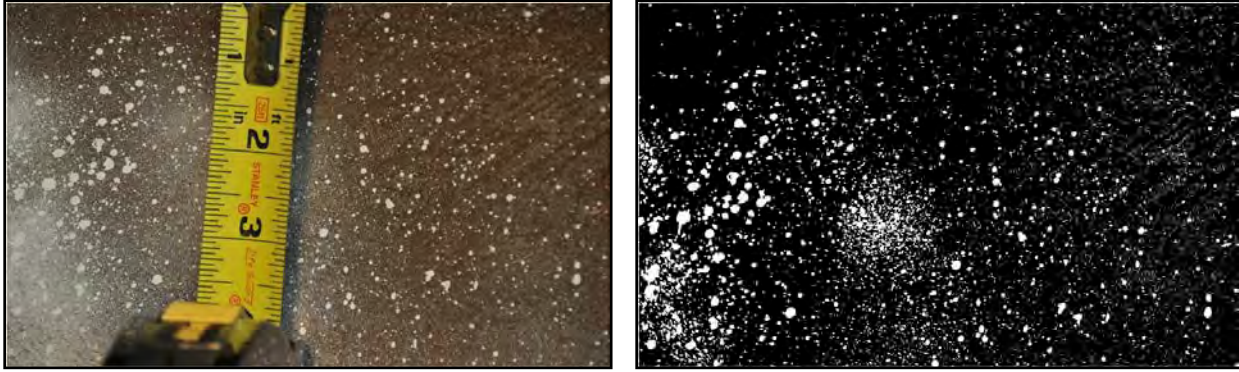
Figure 9-5: Sample Measurements from Pattern and Post -Processing (Ahlborn et al. 2010). Speckle pattern on I-beam on left and post-processing image showing contrast on right.

The open source MATLAB algorithm was initially used to calculate strain from images independent of physical size of the samples. The code allows a displacement vector to be calculated for each sub-grid created from the original grid, which effectively produces a displacement grid for the surface. This is demonstrated in Figure 9-6. The amplitude of these vectors can be extracted and plotted by the X and Y positions for each image to produce a displacement plot of the 2D surface. This software typically reveals pixel position variances in the X and Y positions of the images and leaves the dimension correlation to user interpretation. This code is also an open source program and therefore it can be customized for the user's intent. Nonetheless, this was not the focus of the project; however, some discrepancies in evaluation observed throughout the experimental phases warranted that this path be revisited.

9.2.1.2. Vic-2D Software

Vic-2D optimizes correlation algorithms to provide full-field displacement and strain data for mechanical testing on planar specimens. Actual, in-plane movement can be determined for every point within the measurement area, as well as the Lagrangian strain tensor for those locations. In initial preliminary analysis, both of these software algorithms were utilized. Both solutions allow for a user-specified creation on the grids or area of analysis on the images which could fine tune the measured results correspondingly. A sample area of interest for Vic-2D can be seen in Figure 9-7. In DIC analysis, the size and shape of the area can be selected based on the needs of the user as demonstrated in which an uneven quadrilateral shape is shown on the bar specimen. In this project, with the aim was ideally on commercially available technology and even software, so efforts were focused on Vic-2D which also provided more of a straight forward analysis. Only Vic-2D was evaluated further after the preliminary assessment.
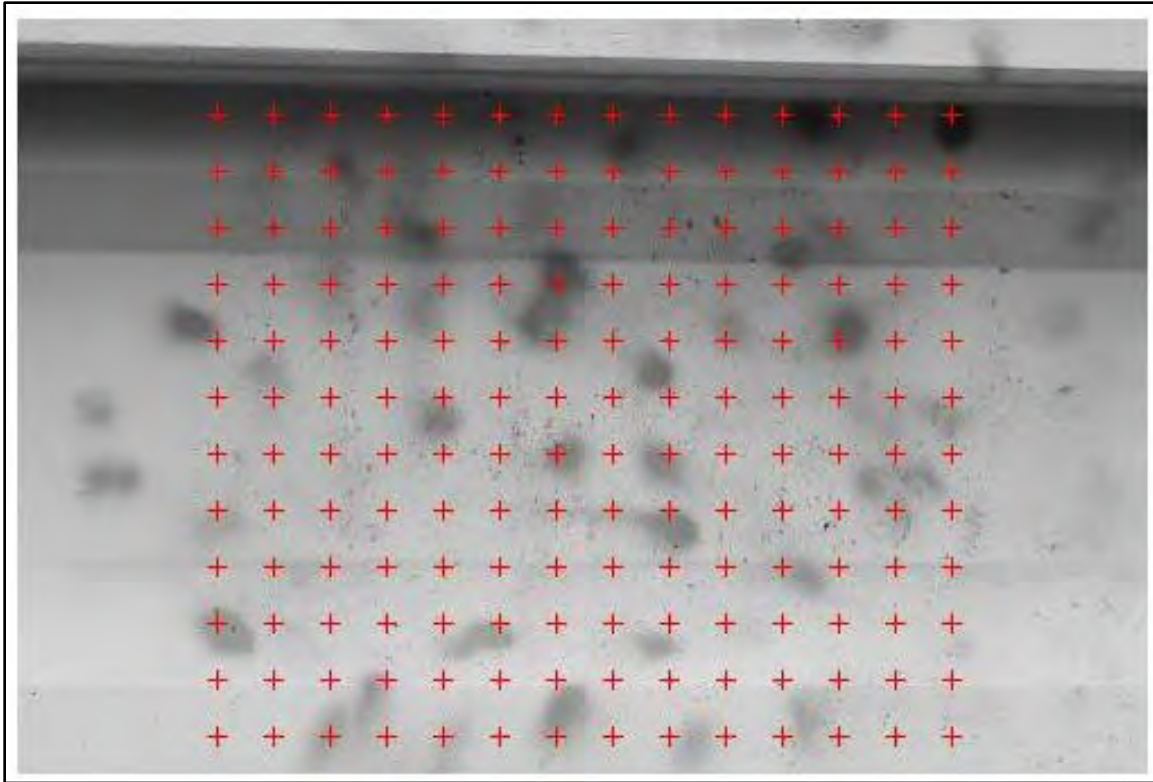
Figure 9-6: Sample grid from MATLAB algorithm on structure surface.
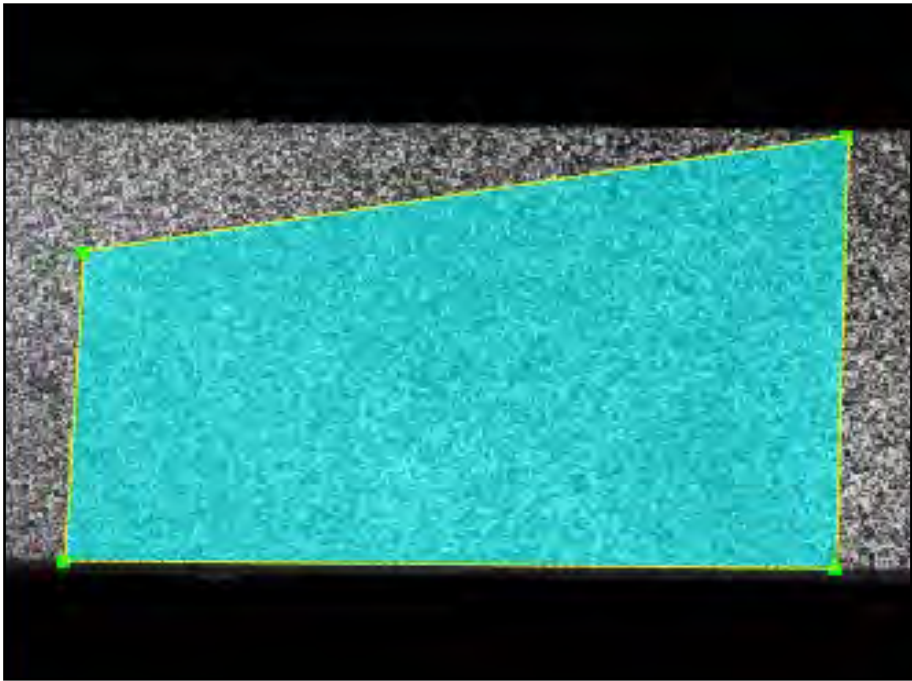
Figure 9-7: Sample area of interest grid from Vic-2D algorithm on structure's surface (Correlated Solutions 2010).

9.2.2.   Preliminary Laboratory Evaluation

DIC was employed in a laboratory experimental setup to verify the technology and assess the applicability for measurements of static and dynamic bridge behavior. To evaluate the concept, several preliminary tests were conducted in laboratory tests as discussed below. For the high resolution digital images, a Canon EOS 7D DSLR camera was selected. The features of this camera include an 18.0 MP resolution capability, high ISO (International Organization for Standardization) light threshold (100-6,400 range), and a capture burst mode of 8 fps. This camera has been researched and used in image testing in order to gain an understanding of the camera's capability and functions.

Different structure samples such as W shape steel members and concrete bridge pylons were tested to evaluate the method (TM n° 15, Appendix C). These tests were completed to emulate static and dynamic behavior and address challenges associated with global metric bridge interaction.   Through laboratory tests, numerous considerations were examined as far as speckle pattern consistencies and diverse materials that could be tested shown in Figure 9-8 revealing a random speckled wood beam specimen undergoing a flexural test. With these considerations analyzed, it was necessary to determine the accuracy of the DIC system measurement with conventional measurements used in the laboratory.

Figure 9-8: Wood Beam with speckle pattern.

Therefore, several tests were done to obtain these measurements. A 16 ft simply supported W10 x 60 steel beam (I-shaped) was subjected to simple flexural tests in the laboratory at varied frequencies and loading capabilities. There was a speckle pattern sprayed on the surface for detection of the pixels during the computer processing. The EOS 7D camera was used with a lens at a focal length of 55 mm. This can be shown in Figure 9-9. This DIC results showed results that agreed well with a linear variable differential transformer (LVDT) that was placed at the mid span location where images were taken. A figure of the sample results from test can be

shown in Figure 9-10. This result was from tested at 0.25 Hz frequency and was intended to measure 0.5 in deflection.

Figure 9-9: DIC Setup for steel W shape (I beam).
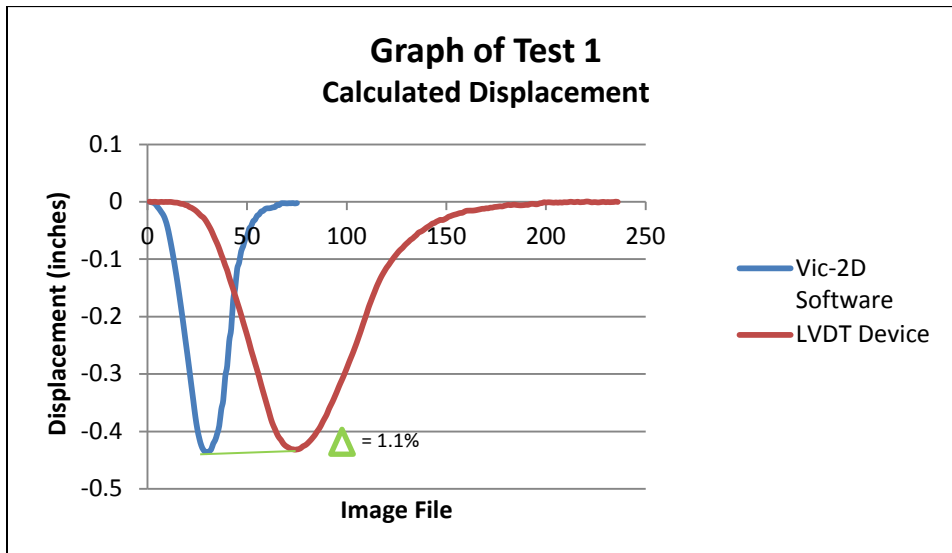
Figure 9-10: Graph of LVDT Result and DIC measurements.

The LVDT measured a value slightly lower than 0.5 in and the DIC software experimental value was compared with the actual measured value obtained. Also, the peak of the displacement curves are identified at different time values due to the non-synchronization of the captured images and actual LVDT measurements. However, the change in position captured through the images and LVDT's still reveal matching movements.   Table 9-1 shows a comparison of a couple scenarios tested for the W10 x 60 steel beam and the corresponding percent errors obtained. In these tests, percent error calculations were used to compare the experimental values with the actual values. The percent error was calculated using Equation 9-1.

$$\% \, Error = \frac{Experimental \, Value - Actual \, Value}{Actual \, Value} \times 100 \qquad \textbf{Equation 9-1}$$

A sample calculation is illustrated below from results in Table 9-1:

$$\% \, Error = \frac{-0.43115 \, in - (-0.43605 \, in)}{-0.43605 \, in} \times 100 = 1.12\%$$

From this series of tests, the percent errors were low and under 5%, a value that could be suggested for acceptable minimal error. A value within 5% error could still prove useful or agreeable in value with some minor acceptable noise variation. A few minor variations of the camera positions on the steel beam was explored in this testing setup although no quantifiable influence on results were obtained at that time. This would also prove useful for the field test later.

Table 9-1: Table of Results from Steel I BeamTests.

Test Number	Expected Displacement (in)	LVDT Displacement Measurements (in)	Vic-2D Displacement Measurements (in)	Percent Error (%) between Measurements
Test 1	-0.5	-0.43115	-0.43605	1.13
Test 2	-0.25	-0.18533	-0.18426	0.57

A 2 x 2 x 8 in Ultra-High Performance Concrete (UHPC) beam that was being explored for fracture behavior characterization was also tested in flexure using a MTS 318.25 810 Material Test System (Krieger et. al 2011). DIC was employed to measure displacement and review strain patterns throughout the loading of the UHPC specimen. The camera was positioned approximately 5 ft away with the EOS 7D camera and a lens of a focal length of 200 mm. In parallel images were captured for the duration of the test and post-processed later using Vic-2D. Figure 9-11 shows a representative speckle pattern (left) and displacement field plot display from Vic-2D (right) with a comparison of results presented in Table 9-2. In this table the values obtained from the 810 Material Test System and Vic-2D shows different results and detailing an 8.87% error. For this test case, not enough contrast in the speckle pattern and lighting issues may have influenced the results as shown in the right image of Figure 9-11. In addition, this specimen cracked during loading, which could have influenced results (Figure 9-11, right).
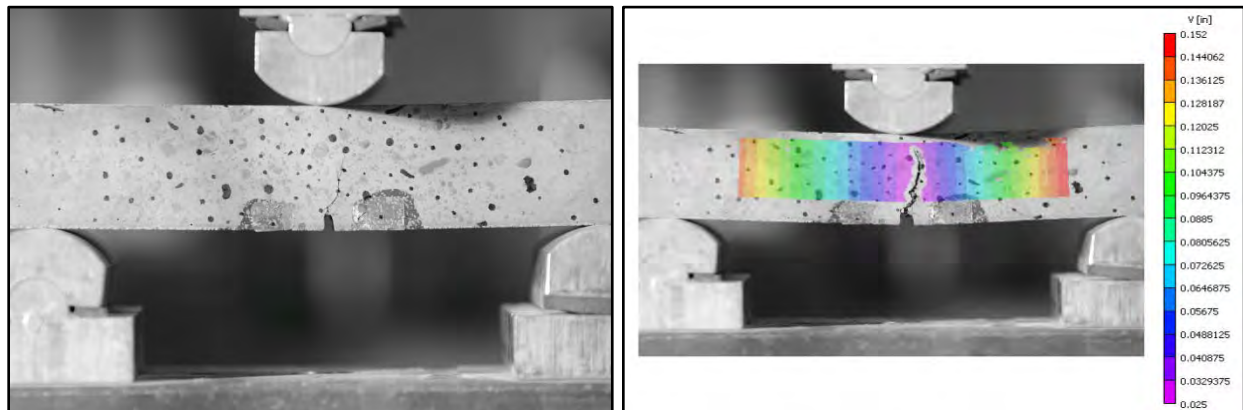
Figure 9-11: UHPC Beam in MTS Machine for compression Test showing speckle pattern of UHPC beam on left and post-processing of image on right.

Table 9-2: Table of results from UHPC test.

Test Number	MTS Displacement Measurements (in)	VIC-2D Displacement Measurements (in)	Percent Error (%) between Measurements
Test 1	0.496	0.452	8.87

It is proposed that with the induced shadow some pixel markers would be lost during correlation comparisons. Ensuring sufficient light and speckle pattern would prove advantageous for field conditions which would encourage field testing to be conducted during peak sunlight hours. Though, it is also suggested that during the night with an adequate light source could also be viable (Santini-Bell et al. 2011).

9.2.3.   Field Deployment

DIC was implemented on an MDOT bridge structure in the city of Clare, MI in order to verify the capabilities of the technique and application for structural health measurements under field conditions. The Mannsiding Road bridge contained three major spans; two approach spans over each shoulder and a center-span over the US-127 NB lanes. Implementation of DIC consisted of a creating a contrasting speckle pattern on the exterior pre-stressed girder, and setting up an elevated (at quarter-span) camera-lens system.

A MDOT bucket truck was used for the creation of these larger and smaller refined marks constituting the speckle pattern which are necessary for tracking pixel movement using DIC (Figure 9-12). A washable water-based spray paint was used for the creation of a speckle pattern on the exterior girder.

Figure 9-12: DIC setup at Mannsiding Road bridge and detail of girder with speckle patterns.

The EOS 7D camera was placed at a 20 ft standoff distance from the target surface on a rigid tripod (4.25 ft) located on a scaffolding platform (10 ft). The overall height of 14.25 ft placed the camera perpendicular with the exterior girder (Figure 9-12 and Figure 9-13). The predetermined bridge span was stressed by both a quasi-static and dynamic live-load generated by a live-load test truck. A live load truck with a weight of 57 kip (Figure 9-13) was used during load testing. The truck was guided along the exterior lane path at a crawl speed below 10 mph.

During loading, images were captured by the EOS 7D camera with an EF 70-200 mm lens on the exterior girder at the quarter span and mid-span location. This test was repeated three more times with two of those cases remaining at focal length of 85 mm and the third was at a focal length of 140 mm.

Figure 9-13: Load truck going over bridge (left) and close-up of camera and tripod setup on scaffolding (right).

The camera was then rotated horizontally approximately 45° angle to capture images on the girder surface at the midspan location. This test was repeated three times at crawl speeds (~10 mph) at a focal length of 125 mm and the third was a focal length of around 200 mm. The speed on the truck was increased to ~40 mph and a series of images were taken at this speed shooting at the quarter-span location. To conclude this testing, a static test was performed with the truck parked at the quarter-point location. A sketch of the truck loading is presented in Figure 9-14. Additionally, a series of images (measurements) taken under true static conditions as well with no truck (load) on the bridge. The dynamic test was performed to determine how accurately DIC can optically sense, and capture, bridge vibration. The dynamic tests were performed at posted speed and were completed to mimic actual service conditions. The images were numbered automatically by the camera's firmware, and each of the images was correlated with the known load applied to the bridge span at that time. The images gathered with the camera were processed in Vic-2D for strain and displacement measurements.
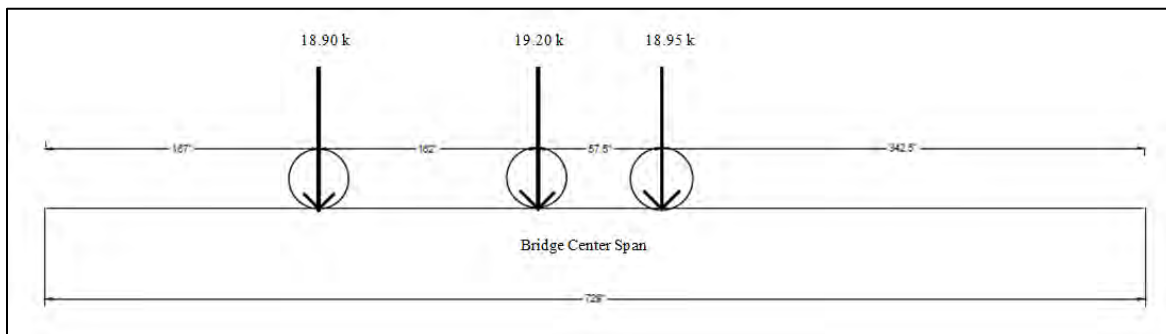
Figure 9-14: Visual Sketch of Wheel Path for Static Positions and Wheel Weights.

9.3.   Results and Discussion

9.3.1.   Field Deployment Results

The next steps following the field deployment involved post-processing the collected images through Vic-2D. Results from this testing would be expected to show the quasi-static behavior where there is a change in displacement and from the loading truck crossing the bridge. The values of change in position (displacement) and image file numbers (time elapse) change from image set to image set. In the analysis of these image sets, there was significant variation in the deflection response during testing that can be shown in Figure 9-15. These results in this figure are for one of the quasi-static test from the truck driving across the quarter span location at crawl speeds.
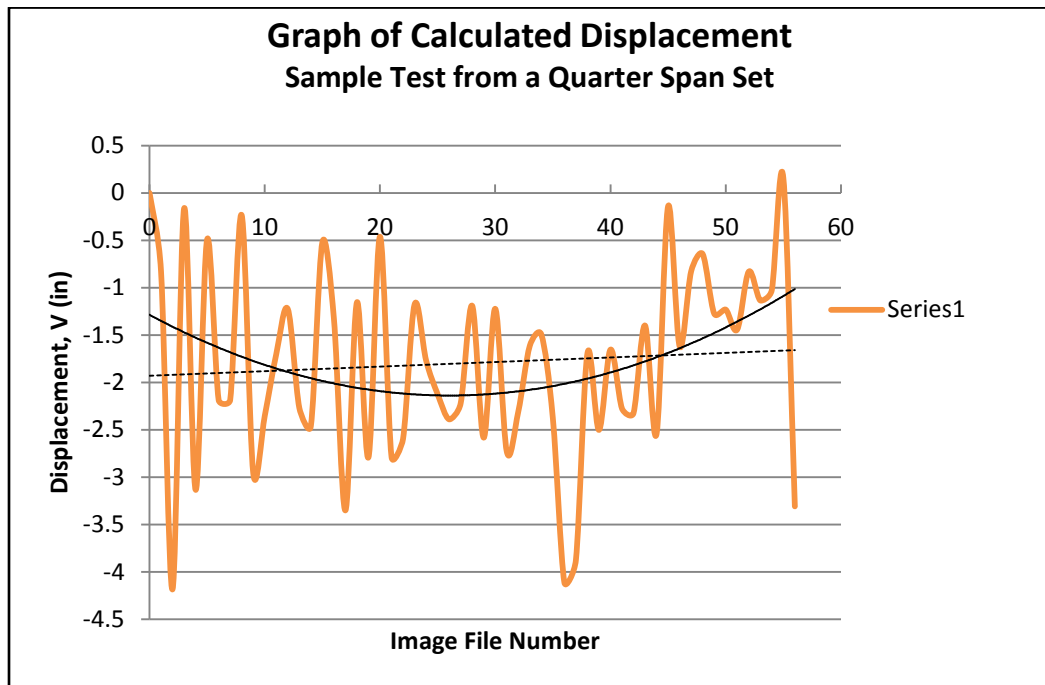
Figure 9-15: VIC-2D plot of calculated displacement for a test series.

There were varied efforts to translate this data to relatable measurements of the bridge's response due to the loading. In the software output contour plots, patterns of higher movement concentration can be displayed as the weight of the loading truck is driven over the mid span testing location (Figure 9-16). In this figure, the dark purple color on the plots reveals the largest displacement (in the negative direction) as the truck load moved across the mid span area of interest. In the first image the greatest load is at the left corner and the second image it moves toward the top center of the area of interest. And correspondingly, in the third image the dark

purple shade of the contour is revealed at the top right of the area of interest as the truck wheel leaves the area of interest. It was difficult to graphically characterize the movement when sets were compared with one another there was not a lot of consistency between the image sets. It was evident in this investigation that the random motion captured in the image processing was due to various environmental and setup effects endured during the field testing.
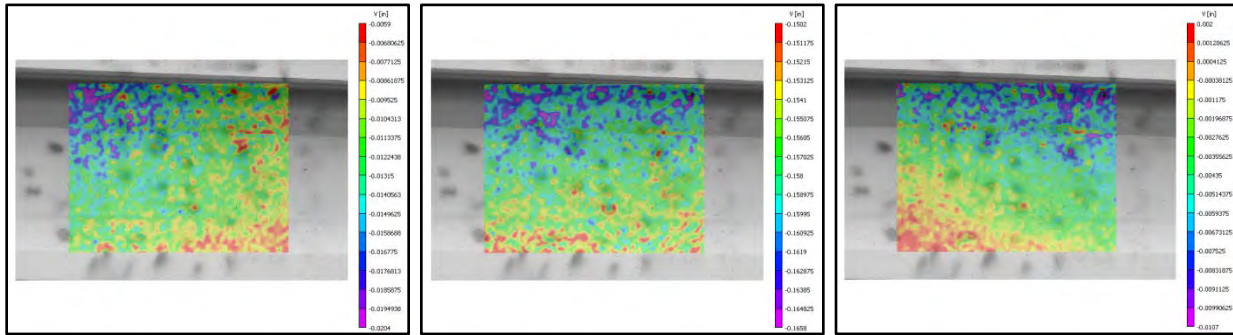
Figure 9-16: Vic-2D analyzed section of tracked displacement along a bridge girder surface due to driving truck load.

9.3.2.   Field Environment Considerations

From the field demonstration, a number of factors were attributed to the erratic processed image sets. Being outdoors and undergoing the outside environment weather conditions were of concern with excessive winds interacting with the camera system. There was also motion from vehicles passing by and the vibrational effects that influenced the results and lead to intermittent graphical plots. In addition, other wind movement in the air could impact camera and lens stability as well as movement to the scaffolding itself especially since the camera system was on a scaffolding platform 10 ft in the air. There were two capturing locations on the bridge girder surface: directly in front of the scaffolding platform (located at quarter span) and the other was located at the mid span location (captured at an angle from the scaffolding platform). In this setting, there was not precise accountability taken into consideration for the rotated camera position and how greatly that would affect the results.

While the technology was evaluated for applicability under field conditions, no conclusions could be drawn as a result of these environmental factors and their influence on the results. Following the ineffective field deployment, the concept of using DIC for in-service performance evaluation was re-evaluated in its entirety including the technique configuration, software algorithm and equipment.

9-18

9.3.3. Retested Laboratory Evaluation

Environmental effects greatly varied result outputs and some form of de-trending procedure or alterations in field setup may need to be implemented for minimum noise capturing. Recall that many of the environmental effects experienced in the field deployment were also mentioned in the literature review. This lead to further investigations of other means to account for the noise to know variability range of accurate measurements and error induced measurements. In this study, it is important to gather a threshold of measurement and coincidently identifying movements that could lead to measurements having large percent error values. As discussed, additional laboratory testing was also done to see how well Vic-2D captures movement together with the dynamic effects of wind and other "outdoor" effects in the camera system as experienced previously in the field.

With the same lens settings, tripod, and camera system a series of tests were completed. A rectangular piece of plywood with a distinct speckle pattern was used at 2 ft and 32 ft from the camera; it was subjected to cyclic movements at two varied displacements on the 810 Material Test System. At the closest position, the focal length was near 25 mm and at the 32 ft position a focal length of 200 mm was used. Figure 9-17 shows the setup of the speckled rectangular board and camera at the two different distance positions. In both images, a light source was placed on the specimen to ensure sufficient pixel tracking from image to image.
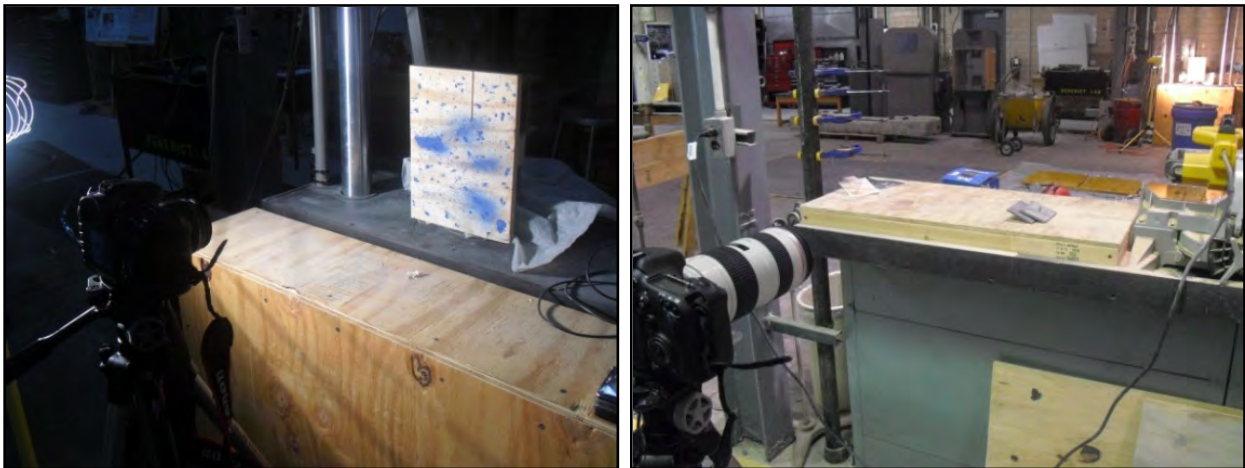
Figure 9-17: Benedict lab testing setups at 2 ft (left) and at 32 ft (right).

At the closest distance, 2 ft, two different scenarios were investigated; with (fan on camera) and without wind. Table 9-3 shows the percent error in values as calculated in Vic-2D as compared to the data collection from the 810 Material Test System; the values had very little error at 1.9%, but with the wind simulation the change increased greatly from the previous 1.9% to 2.39%.

For the 32 ft testing scenario, the camera was placed on the loading platform of a Fairbanks-Morse floor scale located on the MTU Benedict Laboratory (Figure 9-18).

Table 9-3: Test measurement comparisons at 2 ft with wind and no wind.

Test Number/Type	Test Frequency	Expected Displacement	MTS Measurements	Vic-2D Measurements	Percent Error
T1 - no wind	0.25 Hz	0.25 in	0.2468 in	0.2515 in	1.90%
T2 - wind	0.25 Hz	0.25 in	0.2462 in	0.2521 in	2.39%
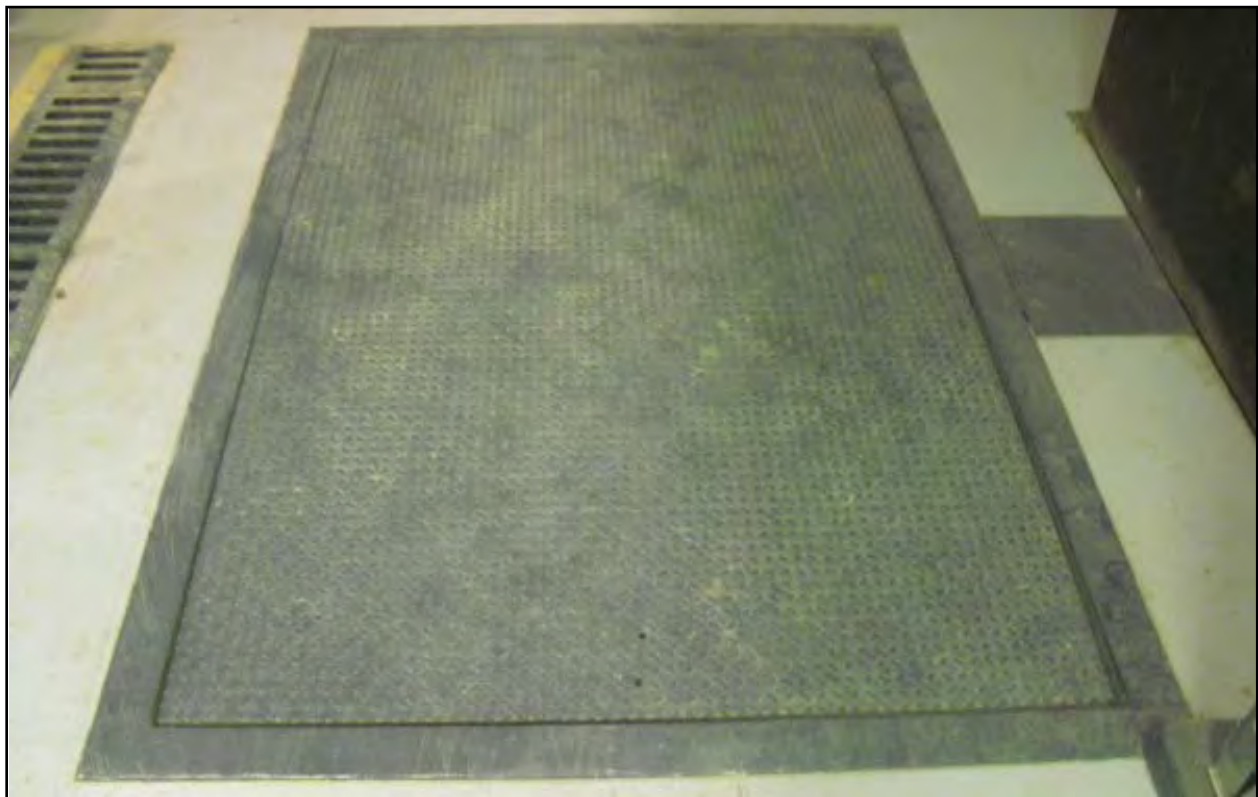
Figure 9-18: Floor scale loading platform used to simulate scaffolding movement.

The floor scale platform can easily move with a person walking or a simple shift weight by placing an object on the scale. The camera and tripod were placed on the platform and images were taken of the rectangle speckled board. This test was repeated with a person moving on the platform to demonstrate a field like simulation of the scaffolding setup. Table 9-4 shows the results from the processed images in Vic-2D compared to the 810 Material Test System recorded

data and the percent error between these results. In this battery of tests, it was shown that the displacement values differ drastically when tests are repeated with and without movement. In Test 1 and 2, there was no movement on the scale and the expected displacement doubled. In Test 3, there was much more movement induced at 0.50 in expected displacement and greater error produced. In Test 4, there was so much movement that the data could not be compared. This graphical representation is shown in Figure 9-19. These tests were deemed comparable to the same type of noise identified in the field results with capricious motion shown in the plot.
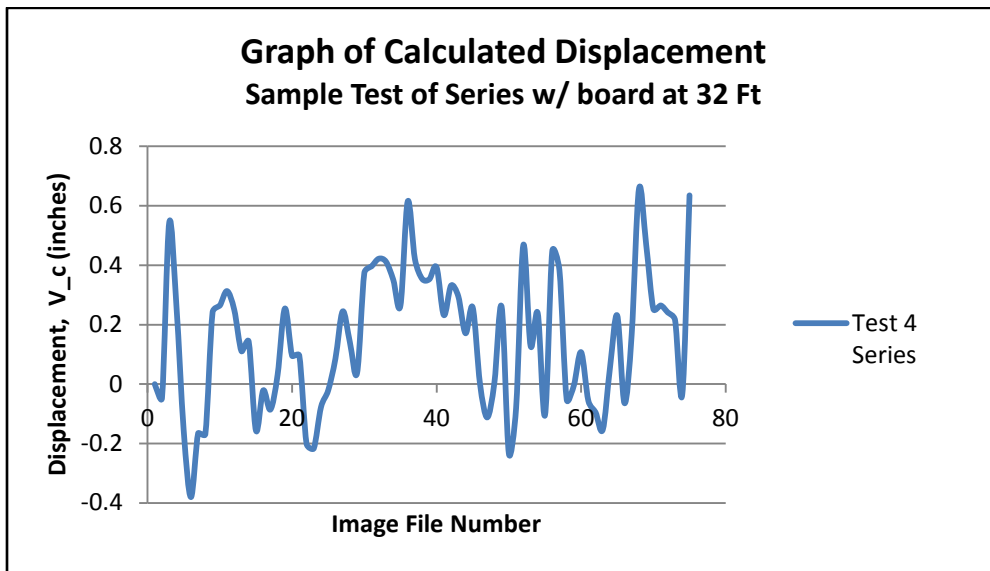
Figure 9-19: Test 4 results from the 32 ft series testing; test performed with floor scale movement.

Table 9-4: Test measurement comparisons at 32 ft; movement and no movement.

Test Number/Type	Test Frequency	Expected Displacement	MTS Measurements	Vic-2D Measurements	Percent Error
T1 – without movement	0.25 Hz	0.25 in	0.2457 in	0.2578 in	4.92%
T2 – without movement	0.25 Hz	0.50 in	0.4966 in	0.5070 in	2.09%
T3 – with movement	0.25 Hz	0.50 in	0.4974 in	0.7414 in	49.05%
T4 – with movement	0.25 Hz	0.25 in	0.2482 in	-----	-----

The challenges related to equipment stability prompted further investigation into the processing algorithms and a more stable data collection system. The 810 Material Test System was used again to monitor movement with a PCB Piezotronics 333B50 piezoelectric accelerometer and transform (integrate) those readings into displacement (Figure 9-20). Using the 810 Material Test System, a known displacement measurement can be used and therefore an easier integration into displacement measurements can be obtained. Measuring this data can enable a measurement of environmental noise (e.g., vibration or movement on the camera) that can be factored out to capture the true bridge movement measurement (Figure 9-20). The accelerometers were connected to a Campbell Scientific CR9000X Measurement and Control System in which results were collected, filtered through, and presented graphically.

Figure 9-20: Accelerometers on the 810 Material Test System.

It was expected that the results of this test would allow for movement tracking using accelerometer data and integrating into position (displaced movement) measurements. A sample of this acceleration data plot is shown in Figure 9-21. These plots show the data from the raw accelerometer measurements and the expected displacement measurements determined using a MATLAB algorithm. In Figure 9-22, the calculated displacement plot of the test data is shown with units of meters and seconds. The measured displacement graph reveals the sinusoidal wave that was expected as the 810 Material Test System moved in a cyclic motion

9-22

for measurement comparisons. In this investigation, correct filtering procedures are evaluated as well as appropriate unit conversion. Both measurements were plotted versus the time.
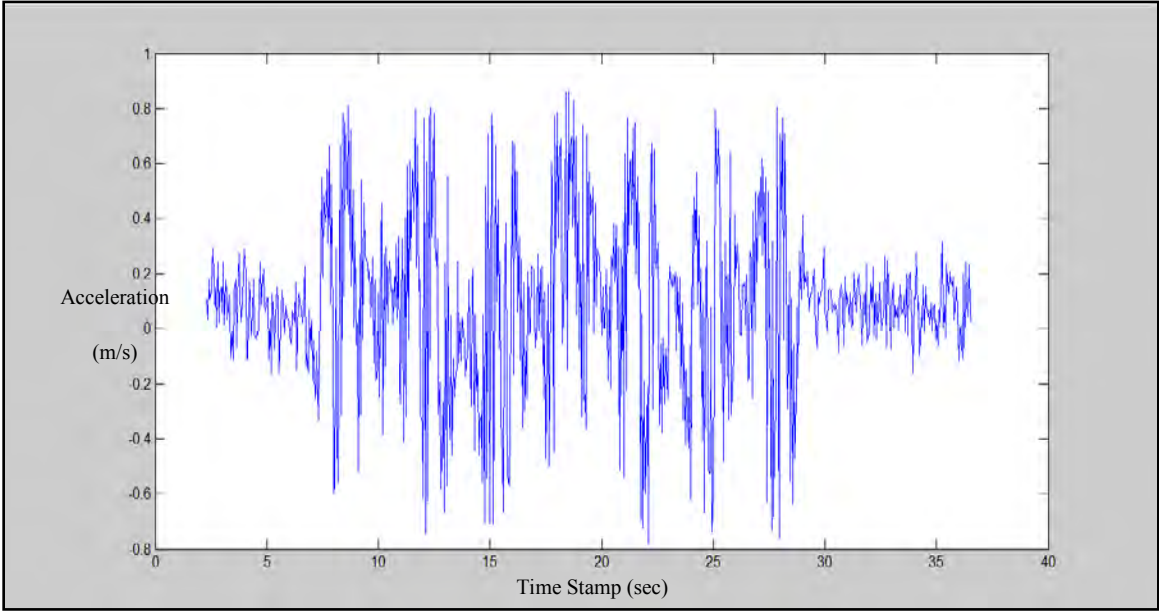
Figure 9-21: Acceleration versus time of camera movement.
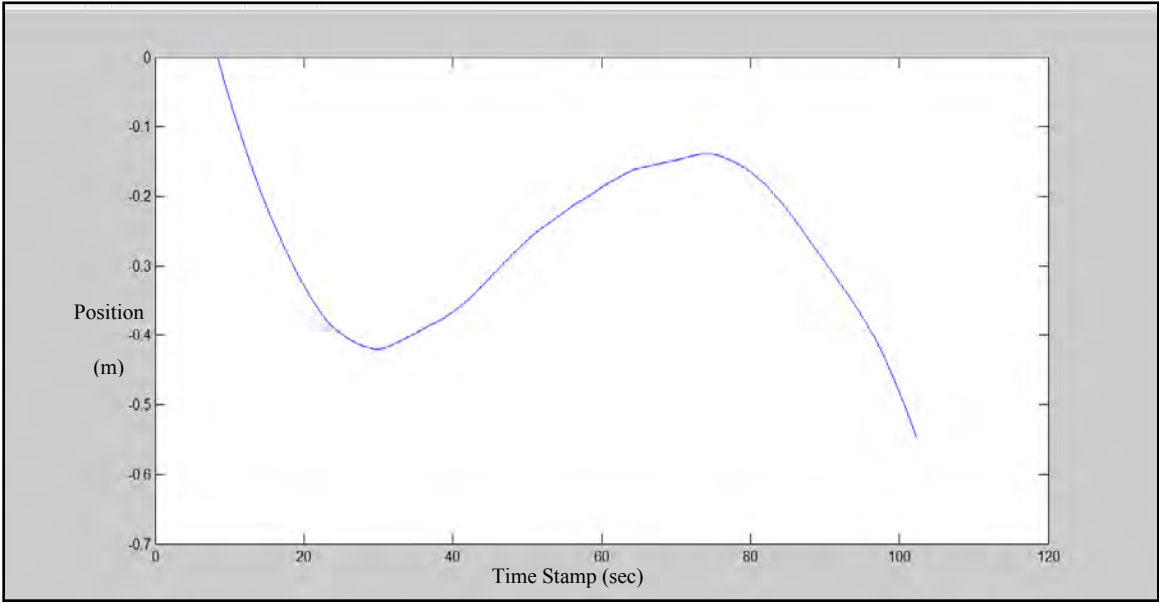
Figure 9-22: Calculated displacement versus time.

As the generic method for capturing motion into displacement measurements on the 810 Material Test System, this was further configured for the camera-lens system.   The camera-lens

system (as used in DIC system) was connected with an accelerometer in order to measure the excessive movement endured and computed the movement as displacement. In this setup, a more stable and heavier surveying tripod as well as a wooden base ensuring a flat secure platform for the camera–lens system was employed.   An additional accelerometer was also placed at the bottom of the tripod for location comparisons at the top and bottom of the tripod. These figures of the tripod and camera-lens setup can be shown in Figure 9-23.

Figure 9-23:   Camera on stable tripod (left) and detailed of mounted accelerometer (right).

The measurements of the camera movement(s) have shown similar results as in the testing system's data, but there were more unknown factors to consider in the acceleration measurement. The calculated position (displacement) measurement for this scenario reveals some alteration in what is expected and other parameters may have to be recognized in the setup.

This expected alteration is derived from the constant "C" which was not captured; this constant "C" is commonly determined from the integration equation of motion for acceleration which is equal to velocity "+ C" and similarly for velocity integration. This method allows for noise to be captured in measurements, but also may require an additional program to account for noise and other parameters associated with system inputs and obtaining correct bridge structure movement.   This could be a promising way to capture this motion, but took additional effort to consider that would lead to additional focus beyond the project scope. So, additional approaches were considered for this evaluation in the post-processing aspect using a computer algorithm for noise minimization.

9-24

9.3.4.   Pros and Cons of Method

The benefits of DIC include the flexibility in location for testing as well as time-of-day for image collection (depending on requirements), use of commercially available software for analysis and ability to provide load performance details with single tests. DIC uses a camera-lens system for the basis of its measurements and can be relocated as need to on different locations on the structure. Varied material specimens such as steel, concrete or wood can be tested using this system and direct correlated measurements can be detailed.

Generally, there are low preparation requirements for this technology as the camera is setup and the testing location is determined and images are captured. For this system, there are generally low overall costs with moderate operating costs. The estimated cost for this field setup was near $16,000 (including camera, software, setup equipment, etc). More details on the cost analysis can be found in Chapter 14. Much of the DIC system cost depends on the requirements needed for particular testing being conducted (e.g., higher grade lens or camera, different paint used for pattern, better more stable tripod) as well as the software algorithm used.

Some challenges of this method include testing factors that supports the notion that DIC may be best suited for controlled laboratory environments. Keeping the camera stable is important for co-registration of photographs in order to correlate accurate movement. Moreover, a more stabilized system with a sturdier tripod was also considered in future field testing environment. As an example, a gyroscopically-compensated camera mount could help in keeping the camera stable and minimized movement within the camera-lens system.

Reduction of the standoff distance would certainly reduce the effects of excessive wind and vibration on the camera-lens system. In this correlation, there are also sensitivities to pattern detection in which there needs to be adequate contrast and/or sufficient lighting for the contrast on the tested specimen to be captured. Initially, when applying the pattern, there needs to be assurance that the pattern will be detected at the imposed standoff distance; a "pre-test" needs to be performed to insure this.

There could be tedious calibration and algorithm processes involved depending on specific analysis desired in analysis. There are also numerous changeable parameters within the software that can alter the results. Algorithm details may require further investigation considering bias errors in the accuracy or precision of the software analysis. Bias interpolation of these results can translate into incorrectly interpreted testing data. More investigation into parameters and how they affect results is a major component of the post-processing data analysis.

As DIC is primarily based on optical imaging and computer processing, some error is prone to occur within the optical alignment and focusing errors that may be associated with the camera and the specimen (Sadek et al. 2003). There are also errors that have to be taken into account concerning the out-of-plane and rotational movement of the images. With DIC, the main

assumption is that the contrast will follow the particle on the image movement. However, out of plane movement may result in some part of the image getting lost. These movements are susceptible to getting ignored in the case of rigid surface displacement (Sadek et al. 2003).

Another major area of error involves the calibration of procedures in particularly between the cameras and the specimen. This is particularly true for the three-dimensional setup in which multiple cameras are used at specified angles.

There are certain constraints incorporated due to the numerical rotation processes that will easily influence the results (Lava et al. 2011). While DIC has hardware and software that is commercially available and ready for deployment, it is a technology that is currently best suited for laboratory work where conditions can be more controlled. There is a future in using DIC in the field, but there needs to be much hardware development specific for bridge condition tests outdoors. Alternatively, fixed-point referencing needs to be incorporated into the software algorithm to subtract the background noise or excessive system movement.

9.3.5. Integration into the Decision Support System

DIC provides useful detailed information on the global level of bridge structures. In this project evaluation, a DSS was developed to encompass the results of remote sensing technologies measurements. This DSS would be a software interface in which bridge inspectors could have access to remote sensing bridge measurements to complement their decision on allocating further maintenance on certain bridge structure. Incorporating this information into the DSS would be advantageous to giving performance measurements of the bridge. In particular, incorporating the deflection information from the images captured from bridge girder due to loading from live traffic.

This information can be transformed to loading distribution along the bridge girder surface. Additionally, this can be translated to give stress distributions along the girder surface as well. This can enhance bridge inspection measurements by providing inspectors with current performance measurements of the bridge structure which could indicate possibly failure on members or excessive strain states.

In long-term evaluation, this could give provide settlement or other transverse movement values if camera position coordinates are exactly registered from image to image; however, the feasibility of this type of measurement is unlikely with today's technology.

9.4. Implementations and Next Steps

9.4.1. Limitations

The limitations of the software consist of the compatibility with the camera-lens system in the testing environment, the applicability of the speckle pattern to be detected (enough contrast), and actual software specifications. This technology has the capability to obtain the measurements expected (shown in a controlled laboratory setting), but needs further development for field deployment. When considering field testing, it is suggested that both the system performance and system algorithms details may need to be particularly evaluated. Additionally, particular lenses can affect the quality of results and aid in determining maximum standoff distances images can be captured for best quality images.   Ideally, continued testing with an adjusted system setup (to better track excessive motion) and instrumentation data correlation would be beneficial in meticulously tracking down displacement in images with time-stamps to track movement of a bridge.

Specific to hardware, a more stable testing platform could be used together with a shorter and sturdier surveying-style tripod to reduce noise. Also, surrounding the camera and lens with a "shield" could possibly eliminate certain wind conditions. Note that accurately assessing wind and vibration factors is very important. The movement of the camera lens could be tracked using an accelerometers and an algorithm; this could allow for lens movement to be possibly factored out in displacement analysis. However, more cohesive analysis of those measurement and respective constant factors in the algorithms would have to be assessed for accurate detection. A gyroscopically-compensated camera mount, such as one of the Kenyon Laboratories Gyro Stabilizers, could also help in keeping the camera still. Reduction of the standoff distance would certainly reduce the effects of wind and vibration. Correspondingly, with additional equipment required, the cost would also increase.

Where DIC might be used for measuring bridge settlement, transverse movement, or detecting a change in bridge length the required temporal resolution makes the technique impractical. To enable the correlation of images separated by six months, a year, or several years, the camera would have to remain in the exact same place, sheltered from environmental interference and anything else that would induce artificial displacements. These displacements are likely inevitable, and though their effect can probably be removed with sophisticated post-processing; only non-rigid displacements and deformations would be preserved. Even when the technique is applied to images separated seconds or less in time, the post-processing is not trivial.

This is particularly applicable to modifications for ideal measurements in long term monitoring. It is possible to obtain long term measurements for bridge length, bridge settlement, or transverse movement. In an ideal system, images in the DIC camera system would be taken from the same

position or be able to be registered through software analysis so alteration in standoff position would not be a factor in the analysis. Certain processing techniques will have to be configured for maximum performance such as co-registration issues from image to image. Also, images would be able to be taken at angles from the shoulder locations and the rotation in camera would be negligible in analysis. Images will yield difficulties in correlation if the images are not taken from the exact locations over time.

The analysis can be performed automatically using an analysis package such as MATLAB software, but requires additional post-processing and tuning for meaningful results. Implementation considerations such as the ones discussed would affect the cost of the system greatly. Furthermore, stationary cameras could be placed on the field site and collected over time pending co-registration of images due to minor movement on the stationary camera that could be endured during weather conditions and other shifts in movements. Higher grade lenses could be employed to get a detailed section of the bridge or the entire bridge surface. Additionally, images could be taken from higher aerial locations and movement for the entire bridge could be tracked revealing bridge settlement, transverse movement and even bridge length as previously mentioned.

9.4.2.   Re-evaluation of Software Algorithms and Noise Detection Approach

Knowing that the change in environment could greatly affect the results, it was proposed to develop a new algorithm to account for the noise. The program was developed in MATLAB and was tailored to measure deformation measurements for structural applications. This algorithm emphasizes using control points (fixed locations) in the image correlation processing. This allows the specimen being analyzed to be compared in image sets taking into account extra motion that may be present. The software creates an area of interest with a corresponding user created grid of analysis. This grid is correlated for change in position on each image in the set of images. Then the control points are identified on the images which gives a reference for the created grid points to be compared to as a stationary point. Having this algorithm collect this measurement proves crucial in minimizing the excessive motion due to wind or other environmental motions. Additionally, in this algorithm a spatial referencing script was incorporated to help relate actual size dimensions to the specimen analyzed.

Vic-2D will be used to evaluate the new post-processing algorithm evaluation and to compare how well it performed. Vic-2D proved to be very accurate in previous lab investigation and would provide a good comparable algorithm.   The program was used for previous image sets to validate the program itself. Figure 9-24 shows an image processed in this refined MATLAB algorithm. This algorithm showed very promising results for previous tests and images as demonstrated with the UHPC beam in Figure 9-24, getting within 5% error of the actual results of these tests. At the top of the photograph there is a control point on the center of the top

loading bar as this was the stationary point in the test. Also, the change in grid points from image to image can be seen where the origin grid points are bright white with a red center and the moved location are the faded white points with the red center. This was then applied to more varied testing positions to determine how well the software would be in detecting displacements at rotated positions that would mimic movement in the field whether rotations to test particular locations or excessive movement in the field.
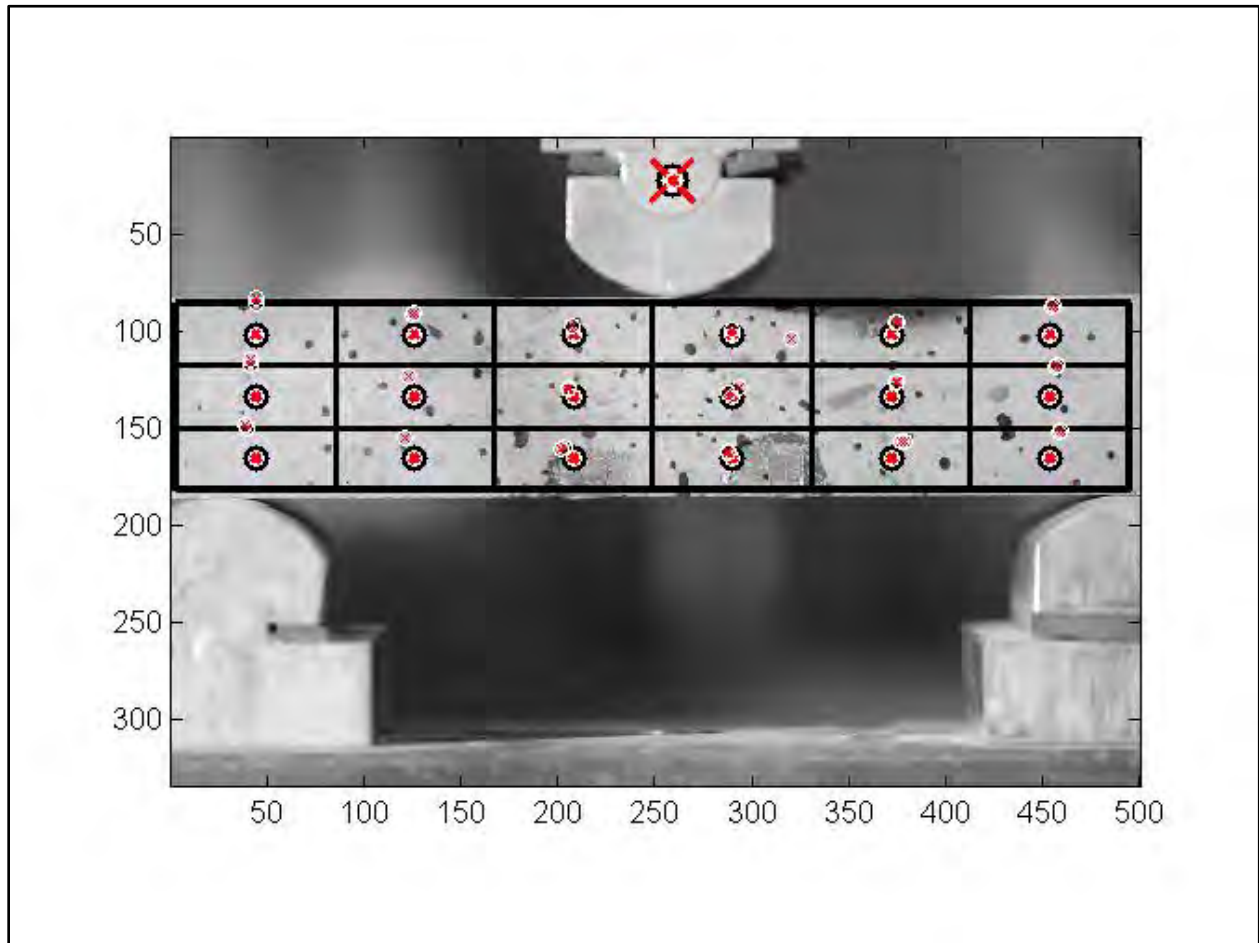
Figure 9-24: Grid display on image using refined MATLAB algorithm.

Several more testing scenarios have been created to test completed for validity of the software and capturing a relationship of simulated environmental effects and the error that would be produced in the system. As mentioned previously, identifying a threshold of percent error of measurement due to movement induced on the camera can help to characterize how much the movement will influence the DIC measurements. This also will ideally create a boundary of when percent error values calculated from the movement also including angle rotation becomes too great and produces non-usable or erratic measurements. This created an investigation with

photogrammetric principles, the underlying foundation of DIC, and relates the position of the projection point (camera) to the change in plane coordinates (points on photographs) with induced rotations. This investigation of photogrammetry principles of colinearity in remote sensing applications allows the exploration the relationship of coordinates in a sensor (image) plane to the object coordinates through the optical center of the camera.   This can provide a known coordinate location of the observed object at its image plane position and the new location due to rotation of the camera in the XYZ directions. These relationships allow for the determination of the effect of changes on sensor coordinates on image and distortion. This is crucial information that could be related to in-field environment and the actual delta (or change in position of the coordinates) due to camera movement.

With camera induced rotations at different degree intervals, great variations are expected to be verified in sample results. In a simple case study, the influence of the camera rotation will cause great change as depicted in Figure 9-25. This graph reveals an interpolated graph plot from the photogrammetric principles of the percent error difference up to 10 degrees at the 5 ft location as the specimen is displaced 0.5 in. This type of measurement is all very dependent on the camera and focal length used, the distance from specimen and amount of movement that occurs in testing. The MATLAB program will be useful in capturing motion around the XYZ axes with the identified control points on stationary locations on the images.
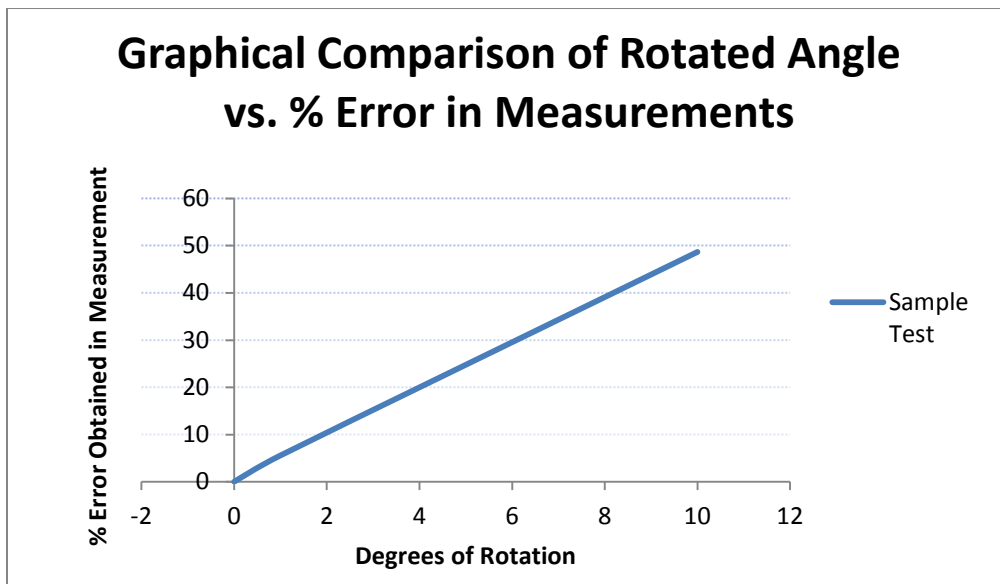
Figure 9-25: Graphical comparison for rotation and percent error obtained.

As in the Figure 9-25 case, the rotated angle considered was measured around the Y-axis. This investigation definitely complements the research for improving field conditions in which if the change in position is known, countermeasures of setup can be completed to minimize those

effects. In this study, it was found that the percent errors of the actual displacement to measured displacements increases with the change in rotation of the camera at a specific location. Continued investigation of this technique in collaboration with laboratory testing will be completed to further advance the technique. In addition, this will be further applied to a steel truss bridge that is setup in the laboratory for more testing evaluation for simulated in-field testing illustrated in Figure 9-26. The steel bridge can be shown here with a sample speckle pattern placed at the mid span location for movement tracking. Current and further investigations include static loading and dynamic testing to simulate bridge behavior in which global metric behaviors. Furthermore, testing will be completed at different elevations and distances to determine range of measurements and where percent errors of measurements are greatest and not effective for quality DIC measurements.

Figure 9-26: Steel bridge specimen used for continued investigations.

9.4.3. Data Combination

This technique can be useful in combination with other technologies for validation and supplementary data comparisons. DIC can be deployed in the field with traditional

instrumentation for verification purposes. These devices include strain gages and deflectometers to track the behavior response of the bridge due to loading. Ideally, DIC allows for a non-contact approach to these measurements. A technology in this investigation that was comparable or complimentary to DIC in particular was LiDAR. Terrestrial LiDAR provides a point cloud representative data model of the bridge. This data is ideal for deck surface measurements and was deemed applicable for measuring global metric behavior. In particular, LiDAR was evaluated effective for bridge settlement and bridge movement. Even though this was not principally investigated during this study, this type of movement can show promise for this challenge and could be coupled with DIC for long-term applications.

In addition, LiDAR had shown promise for live load or vibration detection for static loading conditions (Wanqiu et al. 2010).   This data can be compared during static loading positions when there is no load at a specific location such as the mid-span and compare to an image in which there is a truck load placed at that same location. Additionally, this point cloud data collection can be thoroughly processed and compared with DIC to reveal the change in position of the girder or examined bridge member. Furthermore, this data can also be correlated with a finite element analysis model (FEA) of the Mannsiding Road bridge comparing simulated behavior with actual bridge response. FEA allows for mechanical responses to be detailed due to simulated loading conditions.   DIC can be collaborated to reveal similar mechanical responses such as deflections, stresses and strains.

9.5.   Future Plans and Final Remarks

This DIC investigation is an ongoing study of this technology to employ better configurations for the field deployment environment. This will lead to re-investigation of parameters in the laboratory setup, including a newly created algorithm and an accountability of change (Δ) in position of image coordinates relationship development for DIC. This will enable a percent error scope of how rotations and simulated noise movement influence the DIC measurements. For future bridge comparison, a steel truss bridge as shown in Figure 9-27 located in Benedict Laboratory would provide a test case for implementation for testing alterations and variations of the DIC system and developed algorithms. For this testing scenario, traditional electro-mechanical instrumentation (e.g., LVDTs, deflectometers) will be used as the ground truth for the test. Dynamic loading will be evaluated with a dynamic shaker exciting the bridge and vibration or the live load deflection will be monitored.

Figure 9-27: Walking bridge located in Benedict laboratory at MTU.

Furthermore, more advanced mounting hardware will be investigated for a more stable field deployable setting. Continued efforts will be completed to address the limitations and challenges of this technology, in particular software algorithms and calibration processes. This will be used in future in-field bridge demonstrations to revisit issues experienced in the previous field demonstration. Preferably, more single unit deployable field DIC systems will be explored for managing environmental condition effects. DIC was revealed as very promising for structural integrity evaluation and will be continually investigated for maximum performance measurements as a remote sensing technology for bridge condition assessment.

10. Ultra Wide Band Imaging Example of Ground Penetrating Radio Detection and Ranging

While optical remote sensing technologies provide information about the surface condition of bridge decks, RaDAR systems, employing low frequency electromagnetic waves that penetrate the deck material, provide information about the deck interior. Previous studies have demonstrated that down-looking, low frequency, GPR can image delaminations, defects and rebar within concrete bridge decks, as reviewed in (Vaghefi et al. 2011) and the project's Commercial Sensor Evaluation report found in Appendix A.

Several commercial companies have developed production systems to produce reflectivity maps that are indicative of deck defects. These spatial maps, or more specifically metrics derived from these maps, can be used within the DSS to provide quantitative measures of deck condition which contribute to the overall bridge condition metric. The current program reviewed currently available commercial systems for compatibility and utility with the DSS and conducted a limited set of RaDAR experiments to extend the use of RaDAR technology for bridge assessment.

The RaDAR experiments, conducted under this program as part of the field testing, aimed to extend use of RaDAR technology for bridge assessment in two ways. First, current commercial RaDAR systems used to survey deck condition utilize arrays of truck or cart mounted antennas that are scanned at a vertical orientation close to the deck surface. These systems operate in close proximity to the deck and may require the bridge to be closed for extended periods of time to complete the scan. To mitigate these limitations, an alternate imaging approach was investigated, where a single RaDAR antenna views the deck surface at an oblique angle from the side of a vehicle. This approach would allow a vehicle mounted RaDAR travelling in one lane to produce a 2D image of an adjacent lane, and thus potentially reducing data collection time and interference with traffic. The imaging geometry is also similar to the geometry that would be provided by a standoff airborne RaDAR, so the data collection provided information for assessing the potential utility of a standoff airborne sensor.

The second RaDAR application investigated as part of the field demonstration was the use of low frequency RaDAR to image the interior of concrete box beams. Lack of visual access to the interior of box beams makes condition assessment difficult. Low frequency, 3D imaging RaDAR potentially provides a means of interrogating the structure interior. For each application, a prototype low frequency, wideband RaDAR system was developed using a commercially available transmitter/receiver unit. These systems were used to image bridge structures as part of the summer field demonstrations, and resulting data were evaluated for their utility for bridge condition assessment.

In this section, currently available commercial RaDAR systems will first be reviewed in Section 10.1, and their applicability to the DSS will be discussed. Subsequently, the exploratory RaDAR measurements conducted as part of the field demonstrations will be reviewed in Section 10.2. The RaDAR systems and experiments conducted as part of the field demonstrations will be described, and the results of the experiments and their utility for structure assessment will be summarized. Advantages and limitations of the approaches will be presented, along with recommendations for next steps in Section 10.3.

10.1. Commercial Systems

RaDAR systems probe the environment by transmitting electromagnetic waves, which reflect from surfaces and/or inhomogeneities, which scatter energy back to the RaDAR system. The RaDAR measures the time required for the wave to propagate to the scatterer and back, and this time can be related to the spatial position of the scatterer. GPR systems are designed to transmit energy into material regions, such as the ground or structures, to detect and measure scatterers within those regions. For bridge remote sensing purposes, these scatterers arise from material inhomogeneities, which may be due to normal structure interfaces or due to defects such as subsurface delaminations. Delaminations are a "planar separation in a material that is roughly parallel to the surface of the material" (see American Concrete Institute 2010). It is important to note that RaDAR systems generally do not make direct measurements of bridge structure features and/or material properties. RaDAR returns arise from discontinuities or inhomogeneities in materials. Thus, RaDAR information is "non-litteral" in the sense that the properties of the structure must be inferred by interpreting the strength and location of the sources of RaDAR scattering, rather than being measured directly.

GPR is already commercially available and many companies offer GPR instrumentation for purchase for a wide variety of applications. A representative list of commercial GPR systems is included in Table 10-1.

Some companies perform GPR surveys as a service and do not sell instrumentation; some of these are listed in Table 10-2. Analysis of GPR data can be complex, however, as signals must be "migrated" to identify subsurface features and for some applications the dielectric properties of the medium need to be estimated. While GPR can be used for moisture or chloride measurements, GPR is sensitive to environmental factors such as rain and snow, though some users of commercial GPR systems indicate the effect is not significant (Kim et al. 2003). There is commercial software available for post-processing RaDAR data, most notably the RADAN software suite developed by Geophysical Survey Systems (GSSI), which automatically integrates GPS location data.

Table 10-1: Representative list of some common commercial GPR systems available for purchase.

Instrument	Company	Bandwidth
Profiler EMP-400	Geophysical Survey Systems	1-16 kHz
TerraVision	Geophysical Survey Systems	400 MHz
BallastScan	Geophysical Survey Systems	2.0 GHz
BridgeScan	Geophysical Survey Systems	1.6 GHz
RoadScan 30	Geophysical Survey Systems	500 MHz
StructureScan Mini	Geophysical Survey Systems	1.6 GHz
StructureScan Standard	Geophysical Survey Systems	1.6 or 2.6 GHz
StructureScan Professional	Geophysical Survey Systems	1.6 GHz
StructureScan Optical	Geophysical Survey Systems	1.6 or 2.6 GHz
SIR-20 or SIR-3000	Geophysical Survey Systems	Depends on antenna
OKO-2	Geotech	Depends on antenna
Detector Duo	Ingegneria dei Sistemi	250 or 700 MHz
RIS MF Hi-Mod	Ingegneria dei Sistemi	200-600 or 400-900 MHz
Aladdin	Ingegneria dei Sistemi	2.0 GHz
GPR for Road	Ingegneria dei Sistemi	0.6, 1.6, or 2.0 GHz
Imaging RaDAR Array	MALÅ Geoscience	Depends on antenna
CX Concrete Imaging	MALÅ Geoscience	1.2, 1.6, or 2.3 GHz
ProEx	MALÅ Geoscience	Depends on antenna

Table 10-2: Partial list of companies that perform GPR surveys as a service.

Company	Website
NGPRS	www.ngprs.com
GPA Data	www.gprdata.com
Sensors & Software	www.sensoft.ca
Penetradar	www.penetradar.com
GPR Professional Services	www.gprps.com
Global GPR	www.global-gpr.com
Virtual Underground	www.virtualug.com
GeoView	www.geoviewinc.com

10.1.1. Application to Bridge Condition Sensing

GPR has primarily been used to examine three general areas of potential bridge defects; delamination, moisture and/or chloride ingress, and rebar corrosion (Romero et al. 2000; Shin and Grivas 2003). Mapping of bridge deck delamination is the most common application, particularly for commercial systems. Thus, delamination mapping is of most interest as a data input to the DSS. Characterization of moisture and chloride ingress and rebar corrosion is still more of a research topic.

GPR has been frequently used to locate delaminations in concrete bridge decks. These experiments have constrained the penetration depth of GPR to 7-12 cm at typical stand-off and emission frequencies (Warhus et al. 1994). Voids and areas of potential delamination are mapped with GPR but the dimensions of these areas are not usually known due to the limitations of the technology. By combining SAR with GPR, Scott, Rezaizadeh et al. (2001) indicated potential to measure the dimensions of subsurface features. The FHWA-funded HERMES (High-speed Electromagnetic Roadway Mapping and Evaluation System) Bridge Inspector, the authors describe, was used to locate and characterize the condition of embedded steel reinforcement, detect corrosion-related delamination, as well as locate voids and debonds. HERMES used ultra-wideband sources developed by Lawrence Livermore National Labs emitting in the 0.5-5 GHz range. They were able to penetrate only to 12 cm below the concrete surface, and acknowledged the need for improved range resolution and signal-to-noise ratio as well, but found that SAR processing enabled them to display 2D projections of 3D bridge deck features.

RaDAR has been shown to be sensitive to moisture content. Maierhofer and Leipold (2001), using a GSSI SIR-10 unit operated at 500, 900, 1,000, and 1,500 MHz, determined that by measuring the travel time of the backside reflection, determining the permittivity, and generating calibration curves, the moisture of a mortar structure could be determined to within between 1 and 5% by volume. In place of calibration curves, an inversion model of moisture in concrete might be used in order to estimate the moisture content. Some bridge managers or inspectors may not be interested in quantifying the amount of moisture content and, where that is the case, GPR is also an appropriate choice: it can be used in detecting relative changes in moisture content where strict environmental controls are employed (the technique is sensitive, of course, to moisture held by a bridge after a rainstorm and would be affected by snow or standing water on the bridge deck).

Commercial GPR seems promising for characterizing chloride ingress in girders and the deck subsurface, however. The potential use of GPR for this application was first reported by Maser (1986) when it was observed that RaDAR signal was attenuated in areas of high chloride concentration. The available literature shows that the presence of chloride in a concrete deck increases the material's conductivity and decreases its permittivity. This increase in conductivity results in signal attenuation as less electromagnetic energy is reflected back throughout the

volume (Lim 2001). Kim, Ismail et al. (2003) notes that areas with a high dielectric constant (low electromagnetic velocity) and high attenuation are typically zones of delamination, which are likely marked by high moisture and chloride content.

Rebar, made of metal and therefore highly conductive, causes diffractions in the GPR reflection data (Cardimona et al. 2000), which, when migrated, collapse to the point of origin. Currently, the technique is limited to deformation mapping – the gridding of GPR reflection amplitudes. Harris, Hong et al. (2010) demonstrated that this technique performs just as well or better than standard methods (half-cell potential and sounding) at locating areas of rebar corrosion in most cases. Barrile and Pucinotti (2005) used this technique to characterize the number and position of longitudinal rebar, detect voids, and derive stirrup steps in structural members. Both studies used commercial RaDAR systems; Harris, Hong et al. (2010) utilized a GSSI instrument while Barrile and Pucinotti (2005) used an RIS-family instrument built by IDS (Ingegneria dei Sistemi).

10.1.2.   Examples of Available Commercial Systems

More recently, several commercial systems have been developed into field-deployable products available for bridge inspection. Roadscanners has developed GPR systems for bridge inspection using cart or vehicle-based antenna arrays, which can be used to generate 2D and 3D maps of RaDAR reflectivity and/or GPR signal attenuation. These data can be used to infer bridge deck condition. Roadscanners specifically has Road Doctor PRO software that converts the raw RaDAR data into interpretable spatial maps of observables, which can be used to infer bridge condition.

Curtiss-Wright 3D-RaDAR, produces multichannel antenna arrays for GPR, which can be attached to a vehicle for bridge surface mapping. Using a 200-3,000 MHz bandwidth, the unit can produce 3D maps of RaDAR reflectivity. Penetradar has produced a vehicle mounted 3D imaging system (IRIS: Integrated RaDAR Inspection System), which has a full bridge deck mapping capability and claims to be able to detect areas of deck delamination. An example of a Penetrader spatial map output product indicating areas of delamination is shown in Figure 10-1.
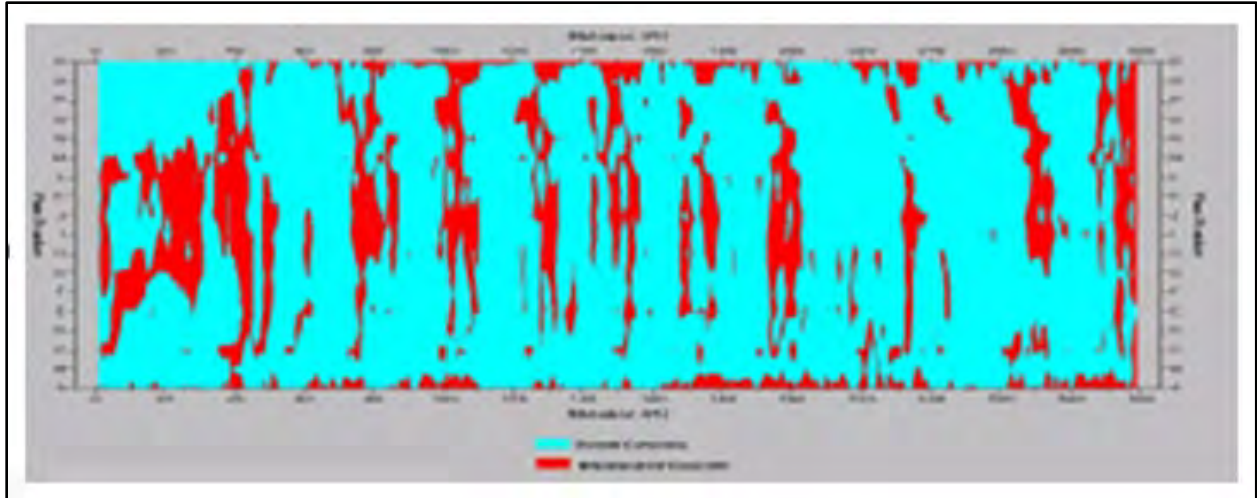
Figure 10-1: Typical GPR bridge deck delamination map produced with IRIS hardware and software. Red areas show locations of delaminated concrete.

The systems mentioned above are just representative sample of the emerging technology. The key point is that there are commercial mapping GPR sensors available that can produce spatial maps of suspected areas of bridge deck deterioration such as sub-surface delaminations. These spatial maps, or more specifically metrics derived from these maps, can be used within the DSS to provide quantitative measures of deck condition which contribute to the overall bridge condition metric. These systems are cited as examples of commercial systems that can provide input to the DSS, and no endorsement of these products or their performance is given or implied.

10.2. Ground Penetrating Radio Detecting and Ranging Experiments

The RaDAR experiments, conducted under this program as part of the field testing, aimed to extend use of RaDAR technology for bridge assessment in two ways. First, current commercial RaDAR systems used to survey deck condition utilize arrays of truck or cart mounted antennas that are scanned at a vertical orientation close to the deck surface. These systems operate in close proximity to the deck and may require the bridge to be closed for extended periods of time to complete the scan. To mitigate these limitations, an alternate imaging approach, where a single RaDAR antenna views the deck surface at an oblique angle from the side of a vehicle, was investigated. The concept is illustrated in Figure 10-2. This approach would allow a vehicle mounted RaDAR travelling in one lane to produce a 2D image of an adjacent lane, and thus, potentially reducing data collection time and interference with traffic. The imaging geometry is also similar to the geometry that would be provided by a standoff airborne RaDAR, so the data collection provided information for assessing the potential utility of a standoff airborne sensor.
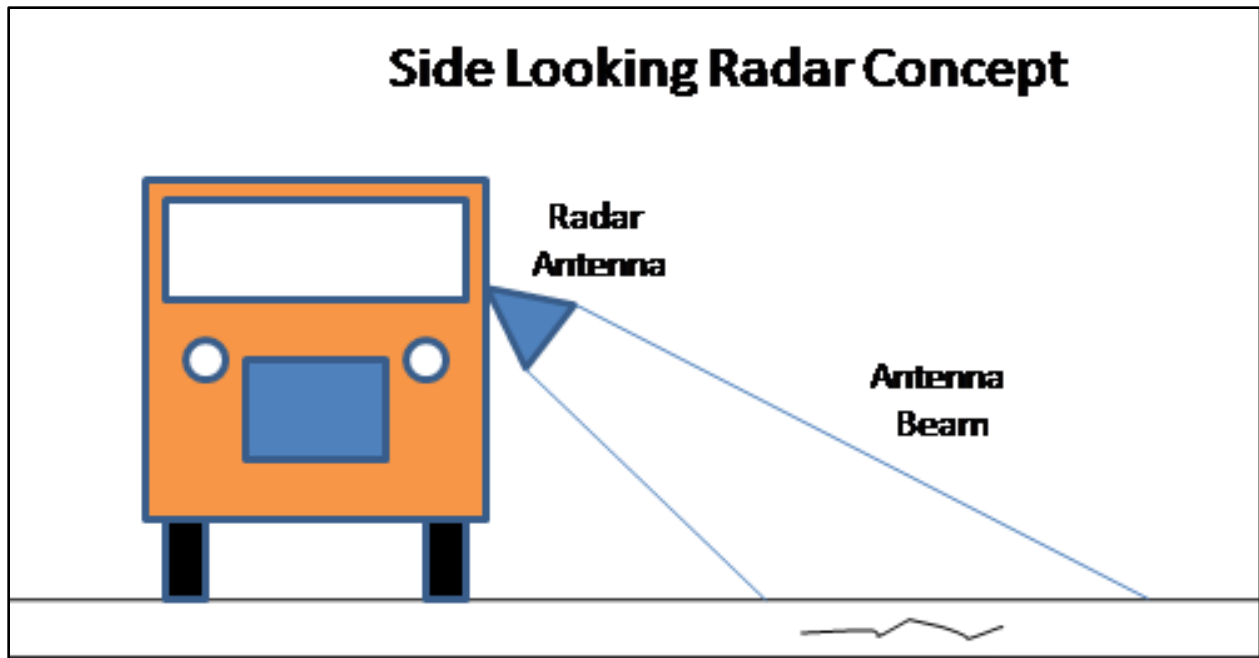
Figure 10-2: Side looking RaDAR concept.

The second RaDAR application investigated as part of the field demonstration was the use of low frequency RaDAR to image the interior of concrete box beams. Lack of visual access to the interior of box beams makes condition assessment difficult. Low frequency, 3D imaging RaDAR potentially provides a means of interrogating the structure interior. For each application, a prototype low frequency, wideband RaDAR system was developed using a commercially available transmitter/receiver unit. These systems were used to image bridge structures as part of the summer field demonstrations, and resulting data were evaluated for their utility for bridge condition assessment.

RaDAR and optical remote sensing measurements of concrete bridge deck and superstructure were conducted in August 2011 as part of the Field Demonstration Task of the Bridge Condition Assessment Using Remote Sensors project. Specifically, data were collected at the Freer Road bridge of I-94 near Chelsea, the Willow Road bridge of US-23 south of Ann Arbor, and the Mannsiding Road bridge of US-127 north of Clare. In addition, measurements of a salvaged concrete box beam were collected at a MDOT facility in Oakland County in September 2011.

To assess the utility of ultra wide band (UWB), low frequency, imaging RaDAR measurements to image the interior of concrete bridge component structures and identify potential structural defects, two types of imaging RaDAR measurements were collected at the test sites. In the 2D imaging modality, the RaDAR sensor obliquely illuminated the bridge deck surface as it was moved along a linear path parallel to the deck surface. This type of data collect produces a 2D map of the RaDAR reflectivity of the deck, which may indicate areas of internal defect and/or delamination. This type of collection is consistent with a concept of operation that has a RaDAR

system mounted on a moving vehicle to produce maps of deck RaDAR reflectivity that identify areas of concern. This type of collection could be performed by a standoff airborne sensor.

In the 3D imaging modality, the RaDAR illuminates the bridge at a normal angle of incidence, and the RaDAR is scanned over a 2D plane parallel to the bridge structure under test. Data from this form of collection can be used to produce a 3D map of the RaDAR reflectivity, which may indicate areas of internal defect. This type of data collection is consistent with a concept of operation that uses the RaDAR system to make a detailed internal survey of a suspect area.

10.2.1.   Field Data Collections

The procedures used to collect 2D and 3D RaDAR measurements will be described in this section. The RaDAR data collected at the test sites will be summarized in Section 10.2.2.

10.2.1.1.   Ultra Wide Band Imaging Radio Detection and Ranging System

A field portable UWBIRS was developed to emulate the performance of commercial RaDAR sensors for the field demonstrations. The RaDAR system consists of a commercially-available AKELA Radio Frequency Vector Signal Generator and Measurement Unit (AVMU) connected to a pair of wideband exponential taper horns. The AVMU operates in a stepped frequency continuous wave (SFCW) mode, with pulse modulation to limit the time delays over which data are collected. The system collects data over 500-3,000 MHz, with a nominal output power of 17 dBm.

The 1.1 lb unit can operate using portable power sources. The RaDAR is controlled using a laptop computer, and all of the instrument's operating parameters are under user control via a graphical user interface. As discussed below, the RaDAR system was deployed on a portable, reconfigurable translation fixture to collect frequency diverse data as the RaDAR sensor was scanned in one and two spatial dimensions at the field demonstrations.

10.2.1.1.1.   Measurement Configuration for 2D Collection

A 2D RaDAR data collection refers to a measurement where the RaDAR collects electromagnetic backscattering measurements over a range of radio frequencies as the RaDAR is moved linearly along one spatial dimension. The resulting data set is a 2D array of scene backscattering measurements as a function of frequency and sensor location.

To collect 2D RaDAR data an apparatus was constructed which moves the RaDAR antenna along one dimension, parallel to the object being measured. This system is made using aluminum framing and an electric motor drive system for consistent sensor motion. The rail along which the RaDAR antenna is translated allows for approximately 2.8 m of sensor motion, which is only

limited by the current size of the side support rails and motor drive mechanism. The system is shown in Figure 10-3. A more mobile apparatus, shown in Figure 10-4, was used to make a series of data collections along the entire bridge deck.
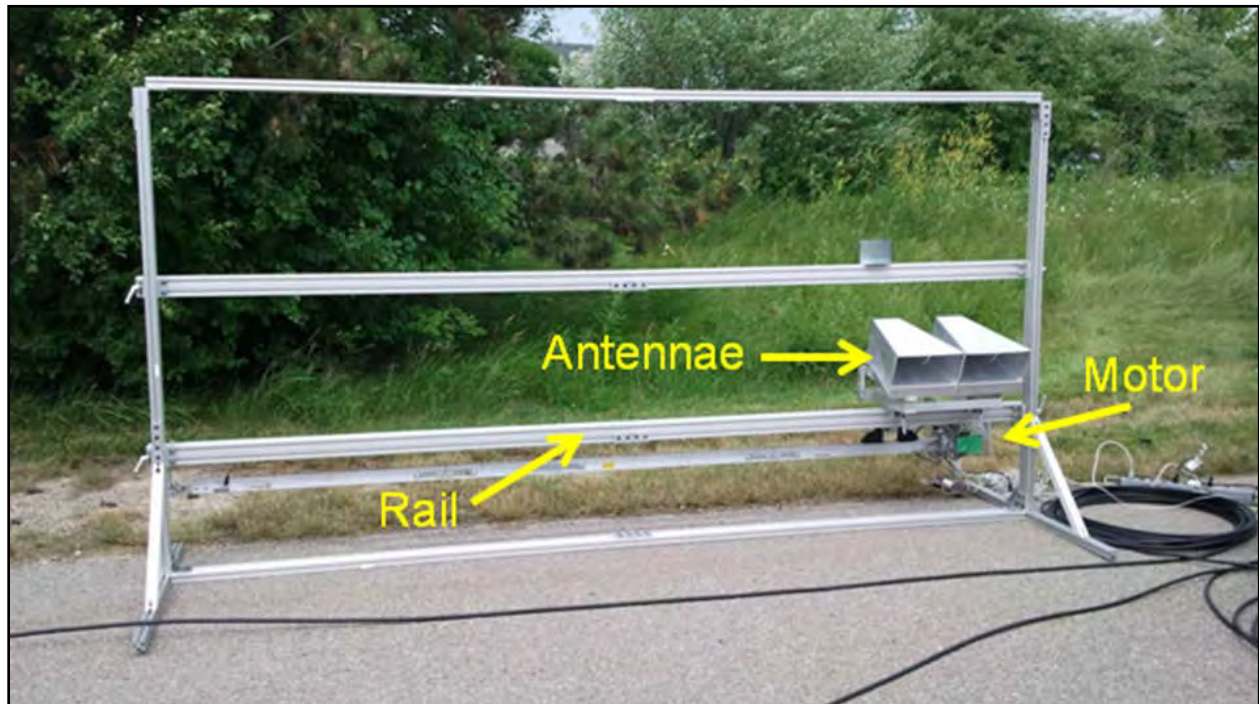
Figure 10-3: 2D field portable RaDAR translator apparatus.

An optical position encoder is attached to the motor to record antenna along-track positions at the start of each RaDAR frequency sweep. The operating parameters of the RaDAR AVMU are configured to illuminate a constrained area of the scene to be imaged via appropriate time gating, and to have the appropriate settings for the particular measurement (e.g., frequency span, gain). In operation, the RaDAR sweeps frequency and collects scene backscattering measurements as the antenna translates down the rail. After the measurement has finished, the 2D data, e.g. scene backscattering verse frequency and sensor location, are saved and post-processed into imagery and/or other products.

Figure 10-4: More "mobile" translator apparatus and RaDAR equipment, which could be adapted for moving vehicle-based deployment.

10.2.1.1.2. Measurement Configuration for 3D Collection

A 3D RaDAR data collection refers to a measurement where the RaDAR collects electromagnetic backscattering measurements over a range of radio frequencies as the RaDAR is moved linearly along two spatial dimensions. The resulting data set is a 3D array of scene backscattering measurements as a function of frequency and the sensor position in two spatial dimensions.

The 3D apparatus is identical to the 2D setup, except the side support rails are lengthened allowing for approximately 2.5 m of translation in that dimension (normal to the motorized rail direction). This added length is necessary to achieve roughly equivalent spatial resolution in this dimension as in the along rail dimension. This 2D translation of the RaDAR sensor results in 3D data - frequency and sensor position in two spatial directions corresponding to the two translation directions. In this configuration the motor drive rail system is set at one end of the side support rails, data are collected in the same manner as the 2D scan, and then the drive rail system is repositioned by a specified amount for the next measurement. These data are saved and then post processed into a 3D RaDAR image.

The 3D apparatus can be oriented with the side support rails either vertical, with the antennas pointing horizontally (at various angles), or horizontal, with the antennas pointing either up or down. This allows 3D measurements to be made of vertical structures such as walls, as well as horizontal structures, such as the underside of bridge structures, in order to attempt to evaluate their sub-surface features. In the vertical configuration the translator apparatus moves the antennas in a plane perpendicular to the ground, while in the horizontal configuration, the translator apparatus moves the antennas in a plane parallel to the ground. The horizontal orientation was utilized to make measurements of the underside of the bridge deck. Post processing is identical in either orientation. Figure 10-5 shows the translator apparatus in the horizontal orientation.
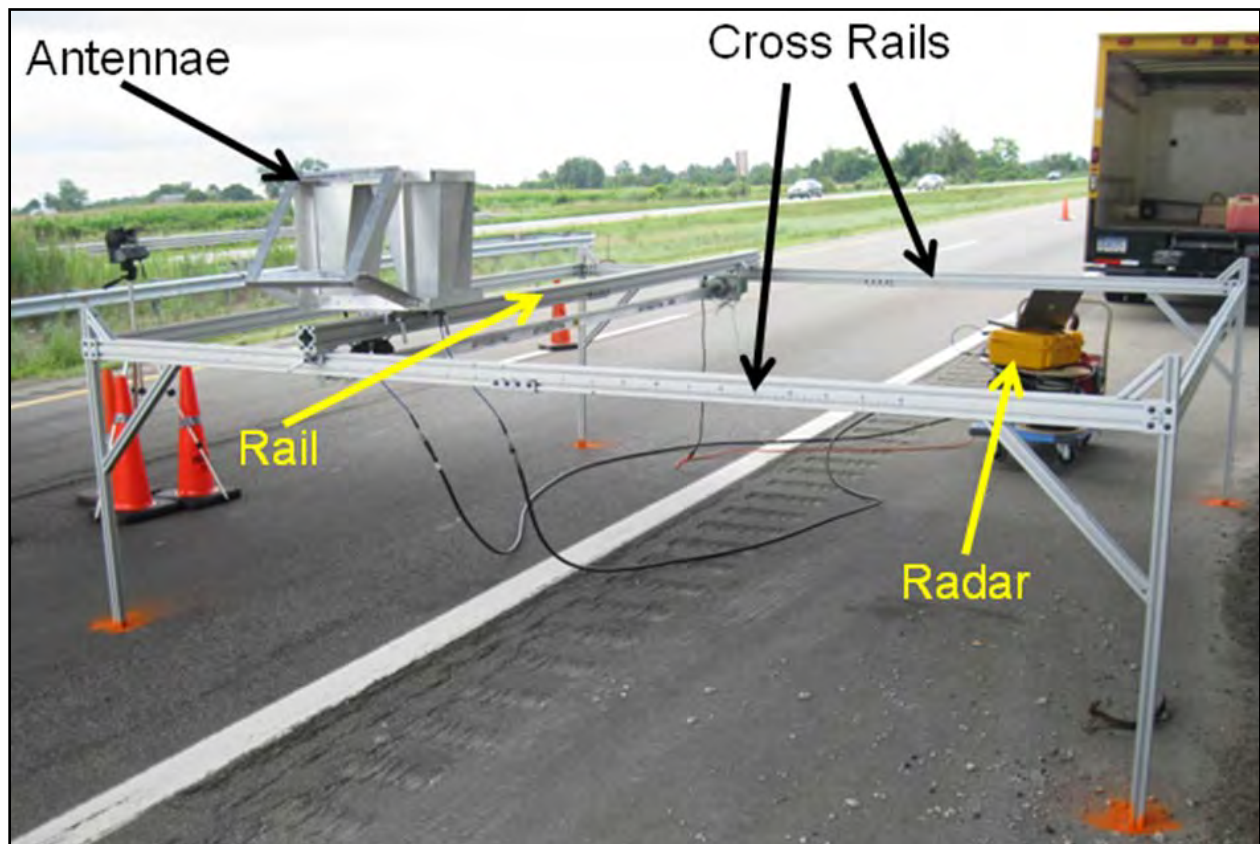
Figure 10-5: Translator apparatus configured for 3D imaging in horizontal orientation.

10.2.1.1.3. Image Formation

2D RaDAR measurements of the scene, specifically RaDAR backscattering measurements as a function of frequency and RaDAR sensor location along a straight line can be processed into a 2D spatial map, or image, of RaDAR reflectivity. The collected data   were processed into 2D images using Back-projection and the 2D Range Migration Algorithm (RMA). A summary of the algorithm and its derivation are given in Carrara, et al. (1995). The algorithm is outlined in Figure 10-6.
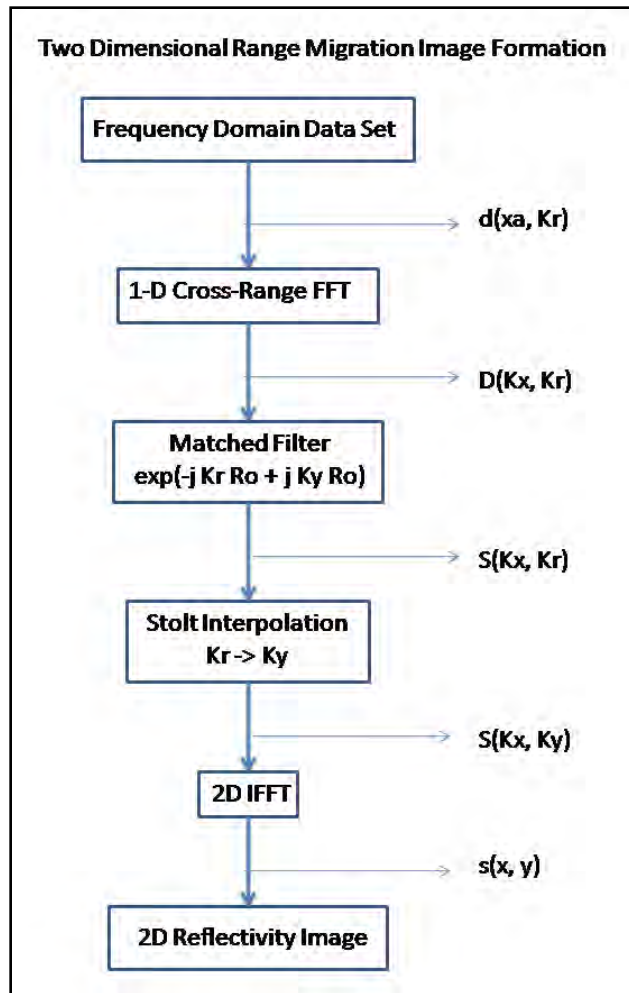
Figure 10-6: 2D range migration image formation algorithm.

Given the RaDAR measurements as a function of position and frequency, the Fourier transform of the data is taken along position, and are multiplied by a matched filter. The resulting data are interpolated in the frequency direction to form an estimate of the image spectrum that is uniformly sampled in spatial frequency space. The 2D Fourier transform is then taken to produce a 2D reflectivity map of the scene.

3D RaDAR measurements of the scene, specifically RaDAR backscattering measurements as a function of frequency and sensor location scanned over a 2D plane can be processed into a 3D spatial map, or image, of RaDAR reflectivity. 3D images can be generated using Back-projection and 3D RMA. 3D RMA was used for much of the 3D data processing since it has lower computational complexity than the Backprokection. The 3D RMA, which was derived in Lopez-Sanchez and Fortuny-Guasch (2000), is outlined in Figure 10-7.
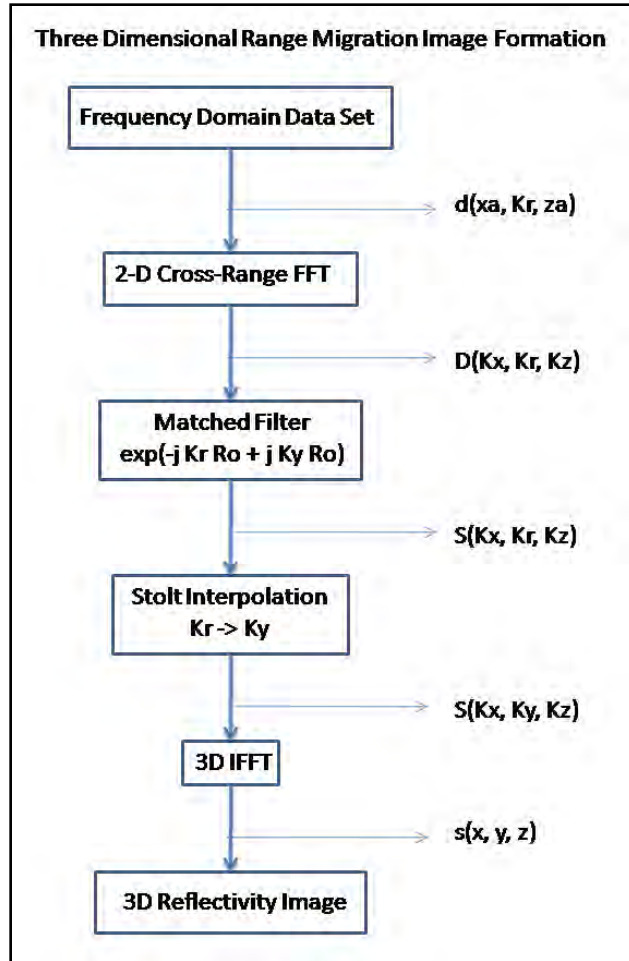
Figure 10-7: 3D range migration image formation algorithm.

The algorithm is very similar to the 2D approach. Given the RaDAR measurements as a function of 2D position and frequency, a 2D Fourier transform of the data is taken along the two position directions, and are multiplied by a matched filter. The resulting data are interpolated in the frequency direction to form an estimate of the image spectrum that is uniformly sampled in spatial frequency space. The 3D Fourier transform is then taken to produce a 3D reflectivity map of the scene.

10.2.1.2.   Deck Measurement Results

As discussed above, bridge deck measurements were made at both the Freer Road and Willow Road bridges. In each case, the resulting data were processed into 2D RaDAR imagery. The resulting imagery was then compared to manual assessments of delamination. The RaDAR data collected at Freer Road was of poorer quality than that collected at Willow Road, so the comparison with ground truth concentrated on the Willow Road data.

At both test sites, 2D measurements of the entire bridge deck were made by setting up the translator apparatus shown in Figure 10-4 in its vertical orientation such that the RaDAR antenna would be moved parallel to the direction of travel on the road. A measurement was taken with 3 fiducial corner reflectors set in the area to be imaged, and then this measurement was repeated with the fiducials removed. The translator apparatus was then moved 10 ft further along the bridge deck and these measurements were repeated. This method of moving the translation apparatus along the road at intervals also served to simulate mounting of the RaDAR to a vehicle and driving in one lane while imaging another. Note that the measurements of the deck with the fiducial targets provided a method of assessing image quality and RaDAR system performance. Since these targets rested on the deck surface, the RaDAR return from these fiducials targets should be localized and focused if the RaDAR system was functioning correctly.

The RaDAR returns were processed into image output, which in turn could be tied to the geometry of the brick deck. 2D RaDAR reflectively maps (images) of the Willow Road deck produced using the range migration algorithm are shown in Figure 10-8 and Figure 10-9. Images of the two lanes of the Willow Road deck when calibration reflectors were placed in the scene are shown in Figure 10-8. The figure shows the Willow Road deck geometry, with potential delamination sites from the ground truth survey, to the left. The 2D RaDAR reflectivity map on a 35 dB color scale in the center, and the map with the delamination site superimposed to the right. These images were generated from RaDAR backscattering measurements spanning the full 750-3,000 MHz frequency range. The point-like returns in the images are the localized returns from the calibration reflectors. The point-like response of the calibration reflectors in the images verify that the collected data have been successfully processed into imagery. The variable, distributed returns are the returns from the deck subsurface.

Images of the two lanes of the deck without calibration reflectors are shown in Figure 10-9. These images show just the returns from the deck. The images to the right show suspected areas of delamination from the manual inspection. The general hypothesis was that areas of delamination show produce enhanced backscattering to the RaDAR, and thus appear as areas of

Figure 10-8: **2D RaDAR reflectivity maps of the Willow Road bridge deck with calibration reflectors.**
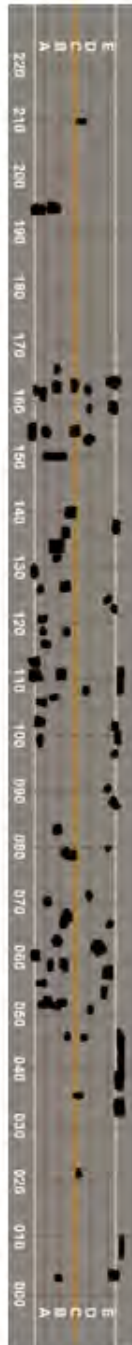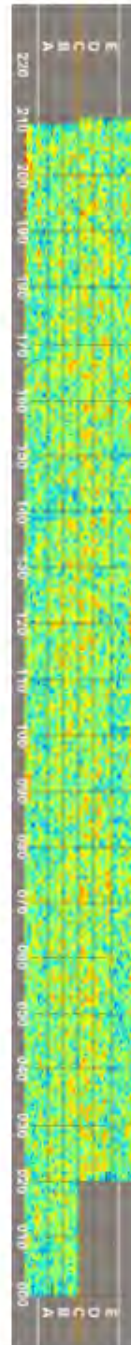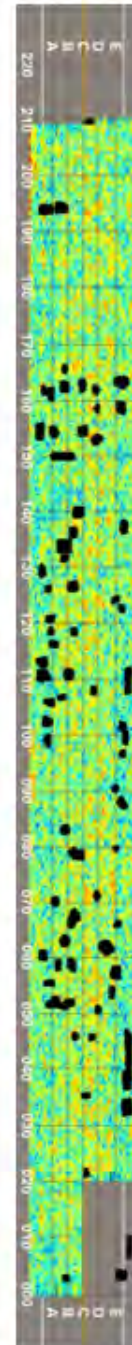
Figure 10-9: 2D RaDAR reflectivity map of Willow Road bridge deck.

higher return. However, the comparison of the images with the ground truth did not show this relationship. It is noteworthy that the Thermal IR also found mostly different delamination areas than the manual inspection – it is possible that both Thermal IR and RaDAR are finding different subsurface deterioration features than traditional manual soundings, which would need coring of the bridge deck to determine with direct ground truth.

RaDAR images of Willow Road deck were also generated with back-projection. The images were georegistered and overlays that indicated the suspected areas of delamination were superimposed. Figure 10-10 shows an image of the Willow Road bridge with the georegistered RaDAR image overlaid on the optical image of the bridge. The composite RaDAR image is the mosaic of the sequence of individual RaDAR images. The red outlines are suspected areas of delamination deduced from a manual inspection of the bridge (via hammer sounding by MDOT partners). The RaDAR image is displayed with a color map where red is the highest level. The lighter yellow/green areas are higher than the blue areas.
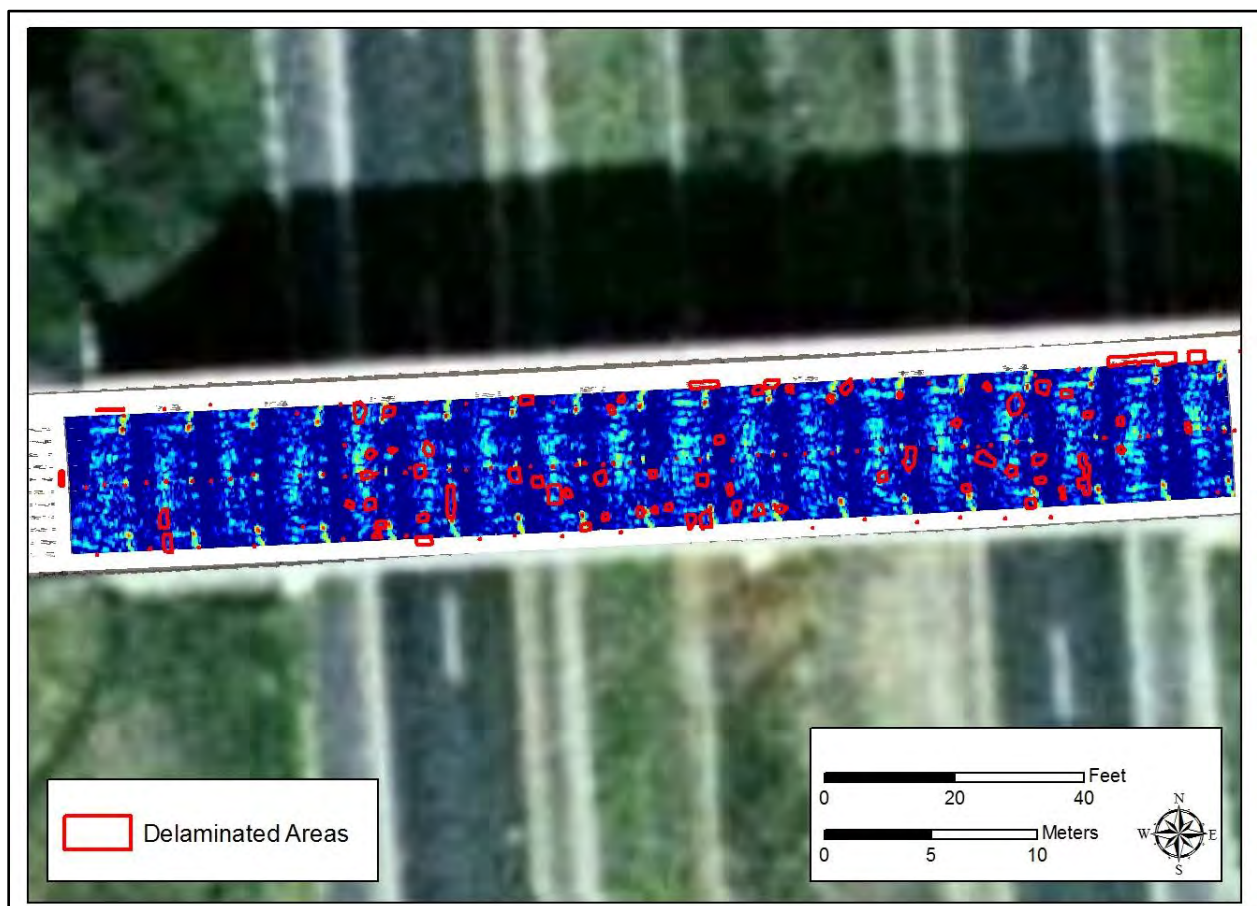
Figure 10-10: Image of Willow Road bridge with georegistered RaDAR image overlaid on optical image. The red outlines indicate suspected areas of delamination.

Note the periodic red dots are the localized returns from the calibration reflectors placed on the surface of the deck. The tight focus of these calibration reflectors indicate that the RaDAR system was working properly and producing quality imagery of targets on the surface of the deck. he areas of blue low level returns between the individual images is due to limitation of the RaDAR illumination used in the collection, and not an inherent limitation of the sensing concept.

Figure 10-11 shows larger displays of local regions of the deck. The side looking RaDAR at oblique incidence concept assumed that delaminations would be manifest by local areas of increased RaDAR reflectivity. Comparing the bright regions (yellow/green areas) of the images to the red delamination outlines, it appears that there is not a good correspondence between high areas of reflectivity and suspect delamination.
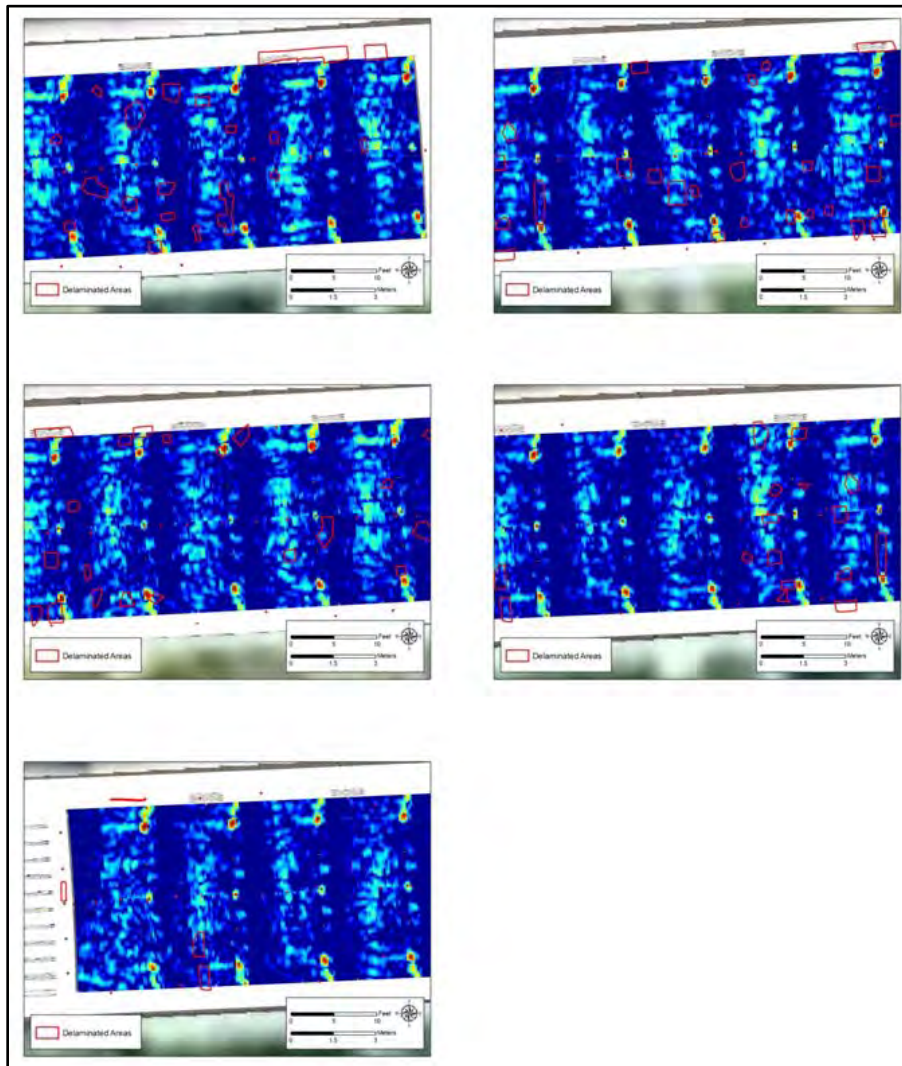
Figure 10-11: Areas of Willow Road bridge deck with red outlines indicating suspect delaminations.

There are two likely reasons that the concept was not demonstrated in the field test data. First, the oblique incidence backscattering from the relatively shallow delamination areas was not strong enough to produce a feature that could be distinguished from the background scattering from the rest of the bridge interior structure. Second, the RaDAR parameters selected for the field test may not have been optimal for the application. Since delaminations occur not far into the deck surface, a RaDAR operating at a higher frequency may have been more effect since only a relatively shallow region of the deck needed to be probed. Deconvolution of the frequency response of the measurement system would also have improved performance, but the required algorithm development was not within the scope of the current effort. The UWBIRS system may also be finding deterioration features not found during the traditional manual hammer sounding.

10.2.1.3.　　　Imaging of Box Beam Interior

Electromagnetic waves from an ultrawideband, low frequency RaDAR can penetrate concrete structures, and in principle, frequency and angle diverse measurements of the backscattered energy can be processed into imagery to provide information about the interior structure. Specifically, discontinuities, transitions, and inhomogeneities in the material structure will backscatter electromagnetic energy to the RaDAR, which appears as localized areas of enhanced RaDAR reflectivity in a RaDAR image.

To assess the utility of RaDAR to image the interior structure of concrete box beam, RaDAR measurements of a box beam salvaged from a recent bridge demolition were collected at the Oakland County Road Commission facility in Waterford, Michigan. The collected data were processed into a 3D map of RaDAR reflectivity to see if interior structure and/or defects were observed.

Photos of the salvaged box beam are shown in Figure 10-12. The front side of the beam viewed from the RaDAR is shown, along with the top and rear sides. The ends of the beam are also shown. Specifically, the right end shows a rough cross-sectional cut of the beam, which gives a general indication of the location of the foam insert and rebar reinforcement.

The portable aluminum frame used to scan the RaDAR antenna over a 2D plane (horizontal and vertical to the ground) parallel to the side surface of the beam is shown in Figure 10-13 in the position used to image the beam.

As sketched in Figure 10-14, the 3D RaDAR measurements of the box beam, specifically RaDAR backscattering measurements as a function of frequency and sensor location scanned over a 2D plane can be processed into a 3D map of RaDAR reflectivity. Specifically, the data were processed into imagery using the 3D RMA, described above.

Front Face of Box Beam (closest to radar)

Radar Deployed in Front of Beam

Top Surface of Box Beam

Rear Face of Box Beam

Right End of Box Beam (viewed from radar)

Left End of Box Beam (viewed from radar)

Figure 10-12:   Photographs of the salvaged box beam used in the 3D GPR imaging experiments.

Figure 10-13: Portable imaging RaDAR mounted on a 2D Translation stage parallel to side of Salvaged concrete box beam at measurement site at Oakland County Road Commission site in Waterford, MI.
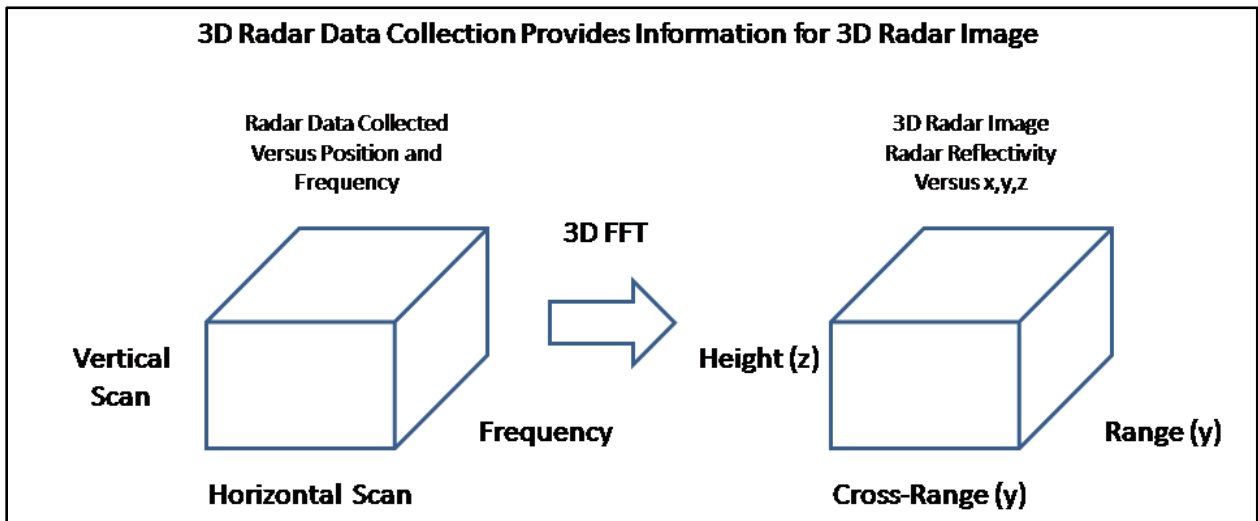
Figure 10-14: 3D RaDAR collection provides information to form a 3D RaDAR image.

The 3D RaDAR image is a 3D spatial map of RaDAR reflectivity. Material discontinuities, transitions and/or inhomogeneities reflect electromagnetic energy back to the RaDAR and result in localized areas of enhanced RaDAR reflectivity in the image. Thus, areas of high intensity in

the image indicate the spatial location of inhomogeneities in the image. These inhomogeneities could be associated with defects or deterioration if there should not be any change of material in that spatial location.

One method of visualizing the 3D RaDAR image is to examine 2D cuts through the 3D volume. Figure 10-15 shows a cut through the volume at a fixed height. This is equivalent to a plane view of the beam (e.g., looking down on the beam from above). The intensity of the RaDAR image is displayed on the 40 dB color scale shown to the right. The RaDAR illumination is from the bottom of the figure. The magenta box indicates the approximate exterior dimensions of the box beam from this view. The long red linear feature is the scattering from the front surface of the beam closest to the RaDAR. The localized returns (in yellow in the display) above the red line are returns from inhomogeneities within the beam.
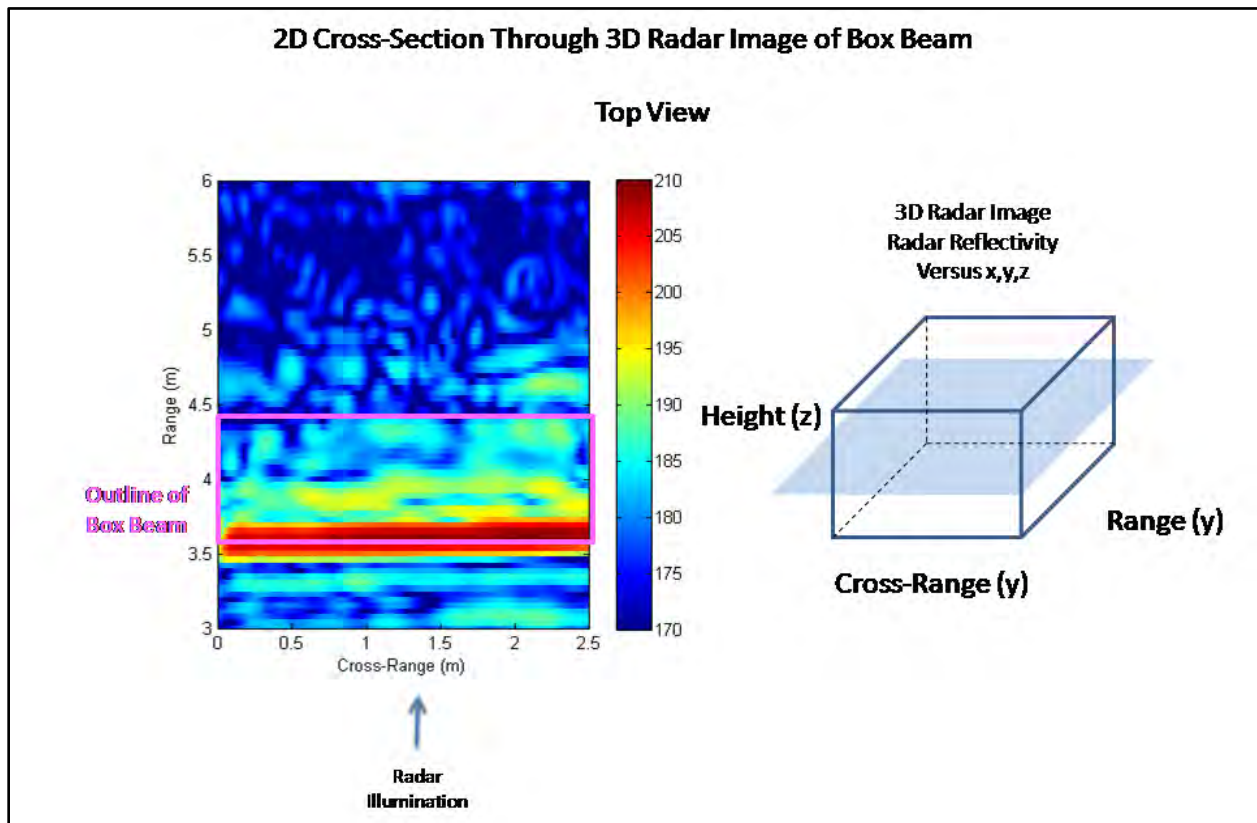
Figure 10-15:   2D cross section through the 3D RaDAR image of the box beam viewed from the top of the box beam.

Figure 10-16 shows a cut though the volume at a fixed position along the beam. This is equivalent to viewing the beam from an end of the beam. Again the intensity of the image is displayed on the 40 dB color scale shown to the right. The RaDAR illumination is from the left side of the figure. The magenta box indicates the approximate exterior dimensions of the box

beam from an end view. The red linear feature is again the scattering from the front surface of the beam closest to the RaDAR. The localized returns to the right of the red line are returns from inhomogeneities within the beam.
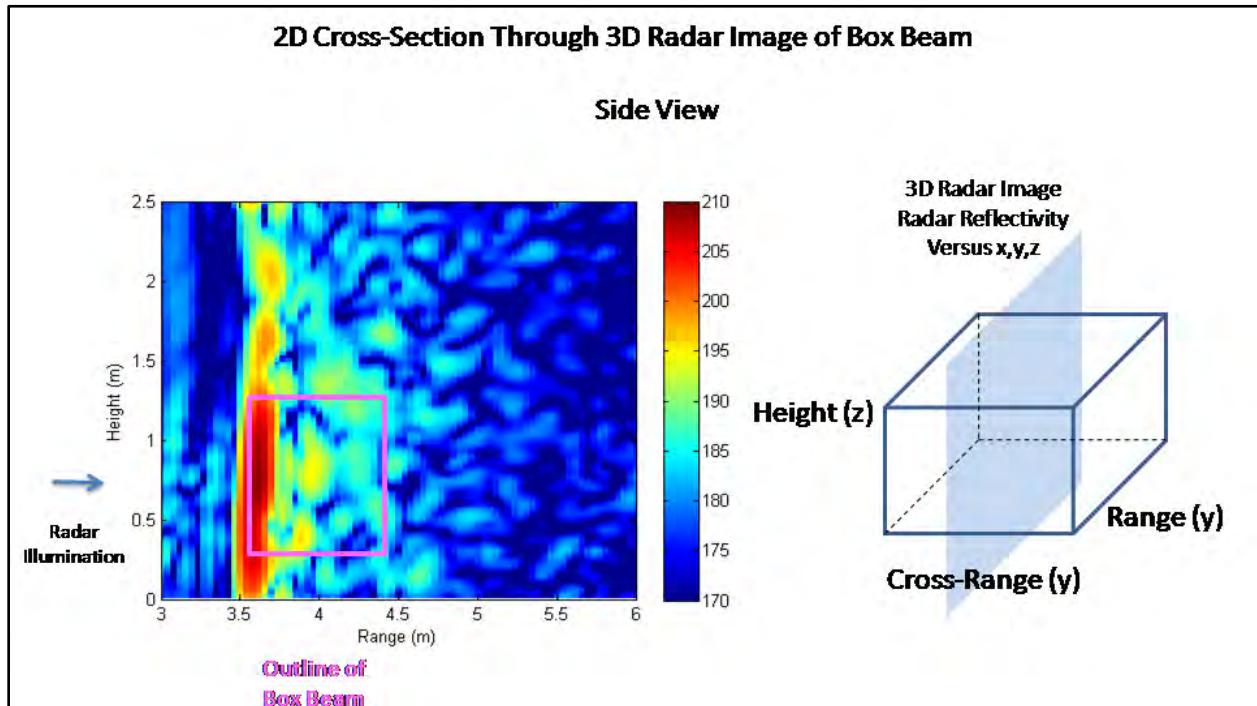
Figure 10-16:   2D cross section through the 3D RaDAR image of the box beam viewed from the end of the box beam.

Thus, these data indicate that RaDAR imaging is able to sense features within the beam. To determine if the interior features are normal structure or defects, an as-built plan or a destructive forensic investigation of the beam would be necessary. Unfortunately, neither was an option for this salvaged beam.

10.3.   Benefits, Limitations and Next Steps

GPR systems, employing low frequency electromagnetic waves that penetrate bridge material, can provide information about the condition of the interior of bridge decks and structures. Previous studies have demonstrated that ground penetrating RaDAR can potentially image delaminations, defects and rebar within concrete bridge decks, and several commercial companies have developed production systems to produce reflectivity maps that are indicative of deck defects. These spatial maps can be used within the DSS to provide quantitative measures of deck condition which contribute to the overall bridge condition metric.

Limitations of current commercial systems are the time required to collect the RaDAR data and extensive verification that inhomogeneities observed in RaDAR imagery can be uniquely associated with different defect types. Future research should address these limitations by developing more efficient methods of RaDAR data collection to address and by conducting more controlled tests of commercial RaDAR systems to develop quantitative relationships between RaDAR image features and known defect and/or failure mechanisms.

Even though sensor development was not a focus of the current research program, a limited set of RaDAR experiments were conducted to extend use of RaDAR technology for bridge assessment and address some of the limitations of current systems. First, current commercial RaDAR systems used to survey deck condition utilize arrays of truck or cart mounted antennas that are scanned at a vertical orientation close to the deck surface. These systems operate in close proximity to the deck and may require the bridge to be closed for extended periods of time to complete the scan. To mitigate these limitations, an alternate imaging approach, where a single RaDAR antenna views the deck surface at an oblique angle from the side of a vehicle, was investigated. This approach would allow a vehicle mounted RaDAR travelling in one lane to produce a 2D image of an adjacent lane, and thus, potentially reducing data collection time and interference with traffic.

Bridge deck RaDAR imagery collected at oblique incidence angles during the field tests did not show features that corresponded to delamination areas. There are two likely reasons that the approach was not demonstrated in the field test data. First, the oblique incidence backscattering from the relatively shallow delamination areas was not strong enough to produce a feature that could be distinguished from the background scattering from the rest of the bridge interior structure. Second, the RaDAR parameters selected for the field test may not have been optimal for the application. Since delaminations occur not far into the deck surface, a RaDAR operating at a higher frequency may have been more effect since only a relatively shallow region of the deck needed to be probed. Deconvolution of the frequency response of the measurement system would also have improved performance, but the required algorithm development was not within the scope of the current effort.

The RaDAR imaging of the interior of a salvaged concrete box beam was demonstrated. However, lack of ground truth information on the interior of the box beam, such as plan or a destructive inspection, limited assessment of the utility of the results. Low frequency, 3D imaging RaDAR provides a means of interrogating unaccessible bridge structure interiors. Its potential justifies further demonstrations and quantitative evaluation on both test items and actual box beam bridges.

11. Synthetic Aperture Radio Detection and Ranging Applications

Applications SAR were investigated for utility for bridge condition assessment (the project's GPR technology investigation also used principles of SAR for UWBIRS). In particular, the assessment of bridge settlement and overall bridge deck condition were thought to be areas that SAR data could be used effectively, based on recent studies and applications.

SAR images are coherent RaDAR images in 3D, where the first two coordinates specify the spatial location of a signal and the third coordinate contains the phase (Curlander and McDonough 1991). It is the phase information from which height or depth measurements are made. SAR data collection is characterized by the translation of an antenna or multiple antennas along a baseline to simulate data collection as if it were conducted by a single, large antenna (aperture). The two techniques discussed here both utilize SAR data. They differ in that InSAR utilizes a pair of images of the same scene, separated in time or look angle, and the SAR speckle investigation need only use a single SAR image.

InSAR displacement mapping (D-InSAR) techniques have demonstrated utility in detecting sub-centimeter resolution elevation changes over time in studies of land subsidence and in studies of smaller-scale targets such as buildings (Crosetto et al. 2002; Tao et al. 2004). In this analysis, the project team sought to assess the potential to detect bridge settlement for two bridges where known elevation changes have occurred by using 2-pass D-InSAR with commercially available SAR imagery from the ERS-2 satellite.

Another application of SAR for bridge deck condition assessment attempted to exploit the phenomena of speckle. Coherence speckle, often observed as "graininess" in RaDAR backscatter images, is produced due to phase differences between picture elements (pixels) in the scene (Dresel et al. 1992). In turn, these phase differences in the image correspond to phase differences between scattering elements in the scene such as height differences on the order of the RaDAR wavelength (or optical wavelength in the case of optical speckle from coherent light sources). If a surface is rough at that scale then the speckle pattern observed may contain a measure of that roughness. This was previously shown to have promise in assessment road surface condition (Brooks et al. 2007). In this investigation, the project team attempted to correlate the roughness thus measured with bridge deck condition from established techniques, namely the NBI inspection.

11.1. Methodology

Three study bridges with known elevation changes were identified for the InSAR application. Two were railroad bridges at USDOT Federal Railroad Administration (FRA) Transportation

Technology Center (TTC) in Pueblo, Colorado. These two bridges had features that were recently elevated at a scale of several centimeters. The third was a road bridge near Brimley, MI, that MDOT officials cited as having settled several centimeters from 2006-10. Table 11-1 summarizes each study bridge by location, timing and degree of elevation change, and notes on imagery acquisition and processing.

Table 11-1: Study bridges used to evaluate InSAR for detection of bridge settlement.

Bridge	Description	Estimated Elevation Change	Time of Change	Processing Notes
TTC#1	2-span concrete bridge, walkways and sides elevated	10 cm increase	July/Aug. 2010	Imagery for 'before' and 'after' acquired, and successfully processed
TTC#2	3-span concrete bridge, deck and 100 ft in both directions elevated	5 cm increase	May 2011	ERS/ENVISAT SAR imagery not available for 'after' date, but used as control, since right next to TTC#1
Brimley (MI)	Gradual settlement from 2006-2010	~2-5 cm decrease	2006-2010	ERS/ENVISAT SAR imagery not available for location after 2006 – attempted with 2001 and 2006 images

For each 'before' and 'after' date and location, ERS-1, ERS-2, or ENVISAT SAR imagery was acquired for InSAR analysis. For TTC#2, SAR imagery was not available for the 'after' date, but since it is located adjacent to TTC#1 (Figure 11-1), it still held value as a control site. From the Brimley bridge, no SAR imagery was available for the location after 2006, so the analysis team attempted InSAR analysis for a 'before' image from 2001 and an 'after' image from 2006.

The commercial image processing software ERDAS IMAGINE 2011's D-InSAR module was used to perform the analysis for each bridge. This module performs the following processing steps: co-registration; subsetting; DEM referencing; spectral shifting; coherence and interferogram generation; phase unwrapping; baseline refinement; and rectification and displacement calculation.

Figure 11-1: Study bridges used to evaluate InSAR for detection of bridge settlement.

For the SAR speckle application, airborne SAR imagery for three demonstration bridges (Freer Road, Willow Road, and Mannsiding Road NB – Table 11-2) was purchased from Intermap, which has commercialized InSAR airborne imagery for elevation data creation. The data were single-look complex (SLC) scenes and, as such, needed to be further processed; the data were byte-swapped by word and stamped with an 8-bit complex floating-point header. Images were rotated to align with geographic north (or as near as possible to geographic north). An example scene after these transformations is shown in Figure 11-2. The MTRI image manipulation libraries were used to affect these and the following transformations described.

Table 11-2: Metadata for SAR speckle data purchased from Intermap.

Site	Collection Date	Transmitted Bandwidth	Antenna Length	SLC Azimuth Resolution	SLC Range Resolution	SLC Azimuth Posting	SLC Range Posting
Willow	May 6 2005	135 MHz	1.2 m	0.6 m	1.11 m	0.5 m	0.999 m
Freer	May 6 2005	135 MHz	1.2 m	0.6 m	1.11 m	0.5 m	0.999 m
M'siding	July 2 2007	135 MHz	0.8 m	0.6 m	1.11 m	0.3 m	0.999 m

The images were subset to focus on an area immediately surrounding the bridge deck. The images from Willow Road and Freer Road were not able to be used for analysis as, upon close

inspection, it was realized that the look angle was not sufficient to illuminate enough of the bridge deck. The image of the Mannsiding Road NB bridge, however, was illuminated properly and provided several bridge deck pixels which could be extracted (Figure 11-3).

Once the scene subset is acquired, the bridge pixels are manually delineated. Then, two pixels, one maximally and one minimally bright, are embedded in the subset among the bridge pixels (technically, a bridge pixel is replaced by each of these). This is done so as to allow the analyst to estimate the speckle contrast range. This will indicate the range of deformation it is possible to detect with this technique.
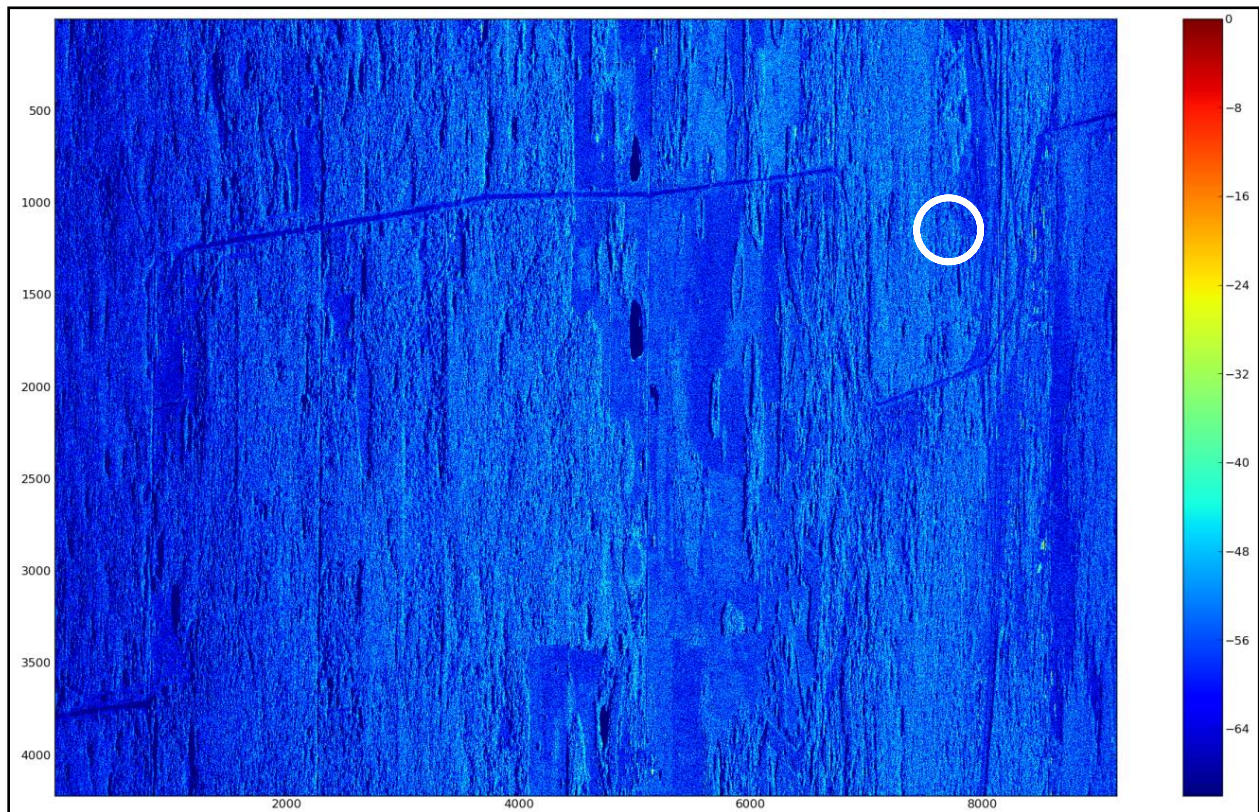
Figure 11-2: SAR image of Mannsiding Road and its wide surroundings where Mannsiding Road NB has been circled in white; color bar shown with dB scaling.

A 2D sliding window operator is used to generate two images, the maximum and minimum pixel values around each pixel. The maximum image is divided by the minimum image to enhance speckle contrast. A 3 x 3 pixel image-window seems to be ideal in the case of Mannsiding Road NB bridge, where the deck width is 9.5 m according to NBI Item 52. Having approximated the width of the bridge in pixels (15.5), the effective resolution was determined to be 61 cm/pixel (this compares very well with the calculated azimuth resolution). This means that 3 x 3 window operates on an area ~1.8 m^2, a 5 x 5 pixel image-window on an area ~3.1 m^2, and a 7 x 7 window on an area ~4.3 m^2. As areas of spalls and patches on a bridge deck surface are closer in size to a

3 x 3 window, this is better suited for this analysis than larger windows. It is possible that the 3 x 3 window is too coarse to be sufficiently sensitive to bridge deck condition indicators.
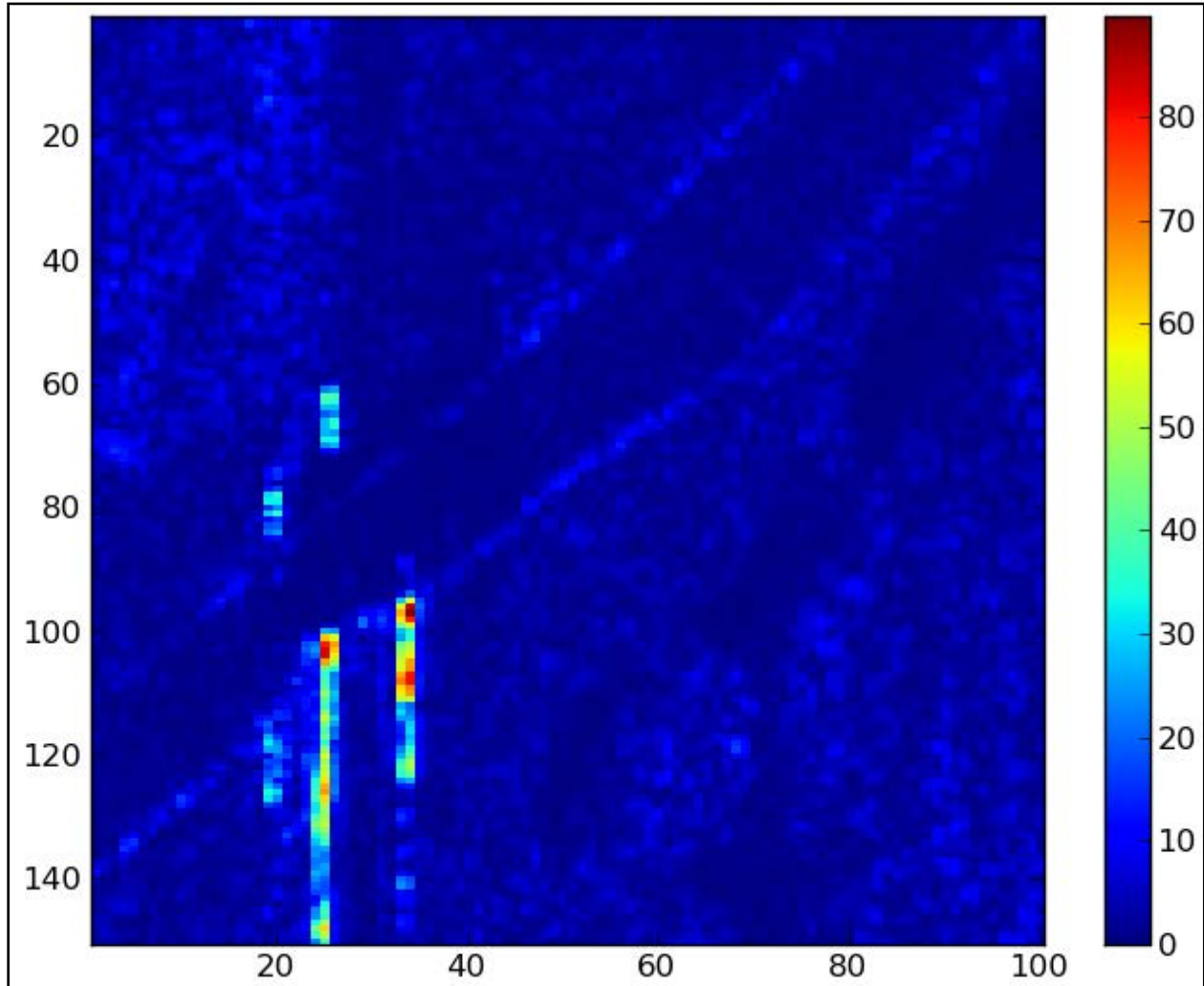
Figure 11-3: Close-up of the Mannsiding Road NB bridge; the bright pixels in vertical lines likely correspond to vehicle traffic beneath the bridge, which can be seen outlined by lighter pixels on the edges of the deck and approach (color bar has arbitrary units).

After the speckle contrast enhancement is performed, the non-bridge pixels in the resulting image (the quotient of the sliding window maximum and the sliding window minimum) are masked out. The bridge pixels can at this point be analyzed and thresholds chosen for a typical high-level decision product with "stoplight" colors (green, yellow, red) (for an example, see Figure 11-4). The chosen thresholds should reflect meaningful deviations in the speckle contrast which, in turn, should correspond to meaningful deviations in the elevation (phase difference) of bridge deck parcels (scattering features). A certain deviation, if determined to correspond to 1 cm

11-5

of offset, might be chosen as the bottom of the "yellow" threshold indicating that such an area has spalls about 1 cm in depth.
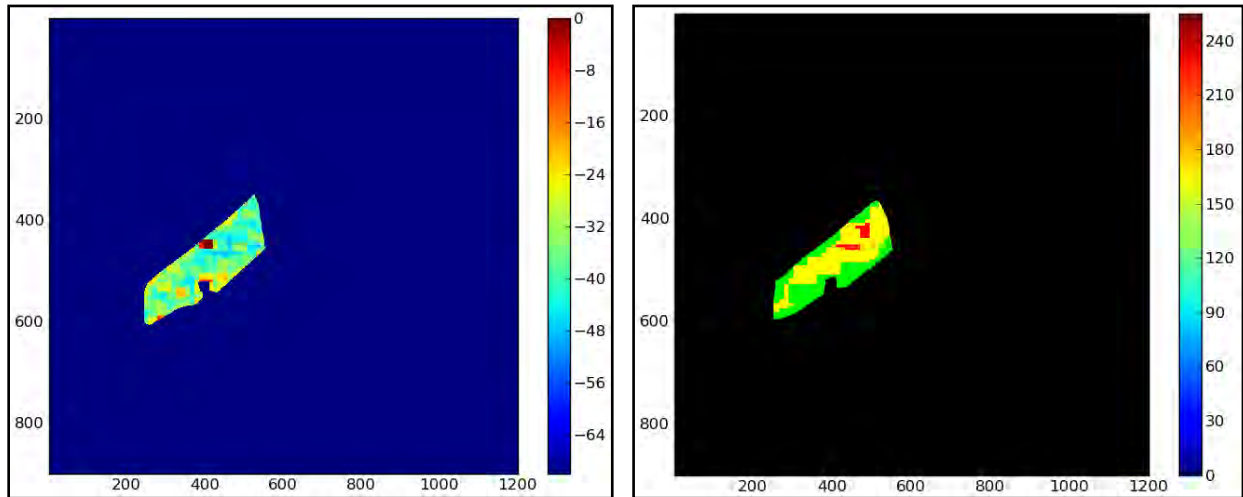
Figure 11-4: Pixels extracted from Mannsiding Road NB image shown after speckle contrast enhancement with dB color scale (left) and after pixel value classification into a "stoplight" decision support image (right).

11.2.   Results and Discussion

Coherence and displacements maps are shown in Figure 11-5 and Figure 11-6 from the InSAR application. For the TTC bridges, the displacement maps shows a 0.5 cm increase of TTC#1 compared to TTC#2 where a 10 cm increase was expected of TTC#1 over TTC#2 (Figure 11-5). For the Brimley bridge, the displacement map shows a ~2 cm increase relative to background levels where a 0-5 cm increase was expected (Figure 11-6). Despite showing the expected trends in elevation change, the displacement maps show little correspondence when compared to ground imagery. Coherence maps show that signal return from the bridges was very low which inhibits D-InSAR algorithms from reliably detecting changes in elevation.

The principal conclusion is that the commercial SAR imagery used in this task was promising although not optimal for detection of bridge settlement due to relatively coarse horizontal resolution (>6 m) which affected the vertical resolution change detection. Additionally, displacement detection may have been hampered by low RaDAR return of paved roads.

In the case of the SAR speckle investigation, as the most recent available image from Intermap for the Mannsiding Road bridge was acquired too long ago, before the field demonstrations began, and no other field data proximate to the acquisition date has been obtained, it is not possible to take this investigation much further within this project. The effective resolution of 0.6 m and the coarsening effect of speckle contrast enhancement may render the results unsatisfactory for condition assessment of features that are generally smaller.
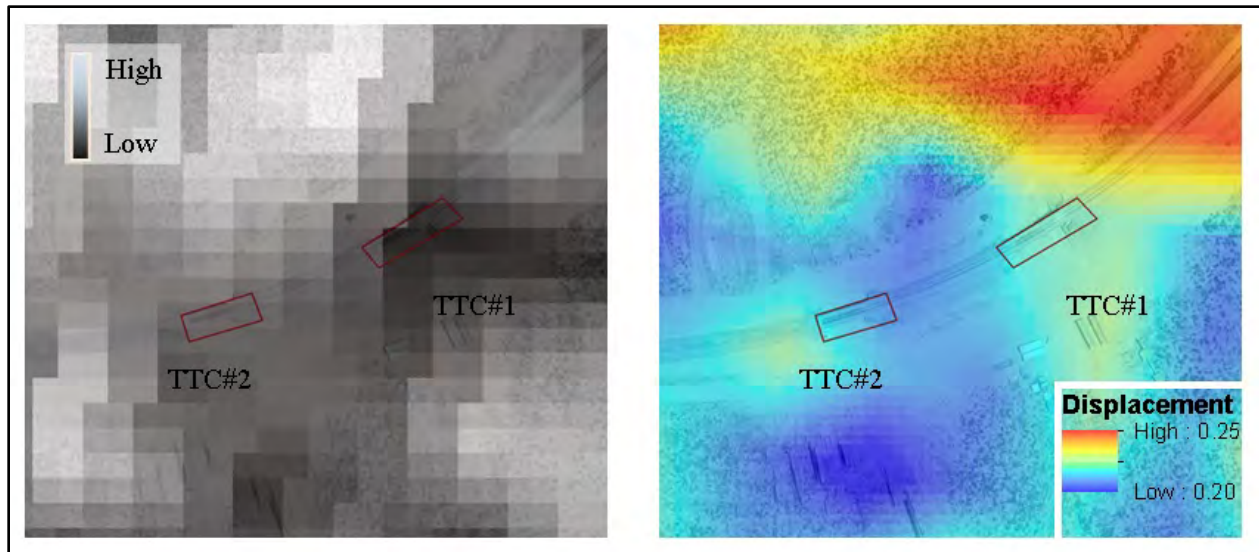
Figure 11-5: TTC bridges – coherence on left image and displacement on right image. Expected change; 10 cm increase (TCC-1) and no change (TCC-2). Observed change; TTC-1 ~0.5 cm increase relative to TTC-2.
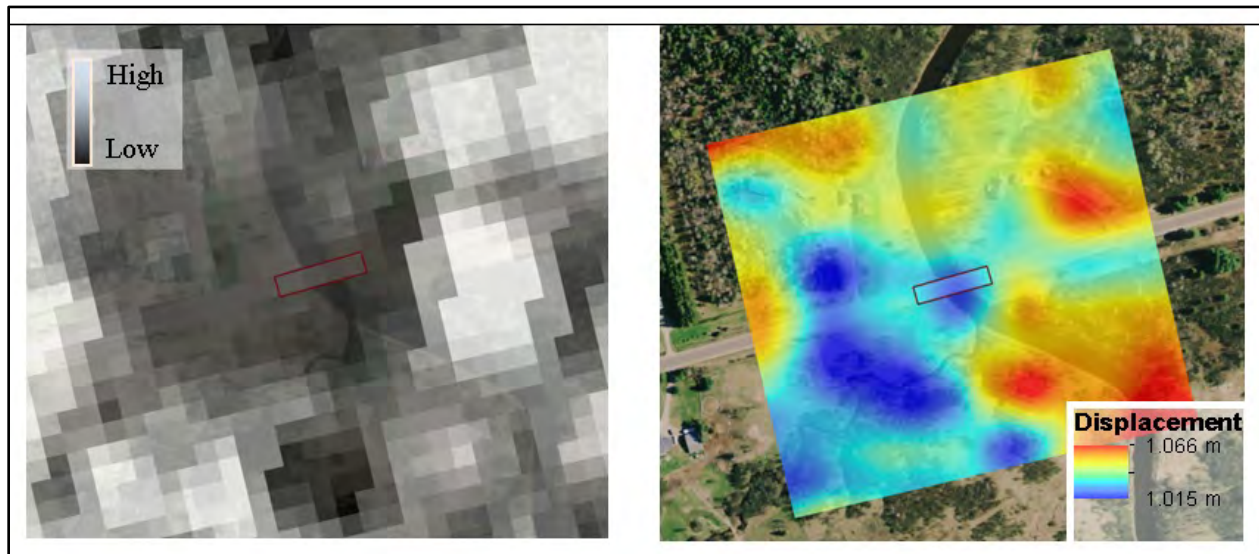
Figure 11-6: Brimley area bridge, Michigan. Coherence on left image and displacement on right image. Expected change; 0-5 cm decrease. Observed change; ~2 cm decrease relative to background.

11.3.   Next Steps and Implementation

While experimental work has demonstrated successes with detecting bridge settlement via InSAR (Zhang et al. 2010), the project team was not able to replicate these results using the tested commercial SAR imagery and ERDAS IMAGINE's out-of-the-box D-InSAR algorithms. Zhang et al. (2010) relied on a series of stable coherent points across a bridge that spanned 32.5

km to register multi-pass PALSAR (higher horizontal resolution than ERS-2 SAR) datasets. Given this, future explorations may be better served using higher horizontal resolution SAR data with targets having static, high-return coherent points.

RITA is currently funding work by Scott Acton at the University of Virginia (RITA-RS-11-H-UVA) evaluating InSAR products and graph theory methodologies to detect sinkholes, landslides, and displacements relevant to transportation infrastructure (Acton et al. 2012). This more in-depth work has the potential to more fully evaluate the potential of InSAR data for bridge condition assessments such as the amount of settlement and should be followed for results.

Given imagery with the appropriate look angle and an acquisition date proximate to a bridge scoping or inspection date, SAR speckle analysis for bridge deck condition shows promise for more frequent condition assessment in terms of surface roughness and/or depth of spalls.

12. Use of Multispectral Satellite Imagery

Commercial high-resolution multispectral satellite imagery, such as WorldView-2, IKONOS, and GeoEye-1, has a spatial resolution of up to 0.5 m which is a relatively coarse resolution when compared to other more "onsite" remote sensing techniques, but relatively high resolution when compared to traditional remote sensing data such as Landsat. For this technology, evaluation, the project team used the "VIS2" band differencing technique that was applied under the Transportation Applications of Restricted Use Technology (TARUT) study at MTRI (Herold and Roberts 2005; Brooks et al. 2007). This technique was developed to determine the condition of road surfaces using high-resolution satellite imagery.

During the TARUT study, multispectral satellite imagery was used to determine the condition of a road surface. This was done by breaking the road into tenth of a mile segments for analysis. A value that represents road condition was generated by subtracting two spectral bands for each road segment. The VIS2 algorithm uses blue spectral information (approximately 490 nm) and near-infrared (approximately 890 nm) as the input for condition analysis.   Subtracting the blue band from the near-infrared band produces an integer value (VIS2) correlated with road condition. These spectral variables were found to respond most highly to degradation in road surface characteristics by both Herold and Roberts (2005) and Brooks et al. (2007). The TARUT study analyzed what these values are for different pavement conditions; the application for this study is the first known attempt to apply it specifically to assessing bridge deck conditions. If it was to work, then any bridge were commercial satellite imagery is available or could be collected would be quickly assessable for a proxy of its deck surface condition.

Readily available archived multispectral commercial satellite imagery was acquired for all of the demonstration bridges. The imagery for the Freer and Mannsiding Road bridges came from the IKONOS satellite (launched in 1999) and the imagery for the Willow Road bridge was from WorldView-2 (launched in 2009). Each archival satellite image scene (one per bridge) cost in the $100-$300 range. The first step in the process was to pan-sharpen the imagery. Since the resolution of the multispectral bands (approximately 2 m) are less than the panchromatic band (up to 50 cm with WorldView-2), a technique called pan-sharpening is used to increase the resolution of the multispectral bands by comparing them to the panchromatic band (Te-Ming et al. 2012). Figure 12-1 shows the difference between the multispectral bands, panchromatic bands, and the pan-sharpened image.

The next step was to take the band centered around 490 nm (blue range of the spectrum) and subtract it from the band that is centered around 890 nm (near infrared) – Figure 12-1 D and Figure 12-2 show the derived results. This would generate a value that should be correlated to road condition. The values from all the pixels of a bridge deck were averaged to get one value per bridge which can be compared to NBI values.
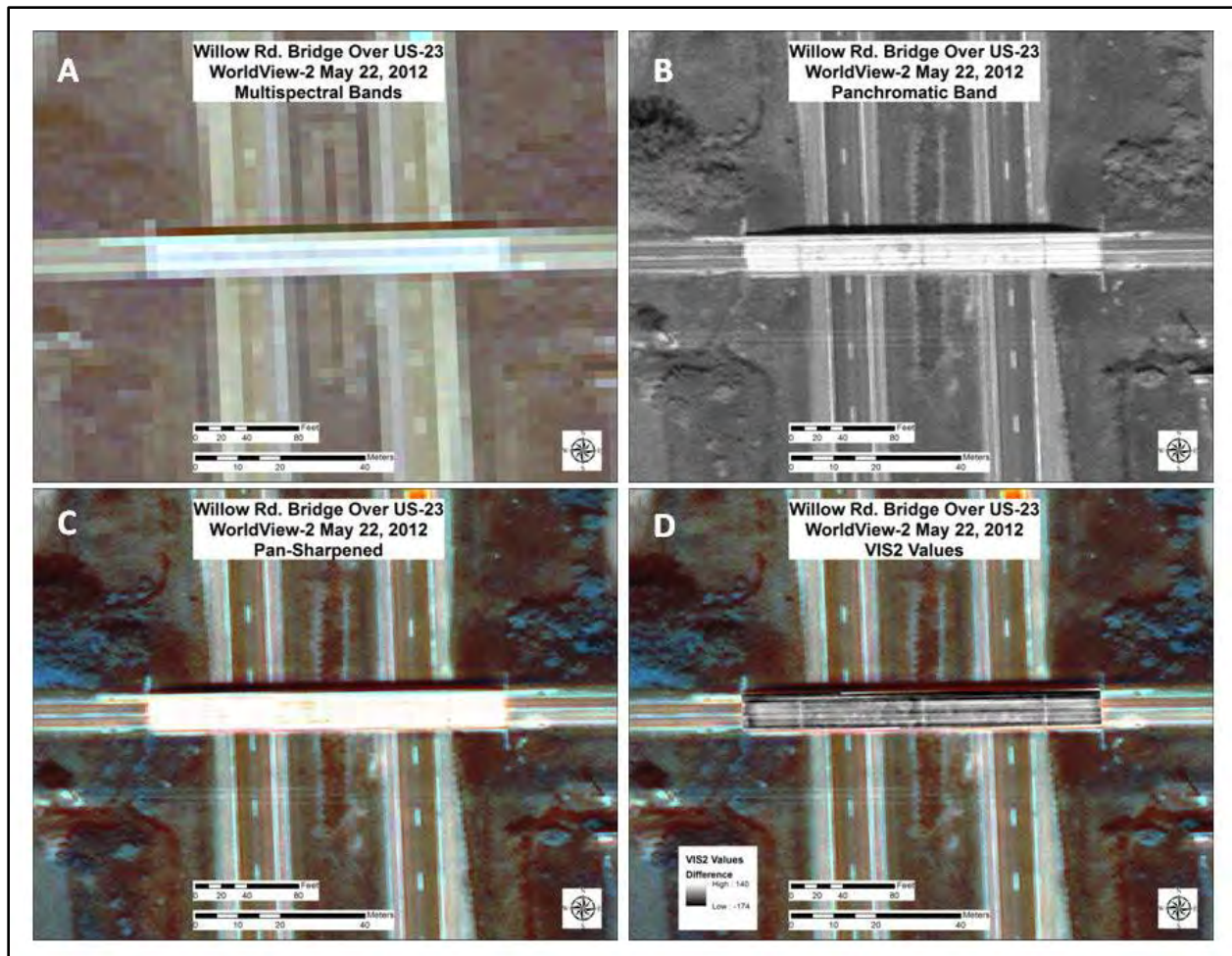
Figure 12-1: WorldView-2 image of Willow Road. Multispectral bands (A) have a resolution of 1.85 m while the panchromatic band (B) has a resolution of 0.5 m. The pan-sharpened (C) band has a resolution of 0.5 m. The derived VIS2 pixel values for Willow Road are shown in image D.

12.1. Results and Discussion

The analysis of the multispectral satellite imagery was not successful at producing a result that could definitively tie to the condition of a bridge deck. The values that were produced from the from the VIS2-band differencing technique were not comparable to the values that were generated by the previous TARUT study. Since there was too few bridges used in the field demonstration and their NBI ratings were close to each other, the project team was also unable to statistically correlate the values that were derived from the bridges to their condition ratings. The reasons for not producing comparable results are not clear, but more likely possibilities exist. In the TARUT study, approximately 19 miles of road in were classified into over 190 1/10-mile segments, allowing for a clear pattern to be determined between VIS2 values and road condition. With only four bridges, the opportunities for a pattern to be discernible were fewer. It could be

that with a larger data set, VIS2 values could still be correlated with bridge deck surface condition.
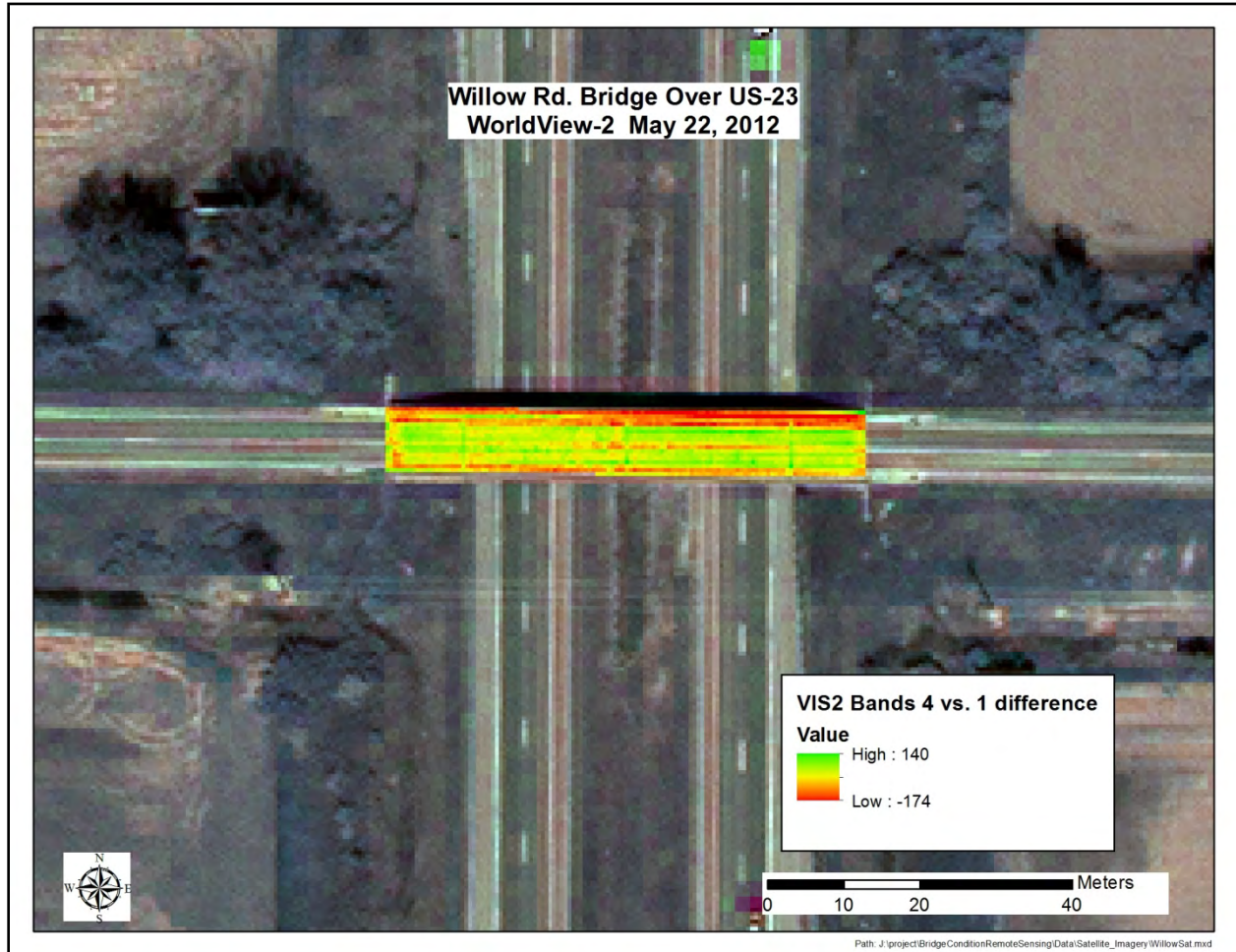
Figure 12-2: The VIS2 calculation displayed in color for the Willow Road bridge using WorldView-2 commercial high-resolution satellite imagery. Red and green areas (relatively low and high values) show high contrast between the blue and infrared spectral band information.

Also, on close visual inspection of the imagery, some areas of large contrast (in red in Figure 12-2) appear to either be wet areas and/or areas in shadow. This was not encountered in the TARUT study and could be reducing the usefulness of the VI2 results.

12.2. Implementation and Next Steps

If an analysis of a larger bridge deck data set did show a clear pattern between VIS 2 values and bridge deck surface condition, then commercial high-resolution satellite imagery could be used as a rapid and readily available condition assessment tool at relatively low cost. Trying to obtain

satellite imagery with little shadow and dry conditions may also help. Such results could then be integrated into bridge management systems including the project's Bridge Condition Decision Support System.

At this point, however, additional efforts are not recommended for this technology unless it could be done for a larger set of bridges.

13. The Bridge Condition Decision Support System

The DSS is a software architecture designed to support bridge managers in their analysis of bridge condition data and asset management for bridges. The version released at the end of the current USDOT RITA project was developed as a demonstration of the necessary features and the potential capabilities of such a system. The DSS evolved during interdisciplinary discussions between project team members, partners at MDOT, the TAC members, and other bridge management experts.

Requirements for the DSS were generated from interactions with bridge managers and inspectors. A series of technical memos provides documentation of developing these requirements and turning them into an effective demonstration DSS (TM n$^{\text{o}}$ 10, n$^{\text{o}}$ 16, n$^{\text{o}}$ 21, and n$^{\text{o}}$ 24 in Appendix C). Team members shadowed MDOT inspectors during regular NBI-compatible inspections (FHWA 1995) and received demonstrations of decision workflows based in existing decision support frameworks such as MDOT Michigan Bridge Reporting System (MBRS). The MBRS, taken together with the Michigan Bridge Inspection System (MBIS), constituted the existing information technology solutions for managing bridge condition information at MDOT (the access page for these tools is at <www.michigan.gov/mdot/0,1607,7-151-9625_24768_59528---,00.html> as of July 2012).

MBRS was used to look up bridge inventory and condition information for asset management decisions while MBIS was used to update the same sources with new information from NBI inspections and scopings; both were web-based. Both were designed to be used in an asset management framework and, as such, this became a requirement for the DSS as well and shaped many of its proposed features.

The DSS was initially conceived of as a web-accessible database application for accessing, visualizing and analyzing bridge condition information. Early on, distinctions were made between established bridge metadata (inventory data), new condition information from routine NBI inspections (inspection data) and condition information derived from remote sensors (remote sensing data). Inventory data consist of bridge metrics such as deck width, total length, the number of lanes, the latitude and longitude of the bridge, the facility it carries, the feature(s) it intersects and many other items that do not change often and sometimes never change in a bridge's lifetime. Inspection data include items required by routine NBI inspections such as the NBI deck, superstructure, substructure and culvert ratings. The DSS was also planned to be "map-centric" in that it would explicitly tie the geographic representation of bridge condition data to analysis and visualization; geographical DSS tools can significantly help interpretation and use of often complex data (Kingston et al. 2000; Sugumaran and DeGroote 2010).

Another goal of the DSS is to provide a comprehensive bridge condition signature for which it will be necessary to synthesize measures of bridge condition from the disparate remote sensing, inspection and inventory datasets. The DSS was also conceived of as supporting inspection operations with support for "ruggedized" mobile devices (ideally, tablet computers) that could be used to locate bridges on a map, get directions to and from bridges, access multiple historical inspection reports, and to log inspection data including a photo log while conducting the inspection.

The DSS must model existing decision-making workflows tailored to different asset management goals and to different users within a transportation agency (Figure 13-1), a requirement clearly communicated by the project TAC. It must provide a user-friendly interface for executing queries on bridge inventory data and up-to-date bridge condition information from recent and historical inspections. Ultimately, it must integrate data from remote sensors both for visualization and analysis purposes. To meet these requirements and support decision makers, a database-driven web application built on web standards and using open-source technology wherever possible was planned.
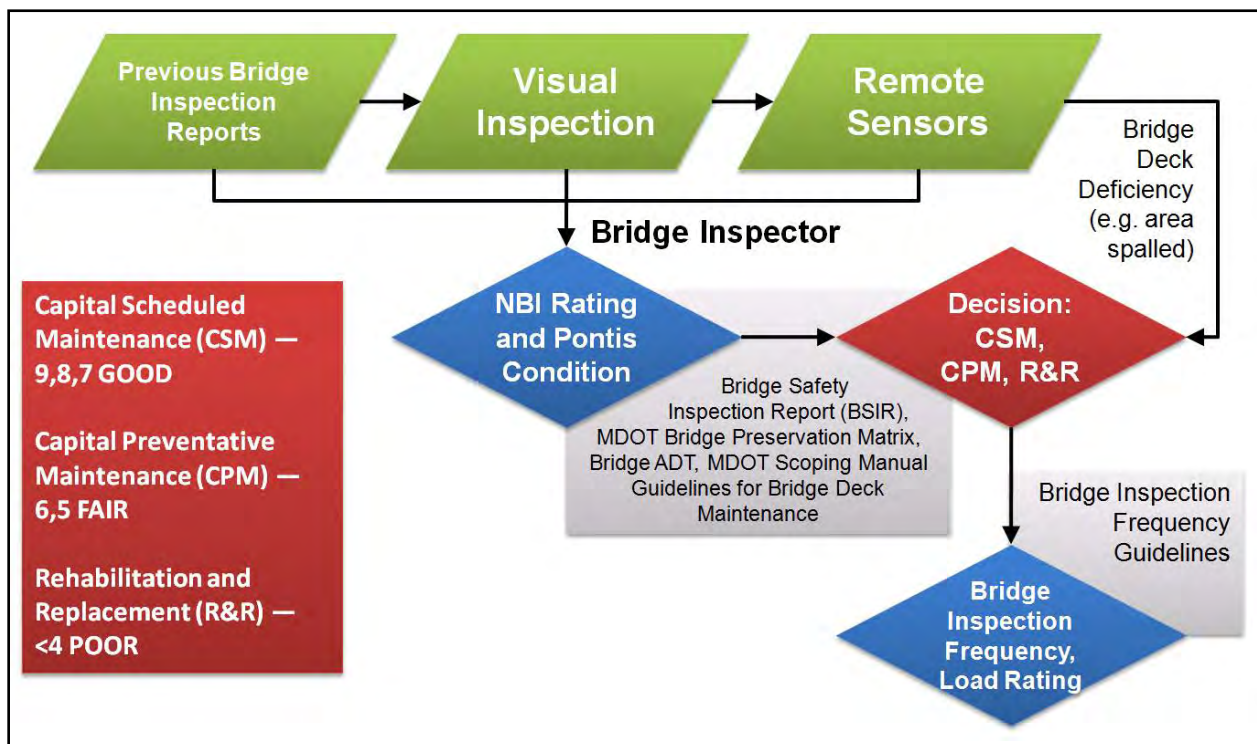
Figure 13-1: Example decision workflow for bridge managers and inspectors based on past NBI data, new NBI inspections, and remote sensing data.

13.1. Design and Development

The DSS can be described in terms of two major dichotomies or components, the client and the server (both are computers) or the application layer and the service layer (Maffeis 2003). The client computer is used by a decision maker who loads the DSS application into his or her web browser. There can be multiple client computers with simultaneous connections to the server, which is a computer or network of computers that handles requests for data that come from the client computer(s). The DSS application, multimedia and the data themselves are hosted on the server, though the database might be physically or virtually separate from the web server, as depicted in Figure 13-2. Also depicted in the figure is the dichotomy between the application layer, which comprises the web application loaded into the client computer's browser, and the service layer, which comprises the various web services that respond to requests for data. Principles of Asynchronous Javascript and XML (AJAX) and Representative State Transfer (REST) were used in the design and construction of the client-server interface to develop a fast and flexible web-based DSS tool.
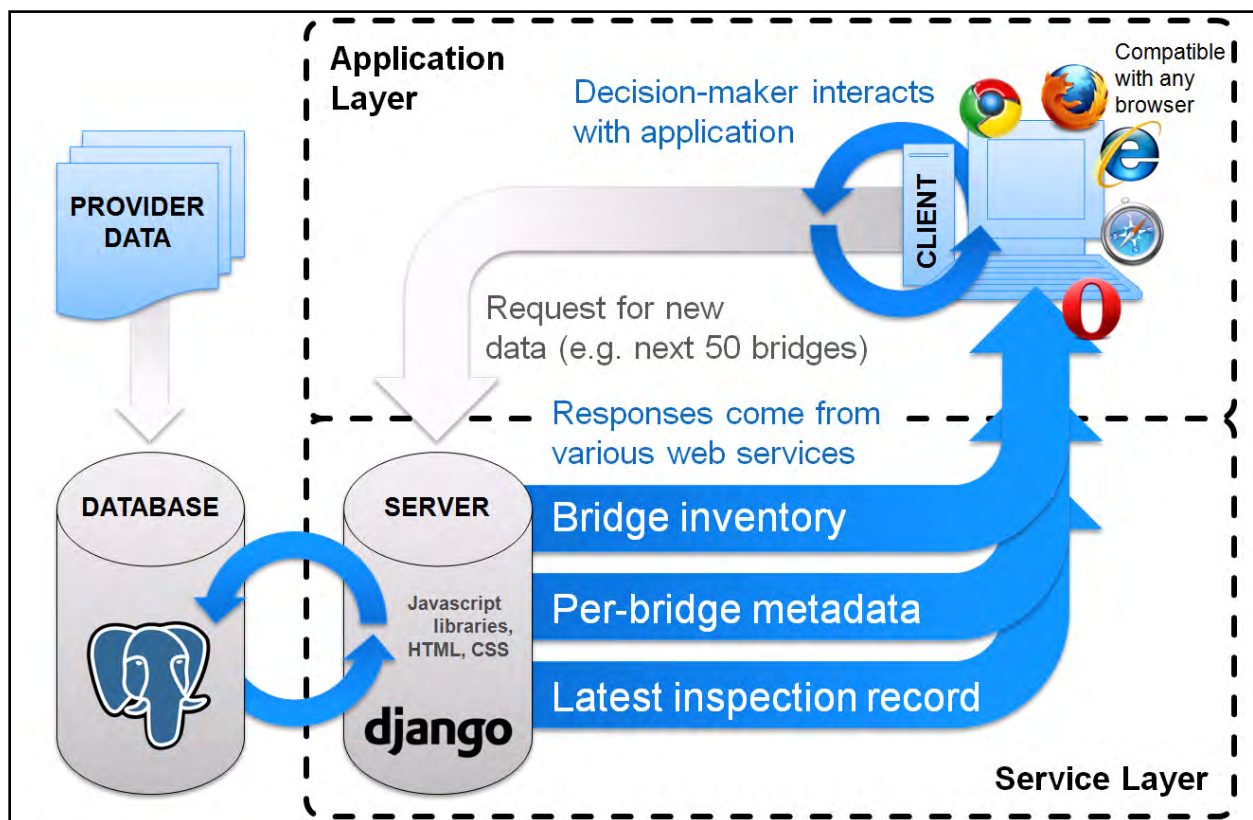
Figure 13-2: Concept diagram illustrating the components of the software architecture in the application and service layers, the location of the client and server within these, and how they communicate with each other.

The software architecture chosen for the DSS is based on a LAMP (Linux-Apache-MySQL-PHP/Perl/Python) stack where Python is the programming environment and PostgreSQL has been substituted for MySQL. Sometimes this variant is referred to as LAPP. This solution stack has been used often by the project's development team for a variety of geospatial applications and is favored by the open-source geospatial software development community. A discussion of the available alternatives to this solution stack in whole or in part can be found in Section 13.2.2. Following in this section is a description of the architecture's components and operations.

13.1.1. Client-server Architecture

The DSS exposes bridge data for decision support through a series of web services hosted on an Apache server. The database management system (DBMS) chosen is based on PostgreSQL, a popular open-source, relational database (Douglas 2006). The PostGIS extension is used in the PostgreSQL database to provide support for geospatial objects. The web services are programmed in Python using the Django web framework, a database application programming interface (API) that allows (among other things) for database queries to be parameterized and executed programmatically. The parameterization of queries is done in the application layer, on the client, by decision makers who, for instance, wish to look at the first 50 bridge records in the inventory sorted by structure number. Such a request is handled by the web server which delegates Django to construct a database query and return the desired results, encoded in Javascript Object Notation (JSON, a more compact alternative to XML), through one of the many RESTful web services that constitute the client application's interface with the database. These requests are made asynchronously, which means the web browser executes them in the background so as to minimize the decision-makers wait time. The client application responsible for making these requests is a Javascript program, utilizing the ExtJS framework, which contains all the logic necessary to provide the decision-maker with an informative, user-friendly experience allowing data manipulation all on its own until more data are needed. The application also retains its own state; it remembers what the user has done in the same session so that, after filtering a table of bridge records, a subsequent sort operation returns only the filtered records, which speeds up the DSS look and feel.

In addition to the Apache-Django server that holds the application code and responds to the majority of data requests, there are separate virtual servers used to actually hold data. The database is itself a server and the remote sensing imagery displayed in the DSS are streamed from one of two imagery servers. While Django mediates requests for data between the client and the database, the client makes requests directly to the imagery servers. The two servers in use in the demonstration version of the DSS are instances of GeoServer, a popular open-source solution, and ArcGIS Server, the web-mapping product of ArcGIS software suite. Each of these streams remote sensing imagery through a web mapping service (WMS), a communication protocol standardized by the Open Geospatial Consortium (OGC). On the client-side, WMS requests are constructed by the application framework (ExtJS) and responses are interpreted by

the Google Maps API, the mapping library selected for the DSS. The WMS responses are image tiles; they are displayed in a Maps instance in the same manner as the built-in roads layer and satellite imagery of Maps itself.

13.1.2.   Data and Database System

A project partner and representative state transportation agency, MDOT, currently manages bridge inventory, inspection and work records using the Bridge Management System (BMS), one of six management tools available in their Transportation Management System (TMS). Employees usually interface with the BMS through Pontis, an FHWA-contracted software program first released in 1992. Pontis thus represents a de facto standard for nationwide bridge management (Thompson et al. 1998). For this reason, the DSS was designed to incorporate the same data structures used by Pontis and found in the BMS. Directly reading from BMS was not an option because Michigan's BMS utilizes Oracle Spatial, a proprietary DBMS, on the back-end.

The project team does not have an Oracle license and obtaining one is cost-prohibitive; without it, the project team cannot obtain the software libraries required for the DSS to connect to Oracle databases. This necessitates exporting data from BMS and inserting it into the DSS database and, consequently, the inventory and inspection data available through the DSS are only contemporary with the dates of these exports. In the DSS, the date of the most recent export was made clear to users and the DSS was designed so that newer data could be easily integrated.

There were some challenges to implementing a relational database-driven framework that uses data from Pontis. The BMS, based on what Pontis requires, implies the use of foreign key relationships which simply do not exist in the database. According to BMS metadata, the bridge key is the "primary structure identifier in Pontis" and is described as such for each of the multiple tables that use it. To maximize the expressive power of the database framework, the DSS developers made new foreign key relationships to the Pontis bridge table on the bridge key.

Another challenge stems from the fact that the Pontis schema was not designed to support an object-oriented web framework. This problem is referred to as object-relational impedance mismatch (Ireland et al. 2009). The premier example from this project is the result of a query to visualize the latest bridge condition information for every one of the thousands of bridges in Michigan along with their geographic location. This query is easily executed in a relational context; however, to utilize the results of the query in the DSS, the query would need to be executed anytime the user wishes to page through the 12,000 unique bridge records returned (in the case of the MDOT inventory). The solution employed in the DSS is to store the results of this query in an intermediate table. This enables faster access through the web-based DSS tool for users, such as transportation agency bridge operations staff.

13.1.3.   Integration of Remote Sensing Data

The integration of remote sensing data is perhaps the most important feature of the DSS. Remote sensing data from disparate sensors must not only be integrated with and compared to inventory and inspection data but with each other. The approach the project team has taken is to identify the products that can be derived from remote sensing data which are of interest to bridge asset management and the commonalities between the derived products of different remote sensing datasets.

Many of the remote sensing products, such as bridge deck digital elevation models (DEMs), take the form of 2D images of the bridge deck or its interior. These planar maps of bridge deck phenomena are intrinsically geospatial and, once georeferenced, can be displayed in their geographic context. They can also then be integrated with each other and third-party geospatial layers. This map representation is central to the display and visualization of some remote sensing data products such as: DEMs from 3D optics like 3DOBS, derived products from DEMs like the hillshade DEM, deviation from a plane, LiDAR DEMs, Thermal IR, and high-resolution photo-composites from 3DOBS.

These data layers are made accessible in the DSS web application through the WMS protocol. This protocol requests imagery "tiles" from the WMS server, providing information about the current view extent or map "bounds," zoom level and desired tile size. The web application then receives tiles of the image corresponding to positions on a simple numerical grid which it then pieces together to construct a map overlay. The WMS protocol also allows for pixel values and/or data attributes to be queried directly by passing the "getFeatureInfo" parameter in WMS requests. This allows users to "click" on a bridge deck resolution cell and discover, for instance, the elevation difference at that spot in the corresponding DEM as well as any other associated with that pixel.

Some remote sensing products are high-dimensional and require more complex representations. The LiDAR point clouds are one obvious example which, due to the technical limitations of the web browser platform, have not been made available through the DSS. The BVRCS photographic inventory is another example of a remote sensing dataset that requires a more complex representation in the DSS. The photo inventory has two spatial dimensions corresponding to the geographic coordinates of each photo vantage point. In addition, each photo has two dimensions corresponding to the pixel coordinates along each axis of the image. Two representations of such data were planned for the DSS and one was implemented. One choice would be to display the photos in their spatial and perspective context simultaneously in a viewer like Google Street View. The representation that is used in the DSS is simpler and faster to implement. The location of each photo in the inventory is represented on the map by a point which links to the photo data presented, in a pop-up window. An obvious improvement would be to indicate the azimuth of the photo by a pointer, however, as the RCS is mounted on a car

13-6

looking left and right there is not much variation in the look angle. GigaPan photographs are similarly treated in the DSS, with a points layer to represent camera vantage points, each of which links to the GigaPan composite hosted on a third-party website.

Extracted features from remote sensing products, such as spalls or delaminations, should be stored as geospatial objects in a spatial database such as PostGIS so as to enable server-side analysis and processing (e.g., spatial intersects, zonal statistics). However, the developers have encountered problems with importing small features such as spalls and delaminations from ArcGIS shapefiles, the storage format native to ArcGIS where they are created. Imported using PostGIS built-ins or importing from features converted to a text format resulted in a severe loss of fidelity. Consequently, the spall and delamination layers in the current version of the DSS are actually WMS layers. The attribute data for each feature can still be accessed using the getFeatureInfo parameter, however, no server-side analysis or processing can be applied to these datasets.

Finally, the metrics of remote sensing indicators of bridge condition, such as the extent of spalled or delaminated area and IRI calculations should be stored in the database directly.

13.2. Outcomes and Product Delivered

At the time of this writing, the demonstration version of the DSS is accessible online at <geodjango.mtri.org/bridge_dss> after providing a username and password which can be obtained from the project team; it is their intent to support this website as long as possible. MTRI can be contacted for the appropriate information to log on to the DSS. This security was a requirement of the project's MDOT partners since detailed state-managed bridge condition data is available through the DSS.

13.2.1. Current Features of the Web Application

The demonstration version of the DSS attempts to convey several important concepts about bridge condition assessment and decision-making through a web-based, database-driven application:

- Geographic context, visualization, and filtering (down-selection) are important at the bridge inventory level.
- Some aspects of bridge condition, such as deck surface and subsurface condition indicators, have a geographic context and visualization as well, though on a much smaller scale.
- Spatial filtering of bridges in the inventory is equivalent to and should be easily integrated with filtering on other parameters (e.g., condition rating).

- The bridge inventory may be very large and must be partitioned for performance considerations yet comprehensive or aggregate visualization of large numbers of bridges must still be available.
- Frequently-used, high-level decision support visualizations at the inventory level should be immediately accessible.
- Where bridge inspectors interact with the application in the field, ancillary features such as driving directions to a bridge can complement data access and input.

The demonstration DSS was designed, on the front end, to look and feel similar to a familiar desktop application. It primarily features a table of bridge inventory records and a map on which markers are displayed representing the locations of the bridges loaded into the table, termed the "Bridge Metrics" and "Bridge GIS" panels, respectively (Figure 13-3). A whole host of other data visualization and analysis features are access through the various toolbars, buttons and menus along the top of these two panels.
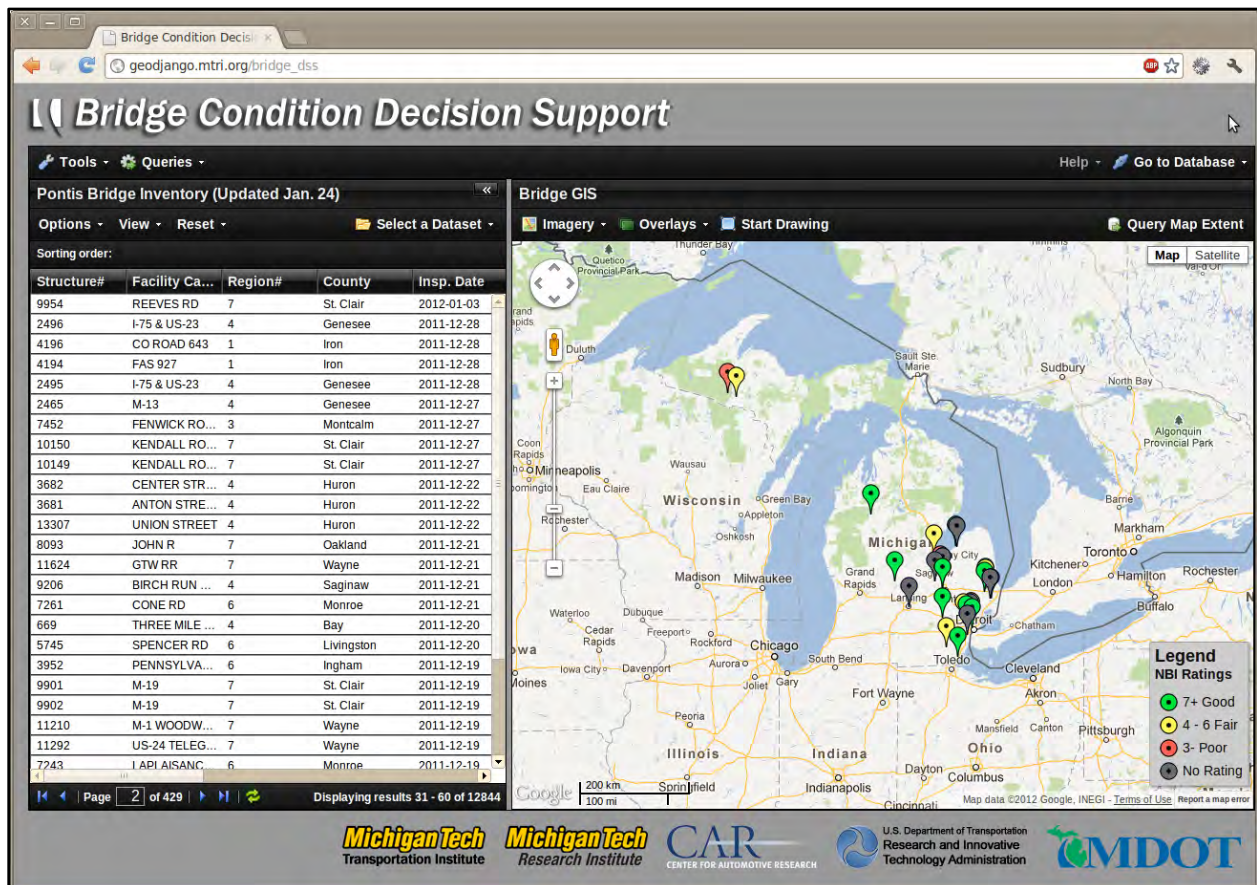
Figure 13-3: Screenshot of the demonstration DSS showing a sample of statewide inventory symbolized by NBI rating.

The Bridge Metrics panel on the left is designed to provide functionality similar to that of Excel, OpenOffice Calc, or any other desktop spreadsheet application. Bridge data are loaded into the table asynchronously and the total number of records available can be paged through, currently set to 30 bridges each time to enable fast performance. The total number of records available is displayed and the client application calculates how many pages are needed for all of them. These records can be sorted and filtered a variety of ways, either through the column headings of some fields (Figure 13-4 left), through the map interface (spatial filtering only) or through a generic utility. The rows of the Bridge Metrics can also be color-coded to match the symbology of the corresponding markers in Bridge GIS (Figure 13-4 right).
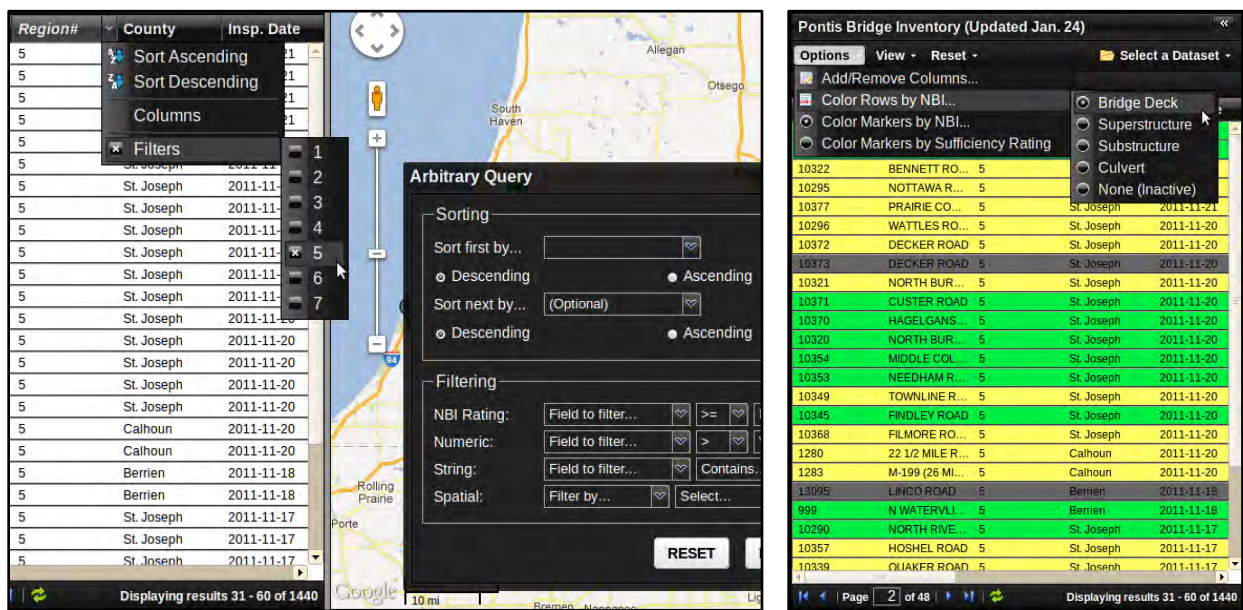
Figure 13-4: Screenshot of the sorting and filtering features and how they are access in the DSS (left) and color-coding of table rows according to NBI Bridge Deck rating, among other choices (right).

Map markers in the Bridge GIS panel are automatically added to the map when bridge records are loaded into the table. These markers are color-coded by NBI Bridge Deck rating by default, but color-coding by other NBI ratings and by sufficiency rating are other options available. Bridge GIS has a lot of features built into it by virtue of the Maps API which is used to render the map. These include a directions service, identical to what is provided through the Maps website, which is intended to help bridge inspectors navigate from bridge to bridge. Bridges do not typically have normal street addresses, which makes them difficult to navigate to using a GPS routing service. The DSS knows the geographic coordinates of every bridge, however, and uses the Maps geocoding service to look up the address. A traffic layer is also obtained from a Maps service, and is designed to complement the directions layer so that inspectors have additional decision support in choosing the exact route (Figure 13-5). Through the Maps API, each map marker has its own pop-up context window (sometimes described as a "callout" and

which is formally called an InfoWindow in the API) which serves as a gateway for bridge-specific decision support features such as the driving directions, attributes, and zoom function of a particular bridge. The basemap imagery that is provided by the Maps API, just as in the Maps website, is also, of course, extremely important to the usability and functionality of Bridge GIS.
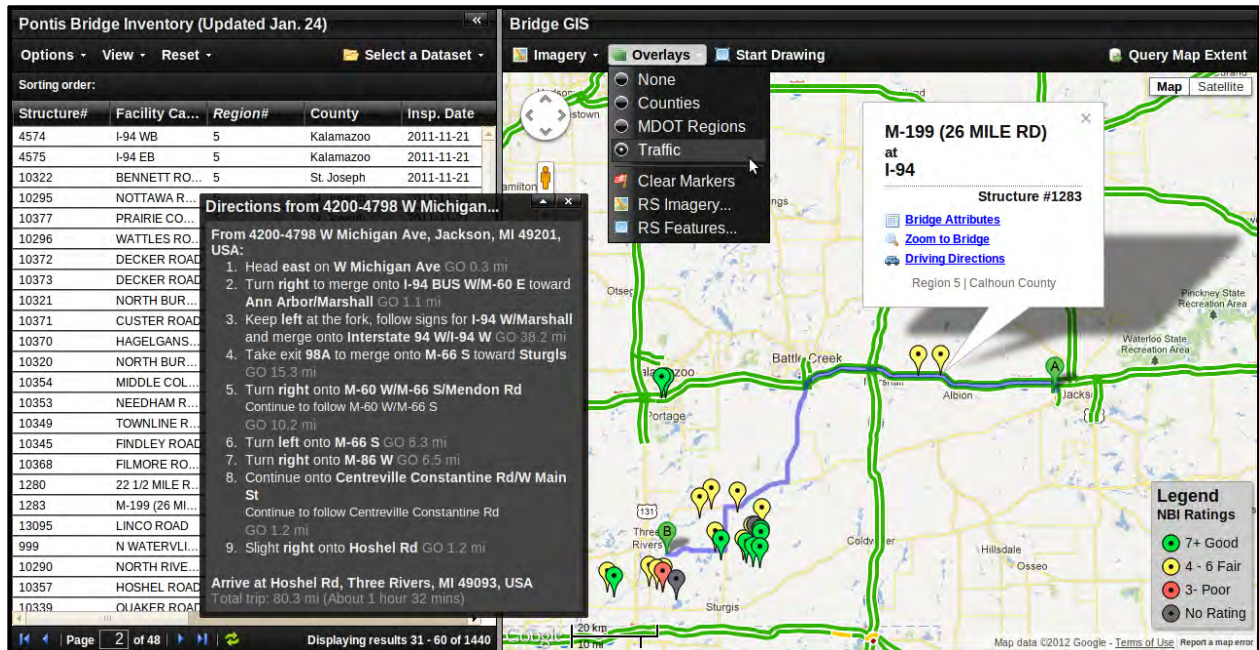
Figure 13-5: Screenshot of the DSS highlighting some of the features built-in to the Maps API, which is used to render the map, including traffic and directions services.

One of the features available through the InfoWindow of each bridge marker in Bridge GIS is the "Bridge Attributes" utility. This launches a pop-up window with three attribute tables that are loaded from the server: that bridge's metadata summary, the complete list of bridge attributes, and the latest inspection record. The bridge's "metadata" is a collection of fields which contain information about the bridge's slow-to-change, ancillary inventory information, such as bridge length and the number of lanes, but also its most recent NBI inspection and sufficiency ratings. The complete list of bridge attributes is the complete list of bridge metadata including most of the NBI or structure inventory and appraisal (SI&A) items. The bridge's latest inspection record is available as well so that, beyond the ratings available in the metadata summary, information such as the inspector's name and the previous inspection date are available. A powerful and useful feature of Bridge GIS is spatial querying, which can be accessed through added overlays or by the drawing utility. In the example shown in Figure 13-6, the drawing utility has been used to draw an arbitrary polygon on the map with the goal of spatially querying all the bridges along or near a highway corridor. The individual markers (red flags) that mark the vertices of this polygon can be adjusted and the spatial query executed again.

13-10
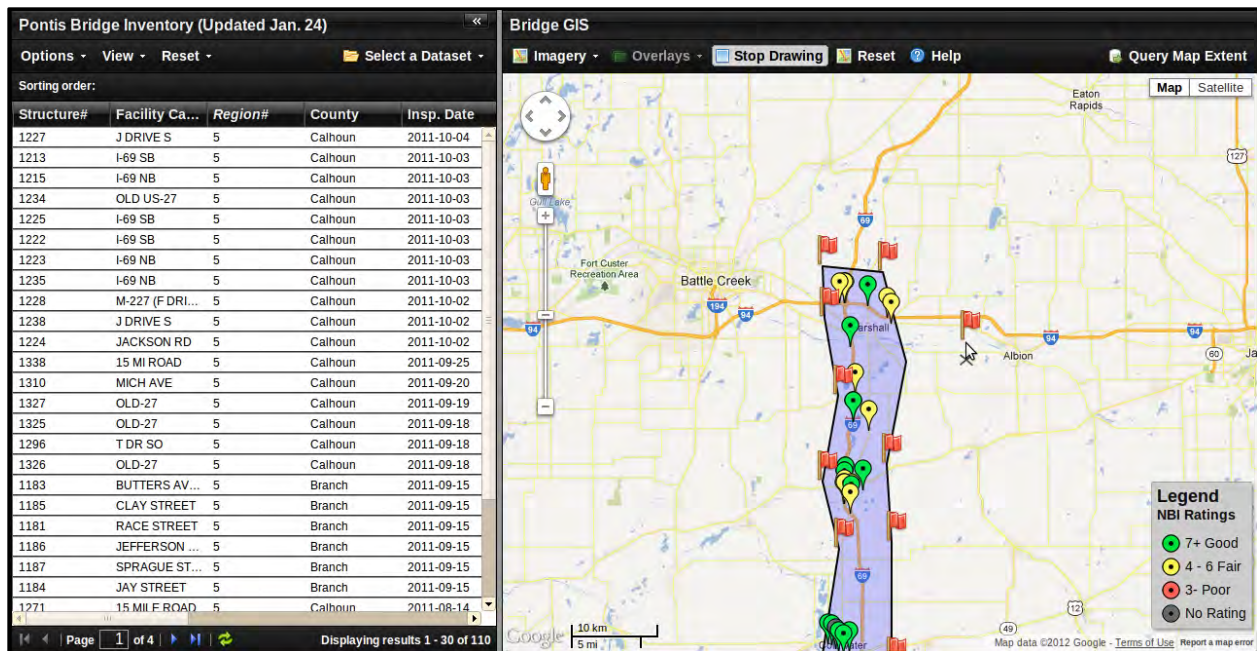
Figure 13-6: Screenshot showing an arbitrary polygon drawn to show how to spatially query the bridges along a highway corridor.

Bridge GIS also has a button, "Query Map Extent," which will apply a spatial query using the bounds of the current map window so that all the bridges "currently in view" are retrieved from the server. This can often be a faster way of filtering to bridges in a certain area defined by panning and zooming the map. In addition, users can apply preset spatial filters by county or by transportation agency region through overlays that helpfully define the area-of-interest and make the spatial filter itself only a double-click away (Figure 13-7).

Many of the more advanced features of the DSS are only available to explore with a subset of MDOT's bridge inventory – the field demonstration bridges (Freer, Willow, and Mannsiding). Each of these bridges has a number of features in its pop-up context window that are not available to other bridges. These are mostly oriented around remote sensing datasets that were only collected for those bridges. BVRCS is one example, as are GigaPan deployments; both are displayed on the map by markers that indicate where the photos were taken from (Figure 13-8). BVRCS photographs thus allow decision-makers to virtually "walk" the bridge from a computer. GigaPan photographs also allow decision-makers to view the bridge in great detail from multiple angles without leaving the office. With multiple photo collections, bridge managers could easily visualize change over time via these photo inventories.
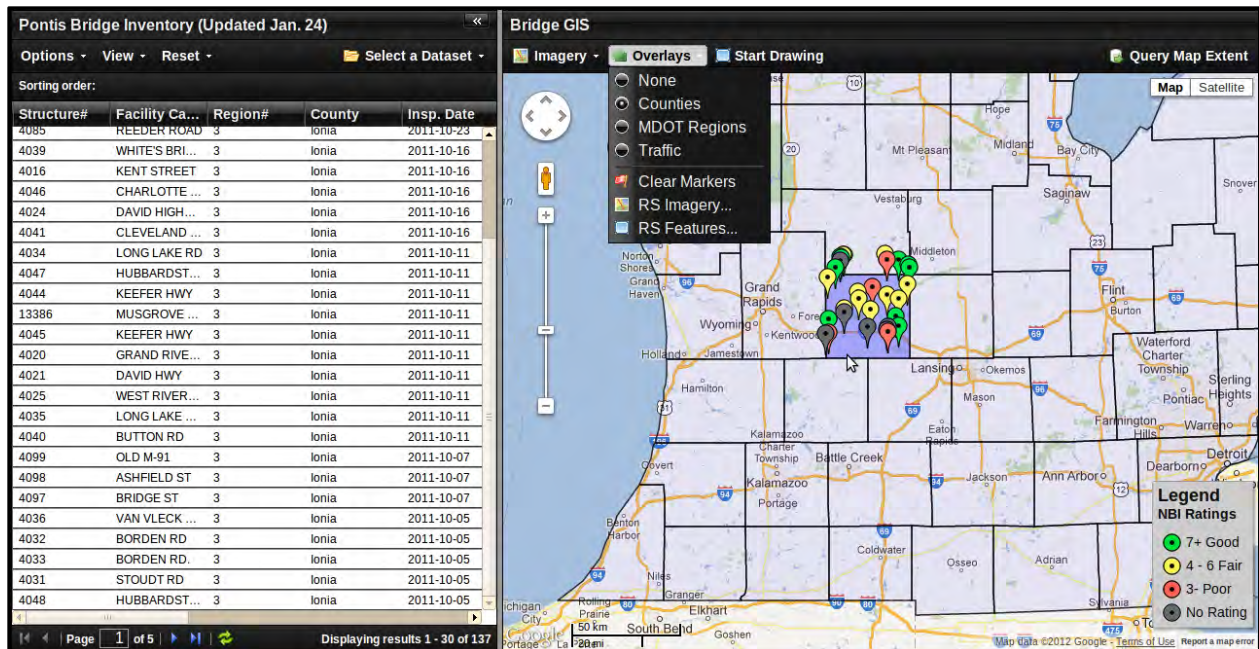
Figure 13-7: Screenshot of the DSS with a counties overlay where each county polygon serves as the handle for a spatial filter to that county; this enables users to find all the bridges in a county of interest.
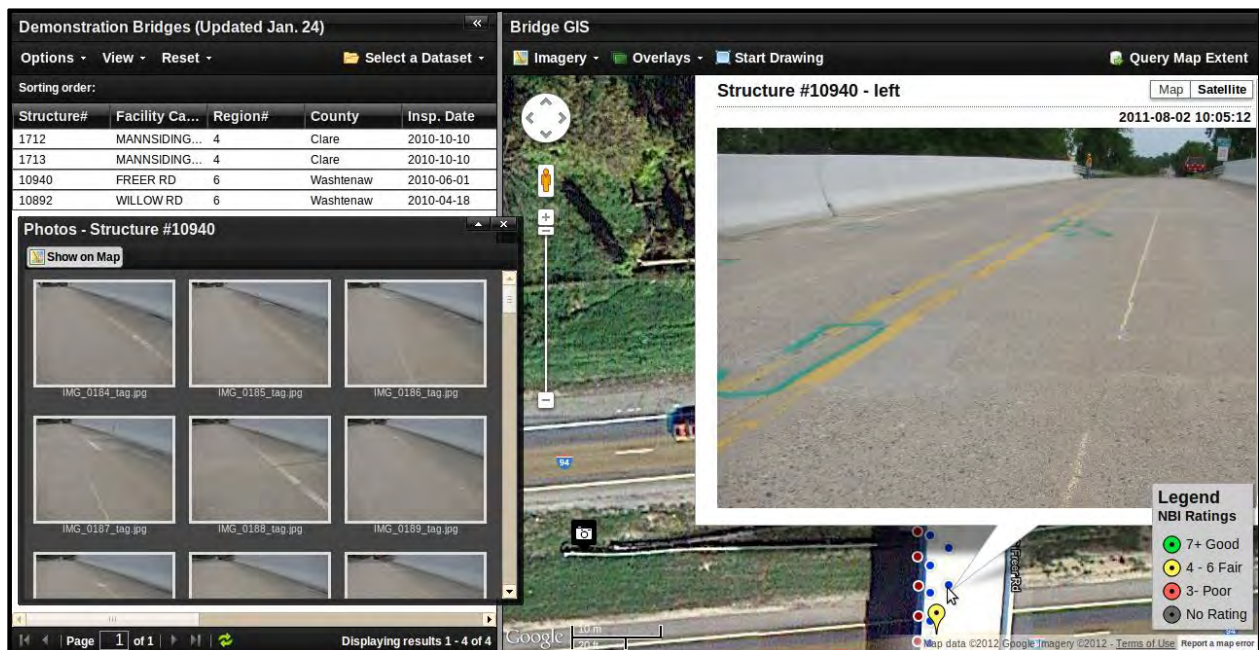
Figure 13-8: Screenshot showing the BVRCS and GigaPan photos accessed in the DSS.

The other remote sensing datasets available are displayed as overlays in the map window. These include a variety of remote sensing products developed as part of the technology evaluation in this project.

Screenshots in this chapter show the DEM from 3DOBS with a color-ramp and spalls digitally extracted as an overlay (Figure 13-9 left), the high-resolution photo-composite from 3DOBS (Figure 13-9 right), and the "hillshade" version of the 3DOBS DEM (Figure 13-10) that displays a 3D effect that provides a sense of the elevation change in bridge surface features such as spalls and patches. These layers can be interleaved with one another and other products to compare results between remote sensing imagery across the bridge deck.
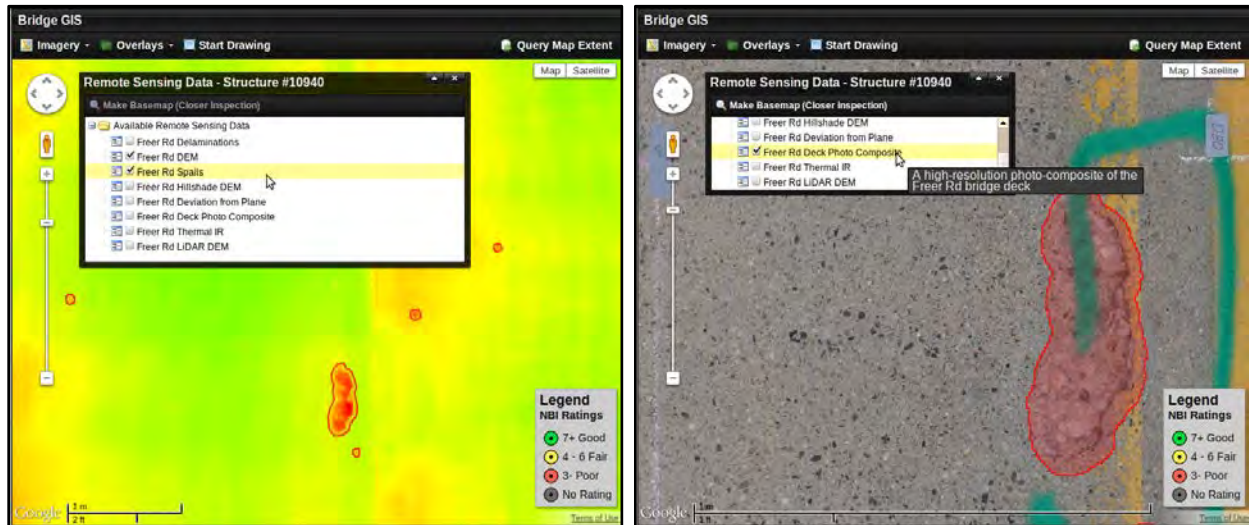
Figure 13-9: Screenshot from DSS of a digital elevation model (DEM) with a color-ramp and spalls outlined in red (left) and screenshot of a high-resolution photo composite showing the same, large spall as outline on the left; note the scale bar at the bottom of each, which is 1 meter in both (right).

Finally, an example of the high-level decision support products that should be available at a glance is the NBI ratings distribution pie chart (Figure 13-11). This tool allows decision-makers to see the distribution of NBI bridge deck, superstructure, substructure and culvert ratings throughout the bridge inventory or in a given agency region at a glance. The charts can be modified (slices separated or removed) and downloaded by users as image files or printed. Moving the mouse over any slice generates a pop-up that displays the rating and the percentage of bridges that have it in the inventory.

This capability was a high-priority request of the project's DSS Focus Group.
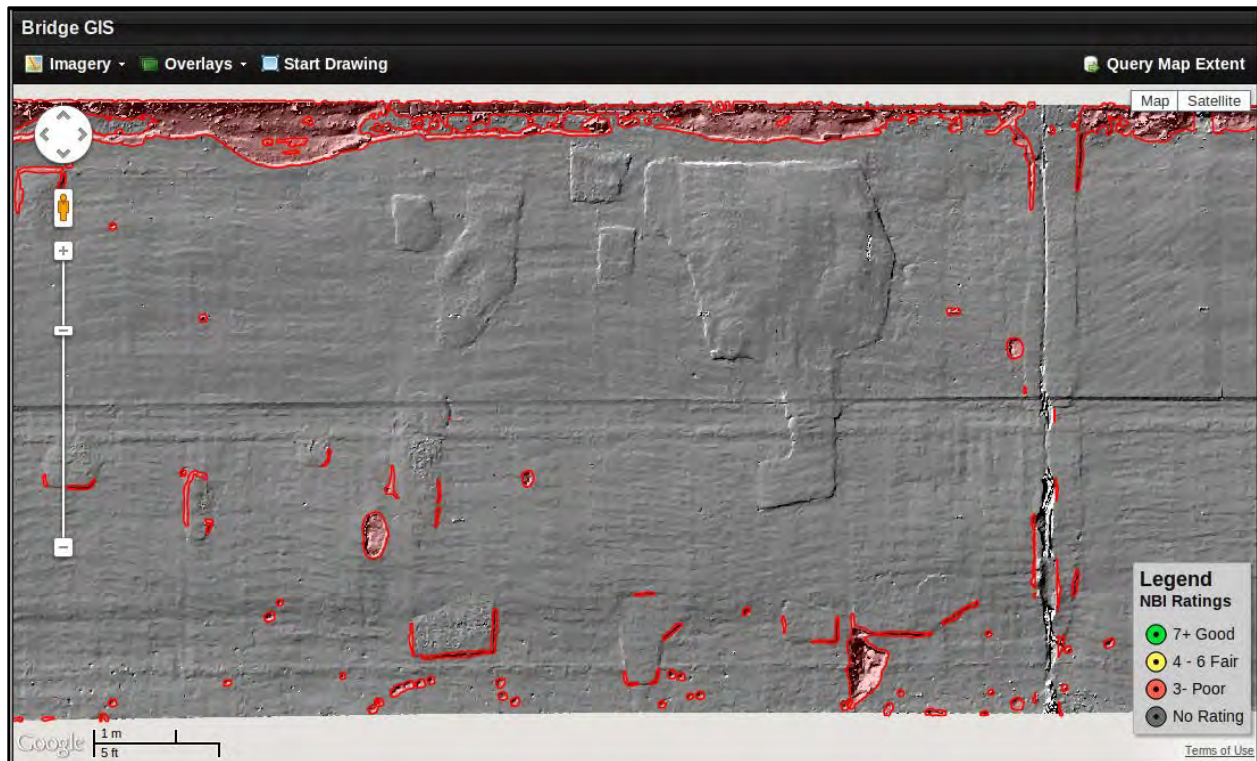
Figure 13-10: Screenshot from the DSS of the hillshade DEM layer for the Willow Road bridge with spalls outlined in red; note that bridge joints have been removed from the spalls layer and that the vertical accuracy is so fine that patches are clearly seen.

13.2.2. Alternatives and Justifications

The project team made technology selections for the DSS based on early requirements, considerations of the target user, and the environment the DSS was to be implemented in. In some cases, choices were made between multiple programming languages, computing frameworks, and software libraries that offer equivalent benefits and limitations. In such cases, the project team opted for those technologies with which it is more familiar and were well-suited to the DSS requirements. The project team's considerable experience with the Python programming language, the Django web framework, and PostgreSQL-PostGIS databases was certainly a factor in their selection. However, these are also appropriate choices on their own merits. It should also be noted that the selection of any particular technology is not always independent of other selections.

As previously mentioned, the solution stack chosen for the DSS web application is based on LAMP; a variant termed LAPP. The adoption of Linux as the server operating system (OS) was a clear choice for the development team, given that it is free, lightweight and easy to develop on and deploy. However, the server stack could be ported very easily to a Windows machine and potentially Apple Mac OS X as well. Apache, the web server in the DSS architecture, was

another obvious choice. It is the most popular HTTP (hypertext transfer protocol) server in use today, estimated to serve over half of all active websites and running on close to 65% of the top servers across all domains (Netcraft 2012). It is also very secure and robust. HTTP Basic authentication has been implemented for the DSS on its Apache server and more secure authentication protocols, such as HTTP Digest, are also supported.
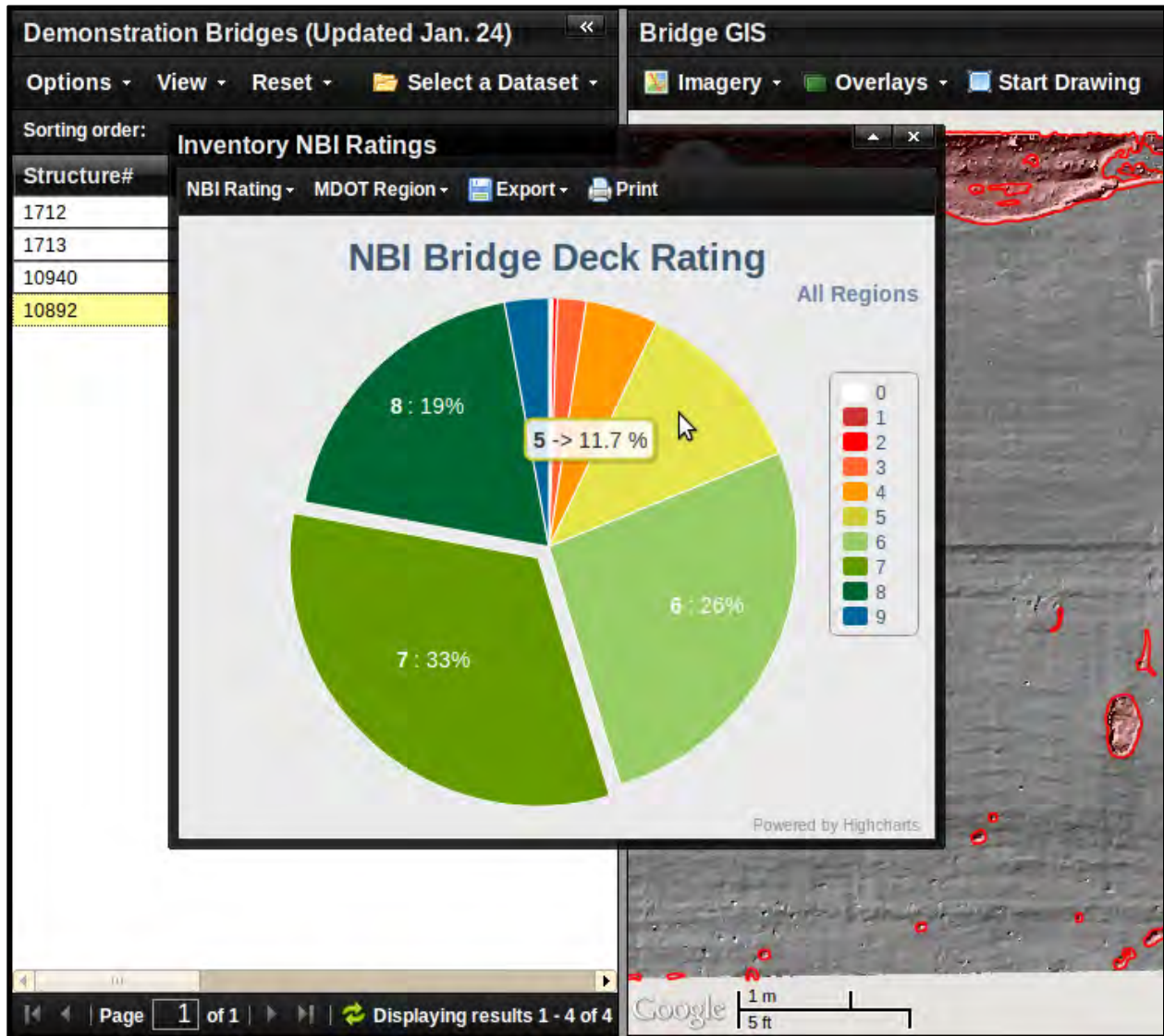
Figure 13-11: Screenshot of the NBI ratings distribution pie chart in the DSS.

The Python programming environment was chosen based on the language's maturity, high-level of expression, and popularity which practically means a large community of developers to turn to for support and extensions. Alternatives in the LAMP/LAPP stack include PHP (PHP: Hypertext Preprocessor) and Perl, the latter of which would be largely inappropriate for this type of

application. PHP, however, is a popular choice for dynamic publishing and database-driven web applications and would be a good alternative for future implementations of the DSS if a PHP framework based on the model-view-controller (MVC) paradigm could be selected. The current DSS demonstration version uses an MVC framework; it is key to the rapid development and deployment of the DSS (Leff and Rayfield 2001). Ruby is another popular, high-level programming language virtually equivalent to Python. Both are dynamically typed and object-oriented.

Selecting the Python programming environment narrows the selection of a server framework. Pylons, Django, TurboGears, Grok and CherryPy are just a few examples of web frameworks to choose from in the Python environment. The project development team selected Django from among these largely because it is familiar; however, the MVC-style and built-in template language make Django more attractive than many of its alternatives.

The selection of a DBMS is an example of a choice that influences other technology choices: an architecture based on one DBMS will only be able to support server frameworks that possess the appropriate database middleware. The back-end DBMS chosen for the DSS, PostGIS, is based on PostgreSQL, a popular open-source DBMS. There are several other relational DBMS flavors available including MySQL, SQLite, Microsoft SQL Server, and Oracle. What PostgreSQL offers in comparison to other relational DBMS flavors is equal or better scalability, support for geospatial objects (with PostGIS), the security and flexibility it offers as a database server, and zero cost. Proprietary DBMS flavors such as Oracle, while robust, scalable and generally able to support geospatial objects, were deemed less attractive choices because of their cost which, for the most part, is justified by enterprise-ready implementations and extremely good technical support. These were not pressing concerns for a development team; however, they may be very attractive in future implementations of the DSS.

The adoption of other DBMS frameworks by transportation agencies such as MDOT, which adopted Oracle, does not preclude their implementation of the DSS, however, because of a few important design features. The DSS components are loosely-coupled, which means that changes in one component do not necessitate a change in others; components can be changed or even replaced provided the interface between components is consistent. In RESTful web communications, these interfaces are uniform by nature. In addition, the web framework can support multiple databases and could connect to a proprietary database such as Oracle provided a license and database middleware are available. In the framework selected, the database middleware is provided by Django; all that would be missing is a license.

Differentiation between alternatives on the client-side, in the web browser, was also necessary when selecting the components of the DSS architecture. In this arena, client-side interaction and data handling must come from so-called "native" technologies built into the web browser or from third-party software libraries that users have downloaded and installed themselves. Native support on the client includes structured data formats such as Hypertext Markup Language

13-16

(HTML) and Cascading Style Sheets (CSS), Javascript, the sole programming language of the web, and the browser API known as the Document Object Model (DOM). Software such as Adobe Flash, the Adobe Flex API, Java, and Microsoft Silverlight each must be installed on the user's computer in order to use web applications built with them. As an early goal of the DSS was to enable its use by any authorized user at any time on any machine with any standard web browser, and in particular as federal, state and local government users are often unable to install new software on their computers, the need for third-party libraries was identified as a weakness of deploying with Flash, Flex, Java or Silverlight.

Instead, the Bridge DSS was designed around Javascript which could be interpreted by any browser on any platform. The ExtJS library was selected as a development framework for Javascript; it provides a large number of application components or widgets (e.g., buttons, sliders, windows, toolbars, grids) and ensures cross-browser compatibility by constructing compatible markup (i.e., HTML) and CSS when loaded. There are alternatives to ExtJS, of course, including jQuery, the Yahoo! User Interface, MooTools and others. These are not quite as complete or as comprehensive as ExtJS, however, each would make a good substitute in future implementations of the DSS.

Finally, the selection of a data interchange format for communication between client and server was also one among many choices, the most notable and popular being Extensible Markup Language (XML), a standard maintained by the World Wide Web Consortium (W3C). The project team selected Javascript Object Notation (JSON) over XML, however, because JSON is more compact (requires fewer bytes) than XML for equivalent data and because JSON is essentially Javascript. Yet Another Markup Language (YAML) is yet another alternative, however, the development team considered XML still more appropriate than YAML.

13.3. Implementation and Next Steps

As emphasized throughout this chapter, the current version of the DSS is intended as a demonstration of next-generation bridge management web tools and remote sensing data integration. There are several considerations that must be taken into account before implementing the DSS in a production environment. In general, these considerations take the form of:

- Outstanding feature requests from user testing.
- Potential barriers to adoption and implementation.
- Performance and security issues.
- Unmitigated software bugs.

13.3.1. User Feedback

The Bridge DSS received two formal demonstrations and an initial planning meeting with outside stakeholders. The initial planning meeting was held with the newly-formed DSS Focus Group which includes many members of the TAC. The Focus Group's membership, in total, consisted of:

- Steve Cook, MDOT
- Jason DeRuyver, MDOT
- Dave Juntunen, MDOT
- Rich Kathrens, MDOT
- Bob Kelley, MDOT
- Amy Trahey, Great Lakes Engineering Group

The Focus Group membership fluctuated slightly throughout the project as members were added and others were unable to make meetings. Melissa Knauff, a bridge inspector with MDOT, was invited to the second Focus Group session. Bob Kelley was unable to attend any Focus Group meetings and Beckie Curtiss, also with MDOT, attended the second Focus Group session in Dave Juntunen's place. Each Focus Group was convened with these anticipated outcomes:

- Feedback on the functionality, completeness, ease of use, and relevance of the demonstration DSS
- Feature requests for any missing or incomplete functionality
- Identification of obstacles to implementation at a state transportation agency
- Identification of barriers to user adoption (adoption by decision-makers)

In the first Focus Group session, held April 18, 2011 in Lansing, MI, participants were shown screenshots of the DSS version that was in development at the time. Discussion was based on remote sensing and bridge inventory visualizations within the DSS that might aid decision-making. Team members asked detailed questions about the asset management process employed by bridge managers and inspectors and about what resources would be good references for integrating that decision workflow into the DSS.

The second Focus Group session held March 1, 2012, featured a live demonstration of an advanced version of the DSS followed by a "hands-on" session where participants could use the application themselves. Discussion was focused on the user interface, the ease of the application, and the terms and notation used in data representations. In addition to Arthur Endsley and Colin Brooks who led the DSS demonstration, and Richard Wallace, Mike Forster, and Qiang Hong from CAR who led an adjacent, afternoon session on the economic evaluation of the DSS and remote sensing technologies, team members Jim Ebling (MTRI), Larry Sutter (MTTI), and Bob Shuchman (MTRI Co-Director) were in attendance.

The near-final demonstration version of the DSS was shown to the TAC and the program sponsor Caesar Singh in a remote webinar during two sessions, April 26 and 27, 2012. Attendees were encouraged to log-on after the live demonstration and use the application themselves. Much helpful feedback was generated from these webinars and the DSS Focus Group meetings. What follows is a list of the problem reports and feature requests that the project received from all of those engagements. Some of them have already been fixed/implemented but all or listed here as a complete source of the most popular and important aspects to be implemented or addressed in a potential future version beyond this project.

- Map should change focus (pan and zoom to fit) for multiple bridge selections, responding to each new bridge selected (from a table or other assortment)
- Pie charts showing the distribution of NBI ratings in the inventory are very useful visualizations
- Map markers should support multiple symbologies: NBI bridge deck, superstructure, substructure and culvert ratings as well as sufficiency ratings
- Pre-defined charts, such as the distribution of NBI ratings, should offer preset filters such as (the distribution of NBI ratings per) transportation agency region and county
- Charts and graphs should also be available for any arbitrary (filtered) subset of the inventory; for example, the distribution of NBI ratings along a spatially-selected highway corridor
- Require login credentials to access the DSS so as to protect MDOT bridge inventory data (a priority issue that was quickly completed)
- NBI ratings of 'N' (not applicable, not taken) should not be displayed in the NBI ratings distribution charts
- The date of the last TMS export should be displayed on the pie chart
- Charting of historical bridge condition information, namely bridge deterioration curves
- View more than 30 bridges (current per-page limit), in fact, view the entire inventory or filtered set on the map
- Order bridge attribute names by structure inventory and appraisal (SIA) number, which is also the NBI item number
- Map overlays "turned on" for one bridge should be displayed for (all) other bridges in the map without having to activate them on separately
- Users should be able to seamlessly zoom arbitrarily far to inspect map overlays without being limited by the maximum zoom level of the basemap or having to set overlays as basemaps
- Bridge summary data should be available by simply moving the cursor over bridges in the map window; that is, the summary should be launched by "mouseover" events not only by "click" events

- In addition to driving directions from a street address, latitude-longitude pair, or an agency office location, there should be the option of getting directions to a structure from another structure (bridge-to-bridge directions)
- Aggregate (GROUP BY) queries are needed so it is possible to answer questions such as, "What are the worst bridges by sufficiency rating in each county?"

13.3.2.   Potential Barriers to Adoption and Implementation

The demonstration version of the DSS runs on an Ubuntu Linux virtual machine through the Apache server. The PostgreSQL/PostGIS database server is running on a different machine but there is no reason it can't be hosted on the same machine. This virtual machine, or a dedicated server, could be easily ported to another computer at any transportation agency. The barriers to implementation, therefore, lie primarily in the integration of the server software with an existing network. This may manifest as network security incompatibilities and/or a lack of information technology (IT) support, neither of which are insurmountable.

The most likely difficulty for integration of the DSS server framework with an existing network would be an incompatible database server. This difficulty would arise in the attempt to have the DSS read data directly from a Pontis-like database. This problem can be mitigated by exporting data from the Pontis-like database, however, this is inefficient. If the adopter decides to connect the DSS to an existing database, the target database must be supported by the DSS middleware, Django. This limits support to MySQL, SQLite, PostgreSQL, and Oracle databases, however, it is possible to write extensions to the middleware that allow it to support any database whatsoever.

If the database is already supported, there still exists the challenge of modeling the database's existing tables in the DSS, as it is not recommended that Django, the DSS database middleware, manage them directly. This challenge persists for future adopters because the project team was not able to connect the DSS directly to a Pontis-like database during the study.

Barriers to adoption are hard to predict. Though none were identified by the Focus Group participants, they may yet exist. One potential barrier at MDOT may be their inevitable adoption of an improved MBRS, an early version of which was demonstrated to the project team. While still in development, the new version of MBRS has been significantly improved from the existing version. Many features and concepts exemplified by the Bridge DSS can also be found in the developing MBRS. The project's DSS appears to be serving as inspiration for future development in this area. Nonetheless, when transportation agencies develop their own next-generation bridge management systems they are less likely to adopt the DSS as-is.

Flexibility and customization should always be design goals for future DSS development so as to maintain its relevance.

13.3.3.   Needed Improvements for Implementation

Over the course of the project it has been necessary to redesign some aspects of the software architecture and add in additional capabilities by linking additional software libraries. Before any new features are added it is strongly recommended that the code be refactored or rewritten to be more implementation-ready and performance-hardened. As several of the needed improvements identified by the Focus Group are feature requests with respect to the user interface, a new design phase should commence in which these requests are taken into consideration before refactoring. Much of the existing code will be re-used, of course, but many structures in the code should be generalized and modified to fit new or existing classes and functions. Most importantly, the interfaces between application components need to be standardized so it is easy to add new components. With this new architecture in place based on defined requirements the DSS code will have a longer support life and ultimately be more reliable and flexible.

Another necessary improvement to the DSS arises from the current implementation of filtering and sorting. In the DSS, bridge inventory records can be sorted locally, sorted remotely, and filtered remotely. In local sorting, the 30 bridge records currently loaded are sorted on a field ascending or descending. In remote sorting, the entire table of records stored on the server is sorted. Filtering is always done remotely, as it must be done by the server operating on all records available. These distinctions are supposed to be invisible to the user but in testing it seems to be too complicated for practical use. Local sorting is likely not necessary, and sorting and filtering should always be done on the server. A good design principle from REST can guide development here: the client application should remember the index number of the first record on the current page, the current sorting parameters and direction, and the current filter parameters and values. When the user changes the page, the client application passes all of these parameters in a request so that the server can reconstruct the query and return the next page. If the user changes filters or sorting, it is up to the developer as to whether or not the same page should be used, but, again, all of the parameters are passed in the request. This is the concept of storing all application state, or information about the application specific to the current user and the current instance, on the client computer only.

The project team has also tested the current version of the DSS on tablet platforms as well. The tool can be used on the Apple iPad and Android-based tablets such as the Samsung Galaxy Tab 10.1. Additional work would be needed to produce a version that was oriented towards the touch-screen-centric model of tablets to enable easier use of the DSS interface. An example version has been generated as part of the project. Also included in an implemented version would be server-based code that would attempt to detect the type of device using the DSS, so that if a user was accessing the DSS from a tablet or smart phone, the DSS would display a touch-focused tablet-compatible version of the interface. Access to remote sensing data and existing Pontis-type bridge data would be very useful to transportation agency users, based on feedback from the TAC, DSS Focus Groups, and presentations about the project to a variety of audiences.

Other general improvements are concerned with implementation in a production environment. To bring the DSS up to an operational capacity without performance degradation, load balancing is needed. Broadly speaking, this can be achieved by using a proxy server to intercept HTTP requests for DSS resources. The proxy server would then delegate one of several server instances to handle the request. Each of these instances might operate on one or more databases or enterprise architecture of databases. The general principle involves the intelligent use of redundancy to increase the amount of computing power available to handle HTTP requests. There are many considerations that must be taken into account here, including the precise scale of load balancing required and the technique used to synchronize database transactions, all of which are beyond the scope of this report. Software virtualization of DSS resources, where parallel processing and throttling are used to efficiently manage HTTP requests, is a near-term goal that will probably meet the performance needs in most implementations. This topic must also be addressed specifically for the image web servers (e.g., GeoServer, ArcGIS Server) as these require particular approaches to load balancing.

A production environment also requires improvements to information security. The demonstration version of the DSS utilizes HTTP Basic authentication solely for its security requirement. This may be insufficient for two reasons, the first a strategic problem and the second a technical limitation. First, weak authentication is used where strong authentication or defense in depth is needed. Second, HTTP Basic authentication sends passwords in clear text, that is, without encryption. Weak authentication is so termed because it rests on the assumption that any user furnishing a valid set of credentials is the user identified by those credentials (an obvious scenario where this assumption fails is one where an attacker has obtained valid credentials). The general solution, defense in depth, can be achieved by adding additional layers of authentication. Strong authentication, the choice solution, is characterized by multiple dimensions of authentication; an example is providing a question and requiring any potential user to give an answer that only the intended user would know in addition to requiring that any potential user furnish login credentials. A more appropriate example for the DSS would be checking the user's IP address against a whitelist of allowed IP addresses in addition to checking for valid credentials. Even with strong authentication, however, the use of HTTP Basic authentication is problematic because the passwords entered by users are not encrypted; anyone monitoring traffic on the network and intercepting communications can read passwords in plain text. HTTP Digest authentication is an alternative supported natively by the Apache server and most web browsers that will allow for authentication to be encrypted.

Finally, what follows is a list of outstanding feature requests and needed improvements identified by the Focus Group. User testing is a key part of proper development and the results from the Focus Group should be used to generate a new requirements document before redesigning the software architecture and refactoring the code.

13-22

- Charts and graphs should also be available for any arbitrary (filtered) subset of the inventory; for example, the distribution of NBI ratings along a spatially-selected highway corridor
- Charting of historical bridge condition information, namely bridge deterioration curves
- View more than 30 bridges (current per-page limit), in fact, view the entire inventory or filtered set on the map
- Order bridge attribute names by SIA number, which is also the NBI item number
- Map overlays "turned on" for one bridge should be displayed for (all) other bridges in the map without having to activate them on separately
- Users should be able to seamlessly zoom arbitrarily far to inspect map overlays without being limited by the maximum zoom level of the basemap or having to set overlays as basemaps
- Bridge summary data should be available by simply moving the cursor over bridges in the map window; that is, the summary should be launched by "mouseover" events not only by "click" events
- In addition to driving directions from a street address, latitude-longitude pair, or an agency office location, there should be the option of getting directions to a structure from another structure (bridge-to-bridge directions) or from the users' current location if the tool is being accessed by a location-enabled device such as a tablet with built-in GPS
- Aggregate (GROUP BY) queries are needed so it is possible to answer questions such as, "What are the worst bridges by sufficiency rating in each county?"

14. Economic Evaluation of Promising Commercial Remote Sensors and Systems

MTU lead an investigation of the utility of remote-sensing technology for bridge condition assessment. This project, performed under contract to USDOT, includes laboratory and field testing of several technologies for bridge condition assessment. As part of Task 6 of the study, MTRI has performed a technical assessment and evaluation of the bridge condition DSS tools, software, and sensor components. CAR was tasked with conducting an economic evaluation of the cost-effectiveness of a broad deployment of remote sensing techniques for bridge condition assessment and DSS for bridge management.

The decision to integrate remote sensing technologies into bridge inspection practices can be viewed as an investment strategy for both the public and private sectors. The economic indices (e.g., capital and operational costs) are critical for quantifying and qualifying the ability of the proposed new technologies to meet the functional and operational needs of the bridge inspection process. This economic assessment is designed to assess the cost effectiveness of remote sensing technologies by comparing marginal costs of employing sensor technologies to the additional benefit that they provide, and therefore to ensure a practical, cost-effective product to be integrated into transportation agency operations.

This assessment includes discussions on bridge inspection and maintenance in the context of declining federal and state transportation revenues, descriptions of existing bridge inspection practices, summaries of remote sensing technologies for bridge condition assessment, and findings of economic evaluation based on different assumptions (e.g., adoption curve of new technologies, time period of analysis, and geographic coverage) and deployment scenarios (e.g., combinations of technologies and service types). This study also examines the benefits of the DSS integrated with remote sensing indicators of bridge conditions. Finally, this study recommends strategies to achieve cost effectiveness of remote sensing technologies.

14.1. Bridge Inspection and Maintenance in the Context of Declining Transportation Revenues

The quality and performance of transportation infrastructure, including highway bridges, are vital to the nation's economy and social well-being. Federal investment in the Highway Bridge Program (HBP) totaled $4.95 billion in 2009, representing 15% of total expenditures of federal funds administered by FHWA (USDOT 2009). Over the past three decades, the HBP (previously HBRRP; Highway Bridge Replacement and Rehabilitation Program) has received increasing federal funds, totaling over $81 billion (see Figure 14-1).
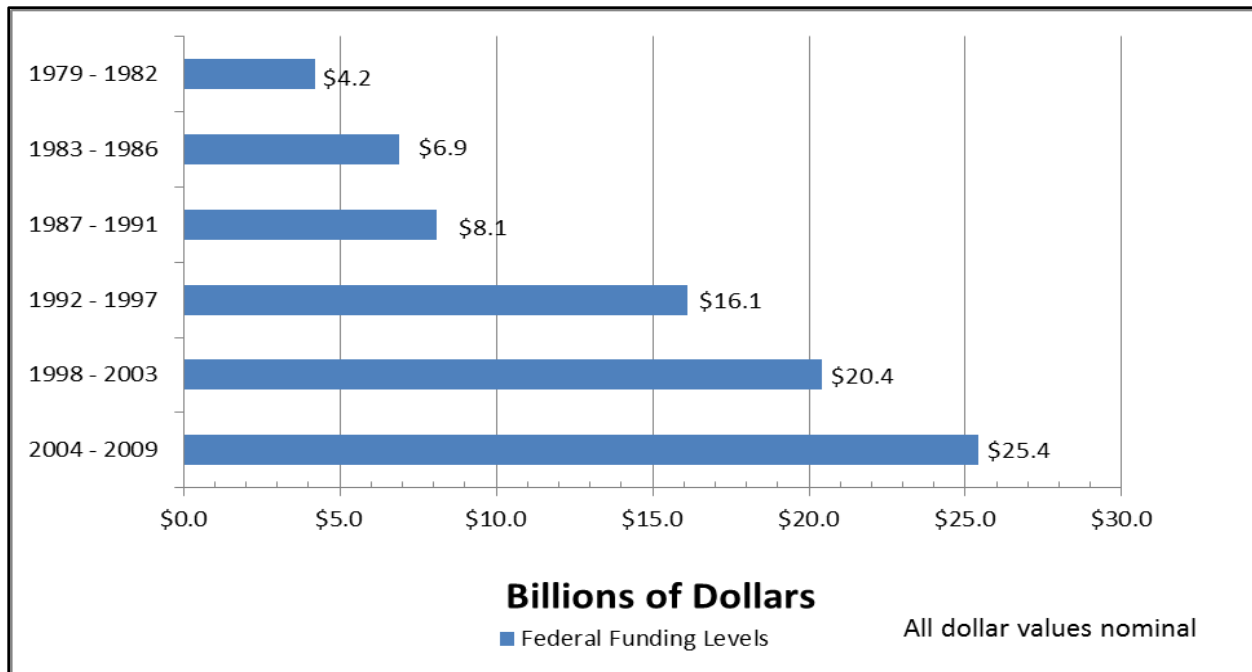
Figure 14-1: Funding levels of the HBP. Data source: 1979-03 data from Bridge Inspector's Manual (FHWA 2006); 2004-2009 data from USDOT Office of Highway Policy Information website <www.fhwa.dot.gov/policyinformation/statistics.cfm>.

Fiscal sustainability of a national HBP remains a challenge as the Highway Trust Fund (HTF), which funds the HBP and other highway programs, is projected to incur significant deficits in the years ahead. Further, the purchasing power of funding currently available for bridge maintenance, rehabilitation, and replacement is also declining (GAO 2010).

Addressing the scope of deficient bridges will be a bigger challenge as larger numbers of bridges built after 1950 reach expected service lives; as shown in Figure 14-2 the correlation between bridge age and condition is strong. About 21% of nation's bridges were built before 1950 and are over 60 years of age. More than 40% of these "old" bridges were either structurally deficient or functionally obsolete as of 2010 (Figure 14-3). Bridge repair and replacement needs will likely soon exceed available funding from federal and state sources.

An increasing pressure to improve economic efficiency of expenditures has created the necessity of BMSs and effective life-cycle cost management. The National Cooperative Highway Research Program (NCHRP) recently conducted a domestic scan focusing on practices among DOTs for identification, prioritization, and execution of programs for management of highway bridges. One of the scan team's key recommendations for bridge management decision-making is to adopt element-level bridge inspection programs and establish standard condition states, quantities, and recommended actions (i.e., maintenance, preservation, rehabilitation, replacement) to match the operational characteristics of state and local bridge maintenance and preservation programs (Weykamp et al. 2009).
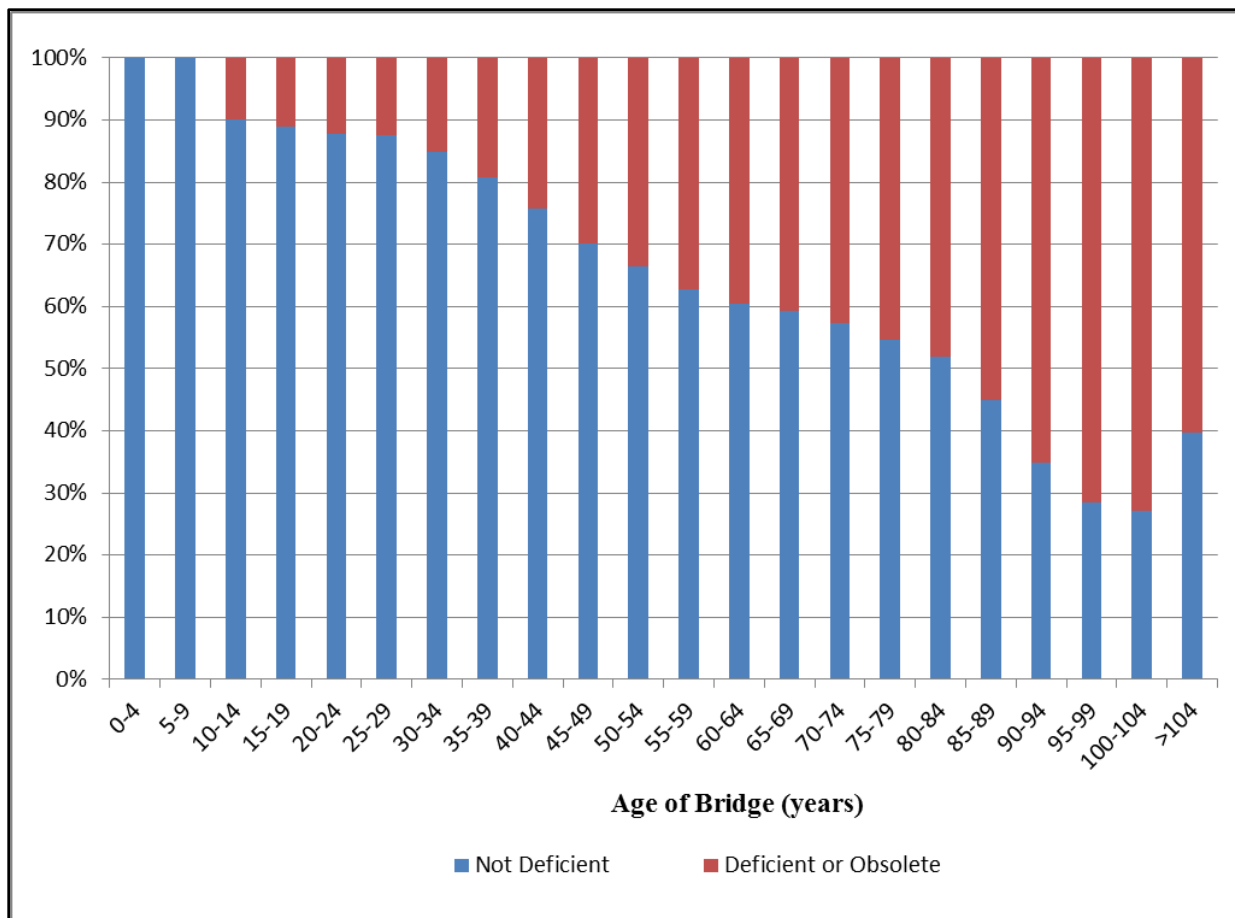
Figure 14-2: Age of bridge strongly correlated with condition (deficient or not). Data source: 2010 National Bridge Inventory (NBI) data.

Bridge management systems are data-driven and based on a strategic, systematic, and balanced approach to managing bridge preservation and replacement needs. The main components of bridge management are condition assessment, planning, life-cycle analysis, and maintenance management. Bridge inspection data and condition rankings are essential to BMSs in order to optimize the use of available funds and help local, state, and federal agencies make smart maintenance and rehabilitation decisions. Research suggests that preventive maintenance (PM) is a cost-effective way of extending the service life of highway bridges. For every dollar spent on the PM program, $4 to $10 was saved in the rehabilitation program (Adams et al. 2008).

FHWA recently introduced a new bridge safety initiative to improve bridge inspection and management practices. This new process is based on objective, statistical data – providing for greater consistency in bridge inspections and more strategic approaches to identifying problem areas by using defined criteria for 23 key metrics (USDOT 2011). Such strategy parallels and complements bridge management systems and will improve bridge investment decisions at all levels.
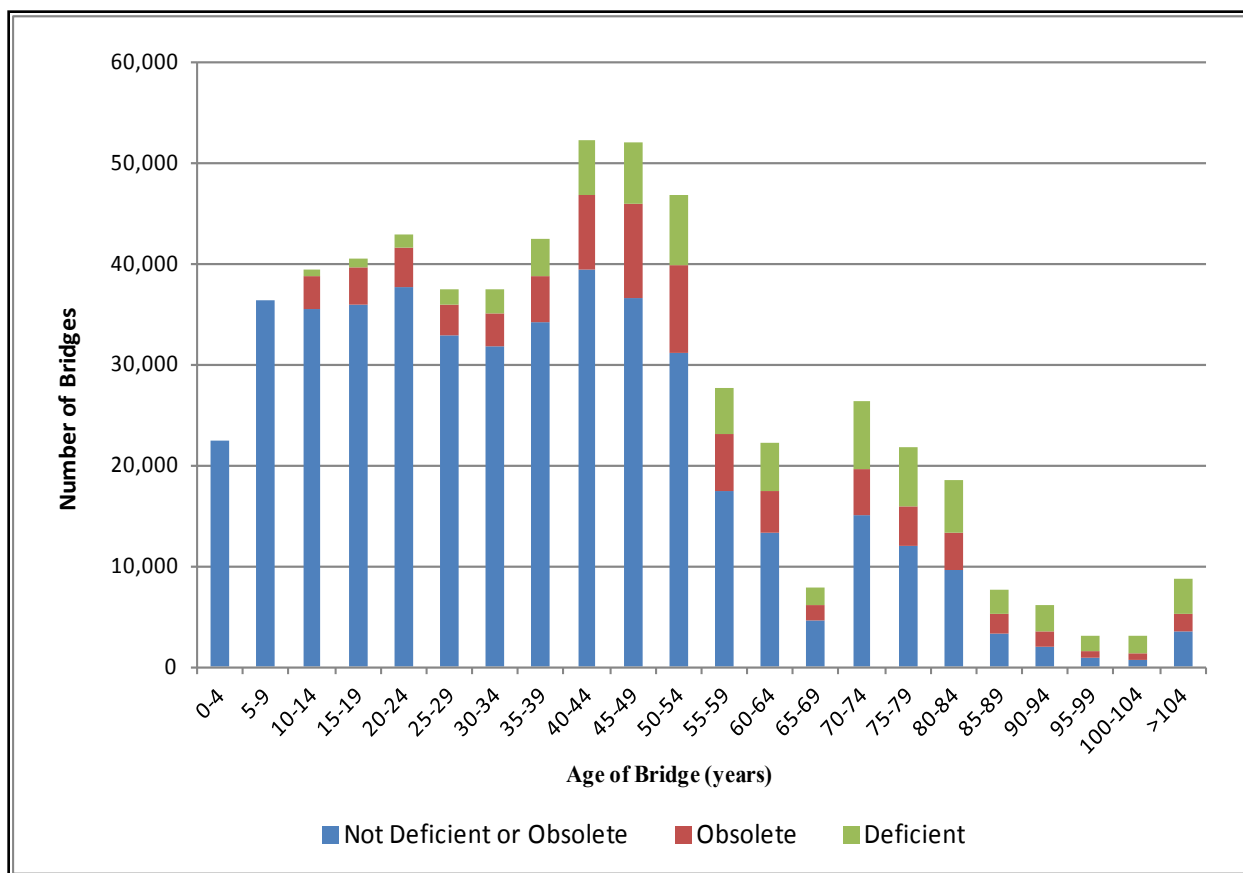
Figure 14-3: High percentage of older bridges are obsolete or deficient. Data source: 2010 National Bridge Inventory (NBI) data.

14.2. Description of Existing Bridge Inspection Practices

Federal regulations define eight types of bridge inspections (routine, fracture-critical, underwater, damage, hands-on, in-depth, initial, and special). Three of these, routine, fracture-critical, and underwater inspection, occur at intervals set by regulation (TRB 2007). In most cases, the NBIS suggests a 24-month interval for routine inspections. Some states, such as Minnesota and Ohio, require routine inspection at 12-month intervals. Bridges with condition problems tend to be inspected at a 6-month, or even 3-month, interval.

Routine inspection is described as "regularly scheduled inspection consisting of observations and/or measurements needed to determine the physical and functional condition of the bridge, to identify any changes from initial or previously recorded conditions, and to ensure that the structure continues to satisfy present service requirements" (TRB 2007).

All routine bridge inspections, by federal mandate, require rating of five major bridge components: bridge deck, superstructure, substructure, channel and channel protection, and culvert condition. Most transportation agencies and owners collect data beyond the NBIS and federal mandates to support their bridge management program (Alampalli 2010).

Currently most inspections are visual based, even though NDE methods are becoming popular in augmenting the visual inspections and subsequent evaluations advocated. Traditional structural health monitoring techniques include:

- Strain gauges
- Deflectometers
- Accelerometers
- Live load vehicles
- Hammer-sounding
- Chain-drag

Federal regulations identify four staff positions for bridge inspection programs:

- Program manager: The individual in charge of bridge inspection, reporting, and inventory.
- Team leader: The individual in charge of an inspection team and responsible for planning, performing, and reporting field inspections.
- Load rater: The individual with the overall responsibility for bridge load rating.
- Underwater bridge inspection diver: Individual(s) performing inspections, by diving, of submerged components of bridges.

State DOTs may use different staff titles for each of the above four positions. For example, Michigan has one state bridge inspection manager, seven region bridge engineers, 15 bridge inspectors, and 15 inspection assistants. Most state DOTs use two-person inspection teams, including Michigan. Local agencies and consultants often use single-person teams.

Federal regulations require training for program managers and inspection team leaders in an FHWA-approved comprehensive course in bridge inspection. Federal regulations do not establish qualifications for inspection team members working under the direction of an inspection team leader (TRB 2007).

In Michigan, professional engineers must complete the NHI 2-week training class. A non-professional engineer needs two years of training in addition to the 2-week training class. After obtaining five years of inspection experience, non-technical inspectors can become an inspection team leader.

14.2.1. Cost Estimates of Current Bridge Inspection Techniques

Estimating bridge inspection costs is complicated because the data are not readily available in most cases. Agency experience or budgets are the only practical source for cost estimates. As previously discussed, state DOTs are required by federal law to inspect all bridges owned and maintained by the states at least once every 24 months. Most DOTs include regularly scheduled inspections costs in their "normal" or "preventive" maintenance budget because bridge inspection is often part of a DOT overall highway maintenance, repair, and traffic operations program (TRB 2003). This study collected data through a literature review and face-to-face interviews with MDOT partners to establish realistic agency cost estimates of current bridge inspections. This bridge inspection cost information is summarized in Table 14-1.

Table 14-1: Sample of Bridge inspection costs by state, county, and city.

State/County/City	Bridge Inspection Costs	# of Bridges Inspected Annually	Period	Annual Inspection Cost Per Bridge	Type of Inspection Services
Connecticut	$22.9 million	2,815	FY2010	$8,135	$15.8M for contractors; $7.1M for in-house
Wisconsin	$2.32 million	2,542	FY 2006-07	$917	$1.01M for contractors; $1.3M for in-house
Armstrong County, Penn	$482,172	34	2010 to 2015	$2,398	Contract service with PennDOT
City of Tulsa, Oklahoma	$98,000	256	2007 - 2008	$383	Contract service
City of Tulsa, Oklahoma	$130,000	256	2005 - 2006	$508	Contract service
Tulsa County, Oklahoma	$70,000	195	2007 -2008	$359	Contract service
City of Sapulpa, Oklahom	$4,500	11	2009 - 2010	$409	Contract service
Coal County, Oklahoma	$18,300	52	2009 - 2010	$352	Contract service
Garvin County, Oklahoma	$73,200	272	2009 - 2010	$269	Contract service
Logan County, Oklahoma	$88,000	231	2007 - 2008	$381	Contract service
Oklahoma Turnpike	$150,000	399	Since 1998	$376	Contract service

The average inspection cost per bridge varies significantly from place to place. For example, Connecticut's DOT oversees inspection of about 5,300 highway bridges and 330 railway spans in the state, and spent around $22.9 million on private bridge inspection services and in-house inspection for FY 2010 (ConnDOT 2011). On average, this translates into an annual inspection cost of $8,135 per bridge in Connecticut (assuming that 50%, or 2,815 bridges, were inspected each year).

In 2008, the Wisconsin Legislative Audit Bureau conducted a limited-scope review of the Wisconsin Department of Transportation (WisDOT) bridge inspection program that included FY 2006-07 bridge inspection expenditures by state staff and consultants ($1.31 million and $1.01 million, respectively). Wisconsin has 5,188 state-owned bridges, and the on-time inspection rate

is 98%; thus, 2,542 bridges, were actually inspected in one year. As a result, the average inspection cost was $917 per bridge for FY 2006-07 (Wisconsin Legislative Audit Bureau 2008).

Inspection costs also have been reported in Pennsylvania and Oklahoma. Armstrong County in Pennsylvania recently signed a bridge inspection contract with PennDOT (Pennsylvania Department of Transportation) that will be in effect from 2010 through 2015. The average inspection cost is $2,398 per bridge. In Oklahoma, an experienced bridge inspection service provider charged from $269 to $508 per bridge for state, county, and city-owned bridges (Oklahoma Department of Transportation 2010). The inspections are for the NBIS inspection program, and include updating the Pontis database, reviewing the load ratings and updating where necessary, preparing reports with Pontis data and work candidates, and coordinating load postings and overhead clearance signage.

14.2.2.   Time Spent on Inspections

While the time required for a bridge inspection varies according to the type and design of the bridge, the Inspection Manual published by Ontario Ministry of Transportation (MTO) states that an inspector should plan to spend at least two to three hours at a typical bridge site to adequately assess the condition of all elements. Insufficient time spent on inspections increases the risk that serious deficiencies will be missed, especially in older structures and bridges that have a history of problems. On average, inspectors conducted three to five inspections in a single day. Larger bridges take longer to inspect (Ontario Ministry of Transportation 2009). In Wisconsin, most routine inspections take less than one day to complete, and some take less than an hour, though inspections of bridges with complex designs or structural problems can last several days (Wisconsin Legislative Audit Bureau 2008).

Another study found that visual inspections rely upon the inspector having access to all components of a bridge; therefore, methods of gaining access to an elevated bridge are critical to inspection times. The two primary access methods are access equipment and vehicular (aerial) lifts. Access equipment includes ladders, rigging and scaffolds. Typical vehicular lifts are manlifts, bucket trucks, and under-bridge inspection vehicles. Usually, employing a vehicular lift will be less time-consuming than deploying access equipment; however, the time savings will be offset by the higher costs associated with operating vehicular lifts (Leshko 2008).

14.2.3.   Findings from Interviews with Bridge Inspection and Management Experts

Interviews with bridge inspection and management experts, including MDOT partners, were conducted in August and September, 2011. The purpose of the interviews was to quantify costs of traditional bridge inspection methods, such as time and labor requirements for bridge inspection, equipment needs, costs of special bridge inspection, and overall annual budget for

bridge inspection program in Michigan. For the list of interviewees, interview questions, and MDOT partners' responses, see Appendices F.1 and F.2. Following is a summary of the interviews.

Michigan has 4,397 state-owned bridges. For routine bridge inspections, nearly 100% are done by MDOT inspectors. MDOT also owns about 200 over-water bridges that often require assistance by contracted consultants. The on-time inspection rate at MDOT is 99.8%. Only a few bridges may be delayed due to special conditions. Special-needs bridges may be inspected more frequently than the standard 24-month interval. Such special-needs bridges include:

- Moveable bridges
- Fracture-critical and fatigue-sensitive bridges
- Special needs bridges
- Complex and/or large bridges
- Underwater bridge inspections

Michigan's annual budget for bridge operations is $185 million. This budget increased from $28 million in 1997 with the adoption of a one-cent per gallon gas tax, which goes directly to MDOT to fix seriously deficient bridges on the state road system. The annual budget for in-house and contract service was about $2 million in 2010, and this includes routine inspection, the bridge asset management program, and contract services. This translates into an inspection cost of about $900 per bridge.

Bridge inspection time includes time spent at the bridge and additional time of preparation and data processing. Typically, preparation for inspection (e.g., review of historical inspection reports) requires about 10-20% of total inspection time (including both on-site and additional time). The actual field inspection requires about 70-80% of total inspection time. Data entry requires the remaining 10% of total bridge inspection time.

A typical 3-5 span bridge will require 4-6 hours of on-site inspection time. The deck, superstructure, and substructure each take about 30% of this inspection time, while the remaining 10% of the time is spent on approaches. All routine inspections can be done without interrupting the traffic.

14.2.4.   Bridge Scoping

Bridge scoping is a more rigorous bridge inspection process. The purpose of bridge scoping is to evaluate a bridge for various repair alternatives, recommend the most economical rehabilitation or treatment, and develop a scope of work and cost estimate for the selected alternative. The work for each bridge scoping includes two major steps: site review and engineering analysis.

According to MDOT, about 167 state-owned bridges were scoped in 2010 at a total cost of $1,557,960, or $9,329 per bridge, on average. All bridge scoping was conducted by outside engineering contractors. Bridge scoping costs are not included in the routine inspection costs given in Table 14-1.

14.3. Remote Sensing Technologies for Bridge Condition Assessment

While cost-benefit analysis can be straightforward in cases with known or measurable costs and benefits, the analysis of remote sensing technologies is complex because neither the true benefits nor true costs can be measured with certainty. Additionally, the current technologies are being assessed as part of an applied research project. Once implemented on a commercial basis, the cost of these technologies is likely to fall significantly. One first important step for this study was to collect and analyze cost-data through field demonstration and associated technical assessment of these technologies.

Three MDOT bridges were selected for field demonstration in August 2011. The bridges provide a variety of conditions from poor to good and are the same type (pre-stressed concrete I-beam with concrete deck) to provide comparability between remote sensing results but under different condition ratings. The bridges, their location, and 2011 field demonstration dates are listed below:

- MDOT n$^{\underline{o}}$ 10940: Freer Road over I-94, Washtenaw County, August 1-3
- MDOT n$^{\underline{o}}$ 10892: Willow Road over US-23, Washtenaw County, August 3-5
- MDOT n$^{\underline{o}}$ 1713: Mannsiding Road over US-127, Clare County, August 8-10

The remote sensing technologies and the specific systems used to deploy these technologies on the three selected bridges included:

- 3DOBS
- BVRCS
- GigaPan
- LiDAR
- Thermal IR
- DIC
- UWBIRS
- SAR

A cost-data collection form was developed with a purpose of documenting detailed inspection activities on the bridge, including types of technology and equipment use, personnel, set-up time, running time, traffic closure etc. The most significant limitations of these technologies, based on

observations from field demonstrations at least, are speed of collection and traffic disruption (Table 14-2).

Table 14-2: Benefits and Limitations of Technology.

Technology	Benefits	Current Limitations
3DOBS	• Low capital cost • Rapid deployment • Useful metrics (% area and volume, and location of spalls) • International Roughness Index (IRI)	• Speed of collection (<5 mph) • Traffic disruption • 5 mm resolvable features (with current deployment; capable of higher-resolution)
BVRCS and GigaPan	• Low capital cost • Rapid deployment • Useful metrics (easily viewable geo-tagged photo inventory, can compare condition over time with multiple inventories)	• Automation of analysis • Not yet at highway speed • GigaPan storage
Thermal IR	• Useful metrics (% delamination, detects subsurface defects) • Qualitative and quantitative assessment tool	• Collection time • Traffic disruption • Camera specifics • Data processing time and user interpretation
SAR	• Bridge settlement from satellite imagery • Road and bridge roughness of multiple bridges	• Need satellite image pairs before and after settlement • Need good geometry from SAR imagery to see road roughness
UWBIRS	• Potential for useful metrics (e.g., % spall and delamination) • Detects surface and subsurface defects • Similar commercial 3D systems are becoming available.	• Not yet a commercially viable technology as deployed. • Speed of collection (<5 mph)
DIC	• Can track changes in mechanical behavior over time • Useful metrics: remotely captures deflection, strain field and vibration (global system metric)	• Environmental effects: error induced by wind and traffic flow, more ideally suited in current form for controlled environments • Deployment time and cost
LiDAR	• Potential for useful metrics: % spall and delamination • Detects surface	• High capital cost • Speed of deployment • Appropriate integration in bridge condition assessment framework

14.4. Economic Evaluation of Bridge Inspection Using Remote Sensing Technologies

The decision to integrate remote sensing technologies into bridge inspection practices can be viewed as an investment strategy for both the public and private sectors. The economic indices

(e.g., capital and operational costs) are critical for quantifying and qualifying the ability of the proposed new technologies to meet the functional and operational needs of bridge inspection processes. Therefore, a high quality economic evaluation should provide "value for money" information to those making decisions about the investment of new technologies and the allocation of limited bridge inspection resources. This section will discuss overall economic evaluation methods for new technologies, assumptions and deployment scenarios of remote sensing technologies, results of economic evaluations, and benefits of the DSS.

14.4.1. Economic Evaluation Methods for New Technologies

The economic evaluation of remote sensing technologies tends to be very complex. The task of evaluation involves determining the value of rapidly evolving technologies or products (both hardware and software) in an environment in which market data from real-world practices is limited. Further, the outcome indicators of traditional bridge inspections and those derived from using remote sensing technologies are not always identical; thus, it is often difficult to create head-to-head comparisons. For example, some remote sensing technologies are creating higher-resolution indicators of bridge condition than have traditionally been available to transportation agencies, such as the bridge deck digital elevation model created through the 3DOBS. Third, the benefits of using remote sensing technologies and the associated DSS are not easily assigned a monetary value without linking them to a broader context, such as life-cycle cost of bridge analysis and the benefits of optimized bridge management system.

There are many types of full economic evaluation techniques, including cost-utility analysis (CUA), cost-effectiveness analysis (CEA), cost-minimization analysis (CMA), cost-benefit analysis (CBA) and cost-consequence analysis (CCA). None of these techniques are absolutely perfect for application to the bridge condition assessment using remote sensors context due to the unique research questions raised, the condition of interest, and the availability of data on outcomes. To address these challenges, this research relied on the technical assessment of each technology, interviews with MDOT stakeholders, previous research findings, and field cost collection. Additional considerations include a forecast of field costs once tested technologies have been incorporated into a standard concept of operations (CONOPS) for bridge assessment to develop application scenarios and conduct relative cost analysis, similar to what the cost would be once these technologies were implemented on a commercial basis. During the analysis process, the factors explored below will influence final evaluation approaches:

14.4.1.1. Adoption Curve

The adoption of new technology tends to follow similar patterns, and this can be expected to apply to bridge condition assessment technology, too. Thus, these technologies are likely to be

adopted over time following familiar patterns, such as the one shown in Figure 14-4 based on theoretical models for the diffusion of innovations.

By using this general model, this study assumes three market penetration rates: 10%, 30%, and 50% of state-owned bridges that will use remote sensing technologies annually. Since the traditional inspection schedule is 2 years, an annual rate of 50% implies that all bridges are being inspected with remote sensing technology.
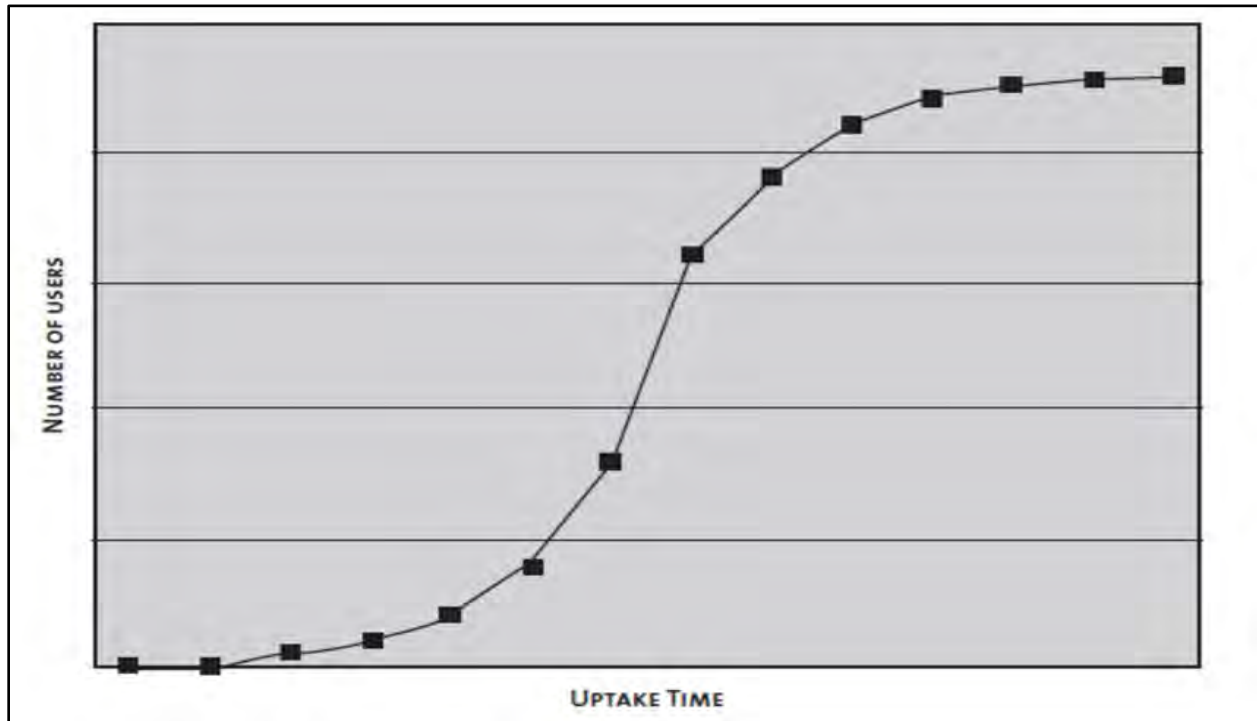
Figure 14-4: Generalized Adoption Curve for a New Product or Technology. Source: Robert H. Potter. Technology Valuation: An Introduction. 2007. <www.iphandbook.org/handbook/ch09/p02>.

14.4.1.2.   Time Period of Analysis

The time period for an economic evaluation should maximize the anticipated economic efficiency of the alternatives. The capital costs should be spread over their economic life (e.g., five years or longer, depending on the technology). To a large extent, the time period will be determined by the technical or functional obsolescence of a product, especially when new products become available on the market. Considering the rapid development of sensing and communication technologies, the equipment replacement frequency could be as short as a few years; this frequency can be longer when transportation agencies make use of purchased technology for as long as possible in budget-limited environments.

14.4.1.3. Geographic Scope of the Analysis

The area included in the analysis is the State of Michigan, which has 4,397 state-owned NBI-length bridges and 6,500 local NBI-length bridges in 2011. As new bridge condition assessment technologies are adopted, we can expect them to be applied to more and more bridges over time related to the adoption rate discussed previously. We also investigated the potential for broad deployment in adjacent states, such as Indiana, Illinois, Wisconsin, and Ohio, to reduce marginal costs. However, it was found that the State of Michigan is a large enough geographical area to take advantage of economies of scale.

The assumption of broad multi-state deployment may be most appropriate if the likely CONOPS is for DOTs to contract out remote sensing services for bridge condition assessment as needed, rather than engage in outright purchase of hardware. DOTs frequently contract out current remote sensing data needs, such as high-resolution aerial photography collection and LiDAR data collection, from commercial services firms, such as Woolpert and Aerocon, and may choose to do so for new remote sensing technologies, as well. These two possibilities – to purchase hardware or to purchase services – may well be the most important distinction in developing the CONOPS, and the recommended option may vary by technology and perhaps even by agency.

14.4.2. Quantifying Costs of Remote Sensing Technologies

Many factors must be considered during the process of estimating the costs of using remote sensing technologies, such as technology costs (e.g., equipment and/or hardware), labor costs (e.g., operation of sensors, analysis of data), software costs (e.g., needed analytic tools), scheduled maintenance of equipment and hardware, additional costs for data storage and transfer, and road user costs due to traffic disruption.

Some of the above cost elements are relatively straightforward and can be measured based on available market data and the field demonstration cost data collection efforts. Others, those with greater uncertainty, are not easily measured, such as final labor costs associated with inspection and data processing times. Careful analysis will need to be performed to estimate the cost of these technologies once at a commercially available stage, as research costs are not typically representative of implemented technology costs. Thus, the final cost database is being developed based on field demonstration cost data collection, interviews with vendors, and additional research. This study also proposes to distinguish experimental or research-stage costs and CONOPS costs for real-world applications, and would expect CONOPS costs to come down when technologies mature.

The final cost categories include capital (data collection systems and pickup truck), operational (labor and data storage), and external costs (e.g., lane/shoulder closures for certain technologies). Summary cost estimates by category for each technology are as follows:

14.4.3.   Data collection system

Costs of data collection equipment, computer, and software. For example, the Thermal IR data collection system includes cameras, laptop computer, and software. The estimated cost for such a system is $30,000. The mobile LiDAR data collection system is probably the most expensive, which will include digital cameras, 2 to 4 LiDAR scanners in order to generate "point cloud" for the entire bridge in a single pass, positioning systems, laptop computers, and other remote sensing devices. The estimated system cost is from $500,000 and up, depending on system configuration (Yen et al. 2011). Similarly, the data collection system for 3DOBS, BVRCS, GigaPan, DIC, and GPR will cost approximately $34,000, $7,000, $5,000, $5,500 and $200,000, respectively. Some system costs may vary significantly depending on the exact specifications and capabilities of the system. Additionally, rapidly decreasing technology costs may affect these costs in the near future.

14.4.3.1.   Vehicle Cost

Cost of a vehicle is estimated at $800 rental fee per month. This is high-end estimate since special configuration for the vehicle may be needed for most data collection systems. In a comparison of purchase and operate vs. contracted service deployment options, a purchased vehicle depreciation cost of $30,000 is assumed.

14.4.3.2.   Data Storage and Backup Costs

Estimated at $10 per GB per year (e.g., Michigan Department of Technology, Management and Budget provides full service network-attached storage that runs across a T1 for $9.6 per GB per year).

14.4.3.3.   Labor Costs Associated with Data Collection and Processing

The total costs of personnel to collect the data and extract the bridge condition information. It was assumed that all technologies except GigaPan and DIC will be deployed close to highway speed for CONOPS analysis. As a result, the data collection time ranges from 30 minutes to four-hours per bridge (4 hours for GigaPan and 2.5 hours for DIC per bridge), and the data processing time ranges from one to 16 hours per bridge, depending highly on the types of technologies to be selected. To simplify the calculation, it was further assumed a two-person inspection crew was needed for all data collection and a uniform labor rate of $50 per hour for all of the personnel needed for data collection and processing.

14.4.3.4. External Costs

Calculations of road user costs require much location-specific information, such as length of highway affected by the activity, traffic speed during activity, normal traffic speed, annual average daily traffic (AADT), annual average daily truck traffic (AADTT), work zone crash rates, vehicle operating costs, etc. One study suggested that road user cost due to bridge inspections could range from $20,000 to $32,000 per occurrence. Another example is the lane rental fee, which appears to be more appropriate for this study. Lane rental is commonly used in the roadway construction contracting process, meaning that the contractor has to pay for the time or right to use lanes during construction operations. This time component is converted to a cost to the contractor based on estimated road user costs, depending on, for example, whether one lane is occupied as opposed to a lane and a shoulder. In addition, rental rates can be different depending on the time of day (i.e., peak or off-peak travel hours). It was assumed that all technologies except GigaPan and DIC will be mounted on a vehicle and travel close to highway speed. As such, they will not generate any external costs. For the use of GigaPan, one shoulder closure is needed and the hourly fee is $125. For DIC, one shoulder and one lane closures are needed and the hourly fee is $625 (TRB 2000).

14.4.3.5. Service Fee

Contractor's charge per bridge for using certain types of technologies. For example, service fee for Thermal IR and GPR is about $1,300 per bridge excluding road user costs and mobilization charges (Infrasense).

The summarized capital, operational, external, and service costs for all examined technologies are presented in Table 14-3. More detailed comparison of research-stage and CONOPS itemized costs for all technologies are presented in Appendix G.

14.4.6. Assumptions and Deployment Scenarios of Remote Sensing Technologies

As discussed previously, several important factors will influence the outcome of the economic evaluation. These factors include the time period of analysis, geographic coverage, penetration rate or percent of bridges using remote sensing technologies, combinations of inspection techniques, and deployment options. Any economic analysis requires a set of assumptions. The assumptions used for the final cost-benefit analysis are described below:

14.4.6.1. Time Period of Analysis

The timeframe to calculate total costs and benefits was determined primarily by the replacement circle of major equipment. For this study, three different time-period options were chosen for

analytical purposes: 5 years, 10 years, and 15 years. The 5-year replacement circle seems to be close to the optimum, given the rapid advancement of technologies and costs associated with technical support and upgrade.

Table 14-3:   Summary of CONOPS costs and contractor's service fee.

Cost Type	Cost Description		3DOBS	BVRCS	GigaPan	ThIR	DIC	M-LiDAR	UWBIRS
Capital	Data Collection Systems (per set)	Includes major data collection equipment, laptop, and software	$34,000	$7,000	$5,000	$30,000	$5,500	$500,000	$200,000
	Pickup Truck (annual total)	$800 rental fee per month	$9,600	$9,600	$9,600	$9,600	$9,600	$9,600	$9,600
Operational	Data Storage and Backup Costs (per	Size of data files (raw and processed, GB)	0.1	2.0	10.0	1.0	32.0	7.0	0.2
		Data storage rate (per GB)	$10	$10	$0	$10	$10	$10	$10
		Data storage cost	$1.20	$20.00	$0.00	$10.00	$320.00	$70.00	$2.00
	Labor Costs	Data Collection time (hours)	0.5	0.5	4	0.5	2.5	0.5	0.5
		# of Personnel needed	2	2	2	2	2	2	2
		Total data collection staff hours	1	1	8	1	5	1	1
		Data Processing time (hours)	2	1	4	8	4	16	8
		Total data collection and processing hours	3	2	12	9	9	17	9
		Hourly rate	$50	$50	$50	$50	$50	$50	$50
		Total labor costs	$150	$100	$600	$450	$450	$850	$450
	Operational Costs Sub-total (per bridge)	Includes data storage and labor costs	$151	$120	$600	$460	$770	$920	$452
External Costs	Road user costs	When lane and/or shoulder closures are needed	$0	$0	$600	$0	$1,563	$0	$0
			3DOBS	BVRCS	GigaPan	ThIR	DIC	M-LiDAR	UWBIRS
Service Fee	Contractor's Charge per Bridge	Road user costs and mobilization costs are not included	$260	$260	$1,500	$1,300	$1,500	$1,800	$1,300

14.4.6.2.   Geographic Coverage

The area included in the analysis is the State of Michigan, which has 4,397 state-owned NBI-length bridges in 2011. If the geographic area is expanded to four adjacent states (Indiana, Illinois, Wisconsin, and Ohio), then the number of state-owned bridges in this region rises to 32,894. However, it was found that expanding the geographic boundary beyond the State of Michigan did not result in any significant differences in estimated cost.

14.4.6.2.1.   Scale of Implementation

The percent of state-owned bridges that will use remote sensing technologies is the key measure for scale of implementation. The rate tends to be higher for longer time period of analysis (e.g.,

10% for five-year horizon, 30% for ten-year horizon, and 50% for 15-year horizon; this means that all bridges are inspected every other year).

14.4.6.2.2.   Available Inspection Days

Because of the Midwest's typical weather conditions, CAR researchers assumed that bridge inspection can be conducted for seven months of the year (April to October), which is typical of MDOT's inspection period. This is equivalent to a 30-week inspection season. The researchers further assumed that, on average, field inspections will occur three days per week (the remaining days are for planning or limited by weather conditions). This translates into 90 inspection days a year. If an inspection crew can inspect eight bridges per day, then the total number of bridges inspected by a single team within a year is 720.

14.4.6.2.3.   Deployment Options

Because each of the remote sensing technologies has its own advantages and disadvantages, combining several methods may yield better results and take advantage of the unique strengths of each individual technology. Relying on the outcomes of technical assessment of the technologies and the results of second-round stakeholder interview, three service packages (i.e., basic, enhanced, and premium) were developed for final analysis. The basic package includes Thermal IR only. The enhanced package includes Thermal IR and 3DOBS, and the premium package includes Thermal IR, 3DOBS, and UWBIRS.

14.4.6.2.4.   Service Life in Uses

Estimating the service life (in number of uses) of a remote sensing inspection unit provides a simple cost estimation method that bypasses complex calculations involving the preceding factors. Determining the total cost of implementation of a remote sensing technology for a given assumed service life requires only adding the capital (investment) costs and the total operational (per bridge) costs. Estimated per bridge costs then only requires dividing the total cost by the anticipated number of uses. This approach was necessary to compare per-bridge costs of purchasing and operating the technology in-house to contracting the service out without making assumptions about the time period of analysis. Because service life is time-independent, it is assumed in this case that an inspection vehicle is purchased at a cost of $30,000 in capital depreciation over the service life of the inspection unit—as opposed to a yearly leased rate as in more complex analysis.

14.4.6.2.5.   Service Types

Two service types were examined in the study: (1) purchase and operate and (2) contract for services.

The analytical results derived from these assumptions are presented in following section.

14.4.7.   Cost Analysis of Alternative Deployments

The measuring of costs associated with the three deployment options (basic, enhanced, and premium) are conducted in combination with other influencing factors (time period of analysis, geographic coverage, and service type). The measurements include annual total cost, average cost per bridge, and cost types. Year 1 costs are usually higher due to one-time capital investment of data collection systems. The highlights of these analytical results include:

- Annual average per bridge cost for using the basic service of Thermal IR ranges from $476 to $495 for the State of Michigan; the cost of adding 3DOBS or the enhanced service package will be 24% higher ranging from $581 to $612 per bridge; The premium package (Thermal IR + 3DOBS + UWBIRS) costs between $1,001 and $1,105, about twice the basic service (Table 14-4, Table 14-5, and Table 14-6). The cost range is a function of the time period of analysis and scale of implementation.
- Annual average cost per bridge using the "purchase and operate" service model is less than using contract services because of number of bridges in these calculations exceeded the balancing point, which is 72 bridges for the basic service package to 155 bridges for the premium package (see Figure 14-5).
- The selection of time period of analysis (5 years, 10 years, and 15 years) does not have significant impact on annual average costs per bridge, mainly because the capital costs only account for less than 4% of total costs (Table 14-7).
- Labor costs associated with data collection and processing account for the majority of total costs at about 85-95%.
- Data storage costs cannot be neglected (1-2%), especially when data services are charged annually.

Table 14-4: Cost summary for using remote sensing technologies (5-year time horizon, with 10% of state-owned bridges inspected each year).

Service Option	Basic	Enhanced	Premium
Purchase & Operate Cost per Bridge	$495	$612	$1,105
Contract Cost per Bridge	$1,300	$1,560	$2,860

Table 14-5: Cost summary for using remote sensing technologies (10-year time horizon, with 30% of state-owned bridges inspected each year).

Service Option	Basic	Enhanced	Premium
Purchase & Operate Cost per Bridge	$479	$585	$1,018
Contract Cost per Bridge	$1,300	$1,560	$2,860

Table 14-6: Cost summary for using remote sensing technologies (15-year time horizon, with 50% of state-owned bridges inspected each year).

Service Option	Basic	Enhanced	Premium
Purchase & Operate Cost per Bridge	$476	$581	$1,001
Contract Cost per Bridge	$1,300	$1,560	$2,860

Table 14-7: Annual cost breakdown by deployment options (10-year time horizon, with 30% of state-owned bridges inspected each year in Michigan).

Cost per bridge	Basic		Enhanced		Premium	
Capital investment per bridge	$5	0.9%	$10	1.7%	$40	3.9%
Vehicle cost per bridge	$15	3.0%	$15	2.5%	$15	1.4%
Operational data cost per bridge	$10	2.1%	$11	1.9%	$13	1.3%
Operational labor cost per bridge	$450	93.9%	$550	93.9%	$950	93.3%
Total	$479	100.0%	$585	100.0%	$1,018	100.0%
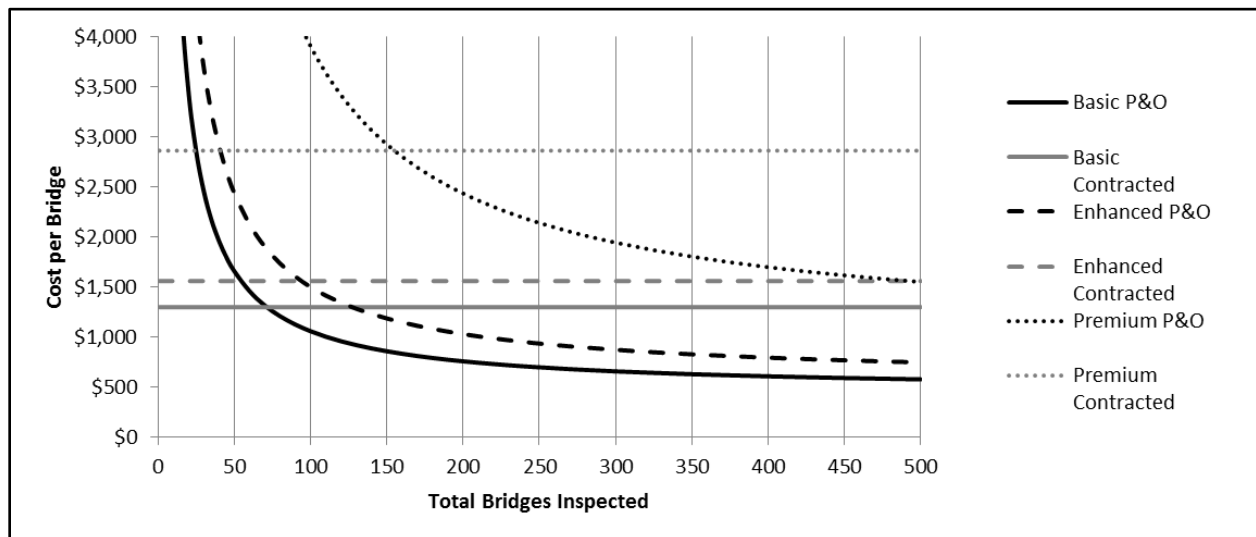
Figure 14-5: Cost per bridge by service options.

14.4.8.   Benefits of Remote Sensing Technologies

Compared to cost analysis, identifying, measuring, and valuing the benefits of remote sensing technologies, are less straight forward and tend to be more complex. From wider technical and economic perspectives, however, the use of remote sensing technologies will have at least the following beneficial consequences: enhancement of technical performance of bridge inspection, early detection of bridge defects and therefor reducing life-cycle costs of bridge maintenance, direct cost savings, safety improvements for bridge inspectors, and the value of the DSS.

First, each technology tested in this study has its own value in terms of providing useful metrics, especially by quantifying, mapping, and visualizing bridge conditions. Some of these additional improvements can be achieved through low capital investment (e.g., 3DOBS) and can be integrated into regular bridge inspection practices with minimum additional operational costs. As suggested in the previous section, a combination of three remote sensing technologies or premium service package (Thermal IR, 3DOBS, and UWBIRS) costs about $1,000 per bridge, but it has the highest added value since they can provide as many as 22 desired measurements of bridge deck surface, deck subsurface, girder surface, girder subsurface, and global metrics in a single run (Table 14-8).

Secondly, inspection costs in general are not that significant in respect to bridge investment since they represent less than 4% of bridge life-cycle costs (construction, maintenance, and rehabilitation etc.) The greater value of remote sensing technologies is likely the benefits of a more efficient bridge management system and new technical capabilities that will lead to timelier detection of problems, resulting in substantial cost savings and longer asset life – if these technologies become practical and cost-effective. Some of the effective diagnosis tools, such as Thermal IR are able to give early detection of bridge construction faults, defects, and deterioration processes. Combined with advanced data processing and visualization tools, these remote sensing technologies can produce a surprising level of information about the inner structure of a bridge. Additionally, the improved interpretability and accuracy of bridge condition assessments will definitely help bridge management agencies make better decisions and develop cost-effective maintenance strategies and procedures.

Thirdly, the outcome indicators of several of the remote sensing technologies field tested are similar to the outputs required in bridge scoping, such as measures of extent of delamination, spalling, and crack areas, and calculation of deterioration percentage. These measures are critical input in developing repair strategies and cost estimates. As discussed previously, MDOT scoped 167 bridges in 2010 with an average cost of about $9,300 per bridge. It is unlikely that remote sensing technologies will substitute bridge scoping completely, but using these technologies to supplement current inspection and analytical work with an estimated cost of $1,000 per bridge (the premium package service of Thermal IR, 3DOBS, and UWBIRS), transportation agencies or engineering firms will likely complete bridge scoping with a smaller budget – in particular when these technologies can be applied without interrupting the traffic, as oppose to the practice of current bridge scoping does.

Finally, remote sensing technologies have great safety implications for bridge inspectors when they can keep bridge inspectors out of traffic for both regular inspection and bridge scoping. The benefits are maximized when these new technologies are mounted on a vehicle and travel at close to highway speed.

Table 14-8: Performance measurement capabilities of 3DOBS, Thermal IR, and UWBIRS.

Location	Challenges	Performance Measurement	Thermal IR	3DOBS	UWBIRS
Deck Surface	Expansion Joint	Torn/Missing Seal	✓	✓	
		Armored Plated Damage		✓	
		Cracks within 2 Feet		✓	
		Spalls within 2 Feet	✓	✓	
		Chemical Leaching on Bottom			
	Map Cracking	Surface Cracks		✓	
	Scaling	Depression in Surface	✓	✓	
	Spalling	Depression with Parallel Fracture	✓	✓	
	Delamination	Surface Cracks		✓	
Deck Subsurface	Expansion Joint	Material in Joint			
	Delamination	Moisture in Cracks	✓		✓
		Internal Horizontal Crack			
		Hollow Sound			
		Fracture Planes / Open Spaces	✓		✓
	Scaling	Depression in Surface (eg. Interior of voided sections)			✓
	Spalling	Depression with Parallel Fracture (eg. Interior of voided sections)			✓
	Corrosion	Corrosion Rate (Resistivity)			
	Rebar Corrosion	Change in Cross-Sectional Area			✓
	Chloride Ingress	Chloride Content through the Depth			✓
Girder Surface	Steel Structural Cracking	Surface Cracks			
	Concrete Structural Cracking	Surface Cracks	✓		
	Steel Section Loss	Change in Cross-Sectional Area			
	Paint	Paint Condition			
	Concrete Section Loss	Change in Cross-Sectional Area			
Girder Subsurface	Internal Concrete Structural Cracks	Internal Cracks (e.g. Box Beam)			✓
		Fracture Planes / Open Spaces	✓		✓
	Concrete Section Loss	Change in Cross-Sectional Area			
	Prestress Strand Breakage	Change in Cross-Sectional Area			✓
	Corrosion	Corrosion Rate (Resistivity)			
	Rebar Corrosion	Change in Cross-Sectional Area			✓
	Chloride Ingress	Chloride Content through the Depth			✓
Global Metrics	Bridge Length	Change in Bridge Length		✓	
	Bridge Settlement	Vertical Movement of Bridge			
	Bridge Movement	Transverse Directions			
	Surface Roughness	Surface Roughness		✓	
	Vibration or Live Load Deflection	Vibration or Live Load Deflection			

14.4.9.   Benefits of Decision Support System

The DSS is developed by the research team as a user-friendly, on-line web mapping tool focused on the needs of the bridge assessment community. It has been designed to be able to integrate existing historical bridge condition data typically collected and used by DOTs, as well as integrate the results of remote sensing technologies, and to create comprehensive bridge health signatures.

A new version of the DSS can also display clearly in mobile tablet-computers such as the iPad and others running the Android operating system to make the DSS readily available to bridge inspectors and engineers in the field. In the end, the DSS will enable more cost-efficient bridge asset management if used as part of a DOT planning processes.

Other benefits of DSS include:

- Reduces the subjectivity of input data, if remote sensing data is provided.
- Increases the accessibility of the data, and makes bridge condition comparisons easier and more accurate.
- Concisely packages key condition information for high level comparisons.

14.5. Conclusions and Recommendations

The quality and performance of highway bridges are vital to the nation's economy and social well-being. Fiscal sustainability of a HBP, however, remains a challenge as the HTF is projected to incur significant deficits in the years ahead. The pressure to increase economic efficiency of expenditures has created the necessity of data-driven, element-level bridge inspection programs and advanced BMSs. This in turn will lead to improved bridge management actions (i.e., maintenance, preservation, rehabilitation, replacement decisions). The use of remote sensing technologies presents a potential alternative to augment current practices by providing both qualitative and quantitative measures of a bridge's condition.

To ensure a practical, cost-effective product to be integrated into transportation agency operations, this economic evaluation assessed the cost effectiveness of remote sensing technologies by comparing marginal costs of employing sensor technologies to the marginal enhancements that they provide. The benefits of remote sensing technologies (both technical and economic) can be optimized by deploying multiple technologies or premium service package at one time (e.g., using Thermal IR, 3DOBS, and UWBIRS together). Under several different deployment scenarios tested in the study, the average cost for using the premium service package was about $1,000 per bridge (or about $480 for Thermal IR only, and $580 for Thermal IR and 3DOBS). The capital cost (equipment and vehicle) accounted for less than 10%. The majority was operational costs (labor cost associated with data collection and processing, data storage). The tipping point for two different deployment options (purchase and operate vs. contract service) was 72 to 155 bridges, depending on the service option – meaning that it would become more cost effective for state agencies to purchase and operate when there are more than this number bridges to be inspected.

The DSS integrated with bridge condition data from remote sensing technologies will increase the accessibility of the data, and makes bridge condition comparisons easier and more accurate. It will also help decision making and resource allocation.

The cost effectiveness of remote sensing technologies is highly dependent on the successful integration with existing bridge inspections (both regular and bridge scoping). It is likely that existing DOT inspection team will fulfill the new functions and responsibilities of using remote sensing technologies. Therefore, it is important to standardize data collection techniques, simplify data processing steps, and develop reporting procedures in order to encourage stakeholders' buy-in.

15. Findings

The current findings add substantially to the understanding of remote sensing technologies for bridge inspection application. For the typical bridge engineer the concept of remote sensing is often associated with satellite imagery and aerial photography for applications in the environmental and earth sciences; however, various remote sensing techniques have been used in infrastructure applications without being specifically labeled as such.

Remote sensing is traditionally defined as the collection and measurement of spatial information at a distance from the data source, without direct contact. Remote sensing technologies are distinct from remote monitoring technologies in that the former does not include attached or embedded sensors such as strain gauges or temperature sensors. Remote monitoring sensors are in direct contact with the bridge component whose characteristics are being measured.

To the bridge engineer, remote sensing can mean the ability to assess the condition or performance of the bridge at a distance, enhancing the inspection process, all without traffic disruption.

Applicable remote sensing technologies for bridge inspection were selected in this project based on the initial literature review. A summary of this study is included in the Commercial Sensor Evaluation and State of the Practice reports (Appendices A and B).

The selected technologies were further investigated during laboratory study and field demonstration stages of the project. Finally, the selected technologies were re-evaluated to reflect the further project findings and achievements. Developing the DSS for bridge inventory and appraisal was one of the main components of this project. The DSS that was developed during the course of this project has the ability to store and display the existing NBI information as well as the results from advanced inspection technologies such as 3DOBS and Thermal IR. Displaying the bridge information in GIS environment and features such as pie charts allow bridge management team to make more viable decisions on the overall condition of the bridge.

This chapter provides an overview of the project findings and technology evaluation as well as field readiness level of each technology and implementation for future bridge inspection practices.

15.1. Technology Evaluation

Evaluating the selected remote sensing technologies for bridge condition assessment was one of the concluding tasks of this project. Remote sensing technologies/systems that were selected include:

- 3DOBS
- BVCRS

- GigaPan
- LiDAR
- Thermal IR
- DIC
- UWBIRS
- SAR
- InSAR
- MSI

These remote sensing technologies were selected for further laboratory study and field demonstration based on the literature review and ratings that were provided in the commercial sensor evaluation report. During the course of this project some of the selected technologies were denominated with a title which best describes the technology performance for bridge inspection. Examples of these cases include 3DOBS which is a technology developed based on the close-range 3D photogrammetry technique or BVCRS and GigaPan which were developed based on Street View-style photography.

After completing the field demonstration and data process stages, these technologies were further evaluated based on the project findings and current knowledge of the project team. A summary of this updated rating is provided in Table 15-1. The main challenges and indicators are almost the same as the initial evaluation at the literature review stage to best imitate the initial evaluation table for comparison purposes.

The basis of the rating methodology was the same as the previous evaluation, however during this evaluation it was decided that there should be a distinction between what is considered as "not achieving the required resolution with a technology" and "Not applicable or not appropriate" for the technology. Therefore, the "N/A" was defined in the methodology section to reflect this perception. Similar to the previous evaluation, all performance criteria (A-H) receive a score from 0 to 2 where a higher score is more satisfactory and zero indicates that the technology does not satisfy the criterion. Criterion that has not been investigated for the specific technology or it seemed not suitable from the early stage of the project was distinguished by a (−). An overall perfect score for each technology would be 16. The rating methodology and definition for each criterion is included in Appendix H.

The results from this evaluation provide additional evidence with respect to the applicability of each technology for each specific bridge health challenge and location of the flaw. Potential remote sensing technologies for identifying bridge health indicators on the deck surface include 3DOBS, BVRCS, LiDAR, Thermal IR, and SAR.

Table 15-1: Performance rating of investigated remote sensors for each challenge.

Location	Challenges	Indicator	UWBIRS	3DOBS	Multispectral Satellite Imagery	Giga-Pan	Terrestrial LiDAR	Thermal IR	Digital Image Correlation	SAR Speckle	InSAR	BVRCS
Deck Surface	Expansion Joint	Torn/Missing Seal	-	12	0	N/A	10	13	-	0	-	12
		Armored Plated Damage	-	11	-	N/A	10	N/A	-	-	-	13
		Cracks within 2 Feet	-	11	0	N/A	10	N/A	-	0	-	13
		Spalls within 2 Feet	-	12	0	N/A	10	12	-	0	-	13
		Chemical Leaching on Bottom	-	-	N/A	13	N/A	-	-	-	-	N/A
	Map Cracking	Surface Cracks	-	11	0	N/A	10	0	-	0	-	13
	Scaling	Depression in Surface	-	12	0	N/A	10	11	-	9	-	13
	Spalling	Depression with Parallel Fracture	-	12	0	N/A	10	11	-	9	-	13
	Delamination	Surface Cracks	-	11	0	N/A	10	0	-	N/A	-	13
Deck Subsurface	Expansion Joint	Material in Joint	-	-	-	N/A	-	-	-	-	-	N/A
	Delamination	Moisture in Cracks	9	-	-	-	-	12	-	-	-	-
		Internal Horizontal Crack	0	-	-	-	-	-	-	-	-	-
		Hollow Sound	-	-	-	-	-	N/A	-	-	-	-
		Fracture Planes / Open Spaces	10	-	-	N/A	-	12	-	N/A	-	-
	Scaling	Depression in Surface (eg. Interior of voided sections)	10	-	-	-	-	0	-	-	-	-
	Spalling	Depression with Parallel Fracture (eg. Interior of voided sections)	10	-	-	-	-	0	-	-	-	-
	Corrosion	Corrosion Rate (Resistivity)	N/A	-	-	-	-	N/A	-	-	-	-
	Rebar Corrosion	Change in Cross-Sectional Area	10	-	-	-	-	-	-	N/A	-	-
	Chloride Ingress	Chloride Content through the Depth	10	-	-	-	-	N/A	-	N/A	-	-
Girder Surface	Steel Structural Cracking	Surface Cracks	-	0	N/A	12	0	0	-	N/A	-	N/A
	Concrete Structural Cracking	Surface Cracks	-	0	N/A	12	0	13	-	N/A	-	-
	Steel Section Loss	Change in Cross-Sectional Area	-	0	-	-	10	N/A	-	N/A	-	-
	Paint	Paint Condition	-	-	N/A	-	-	N/A	-	-	-	N/A
	Concrete Section Loss	Change in Cross-Sectional Area	-	0	-	-	10	N/A	-	N/A	-	-
Girder Subsurface	Internal Concrete Structural Cracks	Internal Cracks (e.g. Box Beam)	9	-	-	-	-	N/A	-	N/A	-	-
		Fracture Planes / Open Spaces	9	-	-	-	-	13.5	-	-	-	-
	Concrete Section Loss	Change in Cross-Sectional Area	-	-	-	-	-	N/A	-	N/A	-	-
	Prestress Strand Breakage	Change in Cross-Sectional Area	9	-	-	-	-	N/A	-	N/A	-	-
	Corrosion	Corrosion Rate (Resistivity)	N/A	-	-	-	-	N/A	-	-	-	-
	Rebar Corrosion	Change in Cross-Sectional Area	9	-	-	-	-	-	-	N/A	-	-
	Chloride Ingress	Chloride Content through the Depth	9	-	-	-	-	N/A	-	N/A	-	-
Global Metrics	Bridge Length	Change in Bridge Length	-	11	-	-	-	-	N/A	N/A	N/A	N/A
	Bridge Settlement	Vertical Movement of Bridge	-	N/A	-	-	N/A	-	N/A	N/A	0	N/A
	Bridge Movement	Transverse Directions	-	N/A	-	-	N/A	-	N/A	N/A	N/A	N/A
	Surface Roughness	Surface Roughness	-	12	0	N/A	16	-	-	10	N/A	12
	Vibration or Live Load Deflection	Vibration or Live Load Deflection	-	-	-	N/A	-	-	13	N/A	N/A	-

Performance Rating of Commercial Remote Sensing Technologies — Rating Based, in Part, on Theoretical Sensitivity for Measurement Technologies

Although all of these technologies are able to resolve the deck surface related challenges, 3DOBS has the best resolution for surface related challenges and showed the most promise for field application. For health indicators associated with girder surface challenges, GigaPan and LiDAR appeared to be the most appropriate technologies while 3DOBS and Thermal IR are not as effective in this case.

For both bridge deck and girder subsurface challenges, the UWBIRS and Thermal IR showed the most promise in resolving the associated bridge health indicators. Technologies that were best suited for resolving global metric challenges include DIC which is applicable for determining bridge live load deflection and vibration measures and 3DOBS which has the potential to investigate the bridge length. Identifying the surface roughness of the bridge deck can be identified using 3DOBS, BVRCS, LiDAR, and SAR. More information regarding the rating methodology for each technology is included in Appendix H.

15.2. Implementation and Field Readiness

According to the technology evaluation findings, some technologies are easier to apply and more relevant to the specific bridge health challenge. 3DOBS is the most promising and lowest cost technology for resolving deck top surface challenges. 3DOBS has the potential to collect high-resolution DEM data of bridge decks using close-range photogrammetry. Size, volume and overall percentage of spalls on the bridge deck can be calculated using the DEM data. Also, other information such as IRI and crack density can be achieved from the results of this technology. In order to obtain better resolution images and increase the speed of data collection higher-end cameras should be used to allow for collecting information by driving over the bridge deck.

BVRCS is another promising tool for assessing the condition of the bridge deck surface and considered as a "near user-ready" technology in this study. The speed of data collection with this technology is mainly dependent on the camera frame rate and has the potential to be applied at higher speeds on the bridge deck. GigaPan is also considered as a "near-user ready" technology. While data collection and process is possible with a least expensive option, higher-end cameras can be used to increase the speed of data collection and process. This technology is mostly applicable for underside of the bridge deck and girders.

Thermal IR imagery is well-recognized in the field of nondestructive testing for detecting subsurface flaws and delaminations. However, the deployment of this technology on the bridge is not always a possible option; considering limitations and effects of the environmental variables. In this case, having a camera with larger field of view can increase the speed of data collection and analysis significantly over the bridge deck. Perhaps one of the main areas that required further investigations is application of this technology for underside of the bridge deck and bridge girders. Further investigation and study is required to develop other selected remote sensing technologies in this project (LiDAR, DIC, and MSI) to make them more applicable for identifying the bridge health indicators.

Further information regarding implementation of each one of the investigated technologies is provided in Chapters 4-12.

15.3. Bridge Signature

It is a primary motivation for the use of remote sensing and non-destructive evaluation in general that the existing protocols for bridge condition assessment describe subjective indicators (e.g., "excessive" cracking or "shallow" spalling). However, some quantifiable metrics of bridge condition are available that could be used to fit remote sensing observations to existing rating schemes such as the NBI (FHWA 1995; MDOT 2009). The quantifiable metrics of bridge condition that are derived from remote sensors, listed in Table 15-2, can thus be correlated to an NBI or IRI rating. Furthermore, these metrics could be used to synthesize user-defined, comprehensive indicators of bridge condition, exemplified by Equation 15-1 for what the authors call the bridge deck surface rating (BDSR) where a, b, c, and d are user-defined weights.

$$BDSR = a \times (\% \ Spall) + b \times (\% \ Delam) + c \times (IRI) + d \times (Crack \ Density)$$ **Equation 15-1**

Table 15-2: Remote sensing technologies and associated useful measures.

Remote Sensing Technologies	Useful measures
3DOBS	% Spalled and International Roughness Index (IRI)
Thermal IR	% Delaminated area
DIC	Deflection, vibration
UWBIRS	% Delaminated area
BVRCS	High-resolution, location-tagged photo inventory
LiDAR	% Spalled and crack pattern
MSI	Overall deck condition

Although ratings such as this can to some extent help bridge management team to have an overall measure of the bridge, some other components such as ADT, structure type or surface overlay, can also influence the decision on bridge maintenance and preservation. Furthermore, visualizations of remote sensing data complete the asset management picture of a bridge by linking the quantifiable metrics of bridge condition to the traditionally more intuitive, visual inspection that is commonplace today in bridge inspection. As bridge decision-makers become

more familiar with using remote sensing data in asset management, the ability to view a thermal infrared image, for instance, or a high-resolution DEM in the map plane and virtually walk the bridge, orienting themselves with oblique photographs from the BVRCS affords them a more thorough understanding of a bridge condition.

At the inventory scale, being able to compare the delamination or spalled area of multiple bridges in a corridor or of a given type to one another, rather than the NBI ratings, will afford the bridge manager or inspector a more accurate and comprehensive view of bridge condition.

15.4. Path Forward

The present study confirms that remote sensing technologies can be used to assess and monitor the performance of bridge infrastructure and improve the efficiency of inspection, repair, and rehabilitation efforts. Most importantly, monitoring the condition of a bridge using remote sensors can help eliminate the need for traffic disruption or total lane closure as remote sensors do not come in direct contact with the structure.

The formal integration of remote sensing technologies into the bridge condition assessment scheme has the potential to enhance inspection practices and provide temporal assessments between inspection cycles, without traffic disruptions. Bringing these technologies together into an understandable environment to support the work of bridge inspectors is paramount and helps to address the issue that no single technology can detect bridge performance alone. By combining the results of individual technologies with a decision support system that is implementable and user-friendly, monitoring and assessing bridge condition can be enhanced and decision-making process for critical repair and replacement can be simplified.

It should be noted that to date there does not appear to be a single method that is capable of providing a comprehensive condition assessment of a concrete bridge deck. The real solution to this challenge is the data fusion of multiple technologies aimed at providing an overall condition signature based on multiple technologies such that commercial available remote sensors can be understood in a broader perspective.

Overall, the nation's bridge assets must be managed in a more sustainable manner. Remote sensing technologies have the potential to transform our current state of bridge condition assessment by helping to take the "guesswork" out of the inspector's toolbox and replacing it with reliable and quantifiable tools to measure several health indicators. When combined with historical data and maintenance records, a unique bridge signature (based on total performance) can be established and monitored over time.

Ultimately, integrating new technologies, such as remote sensing, with proven tools and combining with a decision support system will enhance the way we decide to prioritize critical and dwindling resources to ensure that our nation's bridges are safe.

References

ACI (2001). Protection of Metals in Concrete against Corrosion (ACI 222), American Concrete Institute.

Acton, S., A. Vaccari, et al. (2012). Investigating Interferometric Synthetic Aperture Radar for Transportation Infrastructure Monitoring. Transportation Research Board 91st Annual Meeting. Washington, D.C., Transportation Research Board.

Adams, T. M., M. Kang, et al. (2008). A Systematic Process for Using Federal Aid to Support Bridge Preventive Maintenance. Madison, WI, Midwest Regional University Transportation Center.

Ahlborn, T. M., D. K. Harris, et al. (2010 a). Remote Sensing Technologies for Detecting Bridge Deterioration and Condition Assessment. NDE/NDT for Highways and Bridges: Structural Materials Technology (SMT) 2010. New York, American Society for Nondestructive Testing (ASNT).

Ahlborn, T. M., R. Shuchman, et al. (2010). "An Evaluation of Commercially Available Remote Sensors for Assessing Highway Bridge Condition." From http://www.mtri.org/bridgecondition/doc/RITA_BCRS_Commercial_Sensor_Evaluation.pdf.

Ahlborn, T. M., R. Shuchman, et al. (2011 a). "Technical Mamorandum 11 - Laboratory study progress update." From http://www.mtri.org/bridgecondition/doc/Technical_memo_11_Lab_study_progress.pdf.

Ahlborn, T. M., R. Shuchman, et al. (2011 b). "Technical Mamorandum 15 - Laboratory study progress update, structural modeling and remote sensing response correlation." From http://www.mtri.org/bridgecondition/doc/Tech_Memo_15.pdf.

Ahlborn, T. M., R. Shuchman, et al. (2010 b). The State-of-the-Practice of Modern Structural Health Monitoring for Bridges: A Comprehensive Review.

Al-Omari, B. H. and M. I. Darter (1994). Relationships between International Roughness Index and Present Serviceability Rating. Transportation Research Record 1435. Washington, D.C., Transportation Research Board.

Alampalli, S. (2010). "Special Issue on Bridge Inspection and Evaluation." ASCE Journal of Bridge Engineering **15**(4): 349-351.

American Association of State and Highway Transportation Officials (AASHTO). (2008). "Bridging the Gap: Restoring and Rebuilding the Nation's Bridges." From http://www.transportation1.org/BridgeReport/front-page.html.

American Association of State and Highway Transportation Officials (AASHTO) (2008). Manual for Bridge Evaluation. Washington, D.C.

American Concrete Institute. (2010). "ACI Concrete Terminology - Updated 8/31/10." From http://www.concrete.org/Technical/CCT/ACI_Concrete_Terminology.pdf.

American Society of Civil Engineers (ASCE). (2009). "Bridges | report card for America's infrastructure." Retrieved February 22, 2010, 2010, from http://www.infrastructurereportcard.org/fact-sheet/bridges.

Amey, A. (2010). Beyond State-Level Bridge Counts - Alternative Performance Measures for Evaluating Bridge Conditions. Transportation Research Board 89th Annual Meeting. Washington, D.C.

Aronoff, S. (2005). Remote Sensing for GIS Managers. Redlands, CA, ESRI Press.

ASTM (2007). ASTM D4788-03: Standard test method for detecting delaminations in bridge decks using infrared thermography, American Society of Testing Materials.

Barrile, V. and R. Pucinotti (2005). "Application of radar technology to reinforced concrete structures: a case study." NDT & E International **38**(7): 596-604.

Besnard, G., S. Guérard, et al. (2011). "A space–time approach in digital image correlation: Movie-DIC." Optics and Lasers in Engineering **49**(1): 71-81.

Brooks, C., D. Schaub, et al. (2007). TARUT Pilot Studies Technical Details Report. Ann Arbor, MI, Michigan Tech Research Institute.

Cardimona, S., B. Willeford, et al. (2000). Investigation of Bridge Decks Utilizing Ground Penetrating Radar. International Conference on the Application of Geophysical Technologies to Planning, Design, Construction, and Maintenance of Transportation Facilities. St. Louis, MO.

Carrara, W. G., R. S. Goodman, et al. (1995). Range Migration Algorithm. Spotlight synthetic aperture radar : signal processing algorithms. Boston, Artech House**:** 401-442.

Castro, T., D. V. Jauregui, et al. (2010). A Collaborative Approach for Load Rating of State-Owned Bridges. Transportation Research Board 89th Annual Meeting. Washington, D.C.

CFLHA. (2011). "Chapter 2- LiDAR Hardware." Retrieved December 10, 2011, 2011, from www.cflha.gov/programs/techdevelopment/geotech/LiDAR/documents/04_chapter_2_LiDAR.

Chong, K. P., N. J. Carino, et al. (2003). "Health monitoring of civil infrastructures." Smart Materials and Structures **12**(3): 483.

Chu, X. (2011). Fundamentals of LiDAR Remote Sensing, University of Colorado - Boulder.

Clark, M. R., D. M. McCann, et al. (2003). "Application of infrared thermography to the nondestructive testing of concrete and masonry bridges." NDT & E International **36**(4): 65-275.

Connecticut Department of Transportation. (2011). "Phase 2 Cost-Benefit Analysis of Bridge Inspections performed by Consultant in FY 2010." from http://www.ct.gov/scsb/lib/scsb/Cost_Benefit_Analysis_attachments.pdf.

Correlated Solutions. (2010). "Vic-2D 2009." from http://www.correlatedsolutions.com/index.php/products/vic-2d-2009.

Crosetto, M., B. Crippa, et al. (2002). Quantitative subsidence monitoring using SAR interferometry. Geoscience and Remote Sensing Symposium, 2002. IGARSS '02. 2002 IEEE International.

Curlander, J. C. and R. N. McDonough (1991). Synthetic Aperture Radar: Systems and Signal Processing, Wiley-Interscience.

Dantec Dynamics. "Digital Image Correlation for Deformation Measurement." from http://www.dantecdynamics.com/Default.aspx?ID=1030.

de Melo e Silva, H. and C. Brooks (2011). Summary of Field Demonstration Including Sensor Evaluation and Update of the DSS. Tech Memo 21. Houghton, MI, Michigan Technological University**:** 58.

DeLay, L. S., S. A. LucasKamat, et al. (2008). Taking GIS from the Field to the World Wide Web. Incorporating Geospatial Technologies into SMCRA Business Processes. Atlanta, GA**:** 23.

Douglas, K. (2006). PostgreSQL (2nd Edition). Indianapolis, In, Sams Publishing.

Dresel, T., G. Häusler, et al. (1992). "Three-dimensional sensing of rough surfaces by coherence radar." Appl. Opt. **31**(7): 919-925.

Endsley, A., C. Brooks, et al. (2012). Decision support system for integrating remote sensing in bridge condition assessment and preservation, San Diego, California, USA, SPIE.

Falkner, E. (1995). Aerial Mapping: Methods and Applications. Boca Raton, FL, Lewis Publishers – CRC Press

FHWA (1995). Recording and Coding Guide for the Structure Inventory and Appraisal of the Nation's Bridges; FHWA-PD-96-001, Federal Highway Administration (U.S. Department of Transportation).

FHWA (2006). Bridge Inspector's Reference Manual (BIRM); FHWA NHI 03-001, Federal Highway Administration (U.S. Department of Transportation).

FHWA. (2010). "Deficient Bridges by Material Type of Structure by State." Retrieved July 7, 2010, from http://www.fhwa.dot.gov/BRIDGE/material.cfm.

FHWA. (2010). "National Bridge Inventory (NBI)." from http://www.fhwa.dot.gov/bridge/britab.cfm.

FHWA (2011). Bridge Preservation Guide: Maintaining a State of Good Repair Using Cost Effective Investment Strategies; FHWA-HIF-11-042, Federal Highway Administration (U.S. Department of Transportation).

FHWA (2011). Deficient Bridges by State and Highway System. National Bridge Inventory. Washington, D.C., Federal Highway Administration (U.S. Department of Transportation).

Flood, M. (2001). LiDAR Activities and Research Priorities in the Commercial Sector. International Archives of Photogrammetry and Remote Sensing. **Vol. XXXIV-3/W4:** 3-7.

Frenkel, K. A. (2010). "Panning for Science." Science **330**(6005): 748-749.

Gamache, R. and E. Santini-Bell (2009). Non-intrusive Digital Optical Means to Develop Bridge Performance Information. Non-Destructive Testing in Civil Engineering, Nantes, France.

GAO (2008). Highway Bridge Program: Clearer Goals and Performance Measures Needed for a More Focused and Sustainable Program; GAO-08-1043, U.S. Government Accountability Office.

GAO (2010). Highway Bridge Program: Condition of Nation's Bridges Shows Limited Improvement, but Further Actions Could Enhance the Impact of Federal Investment; GAO-10-930T, U.S. Government Accountability Office.

Gentile, C. (2009). Radar-based measurement of deflections on bridges and large structures: advantages, limitations and possible applications. IV ECCOMAS Thematic Conference on Smart Structures and Materials (SMART'09). Porto, Portugal**:** 1-20.

Gucunski, N., S. Nazarian, et al. (2010). SHRP 2 validation study of performance of NDT technologies in identification and characterization of concrete bridge deck deterioration.

NDE/NDT for Highways and Bridges. New York City, NY, U.S.A., American Society for Nondestructive Testing**:** 121-128.

Hagen, S. B., J. U. Jepsen, et al. (2007). "Shifting altitudinal distribution of outbreak zones of winter moth Operophtera brumata in sub-arctic birch forest: a response to recent climate warming?" Ecography **30**(2): 299-307.

Harris, D., S. Hong, et al. (2010). Practical Evaluation of Bridge Deck Reinforcement Corrosion Using Ground Penetrating Radar, Half-Cell, and Sounding. Transportation Research Board 89th Annual Meeting. Washington, D.C., Transportation Research Board.

Henriksen, S., Ed. (1994). The glossary of mapping sciences, American Society of Civil Engineers.

Herold, M. and D. Roberts (2005). "Spectral characteristics of asphalt road aging and deterioration: implications for remote-sensing applications." Appl. Opt. **44**(20): 4327-4334.

Hutt, T. and P. Cawley (2009). "Feasibility of digital image correlation for detection of cracks at fastener holes." NDT & E International **42**(2): 141-149.

Intelligent Sensing for Innovative Structures (2001). Design Manual 2. Guidelines for Structural Health Monitoring. Winnipeg, Manitoba, ISIS Canada Corporation.

Ireland, C., D. Bowers, et al. (2009). A Classification of Object-Relational Impedance Mismatch. Proceedings of the 2009 First International Conference on Advances in Databases, Knowledge, and Data Applications, IEEE Computer Society**:** 36-43.

Jensen, J. R. (2007). Remote sensing of the environment: an earth resource perspective. Upper Saddle River, NJ, Pearson Prentice Hall.

Kim, S., S. Pakzad, et al. (2007). Health monitoring of civil infrastructures using wireless sensor networks. Proceedings of the 6th international conference on Information processing in sensor networks. Cambridge, Massachusetts, USA, ACM.

Kim, W., A. Ismail, et al. (2003). Non-destructive testing (NDT) for corrosion in bridge decks using ground penetrating radar (GPR). The 3rd International Conference on Applied Geophysics. Orlando, Florida.

Kingston, R., S. Carver, et al. (2000). "Web-based public participation geographical information systems: an aid to local environmental decision-making." Computers, Environment and Urban Systems **24**(2): 109-125.

Ko, J. M. and Y. Q. Ni (2005). "Technology developments in structural health monitoring of large-scale bridges." Engineering Structures **27**(12): 1715-1725.

Küntz, M., M. Jolin, et al. (2006). "Digital image correlation analysis of crack behavior in a reinforced concrete beam during a load test." Canadian Journal of Civil Engineering **33**(11): 1418-1425.

Kutser, T., E. Vahtmäe, et al. (2007). "Photo-library method for mapping seagrass biomass." Estuarine, Coastal and Shelf Science **75**(4): 559-563.

Lava, P., S. Coppieters, et al. (2011). "Error estimation in measuring strain fields with DIC on planar sheet metal specimens with a non-perpendicular camera alignment." Optics and Lasers in Engineering **49**(1): 57-65.

Leff, A. and J. T. Rayfield (2001). Web-Application Development Using the Model/View/Controller Design Pattern. Proceedings of the 5th IEEE International Conference on Enterprise Distributed Object Computing, IEEE Computer Society**:** 118.

Leshko, B. (2008). Access Methods for Bridge inspections. Structure Magazine. **October 2008:** 17-21.

Lim, M. K. (2001). NDE using impulse radar to evaluate material properties in concrete structures. Ninth international conference on structural faults and repair. Professor M. C. Forde. London, UK, Engineering Technics Press, Edinburgh**:** 9.

Lopez-Sanchez, J. M. and J. Fortuny-Guasch (2000). "3-D radar imaging using range migration techniques." Antennas and Propagation, IEEE Transactions on **48**(5): 728-737.

Luhmann, T., S. Robson, et al. (2007). Close range photogrammetry: principles, techniques and applications, Wiley.

Maffeis, S. (2003). Client-server computing. Encyclopedia of Computer Science, John Wiley and Sons**:** 215-218.

Maierhofer, C. and S. Leipold (2001). "Radar investigation of masonry structures." NDT & E International **34**(2): 139-147.

Maser, K. R. (1986). Detection of progressive deterioration in bridge decks using ground penetrating radar. ASCE/EM Division Specialty Conference. Boston, MA**:** 42-56.

McCormick, N. and J. Lord (2010). "Digital Image Correlation." Materials Today **13**(12): 52-54.

McGlone, J. C., E. M. Mikhail, et al., Eds. (2004). Manual of Photogrammetry, ASPRS. MDOT (2009). Michigan Structure Inventory and Appraisal Guide, Michigan Department of Transportation.

MDOT (2011). Transportation Management System (TMS), Michigan Department of Transportation.

Moore, M., B. Phares, et al. (2000). Reliability of visual inspection for highway bridges. NDE Validation Center/FHWA, Federal Highway Administration (U.S. Department of Transportation).

Netcraft. (2012). "March 2012 Web Server Survey." Retrieved May 9th, 2012, from http://news.netcraft.com/archives/2012/03/05/march-2012-web-server-survey.html.

Oklahoma Department of Transportation. (2010). "Off-System Bridge Inspection." From http://www.okladot.state.ok.us/projmgmt/off_system_bridge_inspection_consultants/EC-1321%20-%20The%20Benham%20Companies%20LLC.pdf.

Ontario Ministry of Transportation. (2009). "Bridge Inpsection and Maintenance." From http://www.auditor.on.ca/en/reports_en/en09/302en09.pdf.

Pan, B., K. Qian, et al. (2009). "Two-dimensional digital image correlation for in-plane displacement and strain measurement: a review." Measurement Science and Technology **20**(6): 062001.

Park, H. S., H. M. Lee, et al. (2007). "A New Approach for Health Monitoring of Structures: Terrestrial Laser Scanning." Computer-Aided Civil and Infrastructure Engineering **22**(1): 19-30.

Reutebuch, S., H.-E. Andersen, et al. (2005). "Light Detection and Ranging (LIDAR): An Emerging Tool for Multiple Resource Inventory." Journal of Forestry **103**(6): 286-292.

Romero, F. A., G. E. Roberts, et al. (2000). Evaluation of GPR bridge deck survey results used for delineation of removal/maintenance quantity boundaries on asphalt-overlaid, reinforced concrete deck. Structural Materials Technology IV: An NDT Conference, Atlantic City, NJ.

Sadek, S., M. G. Iskander, et al. (2003). "Accuracy of Digital Image Correlation for Measuring Deformations in Transparent Media." Journal of Computing in Civil Engineering **17**(2): 88-96.

Santini-Bell, E., P. Brogan, et al. (2011). Digital Imaging for Bridge Deflection Measurement of a Steel Girder Composite Bridge. Transportation Research Board 90th Annual Meeting. Washington, D.C.**:** 16p.

Scott, M., A. Rezaizadeh, et al. (2001). Phenomenology Study of HERMES Ground Penetrating Radar Technology for Detection and Identification of Common Bridge Deck Features. McLean, VA, Turner-Fairbank Highway Research Center.

Shin, H. and D. A. Grivas (2003). "How accurate is Ground-Penetrating RaDAR for Bridge Deck Condition Assessment?" Transportation Research Record(1845): p. 139-147.

Shukla, A. and J. W. Dally (2010). Experimental solid mechanics. Knoxville, Tenn., College House Enterprises.

Snay, R. and T. Soler (2008). "Continuously Operating Reference Station (CORS): History, Applications, and Future Enhancements." Journal of Surveying Engineering **134**(4): 95-104.

Sugumaran, R. and J. DeGroote (2010). Spatial Decision Support Systems: Principles and Practices, CRC Press.

Sutton, M. A., J.-J. Orteu, et al. (2009). Image correlation for shape, motion and deformation measurements : basic concepts, theory and applications. New York, Springer.

Tao, C. V. and J. Li (2007). Advances in Mobile Mapping Technology, Taylor & Francis.

Tao, L., L. Jingnan, et al. (2004). Monitoring city subsidence by D-InSAR in Tianjin area. Geoscience and Remote Sensing Symposium, 2004. IGARSS '04. Proceedings. 2004 IEEE International.

Te-Ming, T., H. Ching-Luh, et al. (2012). "An Adjustable Pan-Sharpening Approach for IKONOS/QuickBird/GeoEye-1/WorldView-2 Imagery." Selected Topics in Applied Earth Observations and Remote Sensing, IEEE Journal of **5**(1): 125-134.

Thompson, P. D., E. P. Small, et al. (1998). "The Pontis Bridge Management System." Structural Engineering International **8**(4): 303-308.

TRB (2000). Reducing and Mitigating Impacts of Lane Occupancy During Construction and Maintenance; NCHRP Synthesis 293. Washington, D.C., Transportation Research Board.

TRB (2003). Bridge Life-Cycle Cost Analysis; NCHRP Report 483. Washington, D.C., Transportation Research Board.

TRB (2007). Bridge Inspection Practices: A Synthesis of Highway Practice; NCHRP Synthesis 375. Washington, D.C., Transportation Research Board.

Unwin, A. and D. Unwin (1998). "Spatial Data Analysis with Local Statistics." Journal of the Royal Statistical Society: Series D (The Statistician) **47**(3): 415-421.

USDOT (2001). Highway Bridge Inspection: State-of-the-Practice Survey. T.-F. H. R. Center. Mclean, VA, U.S.A., U.S. Department of Transportation, Federal Highway Administration.

USDOT. (2009). "Expenditure of Federal Funds Administered by The Federal Highway Administration During Fiscal Year 2009." From http://www.fhwa.dot.gov/policyinformation/statistics/2009/fa3.cfm.

USDOT. (2011). "FOCUS: Accelerating Infrastructure Innovations." From http://www.fhwa.dot.gov/publications/focus/index.cfm.

Vaghefi, K., R. Oats, et al. (2011). "Evaluation of Commercially Available Remote Sensors for Highway Bridge Condition Assessment." Journal of Bridge Engineering: 202.

Vosselman, G. and H.-G. Maas (2010). Airborne and terrestrial laser scanning, CRC Press.

Wanqiu, L., S.-E. Chen, et al. (2010). Application of 3D LIDAR Scan of a Bridge under Static Load Testing. Columbus, OH, ETATS-UNIS, American Society for Nondestructive Testing.

Warhus, J. P., J. E. Mast, et al. (1994). Improved Ground-Penetrating Radar, Bridge Decks. Structural Materials Technology Non-Destructive Technology Conference. Atlantic City, NJ.

Washer, G. (2010). Thermal Imaging of Damage in Bridge Soffits. NDE/NDT Conference on Civil Engineering. New York, New York.

Washer, G., R. Fenwick, et al. (2009 b). "Effects of Environmental Variables on Infrared Imaging of Subsurface Features of Concrete Bridges." Transportation Research Record: Journal of the Transportation Research Board **2108**: 107-114.

Washer, G. A., R. G. Fenwick, et al. (2009 a). Development of Hand-held Thermographic Inspection Technologies, University of Missouri – Columbia.